

ISSN 1608-5043 (Print)  
ISSN 1608-5078 (Online)

SCIENTIFIC AND TECHNICAL JOURNAL

# GEORESOURCES

[www.geors.ru](http://www.geors.ru)

V. 20. No. 4. 2018  
Part 1

• Age moving of layers: facts and geological consequences (to the 150th anniversary of N.A. Golovkinsky's fundamental work).....278  
*S.O. Zorina, V.P. Alekseev, E.O. Amon, K.A. Khasanova*

• Analysis of the composition and properties of heavy oils in situ by low field NMR relaxation method.....308  
*V.Ya. Volkov, B.V. Sakharov, N.M. Khasanova, D.K. Nurgaliev*

## GEORESURSY

GEORESOURCES. SCIENTIFIC AND TECHNICAL JOURNAL

**Key title: «Georesursy». Parallel title: «Georesources»****Editor in Chief: Renat Kh. Muslimov**  
Kazan Federal University, Kazan, Russian Federation**Editorial Board**

**Farit A. Agzamov**, Ufa State Petroleum Technical University, Ufa, Russian Federation  
**Lyubov K. Altunina**, Institute of Petroleum Chemistry of the Siberian Branch of the Russian Academy of Sciences, Tomsk, Russian Federation  
**Azary A. Barenbaum**, Institute of Oil and Gas Problems of the Russian Academy of Sciences, Moscow, Russian Federation  
**Eric Delamaide**, IFP Technologies (Canada) Inc., Calgary, Canada  
**Claude Gadelles**, Xytel Inc., Paris, France  
**Jnana Ranjan Kayal**, Institute of Seismological Research, Gandhinagar, India  
**Ilgizar N. Khakimzyanov**, Institute TatNIPIneft Tatneft PJSC, Bugulma, Russian Federation  
**Maxim G. Khramchenkov**, Kazan Federal University, Kazan, Russian Federation  
**Mikhail D. Khutorskoy**, Institute of Geology of the Russian Academy of Sciences, Moscow, Russian Federation  
**Alexander V. Lalomov**, Institute of Geology of Ore Deposits, Petrography, Mineralogy and Geochemistry of Russian Academy of Science, Moscow, Russian Federation  
**Danis K. Nurgaliev**, Kazan Federal University, Kazan, Russian Federation  
**Irina N. Plotnikova**, Tatarstan Academy of Sciences, Kazan, Russian Federation  
**Oleg M. Prischepa**, All-Russian Petroleum Research Exploration Institute, St.Petersburg, Russian Federation  
**Lyalya M. Sitdikova**, Kazan Federal University, Kazan, Russian Federation  
**Antonina V. Stoupakova**, Lomonosov Moscow State University, Moscow, Russian Federation  
**Vladimir A. Trofimov**, Central Geophysical Expedition JSC, Moscow, Russian Federation  
**Noel Vandenberghe**, K.U. Leuven University, Leuven, Belgium

**Editorial office:**

Deputy Chief Editor: Daria Khristoforova. Editor: Irina Abrosimova.  
 Prepress by Alexander Nikolaev. Translator: Alsu Mulile.  
 Web-editor: Artur Sabirov.

**Publisher:** Georesursy LLC**Editorial and Publisher's address:**

1-10, Mayakovsky st., Kazan, 420012, Russian Federation  
 Phone: +7 843 2390530, e-mail: mail@geors.ru

Georesursy (Georesources) is a peer-reviewed scientific and technical journal published since 1999

**The journal is included/indexed in:**

- **Directory of Open Access Journals (DOAJ);**
- **Web of Science Core Collection (ESCI);**
- **CAS (Chemical Abstracts Service) databases;**
- **GeoRef database;**
- **EBSCOhost™ databases;**
- **Ulrich's Periodicals Directory.**

The full-text e-versions of the articles are available on: **www.geors.ru**  
 All the materials of the journal Georesursy (Georesources) are available under the CC BY license (<https://creativecommons.org/licenses/by/4.0/>).

Registered by the Federal Service for Supervision of Communications and Mass Media No. PI FS77-38832

The Journal is issued 4 times a year. Circulation: 1000 copies  
 Issue date: 20.11.2018

© 2018 Scientific and Technical Journal Georesursy (Georesources)  
 Published by Georesursy LLC

**Table of Contents****Geology**

**Age moving of layers: facts and geological consequences (to the 150th anniversary of N.A. Golovkinsky's fundamental work) .....**278  
*S.O. Zorina, V.P. Alekseev, E.O. Amon, K.A. Khasanova*

**On the relationship of oil and gas formation and degassing processes with groundwater decomposition .....**290  
*A.A. Barenbaum*

**Geological and Geochemical Studies**

**Effect of biodegradation processes on the composition and structure of asphaltenes in West Siberian oils .....**301  
*L.S. Borisova, E.A. Fursenko*

**Analysis of the composition and properties of heavy oils in situ by low field NMR relaxation method .....**308  
*V.Ya. Volkov, B.V. Sakharov, N.M. Khasanova, D.K. Nurgaliev*

**Petroleum Geology. Reservoir Studies**

**Study of the lithological characteristics of Domanic deposits of the Pervomayskoe field .....**324  
*A.A. Takhauov, A.A. Titov*

**Types of reservoirs of the Ufa stage of the Republic of Tatarstan. Genesis and reservoir properties .....**331  
*R.F. Vafin, R.R. Khaziev, L.Z. Anisimova, K.Yu. Koluzaeva*

**Oil and Gas Field Development. Drilling and Operation of Wells**

**Simulation of composition changes in reservoirs with large hydrocarbon columns and temperature gradient .....**336  
*A.V. Yashin, I.M. Indruptsky, O.A. Lobanova*

**The safe operations modes substantiation for water source wellbores of the Vadelypskoye deposit .....**344  
*A.V. Seryakov, M.Yu. Podberezheny, O.B. Bocharov, M.A. Azamatov*

**Evaluation of mineral and organic inhibitor effects on bentonite clay .....**355  
*F.V. Degtarjov*

**Gas removal efficiency from a well .....**359  
*A.A. Isaev, R.Sh. Takhautdinov, V.I. Malykhin, A.A. Sharifullin*



Key title: «Georesursy». Parallel title: «Georesources»

**Editor in Chief: Renat Kh. Muslimov**  
Kazan Federal University, Kazan, Russian Federation**Editorial Board**

**Farit A. Agzamov**, Ufa State Petroleum Technical University, Ufa, Russian Federation  
**Lyubov K. Altunina**, Institute of Petroleum Chemistry of the Siberian Branch of the Russian Academy of Sciences, Tomsk, Russian Federation  
**Azary A. Barenbaum**, Institute of Oil and Gas Problems of the Russian Academy of Sciences, Moscow, Russian Federation  
**Eric Delamaide**, IFP Technologies (Canada) Inc., Calgary, Canada  
**Claude Gadelles**, Xytel Inc., Paris, France  
**Jnana Ranjan Kayal**, Institute of Seismological Research, Gandhinagar, India  
**Ilgizar N. Khakimzyanov**, Institute TatNIPIneft Tatneft PJSC, Bugulma, Russian Federation  
**Maxim G. Khranchenkov**, Kazan Federal University, Kazan, Russian Federation  
**Mikhail D. Khutorskoy**, Institute of Geology of the Russian Academy of Sciences, Moscow, Russian Federation  
**Alexander V. Lalomov**, Institute of Geology of Ore Deposits, Petrography, Mineralogy and Geochemistry of Russian Academy of Science, Moscow, Russian Federation  
**Danis K. Nurgaliev**, Kazan Federal University, Kazan, Russian Federation  
**Irina N. Plotnikova**, Tatarstan Academy of Sciences, Kazan, Russian Federation  
**Oleg M. Prischepa**, All-Russian Petroleum Research Exploration Institute, St.Petersburg, Russian Federation  
**Lyalya M. Sitdikova**, Kazan Federal University, Kazan, Russian Federation  
**Antonina V. Stoupakova**, Lomonosov Moscow State University, Moscow, Russian Federation  
**Vladimir A. Trofimov**, Central Geophysical Expedition JSC, Moscow, Russian Federation  
**Noel Vandenberghe**, K.U. Leuven University, Leuven, Belgium

**Editorial office:**

Deputy Chief Editor: Daria Khristoforova. Editor: Irina Abrosimova.  
 Prepress by Alexander Nikolaev. Translator: Alsu Mulile.  
 Web-editor: Artur Sabirov.

**Publisher:** Georesursy LLC**Editorial and Publisher's address:**

1-10, Mayakovskiy st., Kazan, 420012, Russian Federation  
 Phone: +7 843 2390530, e-mail: mail@geors.ru

Georesursy (Georesources) is a peer-reviewed scientific and technical journal published since 1999

**The journal is included/indexed in:**

- **Directory of Open Access Journals (DOAJ);**
- **Web of Science Core Collection (ESCI);**
- **CAS (Chemical Abstracts Service) databases;**
- **GeoRef database;**
- **EBSCOhost™ databases;**
- **Ulrich's Periodicals Directory.**

The full-text e-versions of the articles are available on: **www.geors.ru**  
 All the materials of the journal Georesursy (Georesources) are available under the CC BY license (<https://creativecommons.org/licenses/by/4.0/>).

Registered by the Federal Service for Supervision  
 of Communications and Mass Media No. PI FS77-38832

The Journal is issued 4 times a year. Circulation: 1000 copies  
 Issue date: 20.11.2018

© 2018 Scientific and Technical Journal Georesursy (Georesources)  
 Published by Georesursy LLC

**Table of Contents****Thermal Field of the Earth.  
Geothermal Studies**

**Heat flow from the Earth interior  
as indicator of deep processes** .....366  
*B.G. Polyak, M.D. Khutorskoy*

**Postcollisional evolution features of the  
intracontinental structures formed by  
overthrusting** .....377  
*O.I. Parphenuk*

**Mesozoic-Cenozoic climate and the geothermal regime  
of the oil source Kiterbyutskaya suite of the Arctic  
region of Western Siberia** .....386  
*V.I. Isaev, A.A. Iskorkina, G.A. Lobova,  
T.E. Luneva, E.N. Osipova, R.Sh. Ayupov,  
N.O. Igenbaeva, A.N. Fomin*

**The study of the relationship between thermal  
conductivity and porosity, permeability,  
humidity of sedimentary rocks  
of the West Siberian Plate** .....396  
*A.D. Duchkov, D.E. Ayunov, S.V. Rodyakin, P.A. Yan*

**Complex structural-tectonic zoning of the  
north-eastern part of the Barents Sea shelf** .....404  
*D.S. Nikitin, D.A. Ivanov*

**Geothermal monitoring as a way to predict  
volcanic eruptions and estimate  
geothermal energy resources** .....413  
*A.V. Muravyev*

## ORIGINAL RESEARCH ARTICLE

DOI: <https://doi.org/10.18599/grs.2018.4.278-289>

## Age moving of layers: facts and geological consequences (to the 150th anniversary of N.A. Golovkinsky's fundamental work)

S.O. Zorina<sup>1\*</sup>, V.P. Alekseev<sup>2</sup>, E.O. Amon<sup>3</sup>, K.A. Khasanova<sup>4</sup><sup>1</sup>Kazan (Volga Region) Federal University, Kazan, Russian Federation<sup>2</sup>Ural State Mining University, Ekaterinburg, Russian Federation<sup>3</sup>Borissiak Paleontological Institute of the Russian Academy of Sciences, Moscow, Russian Federation<sup>4</sup>Schlumberger, Tyumen, Russian Federation

**Abstract.** The fundamental facial law, determining the relationship between facies of sedimentary rocks in the sedimentary basin in lateral and vertical extensions, was formulated by the Russian geologist N.A. Golovkinsky a century and a half ago. Theoretical statements and views proposed by Golovkinsky have not lost their importance and relevance nowadays. In the article considered an important aspect of diachroneity (heterochroneity) of layer associations and their litho- and biostratigraphic boundaries. The methodological approach of measuring its degree (the window of age moving) is proposed. Golovkinskiy's conceptions are developing fruitfully within the framework of Seismostratigraphy and Sequence Stratigraphy, and their main content remains in demand in the light of new realities of cognitive process (nonlinear science, NBICS convergence, endovision).

**Keywords:** Golovkinsky's law, facies, sedimentation, diachronism, cognitive process

**Recommended citation:** Zorina S.O., Alekseev V.P., Amon E.O., Khasanova K.A. (2018). Age moving of layers: facts and geological consequences (to the 150th anniversary of N.A. Golovkinsky's fundamental work). *Georesursy = Georesources*, 20(4), Part 1, pp. 278-289. DOI: <https://doi.org/10.18599/grs.2018.4.278-289>

### The background

A century and a half ago, an event took place, the great importance of which the geological community of Russia understood and realized much later. On December 20, 1868, Nikolai Alekseevich Golovkinsky (1834-1897), Privatdocent and Head of the Geological Cabinet and the Department of Geognosy (Geology) and Paleontology of the Imperial Kazan University, defended and published his doctoral dissertation on the Permian formation in the central part of the Kama-Volga basin "(Golovkinsky, 1868). In this work, for the first time in Russian geology, the concept of "facies" was used for practical and theoretical purposes, which was previously introduced into geological science by Swiss geologist A. Gressly (Amanz Gressly, 1814-1865). In the late 1830s Gressly found that even age sediments have paleontological and lithological heterogeneity when tracing them laterally, and he suggested calling the different parts of the same age layers "facies" (Shatsky, 1986; Cross, Homewood, 1997). N.A. Golovkinsky, who applied one of the first among Russian geologists "facies theory and methodology", took the next, really

significant step. It consisted in establishing a "reverse" rule, which states that the boundaries of the lithologically and paleontologically similar layers, when traced along the lateral lines, regularly "slide" in time.

Assessing the age slip of biostratigraphic boundaries, he wrote: "... with each new study, new facts are discovered that reveal the incorrectness of the doctrine of the simultaneous existence and simultaneous disappearance of widespread faunas. The concept of a slow change in the organic population and facies gradually developed and now hardly any geologist..., will reject for different areas the different time of existence of similar forms and the simultaneity of different ones" (Golovkinsky, 1868, p. 152). . Thus, Golovkinsky substantiated the primary asynchrony of any biostratigraphic boundaries. At the same time, the age-related moving of the boundaries was associated not only with the facial differentiation of same-aged layers, but also with the paleobiogeographic features of the faunas.

N.A. Golovkinsky clearly realized that this was in contradiction and hard confrontation with the well-established "ordinary" views on the process of sedimentation. Having formulated the thesis: "the common belief in the sequence of formation of successive layers *is not true*" (Golovkinsky, 1868, p. 125; italics of the author), he also made a reservation that this term is "apparently paradoxical" (ibid.).

\*Corresponding author: Svetlana O. Zorina  
E-mail: [svzorina@yandex.ru](mailto:svzorina@yandex.ru)

© 2018 The Authors. Published by Georesursy LLC  
This is an open access article under the CC BY 4.0 license  
(<https://creativecommons.org/licenses/by/4.0/>)



Russian researchers, Golovkinsky's contemporaries, did not understand and did not accept this revolutionary idea. As a result, the fundamental facies law, which is directly derived from N.A. Golovkinsky's work, was formulated by A.A. Inostrantsev four years later for a different sedimentation mechanism (Inostrantsev, 1872). In the world literature, it is known under the name of J. Walther's law, after the name of German geologist (Johannes Walther, 1860-1937) "re-discovered" and outlined it in his capital report (Walther, 1893-1894). The analogy is with the scientific achievements of the outstanding Russian neurologist and psychiatrist V.M. Bekhterev, who occupied in the years 1885-1893 department of Psychiatry, Kazan University, and delivered at the solemn annual meeting in 1888, the act speech "Consciousness and its boundaries", in which he, long before the founder of psychoanalysis Z. Freud, introduced the concept of the unconscious. The most concise and comprehensive modern wording of fundamental facies law is as follows: "Facies varieties of sedimentary rock from any basin of sedimentation are changed along the stratigraphic vertical in the same order as horizontally" (Sharapov, 1989, p. 97).

In the post-war Soviet period, attention was drawn to the "forgotten" Golovkinsky's law, and it became known in the late 1940s thanks to the articles of G.I. Socratov, associate professor of the Leningrad Mining Institute (Socratov, 1949; Vassoevich, 1949).

To date, a large number of papers of various sizes and contents have been published, in which the history, the essence and significance of fundamental facies law are considered, and among which we especially note the researches of outstanding Russian sedimentologist S.I. Romanovsky (Romanovsky, 1979, 1985, etc.). Some of the publications, concerning the facies law are written by authors of the present article, for example (V.P. Alekseev, 2013; Alekseev, Amon, 2017; Zorina, 2018, etc.).

Avoiding repetition of the main conclusions set forth in the publications of S.I. Romanovsky and other researchers, we highlight here some relevant aspects and patterns that follow from the ideas of N.A. Golovkinsky. We are talking about the diachroneity (or, more generally, heterochroneity) of layered formations and litho- and biostratigraphic boundaries, and the methodological possibility of measuring its (diachroneity) degree, which can be conventionally and very approximately called as the "age-moving window". This is seen in terms of the "prism of time", encompassing both the past and the future.

### Age-moving boundaries

The issues of identifying and recognizing the facts of heterochroneity of the layers boundaries and the

asynchrony of correlated geological bodies and events, measured by any of the methods used in stratigraphic practice (morpholithic, bio-, climatic, magnetic, seismic, radiochronic, etc.), are one of the most "inconvenient" and "undesirable" for discussion in the Stratigraphy and Physical geology (Alekseev, Amon, 2008, 2017). The situation is quite similar with reluctant recognition of the significant role of stratigraphic gaps in the reconstruction of the history of sedimentogenesis in sedimentary basins (Baraboshkin et al., 2002; Amon, Alekseev, 2012; Alekseev, Amon, 2017). This is largely due to the dominance in the minds of specialists of linear paradigms, and, in particular, with the belief in the infallibility of the so-called "onion" model of the concentric-layered structure of the Earth of A.G. Werner (Abraham Gottlob Werner, 1749-1817), who captured the minds of geologists for centuries. As S.V. Meyen noted: "The same age of fragmented areas of one layer should have been taken ... as a matter of course" (Meyen, 1989, p. 140). V.N. Vereshchagin wrote about the formation: "The formation should be characterized by the unity of the time of accumulation, and, thus, the lower and upper boundaries of the formation (in its full extent) should be isochronous. Only a slight difference in the age of the basal layers of formations is allowed" (Vereshchagin, 1980). Such a linear sweep in the 2D metric in its most general form is a consequence of the Stenon principle (Niels Stensen, 1638-1686), according to which in a space filled with a rock, the gradient and time vector at any point are directed oppositely to gravity, and isochronous surfaces are horizontal planes (Gomankov, 2007).

It is noteworthy that in the editions of the USSR-Russia Stratigraphic Code (1977, 1992, 2006 editions) there was no place for gaps, diachronism and cyclicity, just as in the review setting out the achievements and main problems associated with improving the General Stratigraphic Scale (GSS) of Russia (Zhamoida, 2013). Only in supplements to the code, the Appendix 11 "Stratigraphic Gaps" (Supplements to the Stratigraphic Code ..., 2000, pp. 51-54) appeared, in general having the formal and impersonal character. The theme of the diachroneity of strata was practically not reflected in the thematic collection of articles with the promising title "Stratigraphy at the Beginning of the XXI Century – Trends and New Ideas" (2013). Only in the article of A.Yu. Gladenkov in this proceedings briefly labeled "The problem of the diachroneity of the boundaries of biostratigraphic zones", for the solution of which it was rightly suggested: "In specific situations, you must be guided by common sense ..." (Gladenkov, 2013, p. 46).

In translated into Russian the International Stratigraphic Guide, which in our literature was sometimes called the "Code" or "Handbook", the

theme of “diachroneity” was related very carefully – for example, it is present in the semi-recognition that biofacies “can be diachronic” (International Stratigraphic Guide..., 2002, p. 24), or in the statement that “the boundaries of subunits limited by unconformities are always diachronic, to a greater or lesser extent, and therefore never correspond to the boundaries of chronostratigraphic units” (ibid., p. 36).

Meanwhile, in modern stratigraphy, diachroneity (diachronism, diachrony) of layers is understood as a widespread phenomenon, equally inherent in the lithosphere and the paleobiosphere (Alekseev, Amon, 2008, 2017; Amon, Alekseev, 2012, etc.). This state is confirmed by numerous examples described in the new paleontological and stratigraphic literature. Famous stratigrapher F.M. Gradstein in the chapter “Biochronology” of the fundamental work “The Geologic Time Scale 2012” specially noted that “significant diachrony is observed for bioevents, e.g., by plotting them against magnetochrons or isotope spikes in two or more sections” (Gradstein et al., 2012, p. 44). V.S. Tsyganko (2007) supposed that the diachronism of boundaries can be considered as a universal property of formations, series, and other stratigraphic units, and proposed to single out a special type of moving boundaries – parastratigraphic boundaries. S.O. Zorina gave examples of typical diachrony of litho- and biostratigraphic units of the Middle Jurassic, Lower Cretaceous and Paleocene in the Volga region (Zorina, 2006).

According to A.Yu. Guzhikov, asynchrony of paleontologically justified boundaries, which were considered as same-aged, were repeatedly observed in distant sections using independent methods, while the time shift could reach 10 million years (Guzhikov, 2013, 2016; Guzhikov, Baraboshkin, 2006). A.S. Alekseev noted that because of the “obvious diachrony of the borders chosen on a palaeontological basis, the priority was given to physical markers – paleomagnetic, chemostratigraphic, and other events, which are considered to be isochronous” (Alekseev A.S., 2013, p. 10). A direct recommendation on improving the subregional stratigraphic scheme is proposed – that it is necessary to monitor the diachronism of the boundaries of the mapped units and the duration of stratigraphic gaps (Pervushov et al., 2013). The correct consideration was expressed that the bathymetric differentiation forms the litho- and biofacial heterogeneity of sediments, their spatial migration with changes in sea level, and creates a diachronic units a priori, in full accordance with the “moving” of their boundaries according to N.A. Golovkinsky (Sukhov et al., 2013).

The North American Stratigraphic Code not only introduces, explains, and codifies the concepts of

“Diachroneity”, “ Diachronous Categories”, but also regulates the basic operations with diachronic units (North American Stratigraphic Code ..., 2005, Articles 64, 91-94).

Currently, the fundamental facies law and the conclusions of N.A. Golovkinsky concerning the moving boundaries of the layer associations acquired a special meaning and significance due to the introduction and widespread use of the International Geological Time Scale (GTS2012) in everyday geological practice (Gradstein et al., 2012; Ogg et al., 2016). When designing GTS2012, the new and newest, sometimes debated, theoretical achievements in stratigraphy were used; in particular, an event-based approach (event stratigraphy, biological, fossil, climatic, magnetic, geochemical and other events) is widely used, and the term “stage” is given an unambiguous chronostratigraphic meaning. The lower boundaries of the Phanerozoic stages, Proterozoic systems, and the Archean erathems are characterized by specific dates of astronomical (absolute) age (a – Ka – Ma – Ga). Most of the Phanerozoic stage boundaries are labeled with the GSSP-standard points (GSSP – Global boundary Stratotype Section and Point).

There is a strict accounting registry of GSSP, their stratigraphic and geographical coordinates; they received the very popular metaphorical name of “golden spikes” (Alekseev, Amon, 2017; Gradstein et al., 2012; Zorina, 2015). The dual essence of the standard manifests itself: on the one hand, this is a rock sequence, and on the other, a point in it, and it is believed that “golden spikes” are traced in sedimentary basins by means of a principal correlative event (Gradstein et al., 2012).

Many stratigraphers understand and accept the nature and principles of the GTS2012 scale too literally and straightforwardly, quite in the spirit of the traditional “onion-like model” linear paradigm. But such a perception of it contradicts the Golovkinsky’s law, which contains a warning that the boundaries of litho- and biostratigraphic units undergo an age-related moving to a greater or lesser degree. For example, taking into account that the rates of spatial distribution of fossil organisms were not instantaneous, we have to admit that the more farther from the GSSP the point of the first appearance of any index-species (FAD – first appearance datum) is found, the more this FAD point will be declined from the virtual isochron level (Zorina, 2006, 2015).

It is well known and does not require additional substantiation that different faunistic groups in different geological epochs inhabited marine and continental sedimentary basins and disappeared from them at different speeds, therefore the boundaries, based on



traced biological events are diachronic in varying degrees. At the same time, the sequences of biozones that form the basis for most local and provincial zonal scales can be correctly used for age correlation only within a limited area (sedimentary basin or part of it), but not for global correlations. This means that tracing the stage boundaries on a global scale based on the biostratigraphic approach is difficult, since the relatively slow change of one bio-event to another is mainly used (Zorina, 2006, 2015).

This difficulty can be overcome by applying the method of searching and identification in sections the traces of high-speed events or phenomena (Zorina, 2006). Comparing, for example, sequences of magnetic inversions with sequences of much slower events, such as biological events, it is possible not only to show the “slowness” of biological events, but also to determine the “age moving window” of the boundaries of individual biozones and formations.

While providing the comparison, the event of the “greatest stratigraphic weight” (Meyen, 1981, 1989) should be selected, in other words, the fastest events should be chosen (Zorina, 2006, 2015).

Such a comparison was made for magnetostratigraphic and ammonite scales of the sections of the Aptian deposits (Lower Cretaceous) of the eastern Russian Platform and the Western Mediterranean (Guzhikov, Baraboshkin, 2006). The key to answering the question of which of the ammonite zones identified in both areas is the most diachronic and to what is the extent of the diachroneity was the identification of the magnetic chron M0. It turned out that, in accordance with the different position of this chron in the ammonite scales of the regions under consideration, the diachroneity of the ammonite deshaysi zone in the east of the Russian Platform reaches ~ 6 million years.

A significant age-related moving of the lower boundary of the Lower Cretaceous Albian Khanty-Mansiysk Formation was revealed by foraminifera in the West Siberian sedimentary megabasin. Here, the inner sea was ingressed during the Albian with low speeds, and the “moving window” between observation points in the stratotype locality in the Khanty-Mansiysk area and the Southern Urals area is ~ 8 million years (Amon, 2005).

The noticeable diachroneity of the lower boundaries of several formations was recognized in the Paleogene

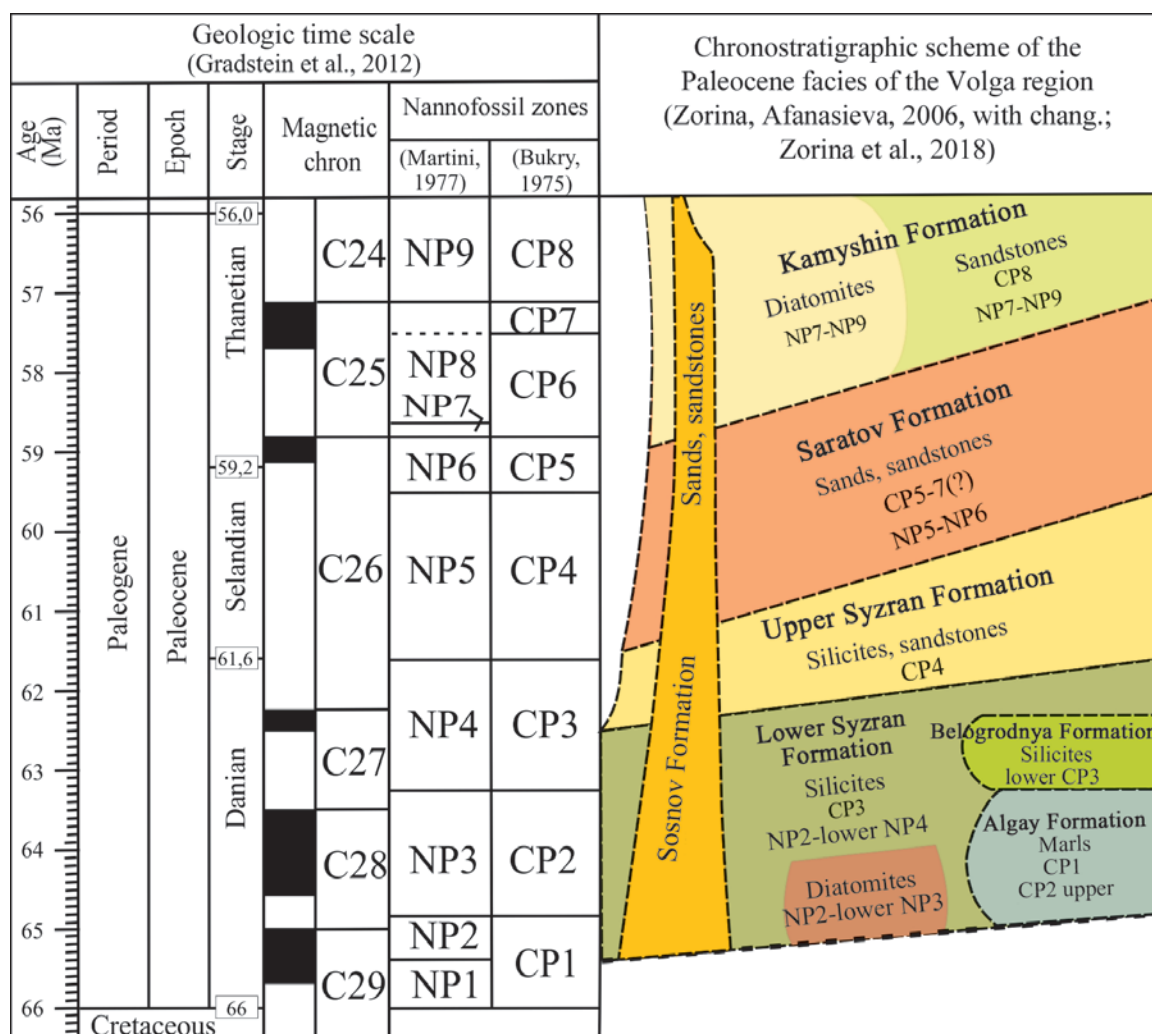


Fig. 1. The diachroneity of the Paleogene strata of the Volga region (Zorina, Afanasieva, 2006, with additions and changes)

sandy-clay-siliceous stratum of the Volga region (Zorina, 2006; Zorina, Afanasieva, 2006; Zorina et al., 2018) (Fig. 1).

Comparison of high-speed bio-events (nannofossil zones) with more short-term litho-events (the formation of lower boundaries of lithostratigraphic units) allowed to state that the end of the accumulation of the base of the Upper Syzran Formation and the beginning of the accumulation of the base of the Saratov Formation coincide with the beginning of the NP5 nannofossil zone from the Martini scale (Martini, 1977) or CP4 zone from the Bukry scale (Bukry, 1975). In other words, the virtual isochronous line drawn on the base of the NP5 zone crosses the entire Upper Syzran Formation from the base to its superface. The “moving window” of the lower and upper boundaries of the Upper Syzran Formation, measured according to the dates in GTS2012 (Gradstein et al., 2012), is 2.1 million years (Fig. 1).

It was also proposed to fix the diachroneity and moving of some levels by metric position of points in sections, measured in meters from the important marker: for example, the level of disappearance of *Samlandia mayii dinocyst* in the Gremyachinsky section in the south-west of the Volgograd area of Lower Volga region, which marks the lower boundary of the Maastrichtian at the base of foraminifera zone LC19, is diachronic relatively ammonite zonation. In the Tercis (Tercis les Bains) section in the south-west of France, which is the GSSP for the lower Maastrichtian, *S. mayii* disappears in 6 meters above the foot of Maastrichtian, and in the Danish basin in 12 meters above this boundary (Benyamovskiy et al., 2013).

We emphasize once again that Golovkinsky's statement about the asynchrony of the litho- and biostratigraphic boundaries allows to apply a methodical technique that reveals and describes the diachroneity of the boundaries and calculates the “moving window”. Additionally, we note that the physical nature of high-speed events, as well as isochronous levels, is different, and we can discuss the limits of their resolution and what is more accurate. These may be, for example, equally applicable:

(a) units of geomagnetic polarity scales due to the short duration ( $<10^4$  years) of geomagnetic inversions (Guzhikov, 2016);

(b) isotope chronometry (Zorina, 2015);

(c) nannofossil zones, for example nannofossil zones in the Paleogene of the Volga region (Zorina, 2006; Zorina, Afanasieva, 2006; Zorina et al., 2018), or marine diatom zones in the Cenozoic of the Pacific region (Gladenkov, 2013);

(d) biological events on dinocysts, as in the Maastrichtian of the Lower Volga region (Benyamovskiy et al., 2013); (e) tempestites, talidites, and black shale episodes in a wide range of regions, systems, and stages

(Zorina, 2006, 2013; Dronov, 2013, etc.).

A recommendation was made when discussing the problem of the boundaries of bio-horizons that: “despite the potential diachroneity, [the boundaries of the bio-horizons] should be regarded as presumptively isochronous” (Gulyaev, Rogov, 2016, p. 57). We believe that the “presumption of isochronism” of the boundaries is valid until the moment when their diachroneity is proven and shown by any of the stratigraphic methods, including those mentioned above.

### Seismic and Cyclic Stratigraphy

The statement of the age-moving of the boundaries of the layers and groups of layer implies the practical need to take into account the diachroneity in two aspects:

(a) identifying and fixing the most high-speed event with the minimal “moving window” and tracing it in the largest number of sections;

(b) the selection of the moment of “fracture” in the change of sedimentation regimes with tracking it laterally.

The first aspect fruitfully develops within the framework of seismic stratigraphy and is based on the isolation and tracing of the unconformities. Undoubtedly, they are very fast, and, in geological terms, almost “instantaneous” events, if we consider one or another sequence of “top down”, that is, from younger sediments to more ancient. It should not be overlooked, as is often done, that the surface of the slice (unconformity) is always diachronic, and the “depth” of the gap can be from minimum to as many as you like.

The second aspect is reflected in the Golovkinsky's schemes, who in his work actually stopped “half a step” from establishing the principle of cyclicity in lithology. Moreover, according to S.I. Romanovsky, the “geological lentil” of N.A. Golovkinsky is the model of migration type cycle (Romanovsky, 1985). The figurative name “lentil” was used by N.A. Golovkinsky to characterize the sequence of layers that have a distinctly flattened shape along the periphery and are similar to the “lentil covering the core” (Golovkinsky, 1868, p. 119). Note that the missing “half-step” was made by Yu.A. Zhemchuzhnikov in the report at the Geological Coal Meeting held in April 1944. He expressed a capacious slogan: “A geologist should think of in cycles” (Zhemchuzhnikov, 1947). At the same time, an extremely important position was formulated, which, unfortunately, is not often taken into account when studying sedimentary strata: “Cyclicity without thorough facies analysis is only a formal, mechanical method. Analysis of facies without cyclicity – like embroidery without canvas – is devoid of a guide rod. Only a combination of these two principles makes the efforts fruitful and leads to the development of each”



(Zhemchuzhnikov, 1947, p.16).

These two aspects illustrate two fundamentally different approaches to identifying sedimentary sequences. The first approach, adopted and developed in seismic stratigraphy, is based, as has been said, on identifying and tracing unconformities in monotonous sequences (Seismic stratigraphy ..., 1982; Supplements to the Stratigraphic code of Russia..., 2000), between the sequences of several orders. The smallest of them – parasequences – have a thickness of several to the first tens of meters and are usually identified from the geophysical well survey data. The two leading types have an asymmetrical structure and are depicted in the form of isosceles triangles, directed by the tip of the vertex in the direction of decreasing the size of particles (in terrigenous strata). They are interpreted as retrogradation (reduction of the size of particles up the section) and progradation (increase in such), corresponding to hemicycles (half cycles) or several cycles (Botvinkina, Alekseev, 1991).

Competent synthesis of seismic, geological, and lithological data can give a lot for theoretical and practical stratigraphy. For example, careful analysis and correlation of data obtained from seismic profiling by reflected waves and deepwater drilling in the Northwest Plate of the Pacific Ocean allowed a deeper understanding of the structure and features of the formation of the sedimentary cover of this region. A warning was issued to “classical” stratigraphers, who, adhering to outdated schemes, often perceived the history of marginal zones of the oceans in the past too straightforwardly; in particular, they did not take into account the lateral diachroneity and rejuvenation of the deposits, accretionary prisms were considered as evidence of the subduction of oceanic sediments, relatively shallow deposits of many areas of the oceans were regarded as deepwater, etc. (Patrikeev, 2013).

The second approach corresponds to the drawing of “lenticles” of N.A. Golovkinsky, in which, speaking figuratively, “proelements of the geometry of sequences” are laid (Nurgalieva, 2016). This approach is focused on the identifying of a turning point (from transgression to regression) fixed by the maximum flooding surface (mfs). In recent decades, it has been intensively used in foreign studies in the framework of genetic stratigraphy, focusing on the identifying boundaries with the highest possible isochronism (Biju-Duval, 2012; Posamentier, Allen, 2014).

Figure 2 shows the correlation of the Lower Cretaceous (Middle Aptian) sediments of the Vikulovskaya Formation at the Kamenny field of the Krasnoleninsk oil and gas bearing area in Western Siberia (Composition, structure and conditions of formation ..., 2011). The near to “plane-parallel”

structure of the sequence, established by tracing the intervals of relatively fine-grained rocks (green color), is distinctly revealed. The thickness of sandy reservoirs VK<sub>1-4</sub> (beige color) is characterized by variations in thickness in the range of 5-15%, which can be caused both by changes in facies composition and differences in post-sedimentary compaction. The information on the structure of the reservoir VK<sub>2</sub> is of the most interest. At relatively small distances (between wells about 2 km), the prograde cyclite in well 160 changes to retrograde ones in well 162, undergoing a distinct inversion of its structure in well column 161, which indicates a greater legitimacy for identifying cycles when the transgressive phase of the development of facies changes to regressive.

We note in passing that much earlier than for genetic stratigraphy, this was introduced into the facial-cyclical analysis developed by Yu.A. Zhemchuzhnikov, L.N. Botvinkina, and others in the 1950s for terrigenous deposits of the Donetsk coal basin. The basic provisions are described in a number of publications (Botvinkina, Alekseev, 1991; Alekseev, Amon, 2017), which shows the importance of the cyclostratigraphic method for studying a wide variety of sediments, including coal-free strata and oil and gas basins.

### Prospects for further research

S.I. Romanovsky, analyzing the creative heritage of N.A. Golovkinsky, noted the subtle and precise aspect that is important for any geological work containing elements of scientific and methodological novelty: “The results of scientific research, no matter how significant they are, inevitably recede before new achievements of regional geology. ... Therefore, it is the creators of theoretical ideas that are forever included in the history of science, but the abundant works on regional geology created by almost every geologist, completely lose their significance over time” (Romanovsky, 1979, p. 6). Indeed, for the knowledge of the Permian deposits of the Kama-Volga basin, the N.A. Golovkinsky’s studies now represent only archival and historical interest. Fundamentally different is the case with the theoretical constructions carried out in his work. Important issues raised a century and a half ago have not lost its relevance, and continue to retain its methodological value, as evidenced by many developments of the 21st century (Berto, 2002; Zorina, 2006, 2015; Krinari, 2010; Lebedev, 2015 and others). Similar issues will excite the minds of researchers in the future, but without being able to predict all possible directions, we’ll dwell on two possible vectors for the development of ideas associated with the name of N.A. Golovkinsky.

The first vector refers to the phenomenon of

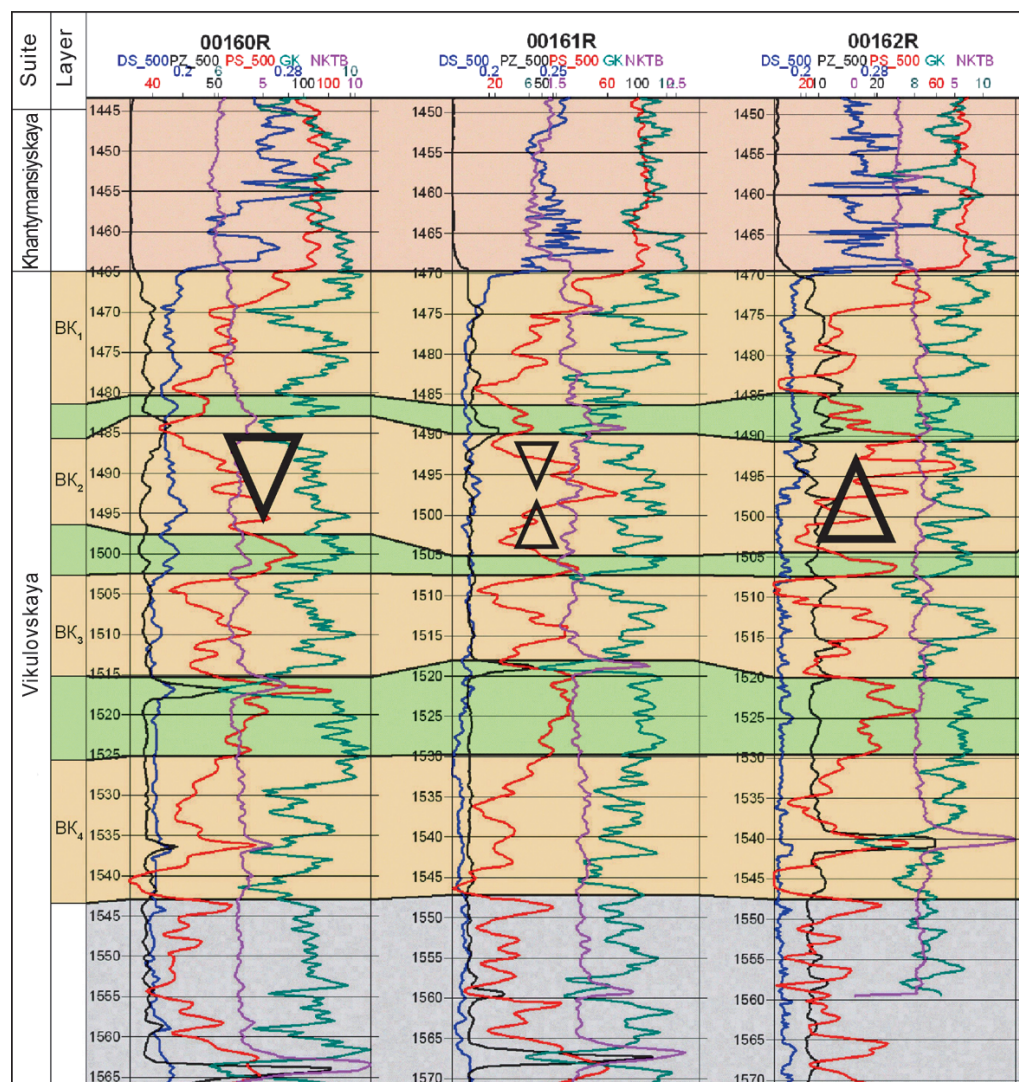


Fig. 2. Well log correlation in the Kamenny field of the Krasnoleninsk oil and gas region, Western Siberia (Composition, structure and conditions of formation ..., 2011). For the reservoir  $VK_2$ , the triangular symbols show the direction of the change in the particle size distribution (the top of the triangle indicates a decrease in the particle size)

the jaggedness of the layer boundaries, which was characterized as follows: "... coastal sediments constantly change the area of their distribution, then pulling into the open sea, then retreating to the coast. This causes uneven serration of the layer; these "teeth" are extremely sharp and elongated, are in the form of thin layers, alternating with the rock of the adjacent layer ..." (Golovkinsky, 1868, p. 126). It also indicates that this jaggedness is due to the rapid displacement of environments during sedimentation in conditions of a small slope of the seabed surface, not exceeding a few angular minutes.

In the development of these ideas, a scheme has been proposed (Alekseev V.P., 2013), reflecting the general structure of the interrelationships of the main parameters controlling the morphostructure of layered units (Fig. 3).

Herewith, issues related to the manifestations of gaps and diachroneity of the layer units are an

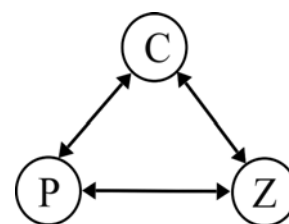


Fig. 3. Interrelations of the main parameters controlling the morphostructure of layered units (Alekseev V.P., 2013). C – moving of layers, interlayers, reservoirs; P – stratigraphic gaps of various durations; Z – lateral jagged borders

object of independent study with their own history and achievements, however, the phenomenon of the jaggedness of the layer boundaries has not been studied much so far. The latter is especially applicable to deep-seated strata, where direct tracing of "thin interlayers" is impossible, due to insufficient resolution of remote sensing methods (seismic profiling), or with large distances between wells.



At the same time, the situation is changing literally “before our eyes” due to the intensive introduction of horizontal drilling into practice. The resulting materials bring invaluable material specifically for lateral tracking of changes or “intermittency” in the composition of “thin layers”. In turn, this inevitably leads to a rational assessment of the orientation of production wells, which gives a significant technological effect.

The second vector is associated with the change of the general scientific paradigm that occurred with the advent of the new Millennium. The transition to non-linear views embraces in all spheres of natural science and humanities, and is particularly evident in the wide development of interdisciplinary and transdisciplinary researches. One of the ways to consider them is the NBICS-convergence – the modern direction of basic science, which assesses the most diverse areas of knowledge at the nanoscale level. Earth sciences are still “on the sidelines” of these studies, but the use of such basic concepts typical of non-linear science as the fundamental facies law allows us to hope for a “breakthrough” in their inclusion in the general trend (Alekseev, Amon, 2017). Some idea of the great opportunities opening up to lithology is provided by the information in Table 1.

In particular, a wide spectrum of manifestation of the main facies law – from the displacement of thin layers in a fraction of millimeters to the moving of the Neocomian clinoforms of West Siberia – can impose a “bridge” from identifying, considering, and accounting for “nano-, micro” objects in geology, physics, biology,

programming etc. to understand the patterns of existence and functioning of the complex “mega-, macro” structures. This is rightly said by K. Mainzer: using an approach based on the theory of complex systems is “... an interdisciplinary methodology to explain the occurrence of certain macroscopic phenomena as a result of nonlinear interactions of microscopic elements in complex systems” (Mainzer, 2009, p. 39).

In addition, modern “revolutionary paradigm changes”, according to E. Morin, imply the rejection of widespread linear mechanistic determinism and recommend the adoption and use of a complex metaconcept, or endo-exo-causality, which corresponds to endo-exo-organization (Morin, 2005, p. 315). Here, “ordinary”, external or exogenous causality should go into comprehension of the unconventional, internal or endogenous essence of the process (Fig. 4).

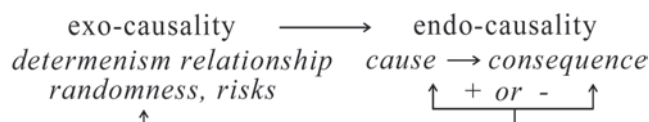


Fig. 4. Complex metaconcept diagram (according to (Morin, 2005))

The study of complex causality, which makes it possible to know and predict the characteristics of the existence and functioning of natural objects – in lithology from the finest layers to sedimentary megabasins – unfolds in an infinite combinatorial dialectic. And, thanks to the ongoing process of improving research

Discipline	System (example)	Elements in the system NBICS	Dynamics	Rank parameter
Quantum physics	Laser	Atoms	Quantum	Formation of quantum structure (for example, optic waves)
Biology	Genetic	Genes	Genetic reaction	Formation of genetic structure
Computer science	Neural networks	Byte	Computational rules, algorithms	Formation of computational network structure
Psychology, medicine	Brain	Neuron	Information dynamics	Pattern recognition
Sociology	Community	Certain individuum, meme	Social interaction	Formation of social structure
Geology: by K. Mainzer	Lava	Molecule	Geological dynamics	Formation of structures (for example, segmentation)
Our understandings	Sedimentary basin	Particle, grain	Accumulation of layers	Main facial law

Table 1. Interdisciplinary applications of the theory of nonlinear complex systems (Mainzer, 2009, p. 40-41; with changes and additions)

tools (horizontal and inclined drilling, isotopy and fine geochemical analytics, remote sensing instruments and methods, computer complexes, neural networks, “big data” technologies, etc.), such combinatorics will always be mobile and internally heterogeneous.

E. Morin names 6 possible combinations of reactions of systems generated by complex causality, when the causes interact and intersect, overlapping each other randomly (Morin, 2005, pp. 315-316):

a) the same causes may lead to different and/or divergent effects;

b) different reasons can cause the same consequences;

c) small causes can lead to very large consequences;

d) great causes may lead to very minor consequences;

e) some reasons are followed by opposite effects, when the reason starts a counter-action directed in the opposite direction: heating → cooling, revolution → counter-revolution, etc.;

f) the consequences of the opposing causes are uncertain, i.e. it is not known whether the reverse actions that will prevail will be negative or positive.

Thus, a whole fan of forms of complex causality is born, and paradoxes of causality constantly arise, which cannot be resolved within the framework of the simplistic approach of mechanistic determination (Morin, 2005, p. 16). One of these paradoxes – the diachroneity of the boundaries of the layer associations, which cannot be solved in the mechanics of the Stenon-Werner models – was brilliantly overcome by N.A. Golovkinsky a century and a half ago, using, perhaps intuitively, the methodology we now call “complex causality.” But there are not a little similar or analogous paradoxes in geology (from the confrontation of the ideas of «fixism» and «mobilism» to the proof of the existence of clinoforms in continental strata or identifying features of paleolandscapes of wetlands, marches and watts in Aptian Vikulovskaya deposits of West Siberia, etc.) and in the future. Note that the paradoxes of causality and their successful resolution stimulate the development of theoretical geological thought, for example, thanks to them, noncontradictory tectonics of lithospheric plates, event biostratigraphy, sequence stratigraphy, cyclostratigraphy, etc., were developed.

Complex causality is non-linear, it is correlative and cyclical, and, in general, constituting one of the foundations of the cognition program of the “method of nature of nature” (La Méthode. La Nature de la Nature) by E. Morin. It partially corresponds to endophysics or “physics from the inside” by O. Rössler (1998) and introduced into the basic principles of endolithology (Alekseev, Amon, 2017). The main facies law in endolithology is given a worthy place, with a statement of both great practical value and significant predictive capabilities.

## Conclusion

In the modern-day turbulent process of knowing nature and the world, it is useful to stop, look back and make a comparison of a range of long-held ideas with today’s realities, and sometimes this comparison shows that some of the former have not lost their relevance. Exactly one and a half centuries ago, in 1868, an event took place that was insufficiently appreciated by contemporaries, but determined one of the main routes in the development of the theory of sedimentary strata. This significant phenomenon was the defense and publication of a doctoral thesis by the privat-docent of the Imperial Kazan University N.A. Golovkinsky, in which a regular “moving” in time of the borders of the visually homogeneous (both lithologically and paleontologically) layers of sedimentary rocks is established. The unusual and revolutionary nature of this geological idea led to the fact that the facies law (namely: the same order of change of facies types of rocks horizontally and vertically) was “rediscovered” only a quarter of a century later by I. Walther, and in the USSR it became widely known only from the middle of the XX century.

The fundamental facies law or the Golovkinsky-Walther law remains in demand and highly significant in modern geological studies. In accordance with it, the diachronism (heterochronism) is characteristic of many geological events and processes. Specificity is manifested only in the accuracy of methods, tools and methods of research that are capable, or not able, to fix the speed of occurrence of events, the so-called “window of moving”. Duration minima taken as “isochrones” are characteristic of episodes of paleomagnethochronometry, isotope chronometry, some short-term bioactivity, as well as the boundaries of complexes of genetically interrelated rocks (cycles, cyclites). In the framework of facies-cyclical analysis, the latter are distinguished by changing the transgressive branch of changing environments of sedimentation to a regressive one, and for genetic stratigraphy – along the surface of maximum flooding. However, the “presumption of isochronism” of the boundaries is valid exactly until the moment when their diachrony is proved and shown by any of the stratigraphic methods.

The relevance of the basic facies law can be extended for future research. On the one hand, this is due to the lack of knowledge of such a common phenomenon as “jaggedness” of layer boundaries, which is especially pronounced when tracing boundaries laterally along the coastline of the receiving reservoir. Here, unlimited prospects are revealed by 3D modeling, which is actively developing in the study of oil and gas objects. On the other hand, the surprising compatibility of the provisions contained in Golovkinsky’s work with



modern philosophical and methodological views and designs of the 21st century is revealed. So, they easily fit into the concept of NBICS convergence, illustrating the importance of interdisciplinary and transdisciplinary researches; in ideas about endo-exo-causality of events within the framework of a wide manifestation of self-organization, etc. This opens up new horizons in theoretical understanding of the processes of sedimentation, as well as prognostics.

Understanding the mechanisms of complex causality in facies-cyclical analysis allows to clarify and streamline the correlation of complex deposits, which is an intransigently important task in the search and exploration of petroliferous strata. These methodological approaches become even more relevant in the development of hard-to-recover resources (reserves) of hydrocarbons.

In general, the fundamental facies law of N.A. Golovkinsky is a striking visionary phenomenon which is inherent in rare (if not the rarest) fundamental geological discoveries.

## Acknowledgments

*The authors are grateful to M.V. Lebedev, who undertook the work of reviewing the manuscript and for making valuable comments which have been very helpful in improving the manuscript.*

*This work was supported by the Program of the Presidium of the Russian Academy of Sciences "The Evolution of the Organic World and Planetary Processes". The studies were carried out according to the Russian Government Program of Competitive Growth of Kazan Federal University, as well as using the funds of the subsidy allocated to Kazan Federal University for the state assignment No. 5.2192.2017/4.6 in the sphere of scientific activities. The work was also supported by the Ministry of Science and High Education of the Russian Federation contract No. 14.Y26.31.0029 in the framework of the Resolution No.220 of the Government of the Russian Federation.*

## References

- Alekseev A.S. (2013). Current state of International Stratigraphic Chart: positive and negative consequences for the general stratigraphic scale of Russia. *General Stratigraphic Scale of Russia: current state and ways of perfection*. Moscow: GIN RAS Publ., pp. 9-13. (In Russ.)
- Alekseev V.P. (2013). Nonlinear-lithological essays. Ekaterinburg: URSMU Publ., 250 p. (In Russ.)
- Alekseev V.P., Amon E.O. (2008). Diachrony of biostratigraphic boundaries as realization of nonlinear process (migration type of stratosedimentogenesis). *Bio- and lithostratigraphic boundaries in the history of Earth*. Tyumen: TyumSOGU, pp. 33-38. (In Russ.)
- Alekseev V.P., Amon E.O. (2017). Sedimentological fundamentals of endolithology. Ekaterinburg: URSMU Publ., 476 p. (In Russ.)
- Amon E.O. (2005). Associations of agglutinated foraminifers from the Khanty-Mansiysk Suite (Albian, Lower Cretaceous) in the Middle and Southern Trans-Urals. *Litosfera = Lithosphere*, 2, pp. 97-134. (In Russ.)
- Amon E.O., Alekseev V.P. (2012). On some "painful" points of modern stratigraphy. *Lithology and Geology of fossil fuels*, vol. VI (22). Ekaterinburg: URSMU, pp. 64-77. (In Russ.)
- Baraboshkin E.Yu., Veimarn A.B., Kopaevich L.F., Naidin D.P. (2002). The study of stratigraphic breaks in the geological survey: guidelines. Moscow: MSU, 163 p.
- Benyamovskiy V.N., Baraboshkin E.Yu., Guzhikov A.Yu. et al. (2013). On the Maastrichtian lower boundary in the International Stratigraphic Scale and its position in the General Stratigraphic Scale of Russia. *General Stratigraphic Scale of Russia: current state and ways of perfection*. Moscow: GIN RAS Publ., pp. 298-303. (In Russ.)
- Berthault G. (2002). Analysis of the basic principles of stratigraphy based on experimental data. *Litologiya i poleznye iskopaemye = Lithology and Mineral Resources*, 5, pp. 509-515. (In Russ.)
- Biju-Duval B. (2012). Sedimentary Geology: Eng. transl. Moscow-Izhevsk: IKI Publ., 704 p. (In Russ.)
- Botvinkina L.N., Alekseev V.P. (1991). Cyclicity of sedimentary strata and methods of its study. Sverdlovsk: URSMU Publ., 336 p. (In Russ.)
- Bukry D. (1975). Coccolith and silicoflagellate stratigraphy, northwestern Pacific Ocean. *Initial Reports of Deep Sea Drilling Project*, 32, pp. 677-701. <https://doi.org/10.2973/dsdp.proc.32.124.1975>
- Catuneanu O. (2002). Sequence stratigraphy of clastic systems: Concepts, merits and pitfalls. *J. of African Earth Sciences*, 35(1), pp. 1-43. [https://doi.org/10.1016/S0899-5362\(02\)00004-0](https://doi.org/10.1016/S0899-5362(02)00004-0)
- Composition, structure and conditions of formation of reservoirs of VK group in the Eastern part of Krasnoleninsky oil field (Western Siberia). (2011). Ekaterinburg: URSMU, 325 p. (In Russ.)
- Cross T.A., Homewood P.W. (1997). Amant Gressly's role in founding modern stratigraphy. *Geological Society of America Bulletin*. 109 (12), pp. 1617-1630. [https://doi.org/10.1130/0016-7606\(1997\)109<1617:AGSRIF>2.3.CO;2](https://doi.org/10.1130/0016-7606(1997)109<1617:AGSRIF>2.3.CO;2)
- Dronov A.V. (2013). Depositional sequences and sea level fluctuations in the Ordovician of Baltoscandia. *Stratigraphy of the early XXI century – tendencies and new ideas*. Moscow: Geokart, GEOS Publ., pp. 65-92.
- Gladenkov A.Yu. (2013). Problems and debatable points of the Cenozoic biostratigraphy and paleobiogeography in interpretation of data based on marine diatoms. *Stratigraphy of the early XXI century – tendencies and new ideas*. Moscow: Geokart, GEOS Publ., pp. 40-64. (In Russ.)
- Golovkinsky N.A. (1868). On Permian formation in central part of Kama-Volga basin. Saint-Petersburg, 143 p. (In Russ.)
- Gomankov A.V. (2007). Geological time and its measurement. Moscow: KMK Publ., 58 p. (In Russ.)
- Gradstein F.M., Ogg J.G., Schmitz M., Ogg G. (Eds.). (2012). The Geologic Time Scale 2012. Vols. 1-2. Oxford-Amsterdam-Waltham: Elsevier, 1176 p.
- Gulyaev D.B., Rogov M. A. (2016). The introduction of the concept of "biohorizont" into the system of official native stratigraphy. *General stratigraphic scale and methodological problems of development of regional stratigraphic scale of Russia*. Saint-Petersburg: VSEGEI Publ., pp. 56-58. (In Russ.)
- Guzhikov A.Yu. (2013). The role of paleomagnetic criteria in justification of unit boundaries in General Stratigraphic Scale of Russia. *General Stratigraphic Scale of Russia: current state and ways of perfection*. Moscow: GIN RAS, pp. 25-28. (In Russ.)
- Guzhikov A.Yu. (2016). The main tasks of actualization of the General magnetostratigraphic scale. *General stratigraphic scale and methodical problems of development of regional stratigraphic scales of Russia*. Saint-Petersburg: VSEGEI, pp. 53-55. (In Russ.)

- Guzhikov A.Yu., Baraboshkin, E.Yu. (2006). Assessment of diachrony of biostratigraphic boundaries via magnetochronological calibration of zonal scales of the lower Cretaceous of Tethian and Boreal belts. *Doklady Akademii Nauk = Proceedings of the Russian Academy of Sciences*, 409(3), pp. 365-368. (In Russ.)
- Inostrantsev A.A. (1872). Geological researches in the North of Russia in 1869 and 1870. Saint-Petersburg, 179 p. (In Russ.)
- International Stratigraphic Guide: An abridged version. (2002). Moscow: GEOS, 38 p. (In Russ.)
- Krinari G.A. (2010). Lithogenesis and Mineralogy of oil-bearing sedimentary rocks. Part 1, the stages of hypergenesis of diagenesis. Kazan: KFU, 64 p. (In Russ.)
- Lebedev M.V. (2015). Clarification of formulation of the law of Golovkinsky-Walther. *Otechestvennaya geologiya = Russian Geology*, 3, pp. 62-69. (In Russ.)
- Mainzer K. (2009). Thinking in Complexity. The Computational Dynamics of Matter, Mind, and Mankind. A new synthesis. Eng. transl. Moscow: LIBROKOM, 464 p. (In Russ.)
- Martini E. (1977). Neue Daten zum Paläozän und Unter-Eozän im südlichen Nordseebecken – Das Nordwestdeutsche Tertiärbecken. *Beitr. Newslett. Stratigr.*, 6(2), pp. 97-105. <https://doi.org/10.1127/nos/6/1977/97>
- Meyen S.V. (1981). From general to theoretical stratigraphy. *Sovetskaya geologiya = Soviet Geology*, 9, pp. 58-69. (In Russ.)
- Meyen S.V. (1989). Introduction to the theory of stratigraphy. Moscow: Nauka, 216 p. (In Russ.)
- Morin E. (2005). La Methode. La Nature de la Nature. French transl. Moscow: Progress-Tradition, 464 p. (In Russ.)
- North American Stratigraphic Code. North American Commission on Stratigraphic Nomenclature (2005). *AAPG Bull.*, 89(11), pp. 1547-1591. <https://doi.org/10.1306/07050504129>
- Nurgalieva N.G. (2016). Basics of the formational analysis of oil and gas bearing strata. Kazan: KFU, 150 p. (In Russ.)
- Ogg J.G., Ogg G.M., Gradstein F.M. (2016). A Concise Geologic Time Scale 2016. Amsterdam-Oxford-Cambridge: Elsevier, 234 p.
- Patrikeev V.N. (2013). Structure, composition and peculiarities of the formation of the Northwestern Pacific plate sedimentary cover (a synthesis of seismostratigraphic and geologic data). *Stratigraphy of the early XXI century – tendencies and new ideas*. Moscow: Geokart, GEOS, pp. 203-217. (In Russ.)
- Pervushov E.M., Guzhikov A.Yu., Kalyakin E.A., Guzhikova A.A. (2013). Sub-regional stratigraphic scheme of upper Cretaceous deposits of the Middle and Lower Volga region. *General Stratigraphic Scale of Russia: current state and ways of perfection*. Moscow: GIN RAS, pp. 25-28. (In Russ.)
- Posamentier H.W., Allen G.P. (2014). Siliciclastic Sequence stratigraphy: Eng. transl. Moscow-Izhevsk: IKI Publ., 436 p. (In Russ.)
- Romanovsky S.I. (1979). Nikolaj Alekseevich Golovkinsky (1834-1897). Leningrad: Nauka, 192 p. (In Russ.)
- Romanovsky S.I. (1985). Dynamic modes of sedimentation. Cyclogenesis. Leningrad: Nedra, 263 p. (In Russ.)
- Rössler O.E. (1998). Endophysics: The World as Interface. Singapore: World Scientific, 204 p. <https://doi.org/10.1142/3183>
- Seismic stratigraphy. Use in the search and exploration of oil and gas. Editor Ch. Peyton. (1982). Moscow: Mir, 846 p. (In Russ.)
- Sharapov I.P. (1989). Metageology. Moscow: Nauka, 208 p. (In Russ.)
- Shatsky N.S. (1986). Amanz Gressly. *Portraits of geologists*. Moscow: Nauka, pp. 184-198. (In Russ.)
- Socratov G.I. (1949). From the history of Russian Geology of the second half nineteenth century (the 50th anniversary of the death of N.A. Golovkinsky and the 80th anniversary of his theory). *Zapiski Leningradskogo gornogo instituta* [Notes of the Leningrad mining Institute], XV-XVI, pp. 41-68. (In Russ.)
- Sukhov S.S., Pegel T.V., Shabanov Y.Y. (2013). The role of regional factors in the development of new generation of stratigraphic schemes, General and International scales (on example of Cambrian of the Siberian platform). *General Stratigraphic Scale of Russia: current state and ways of perfection*. Moscow: GIN RAS, pp. 91-97. (In Russ.)
- Supplements to the Stratigraphic code of Russia. (2000). Saint-Petersburg: VSEGEI Publ., 112 p. (In Russ.)
- Tsyganko V.S. (2007). Formation and horizon: types of boundaries and their relationship. *Geologiya i geofizika = Geology and Geophysics*, 48(8), pp. 862-870. <https://doi.org/10.1016/j.rgg.2007.07.002> (In Russ.)
- Vassoevich N.B. (1949). Layering and facies. *Izvestiya AN SSSR = Proceedings of USSR Acad. Sci., ser. geol.* 2, pp. 129-132. (In Russ.)
- Vereshchagin V.N. (1980). Suite as a most important stratigraphic unit. *Stratigraphic Classification. Materials for the Problem*. Leningrad: Nauka Publ., pp. 130-135. (In Russ.)
- Walther J. (1893-1894). Einleitung in die Geologie als historische Wissenschaft. Bd. 1-3. Jena. 1055 p.
- Zhamoida A.I. (2013). General stratigraphic scale accepted in the USSR-Russia. Its meaning, purpose and improvement. Saint Petersburg: VSEGEI Publ., 24 p. (In Russ.)
- Zhemchuzhnikov Yu.A. (1947). Cyclic structure of coal-bearing strata, periodicity of sedimentation and methods of their study. *Trudy IGN AN SSSR* [Proceedings of Geological Institute of the USSR], vol. 90, coal series (no. 2), pp. 7-18. (In Russ.)
- Zorina S.O. (2006). On synchronism of geological boundaries in the middle Jurassic – Paleocene of the Eastern Russian Plate. *Georesursy = Georesources*, 4(21), pp. 31-35. (In Russ.)
- Zorina S.O. (2015). Geochronology and problems of the International Stratigraphic Scale. Kazan: KFU Publ, 40 p. (In Russ.)
- Zorina S. (2018). Development of Golovkinsky's Law (1868): from Lithological "Lentil" to Platform Sequence. Proceedings of Kazan Golovkinsky Stratigraphic Meeting 2017: «Advances in Devonian, Carboniferous and Permian Research: Stratigraphy, Environments, Climate and Resources». *Filodiritto Editore – Proceedings*, pp. 360-363.
- Zorina S.O., Afanasieva N.I. (2006). On the chronostratigraphic relation of Upper Cretaceous and Paleocene boundary stratons in the Middle and Lower Volga region. *Izvestiya VUZov. Geologiya i razvedka = Proceedings of Higher Schools. Geology and exploration*, 4, pp. 3-7. (In Russ.)
- Zorina S.O., Afanasieva N.I., Khairtdinova L.R. (2018). An Event-Based Depositional Model for the Paleocene–Eocene Sandy–Clayey–Siliceous Sequence of the Russian Platform. *Doklady Earth Sciences*, 480 (1), pp. 547-550. <https://doi.org/10.1134/S1028334X1805001X>

## About the Authors

**Svetlana O. Zorina** – DSc (Geology and Mineralogy), Associate Professor, Professor of the Department of Paleontology and Stratigraphy, Institute of Geology and Petroleum Technologies

Kazan (Volga Region) Federal University  
4/5, Kremlevskaya st., Kazan, 420008, Russian Federation

E-mail: svzorina@yandex.ru

**Valery P. Alekseev** – DSc (Geology and Mineralogy), Professor of the Department of Lithology and Geology of Combustible Minerals

Ural State Mining University  
30, Kuibyshev st., Ekaterinburg, 620144, Russian Federation

*Edward O. Amon* – DSc (Geology and Mineralogy),  
Leading Researcher

Borissiak Paleontological Institute of the Russian  
Academy of Sciences

123, Profsoyuznaya st., Moscow, 117647, Russian  
Federation

*Ksenia A. Khasanova* – PhD (Geology and  
Mineralogy), geologist

Schlumberger

4, 50 let Oktyabrya st., Tyumen, 625048, Russian  
Federation

*Manuscript received 11 September 2018;*

*Accepted 29 October 2018;*

*Published 30 November 2018*





# On the relationship of oil and gas formation and degassing processes with groundwater decomposition

A.A. Barenbaum

*Institute of Oil and Gas Problems of the Russian Academy of Sciences, Moscow, Russian Federation*

*E-mail: azary@mail.ru*

**Abstract.** The article is referred to important consequence of the biosphere oil and gas formation concept, according to which the process of hydrocarbons generation in the subsoil and degassing of the Earth are a single natural phenomenon. The main role in this phenomenon is played by geochemical circulation of carbon and water through the Earth's surface accompanied by polycondensation synthesis of hydrocarbons by  $\text{CO}_2 + \text{H}_2\text{O}$  reaction. This reaction is accompanied by a colossal decomposition of groundwater into hydrogen and oxygen within the sedimentary cover of the Earth's crust. Unreacted  $\text{CO}_2$ , as well as  $\text{H}_2$  and most of the methane produced during the reaction are degassed into the atmosphere, while resulting  $\text{C}_{5+}$  hydrocarbons remain under the surface filling geological traps in the form of oil and gas. The article presents the results of model experiments, which make it possible to estimate the rate of groundwater decomposition and on this basis explain the current rate of Earth's degassing, as well as the observed  $\text{CO}_2$ ,  $\text{CH}_4$  and  $\text{H}_2$  ratio in degassing products.

**Keywords:** Earth degassing, carbon and water cycle, biosphere concept of oil and gas formation

**Recommended citation:** Barenbaum A.A. (2018). On the relationship of oil and gas formation and degassing processes with groundwater decomposition. *Georesursy = Georesources*, 20(4), Part 1, pp. 290-300. DOI: <https://doi.org/10.18599/grs.2018.4.290-300>

## Introduction

As is well known, not a single chemical process in the Earth's crust takes place without water (Vernadsky, 1960). Chemical reactions occur mainly in liquid or vapor-aqueous solutions. At the same time, water, as a chemical compound, is very stable and practically incapable of spontaneous decomposition. The  $\text{H}_2\text{O}$  dissociation constant at ordinary temperature equals to  $10^{-14}$ , while the water decomposition constant with release of hydrogen and oxygen equals to  $10^{-83.1}$  (Garrels, Crayst, 1968). Therefore, decomposition of water into hydrogen and oxygen is extremely unlikely without significant energy from the outside. However, the processes of lithogenesis and metamorphism occur with the participation of water in the Earth's crust (Strahov, 1960; Shvarcev, 1975; Uolter, Vud, 1989), in which groundwater decompose with formation of hydrogen due to the release of energy in chemical reactions (Molchanov, 1981).

Groundwater decomposition during the formation of oil and gas has never attracted the attention of either hydrogeologists or oil industry professionals considered the circulation of groundwater and the formation of hydrocarbons (HC) as natural phenomena independent of each other. Hydrogeologists proceeded from the fact that

the decomposition of water into hydrogen and oxygen is so small that it was not taken into account in the balance calculations of groundwater (L'vovich, 1986; Zekcer, Dzhamalov, 1989; Shvarcev, 1996; Zverev, 2007). Petroleum geologists, in turn, believed (Levorsen, 1970; Gavrilov, 1986; Karcev et al., 1992; Batalin, Vafina, 2008) that groundwater in case of its participation in oil and gas formation, only acts as a means of transporting hydrocarbons during oil and gas reservoir formation and destruction, or as a factor affecting rock's composition and reservoir properties. Many geologists hold these views today.

Formation of oil and gas, as well as subsoil degassing, is not without reason attributed to the most problematic issues of geology. Over the past century, these problems have been tried to be solved, however they have not yet been resolved in disputes between supporters of organic and mineral petroleum origin hypotheses. The adherents of the latter hypothesis associate the origin of oil and gas with the influx of carbon-containing gases and fluids from the deep bowels of the Earth (<http://journal.deepoil.ru>). However, the hypothesis of deep degassing contradicts the data of geophysics and cosmogony regarding the internal structure of the Earth and the mechanism of its formation (Zharkov, 1988; Braun, Masset, 1984; Vityazev et al., 1990). To this we add that with the current intensity of  $\text{CH}_4$  and  $\text{CO}_2$  degassing, the Earth's atmosphere would be completely filled with carbon gases in a time period of ~100 years (Barenbaum, 2004).

## New approach to the problem

The role of groundwater in the processes of oil and gas formation and degassing began to be revised in the mid-1990s. At this period in our country was discovered the replenishment of hydrocarbon reserves within “old” oilfields. In addition, it was turned out (Sokolov, Guseva, 1993) that the formation of oil and gas is a modern process, which depends on production conditions at oilfields. To date, this phenomenon has received a theoretical justification and explanation in the biosphere concept of oil and gas formation (Barenbaum, 2004, 2010, 2013, 2014, 2015, 2017). Drawing on the ideas of V.I. Vernadskiy about the biosphere (Vernadskiy, 2001), this concept revealed the participation in the oil and gas formation of the biosphere carbon cycle inextricably linked with the circulation of meteorogenic waters through the Earth’s surface. Therefore, this cycle is mainly regional in nature, and its characteristic turnaround time is close to the carbon cycle in the biosphere of ~30-40 years (Kondrat’ev, Krapivin 2004).

According to the biosphere concept, meteorogenic water penetrating deep enough into the Earth’s crust carries both significant amount of oxidized carbon ( $\text{CO}_2$ ,  $\text{HCO}_3^-$ ,  $\text{CO}_3^{2-}$ ) and water-soluble organic matter, which are involved in the formation of gas-oil hydrocarbons. Moreover, if carbon-containing substances in hydrocarbons act as carbon donors, then water itself, while decomposing, serves as a donor of hydrogen.

Today there are numerous facts confirming validity of the biosphere concept. One of its most important conclusions is that oil and gas hydrocarbons are formed in the polycondensation reaction of  $\text{CO}_2 + \text{H}_2\text{O}$  synthesis during geochemical cycle of biosphere carbon and water across the Earth’s surface. This reaction is accompanied by the decomposition of a large mass of water in the Earth’s crust, which leads to the formation and penetration into the atmosphere of significant amounts of  $\text{H}_2$ ,  $\text{CH}_4$ ,  $\text{CO}_2$  and  $\text{N}_2$  (from air dissolved in water).

This article develops the concept stating that generation of gas and oil hydrocarbons and the degassing of subsurface is a single natural phenomenon caused by decomposition of huge amounts of water in the rocks of the Earth’s crust, which is involved with carbon in the geochemical circulation through the Earth’s surface.

Below are the arguments, facts and experimental results that allow to prove this opinion and show that this conclusion is a direct consequence of the biosphere concept of oil and gas formation.

## Initial stage of research

One of the first to notice the formation of hydrogen in the Earth’s crust from water was V.I. Vernadskiy and A.P. Vinogradov (Molchanov, 1981). It was later

established (Semenov, 1959) that the course of many chemical processes, in particular polycondensation reactions, is determined by free radicals, i.e. broken chemical bonds. It was found that free radicals could be generated by intracrystalline defects in minerals. Diffusing to the surface of mineral grains, these defects form an energy-saturated layer that reduces the Gibbs energy of chemical reactions. As a result, reactions thermodynamically possible at a temperature of 500°C and more can occur in the rock mineral matrix under “standard” conditions ( $T = 25^\circ\text{C}$  and  $P = 1 \text{ atm.}$ ).

Reaction of  $\text{H}_2\text{O}$  decomposition with the release of hydrogen involved in the polycondensation synthesis of hydrocarbons from  $\text{CO}_2$  and  $\text{H}_2\text{O}$  is also attributed to such reactions, as shown by V.I. Molchanov (Molchanov, 1981; Molchanov et al., 1988; Molchanov, Gontsov, 1992), N.V. Cherskiy and V.P. Tsarev (Cherskiy, Tsarev, 1984; Cherskiy et al., 1985). These authors have experimentally proved that the energy-saturated layer required for the synthesis of hydrocarbons can be created artificially by mechanical activation of carbon-containing mineral media in presence of water. This layer also appears on the surface of the rock mineral matrix under conditions of their natural occurrence and is affected by the tidal influence of the Moon, as well as tectonic, seismic and other natural processes. A diploma for scientific discovery No.326 (Trofimuk et al., 1982) officially approved this fact.

A necessary condition for the hydrocarbon synthesis is the creation of reducing conditions on the surface of minerals in contact with water, under which water is able to generate «active» atomic hydrogen reacting with carbon oxides. It was identified in the article (Cherskiy, Tsarev, 1984) that sea water contact with samples of carbon-containing rocks mechanically activated by friction generates a wide spectrum of hydrocarbons from saturated, unsaturated, and aromatic, both gaseous, liquid and solid.

The study of crude non-biodegraded oils and natural bitumen showed (Barenbaum, 2007; Barenbaum, Ablya, 2009) that molecular mass distributions of n-alkanes in them are almost identical to those obtained in Fischer-Tropsch synthesis (Glebov, Kliger, 1994), as well as to those which were formed in the experiments of N.V. Cherskiy and V.P. Tsarev at room temperature and atmospheric pressure.

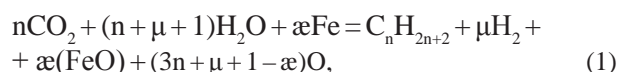
Looking ahead, we emphasize that the following conclusion of the biosphere concept (Barenbaum, 2015; Barenbaum, Klimov, 2015) is fundamentally important: the bulk of “abiogenic” hydrocarbons extracted from the depths in the form of oil and gas come not from some great depths (<http://journal.deepoil.ru>), but directly formed in the sedimentary cover of the Earth’s crust in the reaction of polycondensation synthesis of hydrocarbons from  $\text{CO}_2$  and  $\text{H}_2\text{O}$ .

## Experimental part of the work

In recent years, the reaction of hydrocarbon synthesis from  $\text{CO}_2$  and  $\text{H}_2\text{O}$  has been studied experimentally and theoretically at OGPI RAS when filtering carbonated water (water with dissolved  $\text{CO}_2$ ) through bulk model media containing iron shavings or shale (Barenbaum et al., 2012; Zakirov et al., 2013; Semenov et al., 2014; Barenbaum, Klimov, 2015). In contrast to the experiments of other authors, when modeling the process of hydrocarbons formation from  $\text{CO}_2$  and  $\text{H}_2\text{O}$ , we used the well-known property of Fe to decompose water, generating active hydrogen under room temperature-pressure conditions.

Most of the experimental studies were carried out on the author's equipment (Zakirov et al., 2013; Barenbaum et al., 2012), and the other part of experiments was carried out on a specialized laboratory equipment (Semenov et al., 2014; Barenbaum et al., 2015) at room temperature and pressure close to atmospheric. The experiments made it possible to establish that the polycondensation synthesis of hydrocarbons from  $\text{CO}_2$  and  $\text{H}_2\text{O}$  is accompanied by the formation of free molecular hydrogen.

The corresponding chemical reaction in relation to the synthesis of n-alkanes can be represented by the following phenomenological formula (Barenbaum, 2014):



where  $n$  is the number of carbon atoms in the molecule,  $\mu$  and  $\alpha$  are the stoichiometric coefficients.

Thermodynamic calculations show that the synthesis of hydrocarbons by reaction (1) becomes possible under standard conditions ( $T = 25^\circ\text{C}$  and  $P = 1 \text{ atm}$ ) only with sufficiently complete removal of oxygen from the system. In our experiments, iron shavings served as the necessary "absorber" of oxygen, which also played the role of a "catalyst". In the rocks of the Earth's crust, these functions can obviously be performed by many chemical elements and their compounds.

The experiments generally confirmed the results of V.I. Molchanov, N.V. Cherskiy and V.P. Tsarev. They also showed that if hydrocarbons are deposited in the form of bitumens on iron chips, and oxygen oxidizes its surface, then hydrogen in excess enters the gas phase (Table 1).

Data from Table 1 indicate that in the gas phase there are hydrogen, methane and its homologues, as well as carbon monoxide originally not presented in the system. In this case, the gas phase almost entirely consists of

$\text{H}_2$ . The oxygen arising from the decomposition of  $\text{H}_2\text{O}$  is almost completely consumed on the oxidation of Fe, and its penetration into the gas phase is negligible. The presence of nitrogen, as well as a certain amount of oxygen, is determined by air, which was originally dissolved in water. It is significant that the excess of nitrogen over oxygen is much higher than their ratio in the air.

In our experiments, the yield of  $\text{H}_2$ , as well as yield of  $\text{CH}_4$  and its homologues, depended significantly on the  $\text{CO}_2$  content in carbonated water (Fig. 1). Catalytic activity of the iron shavings was decreasing during the experiments, and the water in the reactor was ceasing to decompose. In all experiments carried out at different reactor volumes and different pressures of  $\text{CO}_2$  in water, a maximum of  $\sim 0.1 \div 1 \text{ g}$  per liter of  $\text{H}_2\text{O}$  have been decomposed in the reactor.

This paper discusses the experimental results (Barenbaum and Klimov, 2015), which allowed for the first time to raise the question on groundwater decomposition rate in the process of oil and gas formation, as well as on the extent of this phenomenon.

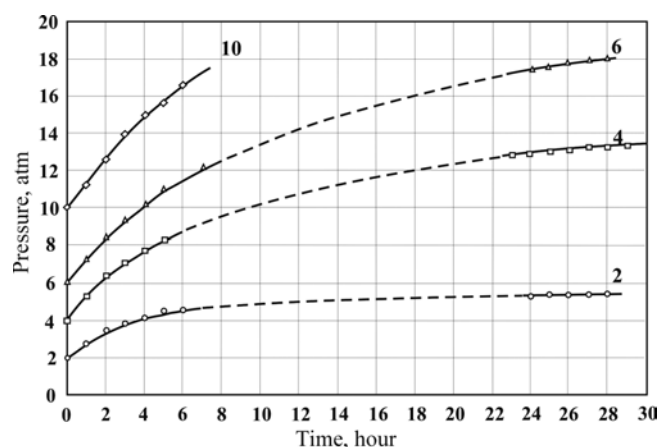


Fig. 1. Changes of pressure over time in the reactor. Curves indicate the saturation of water with  $\text{CO}_2$  at its pressure in the mixer of 2, 4, 6 and 10 atm

## Measuring the rate of water decomposition

Experimental equipment scheme is shown in Fig. 2

The experiment consisted in measuring the volume of gas formed in the reactor (3) some time after it was filled with carbonated water. As a reactor there was used a stainless steel beaker with an internal volume of 45 ml, which was filled with 25 g of fine steel shavings in order to simulate an "activated" rock. Under a small initial pressure,  $\sim 35 \text{ g}$  of carbonated ("meteo-genic") water was poured into the glass, which was emitted by a solution

Component	Hydrogen	Nitrogen	Oxygen	Methane	Ethane	Propane	Butane	2	
Content, %	95.562	3.688	0.657	0.039	0.018	0.0125	0.0049	0.002	0.017

Table 1. Chemical composition of the gas phase after treatment with alkali



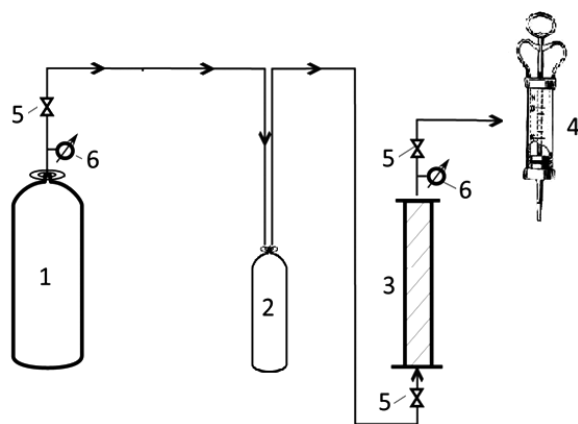


Fig. 2. Experimental equipment scheme. 1 – CO<sub>2</sub> cylinder; 2 – mixer for saturation of water with CO<sub>2</sub>; 3 – reactor with activated medium; 4 – syringe for sampling and measuring gas phase volume; 5 – valves; 6 – manometers

of CO<sub>2</sub> in distilled water. Water saturation by CO<sub>2</sub> was made in 5 l tanks (2), where from a cylinder (1) under pressure of 2-5 atm was supplied chemically pure CO<sub>2</sub>. Water saturation time by CO<sub>2</sub> was assumed 18 hours. The separation of gas from liquid and measuring its volume at the outlet of the reactor was carried out using a syringe (4). The error in measuring the volume of gas with a syringe at atmospheric pressure was ~0.5 cm<sup>3</sup>.

The experiment consisted of filling the reactor (3) with carbonated water from the mixer (2) followed by shut off of the valves at the inlet and outlet of the reactor allowing chemical reactions to take place in it. Along with other possible reactions in the reactor, decomposition of water occurred with the formation of H<sub>2</sub>, which caused an increase in pressure recorded by a pressure gauge (6). The composition of the newly formed gas shows (Table 1) that the pressure increase in the reactor is mainly created by H<sub>2</sub> resulting from H<sub>2</sub>O. Thus, mass of the destroyed water can be measured by volume of the generated H<sub>2</sub>.

In the course of the experiment, 5 cycles of gas

volume measurements were performed, including from 4 to 6 consecutive experiments of different duration. Duration of each cycle ranged from 3 to 6 days. The measurements were carried out at room temperature.

When developing the methodology, a number of factors were taken into account, which could introduce errors into the experimental results. The first factor is associated with the possible ingress of air into the measured volume of gas when it is taken by syringe. The second factor is the necessity to maintain a constant saturation of the water with CO<sub>2</sub> before the start of each experiment, which was technically difficult to control, but it was necessary to ensure reproducibility of different series of measurements. The third source of errors is caused by the fact that after each series of experiments, the reactor had to be rinsed and sealed again before new measurements with the removal of air that had entered it.

The influence of these factors was reduced with the use of the technique explained in Fig. 3, which shows the results of measuring the volume of gas at the outlet of the reactor after one of a series of experiments. The technique consisted in the fact that in the course of the experiment the reactor was repeatedly filled with carbonated water from the mixer, and the volume of gas was measured after different periods of exposure (duration of water presence in the reactor), considered as “background” and “informative” measurements. Measurements with an exposure time of 1 min were considered as background. The gas selected in them almost completely consisted of CO<sub>2</sub>, and its volume corresponded to that which was separated from water as the pressure decreased from initial to atmospheric, at which the measurements were made. Experiments with an exposure time of 21 hours or more were considered informative. In this case, along with CO<sub>2</sub>, the gas also contained H<sub>2</sub> formed from water. The difference effect between informative and background measurements made it possible to measure the amount of the emerged

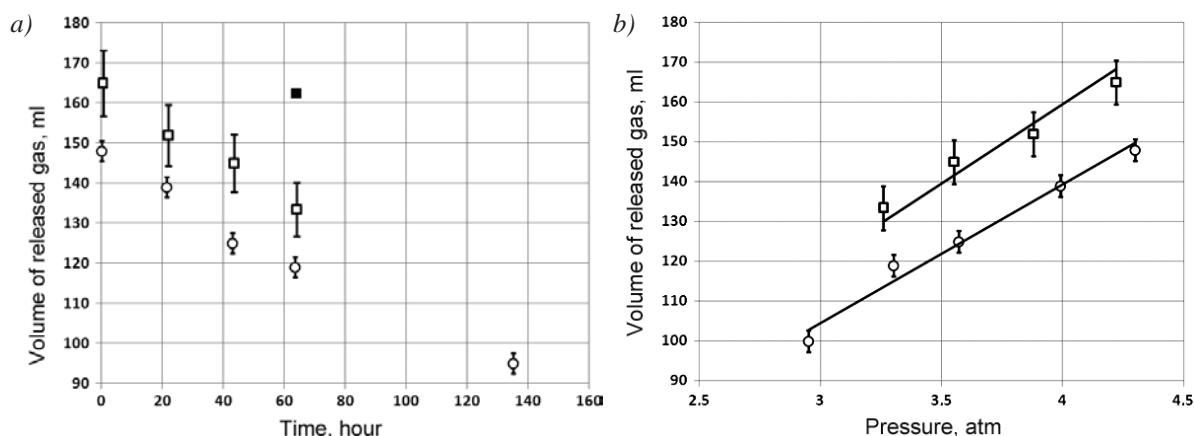


Fig. 3. Volume of released gas, depending on: a) the time elapsed since the beginning of the experiment, b) initial pressure of meteorogenic water in the reactor. Circles – background measurements, squares – informative measurements. Measurement with an exposure of 71 hours is shown by a dark square. Straight lines indicate approximating dependencies. Errors: background – 2.4% rel., informative measurements – 6.8% rel.

$H_2$ , and according to this data, find the amount of water disintegrated in the reactor. As the number of measurements increased in the experiment, the amount of water and the pressure of  $CO_2$  in the mixer decreased with time. The volumes of gas ( $V$ ) released in the reactor also decreased (Fig. 3a). In Fig. 3b the same volumes are given depending on the initial pressure of the gas  $P_0$  in the reactor.

Since the solubility of gases is linearly related to pressure, the  $V(P_0)$  dependences were approximated by straight lines passing through the point  $P = 0$ . Dependences found by least squares method are as follows:  $V = 34.7 P_0$  for the background measurements, and  $V = 39.0 P_0$  for informative measurements. In the latter case, the volume of gas in the experiment with an exposure of 71 hours is recalculated to 21 hours, as for all other measurements.

### Analysis of the experimental results

Since the gas sampling technique was standardized, possible systematic errors during the transition to the differential effect were reduced. Experiments have shown that the replacement of iron shavings, the new preparation of carbonized water, as well as the sequence of background and informative measurements did not affect the difference effect. After averaging the results of a series of experiments performed at initial pressures,  $P_0 = 3.0 \div 4.3$  atm and an exposure time of 21 hours, the difference effect was  $\Delta V = 22 \pm 6$  ml. Assuming that the  $\Delta V$  effect is created by gaseous hydrogen, which at atmospheric pressure has a density of  $\rho_H = 1 \cdot 10^{-4}$  g/cm<sup>3</sup>, the mass of the hydrogen formed is calculated as  $m_H = \Delta V \cdot \rho_H = (2.2 \pm 0.6) \cdot 10^{-3}$  g. Taking into account that the share of  $H_2$  in water is 11.1%, the mass of decomposed water was  $M = m_H / 0.111 = 2.0 \cdot 10^{-2}$  g. Taking into account that the mass of water in the reactor was  $\sim 35$  g, its decomposed part was  $M/35 \sim 5.7 \cdot 10^{-4}$ . From where the rate of carbonized water decomposition in the reactor turned out to be  $\sim 2.7 \cdot 10^{-3}$  g per 1 liter of  $H_2O$ . Hydrogen included in the HC was not taken into account.

Taking into account the effect of flattening (Fig. 1), there was decomposed  $\sim 0.1 \div 1$  g per liter of carbonated water during the experiments. Taking this data as a basis, we inevitably come to the conclusion that in the Earth's crust, and above all in its sedimentary cover, a significant amount of groundwater should be decomposed annually (Barenbaum, 2017a).

The main question is how large this mass of water is and whether it is sufficient to explain the current rate of HC generation, as well as the intensity of  $CH_4$ ,  $CO_2$  and  $H_2$  degassing from the depths.

Biosphere concept of oil and gas formation gives us the answers to these questions (Barenbaum, 2014, 2015, 2017).

### Biosphere concept of oil and gas formation

The fundamental difference of the biosphere concept from other theories is that it requires a balance between the "descending" and "ascending" flows of carbon and water during circulation through the Earth's surface.

When solving this problem, it was identified (Barenbaum, 1998, 2010) that hydrosphere waters, biosphere carbon and atmosphere oxygen form a single geochemical circulation system on our planet. The unity and stability of this system ensures participation in the circulation of living matter, which brings the rate of oxygen and carbon circulation in line with the rate of water circulation within the underground hydrosphere.

At present, the geochemical system of the biosphere is in a state close to stable dynamic equilibrium characterized by the rate of the cycle in terms of  $CO_2$  equal to  $2.7 \times 10^{16}$  g/year. In this state, the main water bodies of the Earth are replenished at a rate of  $(2.0 \pm 0.5) \times 10^{19}$  g/year by waters participating in two circulation cycles (Fig. 4). These waters consist of 87-90% "meteoric" waters, and 10-13% "marine"

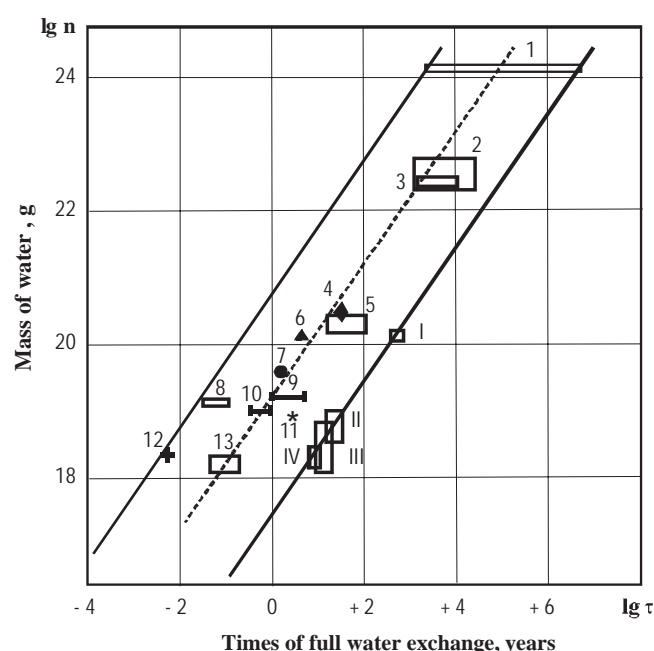


Fig. 4. Comparison of water quantities and times of water exchange for the main natural reservoirs of the Earth: 1 – World Ocean; 2 – groundwater; 3 – glaciers and ice caps; 4 – lakes, impounding reservoirs and swamps; 5 – lakes; 6 – swamps; 7 – sea ice; 8 – water in the atmosphere; 9 – soil moisture; 10 – snow cover; 11 – icebergs; 12 – atmospheric ice; 13 – rivers; dotted line characterizes the average rate of water exchange. Roman numerals indicate data of the biosphere carbon cycle in terms of  $CO_2$ : I – World Ocean; II – living matter; III – soil-silt; IV – the atmosphere. The upper oblique straight line corresponds to meteorogenic waters circulation at a rate of  $C_1 = 5.2 \times 10^{20}$  g/year (L'vovich, 1986), and the lower one corresponds to marine waters circulation through the mid-ocean ridges at a rate of  $C_2 = 2.7 \times 10^{17}$  g/year, which coincides with the circulation rate of  $CO_2$  in biosphere (Barenbaum, 2010).

waters. The first one are of local origin, they are formed in the atmosphere and in the form of rain and snow infiltrate through the Earth's surface subsequently entering the area of water bodies feeding. The second is water belonging to the general system of deep circulation of groundwater through the mid-ocean ridges. They received the name "marine" because of proximity of their salt composition to the waters of the World Ocean. In the groundwater of different regions of the globe, meteogenic waters significantly dominate over the marine waters. This conclusion was obtained for waters of rivers, lakes and glaciers, as well as for waters of deep artesian basins, volcanic areas and waters associated with oil and gas accumulations (Ferronskiy, Polyakov, 2009).

The carbon balance in its cycle through the Earth's surface is provided by 4 components. On the ascending branch of the cycle, these components are natural and anthropogenic flows. The first one caused by subsurface degassing phenomenon (Table 2), in which CH<sub>4</sub> and CO<sub>2</sub> come into the atmosphere from the depths in approximately equal amounts of  $(2.5 \pm 0.2) \times 10^{14}$  g/year (Voytov, 1986). According to measurements of recent years (Voytov, 1999; Syvorotkin, 2002), this component may be ten times greater.

The anthropogenic component is represented by carbon, which is extracted from the depths of the Earth as

fuel in the form of oil, gas and coal. In particular, in 2017 the world produced 4.3 billion tons of oil, 3.8 trillion m<sup>3</sup> of natural gas and 7.8 billion tons of hard coal, which contain  $\approx 14$  billion tons of carbon. Thus, it can be assumed that at the present time, about  $10^{16}$  g of predominantly reduced carbon comes to the surface from the subsurface.

Carbon downstream is also represented by two components. One is associated with the disposal of carbon (organic and inorganic) in sedimentation processes. According to data (Voytov, 1986),  $\sim 2 \times 10^{14}$  g of carbon consisting of  $\sim 2/3$  of carbonates and  $\sim 1/3$  of dead organic matter are buried into the Earth's crust annually. The second component is carbon, which is transported under the Earth's surface by meteogenic (surface) water. Since most of the carbon fuels extracted from the subsoil is burnt and therefore converted in about three times greater amount of CO<sub>2</sub> emitted into the atmosphere, then to balance the ascending and descending carbon flows, it is necessary to supply  $\sim 3 \times 10^{16}$  g of water-soluble CO<sub>2</sub> to the Earth's crust every year. In this case, its content in water should be  $\sim 3 \times 10^{16} / 2 \times 10^{19} \sim 10^{-3}$  g/year, which fully satisfies the actual data (Korzh, 1991).

Under the Earth's surface, water-soluble CO<sub>2</sub> may take part in various chemical reactions, but first of all it participates in the decomposition of H<sub>2</sub>O with the formation of HC and H<sub>2</sub> according to reaction (1).

Geostructural zones	Area mln. km <sup>2</sup>	CO <sub>2</sub>	HC	<sub>2</sub>	N <sub>2</sub>	
<i>In active volcanism on the surface of the Earth</i>						
Explosive stage		5.66	0.066	0.025	?	?
Fumarole stage		10.38	0.170	0.012	?	?
<i>In Alpine fold zones</i>						
In mud volcanoes		3.95	10.68	0.0014	0.16	$22 \cdot 10^{-5}$
Areas of Alpine folding	150	400/119	50/54	10/0.14	40/7.5	$0.35/9.5 \cdot 10^{-3}$
<i>Platforms and ancient folded areas</i>						
Shields	29.4	22.5/1.21	30/0.063	4.2/0.012	4/0.147	0.2/0.001
Blocks of alkali rock	5.1	1.0/0.01	300/1.102	100/0.012	20/0.127	$0.35/8 \cdot 10^{-5}$
Platforms and ancient folded areas, screened by sedimentary cover	316	20/13	150/34.1	6.3/0.18	18./7.11	0.27/0.015
<i>World ocean</i>						
Underwater margins	81.8	20/3.24	150/8.835	4/0.029	5/0.51	0.3/0.0044
Transitional area	30.8	500/30.49	650/14.5	12/0.033	8/0.31	0.6/0.0033
Sea floor	193.9	50/19	300/70	75/1.3	8/1.938	0.15/0.005
Mid-ocean ridges	55.4	600/67	750/30	900/4.48	100/6.93	0.25/0.0025
Total gas		272.89	223.51	6.084	24.732	0.0405

Table 2. Flow density for some gases and the value of their unloading in different geostructural zones according to G.I. Voytov (1986). The figure in the numerator is the gas flow density (cm<sup>3</sup>/m<sup>2</sup> per year), the figure in the denominator is the gas integral discharge ( $10^{12}$  g/year)



Moreover, in case when formed hydrocarbons fill up geological traps (reservoirs) and can stay there for a long time, then light  $H_2$ , together with most of the  $CH_4$ ,  $N_2$  dissolved in groundwater and unreacted  $CO_2$  are degassed into the atmosphere (Table 2).

As is known, oil and gas formation processes are most intensively taking place at the depths of “oil window” (Fig. 5), where the temperature and pressure conditions are determined by hydrocarbons phase composition (Batalin et al., 1992; Batalin, Vafina, 2008).

Fig. 5a (Barenbaum, Batalin, 2001) shows the results of the phase PT-diagram calculation for a hydrocarbons mixture having typical gas-condensate composition:  $CH_4$  (70-85%),  $C_2H_6$ - $C_4H_{10}$  (5-10%),  $C_{5+}$  (10%). According to calculations, this HC mixture can exist in a homogeneous state only from the outside of the two-phase region. Inside this region, the mixture is divided into two phases: gaseous – “gas” and liquid – “oil”. Isoplethic lines show the percentage of liquid phase in the mixture. Straight line characterizes the change in PT conditions with depth on the continents. The points of the straight line intersection with the isoplethic lines determine the percentage of «oil» in the initial mixture at different depths. Fig. 5b shows the curve of “oil” percentage change with the depth according to the diagram in Fig. 5a. The calculation explains well the position and shape of the oil window in the largest oil and gas basins of the world (Sokolov, Ablya, 1999). In case of changes in the composition of HC mixture and thermobaric conditions, the oil window can be deformed and displace along the depth axis (Lapshin, 2000; Batalin, Vafina, 2008).

Oil and gas formation also causes another effects. The first of these is the failure of groundwater hydraulic connection with the surface in the oil window, which is characteristic of relatively shallow depths (Fig. 6).

In zone I, the growth of pressure with depth is

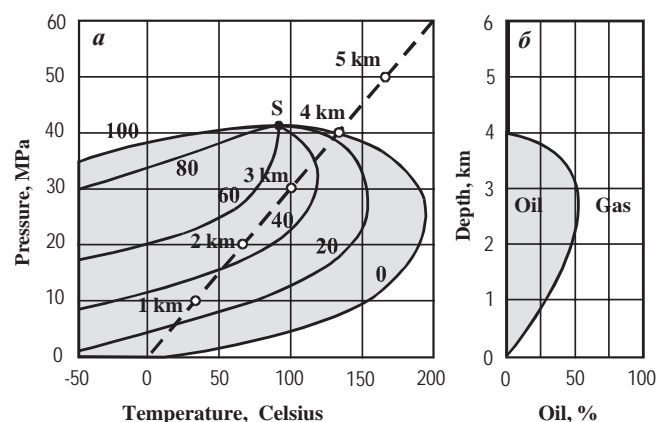


Fig. 5. Phase diagram of the hydrocarbon mixture with isopleths (a) and the oil saturation curve corresponding to this diagram (b): inclined dashed straight line – depth scale corresponding to the hydrostatic gradient typical of continents; S is the critical point of the mixture

created by fluids filling pores and fractures, which form channels communicating with each other and with the surface. In zone III, pressure gradient is determined by the weight of the overlying rocks. Rocks of this zone are characterized by low fracturing and porosity, and if they contain water, this water is in a chemically bound state.

As for zone II – the zone of so-called abnormally low and abnormally high reservoir pressures (Dobrynin and Serebryakov, 1989), until recently it did not receive a clear explanation. The prevailing view was that this zone is formed in oil and gas basins due to inhomogeneous lithological transformation and compaction of sedimentary rocks with increasing pressure and temperature with depth.

This explanation is true, but only in part. In the biosphere concept, this zone arises primarily due to the decomposition of water in the fields of hydrocarbons generation. The process is so intense that free water at the depths of the oil window physically ceases to exist. Owing to the transformation of  $H_2O$  into  $H_2$  and  $CH_4$  degassing into the atmosphere, there is a shortage of reservoir pressures (piezo minimum), which serves as a kind of “pump” (Barenbaum, 2015a), sucking water from the upper and lower horizons.

Another effect is the fact that the water repeatedly involved in the hydrocarbon synthesis is enriched with deuterium – a heavy isotope of hydrogen. According to data (Zykin, 2012), the associated waters within gas reservoirs and containing acidic components, have abnormally high deuterium contents, which are not found in any other natural objects (Fig. 7).

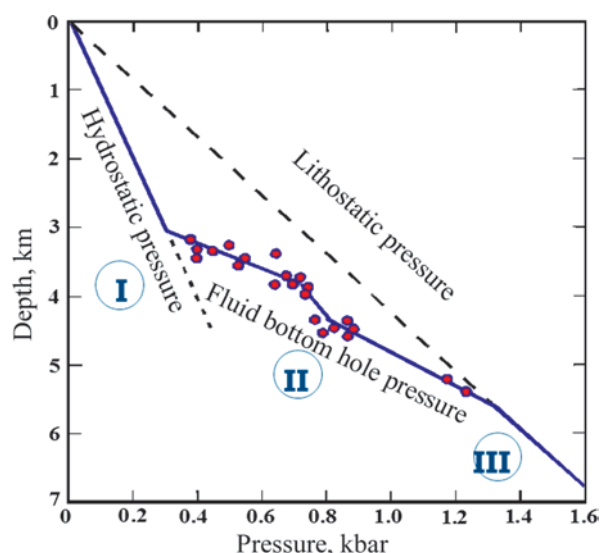


Fig. 6. Changes in reservoir pressure with depth within sedimentary basins caused by the total hydrodynamic pressure zonality in the subsurface crust hydrosphere (according to Dz. Uolter and B. Vud (1989) with changes). The numbers indicate zones of hydrostatic (I), transition (II) and lithostatic (III) pressure gradient

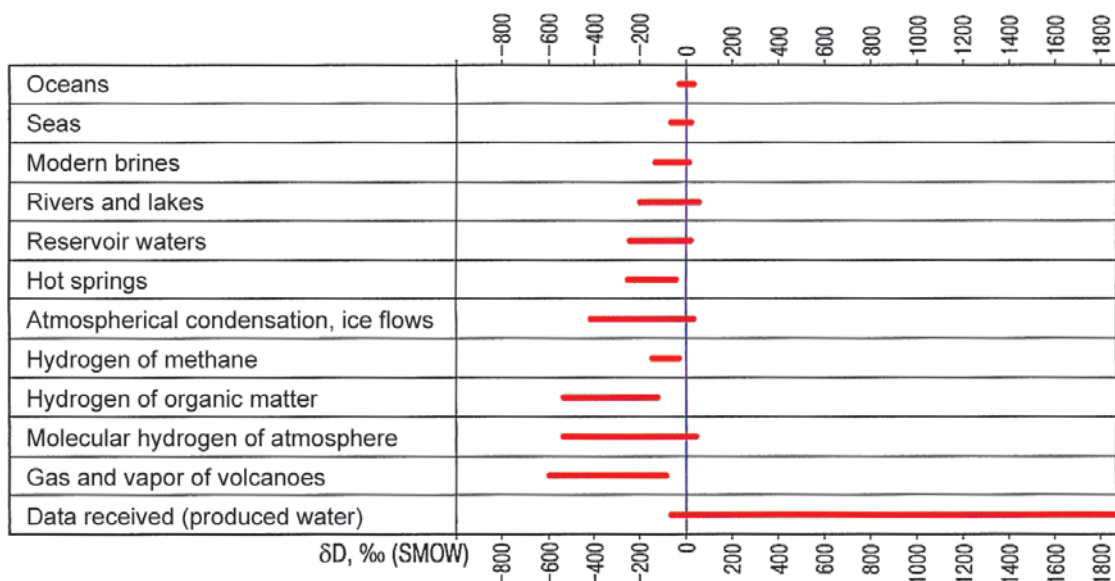
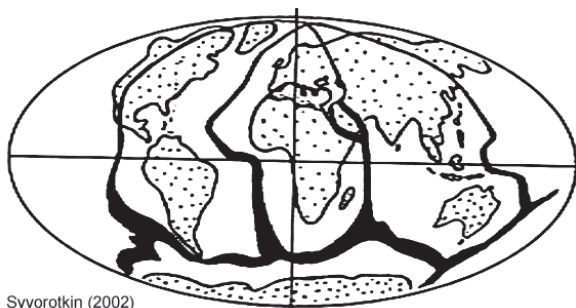


Fig. 7. Variations of hydrogen isotopic composition in natural waters and objects (Zykin, 2012)

### Extent of groundwater decomposition in the Earth's crust

In solving this problem, we proceed from the fact that polycondensation synthesis of hydrocarbons and degassing are processes reflecting different sides of the same phenomenon caused by hydrospheric waters circulation through the Earth's surface and their decomposition in the rocks of the Earth's crust with the formation of hydrocarbons and hydrogen.

Therefore, being connected by formula (1),  $\text{CH}_4$ ,  $\text{CO}_2$  and  $\text{H}_2$  degassing into the atmosphere not only characterize the intensity of the modern HC formation, but also make it possible to judge the mass of water decomposing within the Earth's crust.



Syvorotkin (2002)

Fig. 8. Main degassing channels associated with the world rift system according to V.L. Syvorotkin (2002)

Let us note that the degassing process is exceedingly uneven. According to G.I. Voytov (1986), gas emission in oceans is higher than on the continents. The bulk of the gas enters the atmosphere through the faults of the Earth's crust, primarily through the mid-ocean ridges (Fig. 8).

Maximum degassing occurs in the southern hemisphere of the Earth (Syvorotkin, 2002). The composition of gases and their intensity also vary, showing cyclicity from several minutes to several years (Voytov, 1991). In general, similar amounts of  $\text{CH}_4$  and

$\text{CO}_2$  at a level of  $\sim 2.5 \times 10^{14}$  g/year are degassed from the depths of the globe (Table 2). In later articles (Voytov, 1999; Syvorotkin, 2002), these estimates were increased by about an order of magnitude, so that they can be taken equal to  $\sim 10^{15}$  g/year. Hydrogen degassing rates should also be considered much higher than in Table 2 (Larin et al., 2010).

Let's show that the results of our experiments on the water decomposition satisfy quite well the actual data. To this end, let us assume that annually  $\sim 2 \times 10^{19}$  g of water comes under the surface, which transfers  $\sim 3 \times 10^{16}$  g/year of  $\text{CO}_2$  to the rocks of the Earth's crust. A part of this amount of  $\text{CO}_2$  interacts in rocks with  $\text{H}_2\text{O}$ , participating in hydrocarbons synthesis according to reaction (1). Another unreacted part of  $\text{CO}_2$ , which is about an order of magnitude smaller, degasses into the atmosphere.

Let's consider the part of  $\text{CO}_2$  that took part in the formation of hydrocarbons. According to formula (1), it takes 2.75 g of  $\text{CO}_2$  and at least 2.2 g of  $\text{H}_2\text{O}$  to form 1g of  $\text{CH}_4$ . Let's suppose that all methane formed is degassed from the subsurface. Then, to explain its flux of  $\sim 10^{15}$  g/year into the atmosphere, then  $\sim 2.75 \times 10^{15}$  g of  $\text{CO}_2$  should be consumed annually. Taking into account that  $\text{CO}_2$ , in addition to methane, also participates in the synthesis of heavier hydrocarbons represented by oil and bitumen remained in the depths, for a mass of  $\text{CO}_2$  annually entering the Earth's crust in an amount of  $\sim 3 \times 10^{16}$  g, this estimate looks quite acceptable.

We now turn to the water flow rate. According to the formula (1) an unlimited amount of  $\text{H}_2\text{O}$  may be involved in this reaction. Moreover, the synthesis of hydrocarbons consumes a mass of  $\text{H}_2\text{O}$  approximately 20% less than amount of consumed  $\text{CO}_2$ ; all the excess  $\text{H}_2\text{O}$  goes to the formation of  $\text{H}_2$ . Therefore, if  $\sim 10^{16}$  g of groundwater decomposes annually in the processes of oil and gas formation, this amount is enough to explain

the data of Table 2 on methane and hydrogen.

In this regard, we note that in our experiments was decomposed the maximum  $\sim 0.1 \div 1$  g per liter of carbonated water. If we proceed from this result, then in case of  $\sim 2 \times 10^{19}$  g/year water circulation through the Earth's surface, the decomposition rate of  $H_2O$  will be  $\sim 2 \times 10^{19} \times (10^{-4} \div 10^{-3}) \sim 10^{15} \div 10^{16}$  g/year. That coincides with our estimate of groundwater decomposition rate according to  $CH_4$  and  $CO_2$  degassing data.

Thus, the rate of water decomposition in our experiments is not so far from the rate of this process, on average across the globe.

## Conclusion

The results of the experiments, as well as arguments and facts allow us to state the following:

1. In the Earth's crust, in reactions of hydrocarbon polycondensation synthesis, annually decompose  $\sim 10^{16}$  g of groundwater containing dissolved  $CO_2$ . This process involves not only meteorogenic (on the continents), but also marine (through the mid-ocean ridges and zones of deep faults on the continents) waters.

2. The hydrogen produced during water decomposition, most of the  $CH_4$  and unreacted  $CO_2$  are degassed into the atmosphere, while the HC and part of methane remain in the depths forming oil and gas accumulations in case of favorable conditions. Of course, part of the formed hydrogen combines with  $O_2$  again turning into  $H_2O$ .

3. The main mass of  $CH_4$ ,  $CO_2$  and  $H_2$  is degassed into the atmosphere not from the deep bowels of the Earth, but from the rocks of the Earth's crust and above all from its sedimentary cover. The main role in the processes of oil and gas formation and degassing is played by decomposition of water in the Earth's crust circulating through the surface on the continents. Mass of such water is  $\sim 10^{21}$  g, and its cycle time, like that of the biosphere carbon cycle, is about 40 years (Barenbaum, 2004).

4. It should be assumed that the decomposition of  $H_2O$  mainly occurs in the upper 5 km layer of the Earth's crust. With a mass of free water in this layer of  $\sim 6 \times 10^{22}$  g (Shvarcev, 1996) and a decomposition rate of  $\sim 10^{16}$  g/year, their life time in the underground hydrosphere will be  $\sim 6 \times 10^{22}$  g /  $10^{16}$  g/year, which is approximately  $\sim 6$  million years.

5. Amount of free water on Earth is  $2.1 \times 10^{24}$  g. Of these,  $1.37 \times 10^{24}$  g is in the World Ocean and  $0.73 \times 10^{24}$  g is in the underground hydrosphere. Most of the underground hydrosphere waters-4 are represented by deep-seated waters circulating beneath the continents along permeable horizons, ensuring the geological circulation of water through the mid-ocean ridges. According to data (Baskov, Kiryukhin, 1993), every 8 million years a mass of water equal to the volume of the World Ocean pass through the rift zones of the axial

parts of the middle oceanic ridges. Therefore, the rate of the geological water cycle of the hydrosphere can be found as  $2.1 \times 10^{24}$  g /  $8 \times 10^6$  years =  $2.63 \times 10^{17}$  g/year.

This value coincides with the rate of circulation on Earth of atmospheric oxygen and biospheric carbon, which together with hydrosphere water cycle form a single geochemical system on our planet (Barenbaum, 1998).

These estimates of the rate and extent of groundwater decomposition in the Earth's crust should be taken into account when assessing the petroleum potential of the subsurface.

## Acknowledgments

The author thanks A.N. Pavlov, V.I. Ferronsky and S.N. Zakirov for support and helpful discussions of the problems.

The author is grateful to the reviewer for the questions raised and for a useful discussion of the problems, as well as critical comments which have been very helpful in improving the manuscript.

## References

- Barenbaum A.A. (1998). O postuplenii kosmicheskogo ugleroda i ego krugovorote na Zemle [On the income of cosmic carbon and its circulation on Earth]. *Ekosistemnye perestroiki i evolyutsiya biosfery* [Ecosystem restructuring and the evolution of the biosphere], 3, pp. 15-29. (In Russ.)
- Barenbaum A.A. (2007). Izuchenie uslovii obrazovaniya nefti s ispol'zovaniem teoreticheskoi modeli Andersona-Shul'tsa-Flori [Study of oil formation conditions using the theoretical model of Anderson-Schulz-Flory]. *Vestnik Otdeleniya nauk o Zemle RAN*, 1(25). (In Russ.)
- Barenbaum A.A. (2017). On participation of underground waters in oil and gas formation. *Novye idei v geologii nefti i gaza – 2017: sbornik nauchnykh trudov (po materialam Mezhdunarodnoi nauchno-prakticheskoi konferentsii)* [New ideas in geology of oil and gas – 2017: Coll. papers (based on the proc. of the International Scientific and Practical Conference)]. Ed. A.V. Stupakova. Moscow: Pero publ., pp. 35-39. (In Russ.)
- Barenbaum A.A. (2010). Galaktotsentricheskaya paradigma v geologii i astronomii [Galactocentric paradigm in geology and astronomy]. Moscow: LIBROKOM Publ., 544 p. (In Russ.)
- Barenbaum A.A. (2015). Modern oil and gas generation as a result of carbon cycle in the biosphere. *Georesursy = Georesources*, 1(60), pp. 46-53. (In Russ.)
- Barenbaum A.A. (2017). Oil Origin and Age. *Georesursy = Georesources*, 19(1), pp. 30-37. DOI: <http://doi.org/10.18599/grs.19.1.6>
- Barenbaum A.A. (2015a). On the Problem of the Water Downward Filtration in the Oil-and Gas Bearing Sedimentary Basins. *Georesursy. Geoenergetika. Geopolitika = Georesources, geoenergetics, geopolitics*, 2(12). (In Russ.)
- Barenbaum A.A. (2013). Reshenie problemy proiskhozhdeniya nefti i gaza na osnove biosfernoy konseptsii neftegazobrazovaniya [Solving the problem of the origin of oil and gas on the basis of the biosphere concept of oil and gas formation]. *Ural'skiy geologicheskii zhurnal = Ural Geological Journal*, 2(92), pp. 3-27. (In Russ.)
- Barenbaum A.A. (2004). The Mechanism of Oil-Gas Traps Formation. *Doklady AN = Proc. of the Russian Academy of Sciences*, 399(6), pp. 802-805. (In Russ.)
- Barenbaum A.A. (2014). The Scientific Revolution in the Oil and Gas Origin Issue. New Oil and Gas Paradigm. *Georesursy = Georesources*, 4(59), pp. 9-16. (In Russ.)
- Barenbaum A.A., Ablya E.A. (2009). The molecular mass distribution of normal alkanes of oil as evidence of their polycondensation synthesis. *Organicheskaya mineralogiya. Mater. III Ros. sovesch. [Proc. III All Rus. Meet. «Organic Mineralogy»]*. Syktyvkar, pp. 74-77. (In Russ.)
- Barenbaum A.A., Batalin O.Yu. (2001). Phase transformations of hydrocarbons during the global geochemical cycle. New ideas in the geology and geochemistry of oil and gas. *Neftegazovaya geologiya v XXI veke = Oil and gas geology in the XXI century*, Ch.I, pp. 40-42. (In Russ.)



- Barenbaum A.A., Klimov D.S. (2015). Experimental measurement of the rate of destruction of carbonized water during geosynthesis. *Trudy VESEMPG-2015*. Moscow: GEOKhI RAN, pp. 347-351. (In Russ.)
- Barenbaum A.A., Zakirov S.N., Zakirov E.S., Klimov D.S., Serebryakov V.A. (2015). Physical and Chemical Processes During the Carbonated Water Flooding in the Oilfields. *SPE Russian Petroleum Technology Conference*, Moscow, Russian Federation. SPE-176729-RU
- Barenbaum A.A., Zakirov S.N., Zakirov E.S., Serebryakov V.A. (2012). Method of hydrocarbon and hydrogen production from water and carbon dioxide. U.S. Patent No 20,120,315,215. Washington, DC: U.S. Patent and Trademark Office
- Baskov E.A., Kiryukhin V.A. (1993). Evolyutsiya podzemnoi gidrosfery v istorii Zemli [Evolution of the underground hydrosphere in the history of the Earth]. *Evolutsiya geologicheskikh protsessov v istorii Zemli* [The evolution of geological processes in the history of the Earth]. Moscow: Nauka Publ., pp. 175-182. (In Russ.)
- Batalin O.Yu., Brusilovskii A.I., Zakharov M.Yu. (1992). Fazovye ravновесiya v sistemakh prirodnykh uglevodorodov [Phase equilibria in natural hydrocarbon systems]. Moscow: Nedra, 272 p. (In Russ.)
- Batalin O.Yu., Vafina N.G. (2008). Kondensatsionnaya model' obrazovaniya zalezhei nefi i gaza [Condensation model of oil and gas deposits formation]. Moscow: Nauka, 248 p. (In Russ.)
- Braun D., Masset A. (1984). Nedostupnaya Zemlya [Inaccessible Earth]. Moscow: Mir, 263 p. (In Russ.)
- Cherskiy N.V., Tsarev V.P. (1984). Mechanisms of hydrocarbon synthesis from inorganic compounds in the upper layers of the crust. *Doklady AN = Proc. of the Russian Academy of Sciences*, 279(3), pp. 730-735. (In Russ.)
- Cherskiy N.V., Tsarev V.P., Soroko T.I., Kuznetsov O.L. (1985). Vliyeniye tektono-seismicheskikh protsessov na obrazovanie i nakopleniye uglevodorodov [Influence of tectonic and seismic processes on the formation and accumulation of hydrocarbons]. Novosibirsk: Nauka Publ., 224 p. (In Russ.)
- Dobrynin V.M., Serebryakov V.A. (1989). Geologo-geofizicheskie metody prognozirovaniya anomal'nykh plastovykh davleniy [Geological and geophysical methods for predicting abnormal reservoir pressures]. Moscow: Nedra, 287 p. (In Russ.)
- Ferronskiy V.I., Polyakov V.A. (2009). Izotopiya gidrosfery Zemli [Isotopy of the Earth's hydrosphere]. Moscow: Nauchnyy mir Publ., 632 p. (In Russ.)
- Galkin A.A., Lunin V.V. (2005). Voda v sub- i sverkhkriticheskom sostoyaniyakh – universal'naya sreda dlya osuschestvleniya khimicheskikh reaktsiy [Subcritical and supercritical water: a universal medium for chemical reactions]. *Uspekhi khimii = Russian Chemical Reviews*, 74(1), pp. 24-40. (In Russ.)
- Garrels R.M., Krayst Ch.L. (1968). Rastvory, mineraly, ravновесiya [Solutions, minerals, equilibria]. Moscow: Mir. (In Russ.)
- Gavrilov V.P. (1986). Proishozhdeniye nefi [The origin of oil]. Moscow: Nauka, 176 p. (In Russ.)
- Glebov L.S., Kliger G.A. (1994). Molekulyarno-massovoe raspredeleniye produktov sinteza Fishera-Tropscha [The molecular mass distribution of the products of the Fischer-Tropsch process]. *Uspekhi khimii = Russian Chemical Reviews*, 63(2), pp. 192-202. (In Russ.)
- Karcev A.A., Gattenberger Yu.P., Zor'kin L.M. (1992). Teoreticheskie osnovy neftegazovoy gidrogeologii [Theoretical foundations of oil and gas hydrogeology]. Moscow: Nedra, 208 p. (In Russ.)
- Kondrat'ev K.Ya., Krapivin V.F. (2004). Modelirovaniye global'nogo krugovorota ugleroda [Modeling of the global carbon cycle]. Moscow: Fizmatlit Publ., 336 p. (In Russ.)
- Korzh V.D. (2000). Geokhimiya elementnogo sostava gidrosfery [Geochemistry of the elemental composition of the hydrosphere]. Moscow: Nauka, 243 p. (In Russ.)
- Lapshin V.I. (2000). Fazovye prevrashcheniya gazozhidkostnykh sistem [Phase transformations of gas-liquid systems]. *Gazovaya promyshlennost' = Gas industry*, 2, pp. 11-13. (In Russ.)
- Larin N.V., Larin V.N., Gorbatiykov A.V. (2010). Ring structures due to deep hydrogen flows. *Degazatsiya Zemli: geotektonika, geodinamika, geoflyuidy; nefi i gaz; uglevodorody i zhizn': Mater. Vseros. konf.* [Earth degassing: geotectonics, geodynamics, geofluids; oil and gas; hydrocarbons and life. Proc. All-Russ. conf.]. Moscow: GEOS, pp. 284-288. (In Russ.)
- Levorsen A. (1970). Geologiya nefi i gaza [Geology of oil and gas]. Moscow: Mir, 640 p. (In Russ.)
- L'vovich M.I. (1986). Voda i zhizn' [Water and life]. Moscow: Nauka, 254 p. (In Russ.)
- Molchanov V.I. (1981). Generatsiya vodoroda v litogeneze [Hydrogen generation in lithogenesis]. Novosibirsk: Nauka, 142 p. (In Russ.)
- Molchanov V.I., Gontsov A.A. (1981). Modelirovaniye neftegazobrazovaniya [Modeling of oil and gas formation]. Novosibirsk: OIGGM Publ., 246 p. (In Russ.)
- Molchanov V.I., Selezneva O.G., Zhirnov E.N. (1988). Aktivatsiya mineralov pri izmel'chenii [Activation of minerals during grinding]. Moscow: Nedra Publ. (In Russ.)
- Semenov A.P., Zakirov Ye.S., Klimov D.S. (2014). Sravnitel'nye laboratornye issledovaniya protsessov geosinteza na model'nykh obraztsakh geologicheskikh sred [Comparative laboratory studies of geosynthesis processes on model samples of geological media]. *Tekhnologii nefi i gaza* [Oil and gas technologies], 4(93), pp. 38-44. (In Russ.)
- Semenov N.N. (1959). Osnovnyye problemy himicheskoy kinetiki [The main problems of chemical kinetics]. Moscow: Academy of Science USSR. (In Russ.)
- Shvarcev S.L. (1996). Obshchaya gidrogeologiya [General hydrogeology]. Moscow: Nedra, 423 p. (In Russ.)
- Shvarcev S.L. (1975). Razlozheniye i sintez vody v protsesse litogeneza [Decomposition and synthesis of water in the process of lithogenesis]. *Geologiya i geofizika = Russian Geology and Geophysics*, 5, pp. 60-69. (In Russ.)
- Sokolov B.A., Ablya E.A. (1999). Flyuidodinamicheskaya model' neftegazobrazovaniya [Fluid dynamic model of oil and gas formation]. Moscow: GEOS Publ., 76 p. (In Russ.)
- Sokolov B.A., Guseva A.N. (1993). O vozmozhnosti bystroy sovremennoy generatsii nefi i gaza [On the possibility of fast modern oil and gas generation]. *Vestnik MGU. Geol. Ser. = Moscow University Geology Bulletin*, 3, pp. 48-56. (In Russ.)
- Sokolov V.A. (1971). Geokhimiya prirodnykh gazov [Geochemistry of natural gases]. Moscow: Nedra Publ., 336 p. (In Russ.)
- Strahov N.M. (1960, 1962). Osnovy teorii litogeneza [Fundamentals of the theory of lithogenesis]. Moscow: AN SSSR, V.1, V.2, V.3 (In Russ.)
- Syvorotkin V.L. (2002). Glubinnaya degazatsiya Zemli i global'nye katastrofy [Deep degassing of the Earth and global natural hazards]. Moscow: Geoinformtsentr Publ., 250 p. (In Russ.)
- Trofimuk A.A., Cherskiy N.V., Carev V.P., Soroko T.I. (1982). Yavleniye preobrazovaniya organicheskogo veshchestva osadochnykh porod pod deystviem tektonicheskikh i seismicheskikh protsessov zemnoy kory [The phenomenon of transformation of organic matter in sedimentary rocks under the influence of tectonic and seismic processes of the Earth's crust]. Invention Certificate No. 326. (In Russ.)
- Uolter Dzh., Vud B. (1989). Vzaimodeystviye flyuid-poroda pri metamorfizme [Fluid rock interaction during metamorphism]. Moscow: Mir, 248 p. (In Russ.)
- Vernadskiy V.I. (1960). Izbrannyye sochineniya [Selected Works]. Moscow: AN SSSR Publ., vol. V (In Russ.)
- Vernadskiy V.I. (2001). Khimicheskoe stroeniye biosfery Zemli i ee okruzeniye [The chemical structure of the Earth's biosphere and environment]. Moscow: Nauka Publ., 376 p. (In Russ.)
- Vityazev A.V., Pechernikova G.V., Safronov V.S. (1990). Planety zemnoy gruppy. Proiskhozhdeniye i rannyya evolyutsiya [Planets of the Earth group Origin and early evolution]. Moscow: Nauka, 295 p. (In Russ.)
- Voytov G.I. (1999). Cold methane drainage in Earth's troposphere. Theoretical and regional problems of geodynamics. *Tr. GIN RAN* [Proc. of the Geological Institute of the Russian Academy of Sciences]. Moscow: Nauka Publ., vol. 515, pp. 242-251. (In Russ.)
- Voytov G.I. (1986). Khimizm i masshtaby sovremennoy potoka prirodnykh gazov v razlichnykh geostrukturnykh zonakh Zemli [The chemistry and the magnitude of the modern flow of natural gas in various zones of the Earth geotectonic zones]. *Zhurn. vsesoyuz. khim.* [Journal of the All-Union Chemical Society], 31(5), pp. 533-539. (In Russ.)
- Voytov G.I. (1991). O khimicheskoy i izotopno-uglerodnoy nestabil'nosti svobodnykh gazov (gazovykh struy) v Khibinakh [On the chemical and isotopic-carbon instability of free gas (gas jets) in the Khibins]. *Geokhimiya = Geochemistry*, 6, pp. 769-780. (In Russ.)
- Zakirov S.N., Zakirov Ye.S., Barenbaum A.A. et al. (2013). Natural Geosynthesis of Hydrocarbons and Consequences. *Tr. IV Mezhd. nauchnyy simpozium: Teoriya i praktika primeneniya metodov uvelicheniya nefteotdachi plastov* [Proc. IV Int. Scientific Symposium: Theory and practice of application of enhanced oil recovery methods]. Moscow: VNIIneft', v. I, pp. 130-135. (In Russ.)
- Zekcer I.S., Dzhamalov R.G. (1989). Podzemnyye vody v vodnom balanse krupnykh regionov [Groundwaters in the water balance of large regions]. Moscow: Nauka, 125 p. (In Russ.)
- Zharkov V.N. (1983). Vnutrennee stroeniye Zemli i planet [The internal structure of the Earth and planets]. Moscow: Nauka, 416 p. (In Russ.)

Zverev V.P. (2007). Podzemnye vody zemnoy kory i geologicheskie processy [Groundwaters of the Earth crust and geological processes]. Moscow: Nauchnyy mir, 256 p. (In Russ.)

Zykin N.N. (2012). Poputnye vody neftegazokondensatnykh mestorozhdeniy kak netraditsionnoe syr'e dlya gazokhimicheskogo proizvodstva [Passing water of oil and gas fields as unconventional raw material for gas and chemical production]. *Gazovaya promyshlennost'. Netraditsionnye resursy nefii i gaza* [Gas industry. Spec. Is.: Unconventional oil and gas resources], pp. 38-42. (In Russ.)

### About the Author

*Azariy A. Barenbaum* – PhD (Physics and Mathematics), Leading Researcher

Institute of Oil and Gas Problems of the Russian Academy of Sciences

3, Gubkina st., Moscow, 119333, Russian Federation

*Manuscript received 12 July 2018;*

*Accepted 4 October 2018;*

*Published 30 November 2018*



# Effect of biodegradation processes on the composition and structure of asphaltenes in West Siberian oils

L.S. Borisova<sup>1,2\*</sup>, E.A. Fursenko<sup>1,2</sup>

<sup>1</sup>Trofimuk Institute of Petroleum Geology and Geophysics of Siberian Branch of Russian Academy of Sciences, Novosibirsk, Russian Federation

<sup>2</sup>Novosibirsk State University, Novosibirsk, Russian Federation

**Abstract.** NMR spectroscopy in combination with elemental analysis was used to study asphaltenes in biodegraded oils from Cenomanian pools of West Siberia. The sampling depths vary from 680 to 1800 m, formation temperatures – from 40°C to 70°C. For comparison, we used the data on asphaltenes in non-biodegraded oils of different genotypes. Given that biodegraded oils are very heavy (density: 910-950 kg/m<sup>3</sup>), they are characterized by high boiling point temperatures (145-270°C). Due to the loss of hydrocarbon components, they have higher resin and asphaltene content (9-20%) compared to non-degraded samples. Elemental analysis of asphaltenes in biodegraded and unaltered oils of different genotypes revealed an increasing trend for oxygen content in the asphaltenes from biodegraded samples, which may result from the oxidation of structural blocks of asphaltenes during microbial oxidation. It was shown that the aromaticity of the moderately biodegraded terrestrial-aquatic Novoaganskaya samples tends to increase with a decrease in asphaltene saturation, suggesting that the redistribution of structural groups of asphaltenes may be caused by biodegradation processes. High saturation of asphaltenes in strongly biodegraded Gubkinskaya and Novoportovskaya oils, along with a high degree of substitution of aromatic compounds in asphaltenes in Gubkinskaya oils (terrestrial and aquatic-terrestrial genotype) can be attributed to the formation of asphaltenes during strong biodegradation of hydrocarbon components in these oils.

**Keywords:** asphaltenes, oil, biodegradation, West Siberia

**Recommended citation:** Borisova L.S., Fursenko E.A. (2018). Effect of biodegradation processes on the composition and structure of asphaltenes in West Siberian oils. *Georesursy = Georesources*, 20(4), Part 1, pp. 301-307. DOI: <https://doi.org/10.18599/grs.2018.4.301-307>

Establishing patterns of changes in the properties of oils in the hypergenesis zone since the middle of the last century is an important task of geochemical research, both for the development of the theory of naphthidogenesis, and for solving practical problems aimed at predicting the quality of hydrocarbon fluids. The active influence of hypergenesis is characteristic of shallow oil deposits with low reservoir temperatures, which are often located in the zone of infiltration of meteoric waters. Vassoevich and Amosov (1953) identified two zones of hypergenesis: the lower – cryptohypergenesis, which is characterized by anaerobic environments; upper idiohypergenesis associated with aerobic conditions. Even in the works (Uspensky, Radchenko, 1947; Vassoevich, Amosov, 1953) it was noted that with the active influence of hypergenesis from the bottom upwards along the section, the oil becomes heavier, more resinous, depleted of paraffins and enriched with naphthenic components. To date, it has been established that the most important

factor of hypergenesis, affecting the change in the group and component composition of oils, is their microbial oxidation (Rozanova, Kuznetsov, 1974; Petrov, 1984; Kurbsky, 1987; Kashirtsev, 2003; Philippi, 1977; Peters et al, 2005; Mullins et al., 2007, etc.), which grows from cryptohypergenesis to the idiohypergenesis zone. During biodegradation, mainly hydrocarbons are utilized, with the rate of microbial oxidation decreasing in a certain sequence – from n-alkanes to acyclic isoprenanes and further to polycyclic naphthenes. On the basis of indicators on the hydrocarbon composition, it has been established (Goncharov, 1987; Kontorovich et al., 1991; Fursenko, Borisova, 2006; Peters et al, 1994, etc.) that in West Siberia biodegraded oils are characteristic of shallow Aptian-Albian-Cenomanian and, partly, Barremian pools, where thermo- (reservoir temperatures <70°C) and hydrodynamic conditions are favorable for microbial oxidation of hydrocarbon fluids. In recent years, studies have discussed the effect of biodegradation on the composition and structure of asphaltenes (Gordadze et al., 2015; Mullins et al., 2007; Silva et al., 2008; Meredith et al., 2008; Liao et al., 2009; Snowdon et al., 2016, etc.). The chemical and geochemical features of asphaltenes in West Siberian

\*Corresponding author: Lyubov S. Borisova  
E-mail: [BorisovaLS@ipgg.sbras.ru](mailto:BorisovaLS@ipgg.sbras.ru)

© 2018 The Authors. Published by Georesursy LLC  
This is an open access article under the CC BY 4.0 license  
(<https://creativecommons.org/licenses/by/4.0/>)



oils was the focus of many previous studies (Borisova, 2009; Golovko et al., 2010), however, variability of these parameters during biodegradation was not discussed.

The aim of the work is to study the effect of microbial oxidation on the composition and structure of asphaltenes in the oils of West Siberia. Asphaltenes isolated from biodegraded oils from Cenomanian pools (9 samples) were analyzed. For comparative analysis, we used the data on asphaltenes from non-degraded oils of different genotypes (96 samples).

In the designation of genetic types we used the following classification of West Siberian oils proposed by Kontorovich and Stasova (1964): aquatic ( $C_1$ ) – oils, that were generated by organic matter derived from marine deep-water sediments with hydrogen sulfide contamination, they have high to moderate density, high contents of sulfur, resins and asphaltenes, and are distributed, mainly, in Middle Ob' Region; terrestrial ( $A_1$ ) – oils that are genetically associated with organic matter derived from higher terrestrial plants, lakustrine plankton and benthos, they have light to medium density, and are low in sulfur, resins and asphaltenes, and have high concentrations of solid paraffins, these oils are localized in the northern and arctic regions of the West Siberia; mixed  $C_2$  and  $A_2$  oils replace successively aquatic crudes for terrestrial ones from the Middle Ob' Region to the north. Biodegraded oils, according to previous studies (Petrov, 1984; Goncharov, 1987; Kontorovich et al., 1991; Fursenko, Borisova, 2006; Peters et al., 1994, etc.), are usually very heavy, and have high contents of asphaltenes and resins; on chromatograms (gas/liquid chromatography) they are characterized by a distinct unresolved “naphthenic hump”. N-alkanes in these oils are either absent or present in very low concentrations.

Genetic typification of the studied oils, which was based on the data on physicochemical properties, isotopic composition and distribution of hydrocarbon biomarkers (pristane/phytane,  $C_{29}/C_{27}$  steranes,  $C_{35}/C_{34}$  homohopanes,  $C_{19}-C_{20}/C_{23}-C_{26}$  tricyclic terpanes, etc.) and their spatial localization was discussed in previous studies (Goncharov, 1987; Kontorovich et al., 1991; Peters et al., 1994). In the studied collection, 4 genetic groups of non-biodegraded oils (Fig. 1) are distinguished: predominantly aquatic (16 samples) and predominantly terrestrial (5 samples) genotype; and two groups of mixed genotypes – aquatic-terrestrial (31 samples) and terrestrial-aquatic (44 samples). Biodegraded oils have been identified by gas/liquid chromatography. These oils were collected from Cenomanian pools ( $K_{2c}$ ) from depths of 680-1800 m with reservoir temperatures  $< 70^\circ\text{C}$ . Such conditions are favorable for the microbial oxidation (Rozanov, Kuznetsov, 1974; Petrov, 1984; Goncharov, 1987; Kashirtsev, 2003, etc.). Severely biodegraded oils from the Gubkinskaya and Srednemosoyakhskaya prospects are characterized

by the absence of n-alkanes and acyclic isoprenanes, the presence of 25-norhopanes in the m/z 177 mass-fragmentograms. The remaining samples are only slightly biodegraded oils. Analysis of the distribution of polycyclic biomarkers (steranes and terpanes) shows that samples from the Novoportovskaya, Messoyakhskaya, Srednemosoyakhskaya, Gubkinskaya and Ereminskaya prospects can be attributed predominantly to the terrestrial genotype, whereas samples from the Novoaganskaya prospect are of terrestrial-aquatic genotype.

Biodegraded oils differ significantly from non-biodegraded oils by their physico-chemical properties and group composition (Table 1). Due to the loss of hydrocarbon components, they have higher contents of resins and asphaltenes (9-20%). These are very heavy oils (910-950 kg/m<sup>3</sup>). The biodegraded oils are characterized by a high bubble point (145-270°C). All these characteristics are consistent with our recent understanding of biodegraded oils (see above).

Unlike biodegraded oil samples of a mixed genotype (Novoaganskaya prospect), the biodegraded mostly terrestrial oils (Ereminskaya, Novoportovskaya, Messoyakhskaya and Srednemosoyakhskaya prospects) have lower sulfur, resin and asphaltene contents, while paraffins are either absent or present in trace amounts. The latter may be caused by a strong degree of biodegradation rather than by genetic reasons (Petrov, 1984; Kashirtsev, 2003; Peters et al., 2005, etc.).

### Asphaltene Analysis

The separation of asphaltenes was carried out with petroleum ether with a boiling point of 40-70°C in a ratio 1:40 (Kontorovich, 1973). The composition and structure of asphaltenes were studied by nuclear magnetic resonance spectroscopy (NMR) in combination with elemental analysis.

The high resolution NMR method of protons (PMR), together with data on the elemental composition (integral structural analysis) (Brown et al., 1960; Borisova, 2012), provides information on the distribution of hydrogen and carbon between various structural elements of complex organic compounds. The PMR spectra were studied on a Bruker spectrometer with an operating frequency of 200 MHz. According to the PMR and elemental analysis, the carbon content was calculated in various structural groups of asphaltenes: saturated ( $C_{\text{sat}}$ : in methylene, methine and methyl groups, distant from the aromatic ring and replacing hydrogen aromatic structures) and aromatic ( $C_{\text{ar}}$ : in condensed and peripheral positions). The carbon content in naphthenic structures ( $C_{\text{naph}}$ ) is not included in the 100% of the above groups, but can be quantified as percent of saturated structures. Determination of the mass proportion of carbon, hydrogen, sulfur and nitrogen was carried out on a Flash EA2000 CNHS analyzer. The physical and

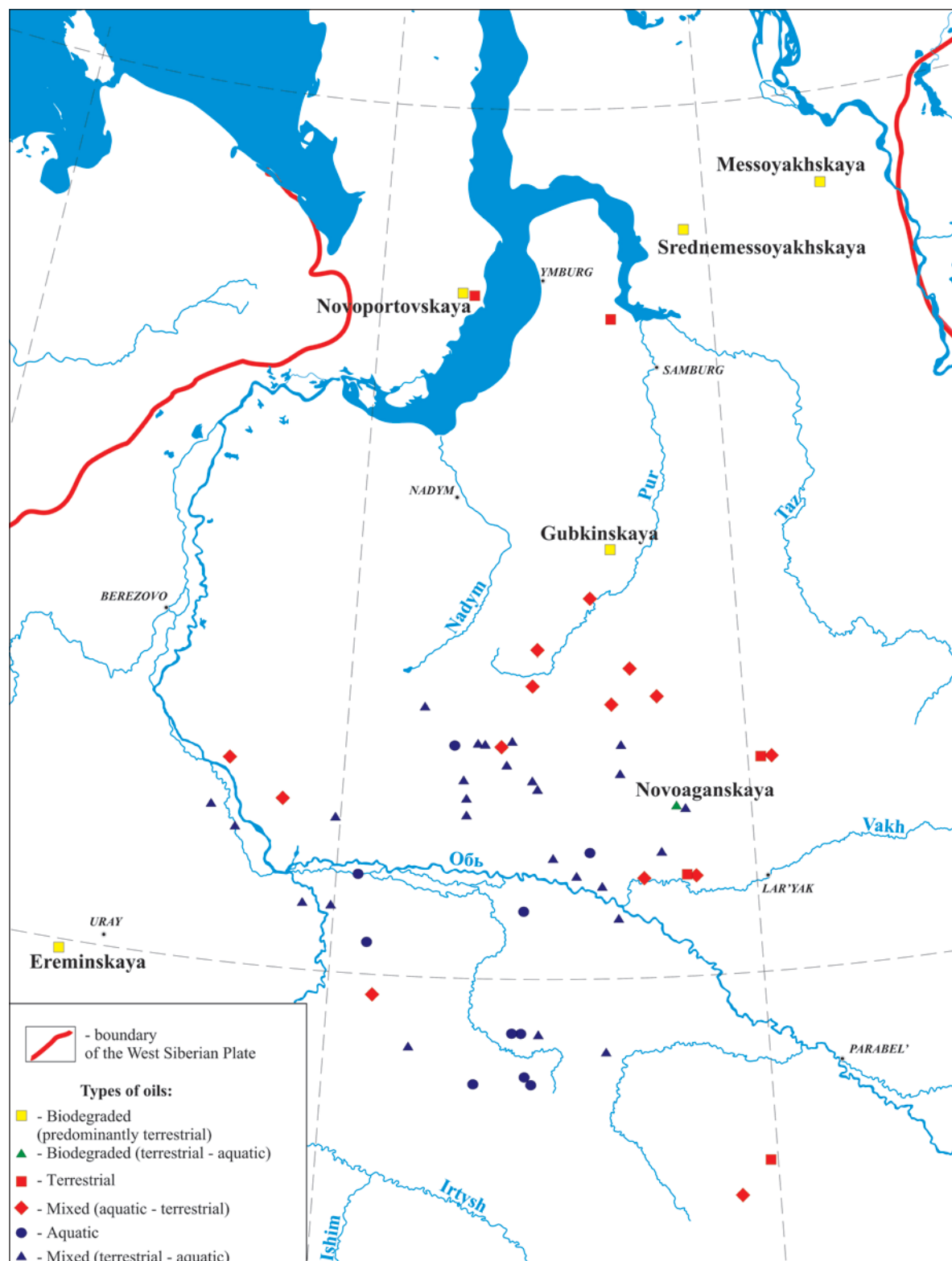


Fig. 1. Schematic map of oil sampling points

physicochemical methods of asphaltene analysis as well as the parameters of spectra acquisition and processing were discussed in detail in Borisova (2012).

### Discussion

The studied samples are characterized by the elemental composition typical of asphaltenes (Table 2, Fig. 2a, b). The hydrogen content of asphaltenes in

biodegraded oils varies from 7.52 to 8.83%, and the carbon/hydrogen atomic ratio ( $(H/C)_{at}$ ) varies from 1.04 to 1.30. They also contain 0.71-1.87% sulfur and 0.30-7.05% oxygen.

The asphaltenes from predominantly terrestrial oils, both biodegraded and non-biodegraded, have lower hydrogen and sulfur contents, lower  $(H/C)_{at}$  ratio compared to aquatic and terrestrial-aquatic

Prospect, well	Depth, m	Density, kg/ m <sup>3</sup>	S, %	Paraffins, %	Resins, %	Asphaltenes, %	Resins/Asphaltenes
<b>Biodegraded oils (terrestrial - aquatic genotype)</b>							
Novoaganskaya, 197	1734-1738	935.1	0.50	2.50	12.90	3.75	3.44
Novoaganskaya, 197	1574-1578	938.5	0.52	0.63	14.46	4.66	3.10
Novoaganskaya, 196	1302-1307	945.6	0.54	0.69	14.92	4.48	3.33
Novoaganskaya, 201	1204-1207	948.1	0.59	0.34	12.16	1.94	6.27
<b>Average values</b>		<b>941.8</b>	<b>0.54</b>	<b>1.04</b>	<b>13.61</b>	<b>3.71</b>	<b>4.04</b>
<b>Biodegraded oils (terrestrial and aquatic - terrestrial genotype)</b>							
Gubkinskaya, 642	1396-1398	914.3	0.37	1.78	7.63	0.43	17.74
Ereminskaya, 5	612-625	950.0	-	0.00	17.10	2.60	6.58
Messoyahskaya, 31	897-899	953.1	0.23	0.01	11.40	1.49	7.65
, 46	888-897	910.0	-	0.00	8.70	0.40	21.75
Srednemesoyahskaya, 25	887-894	953.9	0.24	0.05	9.10	1.97	4.62
<b>Average values</b>		<b>936.3</b>	<b>-</b>	<b>0.37</b>	<b>10.79</b>	<b>1.38</b>	<b>11.67</b>
<b>Genetic types of non-biodegraded oils in the studied collection (average values and scatter)</b>							
A <sub>1</sub> (terrestrial)		858/ (830-887)	0.27/ (0.09-0.56)	8.10/ (3.49-28.10)	5.44/ (2.53-9.83)	0.91/ (0.40-4.14)	4.24/ (1.17-8.47)
A <sub>2</sub> (mixed, aquatic - terrestrial)		851/ (755-918)	0.46/ (0.11-0.83)	3.76/ (2.60-5.68)	7.14/ (1.81-20.24)	1.72/ (0.12- 4.52)	5.24/ (1.51-15.08)
C <sub>1</sub> (aquatic)		887/ (829-925)	1.34/ (0.86-2.17)	3.64/ (2.39-4.59)	9.20/ (3.48-15.61)	4.69/ (0.28-11.16)	3.66/ (0.71-12.43)
C <sub>2</sub> (mixed, terrestrial - aquatic)		874/ (843-926)	0.88/ (0.26-1.77)	3.53/ (1.28-5.43)	12.33/ (4.34-27.58)	2.55/ (0.35-8.10)	7.00/ (1.22-27.66)

Table 1. Physical and chemical characteristics of oils

Prospect, well	Depth, m	Elemental composition, %					(H/C) <sub>at</sub>
		C	H	S	O	N+O+S	
Biodegraded oils (terrestrial - aquatic genotype)							
Novoaganskaya, 197	1734-1738	86.02	8.22	1.79	2.97	5.76	1.15
Novoaganskaya, 197	1574-1578	84.09	8.14	1.34	5.43	7.77	1.16
Novoaganskaya, 196	1302-1307	85.15	8.00	-	4.35	6.85	1.13
Novoaganskaya, 201	1204-1207	88.23	8.73	0.78	1.26	3.04	1.19
Average values		85,87	8.27	1.30	3.50	5.86	1.16
Biodegraded oils (terrestrial and aquatic - terrestrial genotype)							
Gubkinskaya, 642	1396-1398	82.35	8.89	0.71	7.05	8.76	1.30
Ereminskaya, 5	612-625	87.07	7.52	1.87	2.71	5.45	1.04
Messoyakhskaya, 31	897-899	86.15	8.06	1.02	4.77	5.79	1.12
, 46	888-897	85.38	8.23	0.91	4.46	6.39	1.16
Srednemesoyakhskaya, 25	887-894	83.55	7.54	1.26	6.65	8.91	1.08
Average values		84,90	8.05	1.15	5.13	7.06	1.14
Genetic types of non-biodegraded oils in the studied collection (average values and scatter)							
A <sub>1</sub> (terrestrial)		85.64/ (83.13-88.77)	7.57/ (7.11-7.90)	1.32/ (1.19-1.62)	4.74/ (1.88-6.67)	6.79/ (4.12-9.01)	1.06/ (0.96-1.14)
A <sub>2</sub> (mixed, aquatic - terrestrial)		86.57/ (82.76-88.64)	7.83/ (7.26-8.49)	1.64/ (0.48-2.69)	3.05/ (0.54-6.68)	5.60/ (3.19- 9.33)	1.09/ (1.01-1.18)
C <sub>1</sub> (aquatic)		85.80/ (80.03-87.97)	8.17/ (7.72-8.81)	2.80/ (2.49-3.41)	1.22/ (0.20-4.47)	6.82/ (3.69-13.86)	1.14/ (1.08-1.24)
C <sub>2</sub> (mixed, terrestrial - aquatic)		85.33/ (81.59-88.20)	8.08/ (7.51-8.77)	2.51/ (1.17-4.71)	3.39/ (0.47-6.95)	6.60/ (3.03-10.29)	1.13/ (1.05-1.21)

Table 2. Elemental composition of asphaltenes in oils



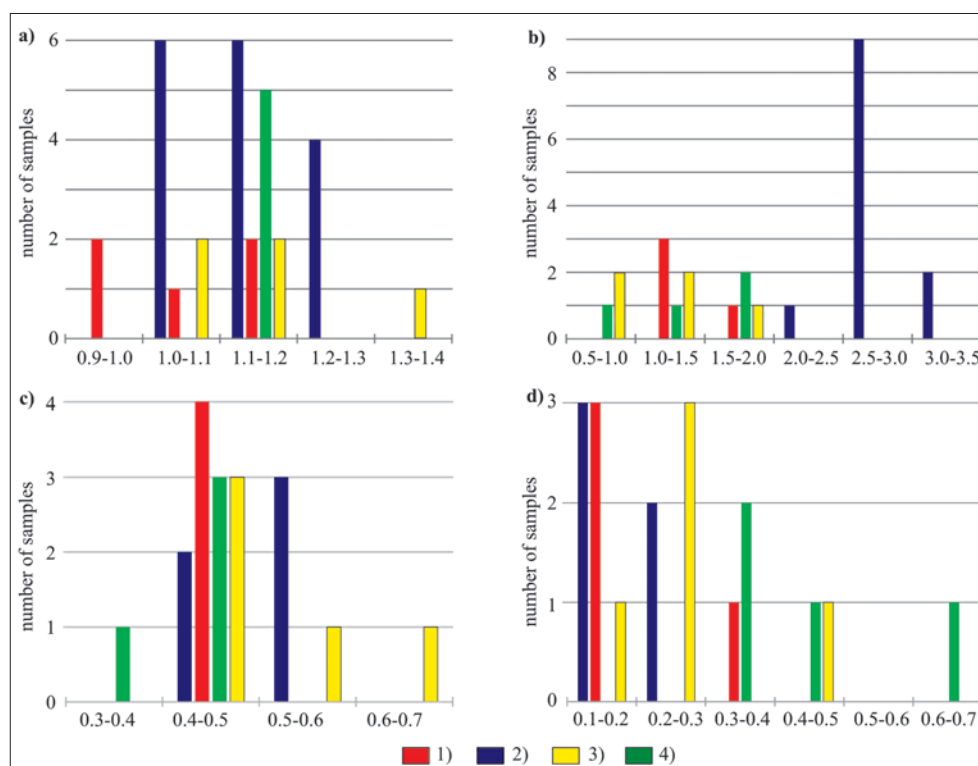


Fig. 2. Histograms of the distribution of elemental parameters: (a)  $(H/C)_{at}$ ; b) S, %) and group composition (c) saturation; d) naphthenic content) of the asphaltenes studied. 1) terrestrial genotype; 2) aquatic genotype; 3) biodegraded samples (predominantly terrestrial genotype); 4) biodegraded samples (terrestrial-aquatic genotype)

samples. However, a comparison of the  $(H/C)_{at}$  ratio by genetic groups shows that this indicator is higher for biodegraded samples. For example, the highest value of this ratio is observed in the asphaltene from severely biodegraded Gubkinskaya oil (1.30), which is classified to be of aquatic-terrestrial genotype, whereas the average value of this ratio in non-biodegraded oils of this group is 1.09 (Table 2). The  $(H/C)_{at}$  ratio varies from 1.16 for asphaltenes in moderately biodegraded Novoportovskaya oil to 1.13 for asphaltenes in non-biodegraded Novoportovskaya oil. It should be noted that asphaltenes in severely biodegraded Gubkinskaya (7.05%) and Srednemessoyakhskaya (6.65%) samples have high oxygen concentrations. Asphaltenes in the moderately biodegraded oils from the Novoaganskaya prospect have higher oxygen content (1.26-5.43%) than those in non-biodegraded oils (1.11%). Based on the results of the experiment on the microbial oxidation of oil from the Ashalchinskoe field, Filatov et al. (2017) showed that these parameters tend to increase in an experimentally biodegraded sample.

Let us consider the features of the structural-group composition of the studied asphaltenes obtained by the PMR method. The studied asphaltenes have almost similar saturation and aromaticity values (Table 3), and the average proportion of naphthenic structures in the composition of saturated ones does not exceed 0.3, except for biodegraded Novoaganskaya samples. The saturation of terrestrial non-degraded samples is lower compared

to aquatic ones, and their naphthenic content, on the contrary, is higher. Several asphaltenes in biodegraded oils of predominantly terrestrial genotype (Gubkinskaya and Novoportovskaya prospects) are characterized by the highest saturation (Table 3), which is significantly higher than that of asphaltenes in non-degraded terrestrial and aquatic samples. Thus, for example, the saturation of asphaltene in non-degraded Novoportovskaya oil is 0.49, and that of biodegraded Novoportovskaya oil is 0.63. At the same time, the naphthenic content of the biodegraded Gubkinskaya sample is comparable to that of the non-degraded terrestrial samples. This sample is also characterized by a high substitution value of aromatic structures and their low condensation. The naphthenic content of the asphaltenes in biodegraded Novoportovskaya oil is higher (0.47) than that of asphaltenes in the non-degraded sample (0.19), and the condensation of the aromatic structures of these asphaltenes is the lowest in the studied collection. The biodegraded terrestrial-aquatic Novoaganskaya samples are characterized by relatively low saturation and strong aromaticity compared to non-degraded aquatic samples. The condensation and substitution of the aromatic structures of the Novoaganskaya asphaltenes show the same variability in the corresponding genetic group of non-degraded samples. The studied asphaltenes of different oil types exhibit no distinct trend in the distribution of saturated structural blocks (methylene and methine groups located in chains and rings far

Prospect, well	Depth, m	Saturation	romaticity	Substitution	Condensation	Naphthenic content
<b>Biodegraded oils (terrestrial - aquatic genotype)</b>						
Novoaganskaya, 197	1734-1738	0.37	0.63	0.08	0.47	0.67
Novoaganskaya, 197	1574-1578	0.46	0.54	0.41	0.63	0.38
Novoaganskaya, 196	1302-1307	0.45	0.55	0.27	0.65	0.42
Novoaganskaya, 201	1204-1207	0.47	0.53	0.43	0.58	0.38
<b>Average values</b>		<b>0.44</b>	<b>0.56</b>	<b>0.30</b>	<b>0.58</b>	<b>0.46</b>
<b>Biodegraded oils (terrestrial and aquatic - terrestrial genotype)</b>						
Gubkinskaya, 642	1396-1398	0.60	0.40	0.79	0.51	0.20
Ereminskaya, 5	612-625	0.49	0.51	0.46	0.77	0.24
Messoyakhskaya, 31	897-899	0.45	0.55	0.41	0.64	0.21
, 46	888-897	0.63	0.37	0.50	0.11	0.47
Srednemessoyakhskaya, 25	887-894	0.48	0.52	0.56	0.59	0.22
<b>Average values</b>		<b>0.53</b>	<b>0.47</b>	<b>0.54</b>	<b>0.52</b>	<b>0.27</b>
<b>Genetic types of non-biodegraded oils in the studied collection (average values and scatter)</b>						
A <sub>1</sub> (terrestrial)		0.47/(0.45-0.49)	0.53/ (0.51-0.55)	0.52/ (0.47-0.61)	0.68/ (0.41-0.89)	0.23/ (0.18-0.35)
A <sub>2</sub> (mixed, aquatic - terrestrial)		0.45/(0.38-0.52)	0.55/ (0.48-0.62)	0.33/ (0.08-0.60)	0.66/ (0.41-0.94)	0.29/ (0.18-0.43)
C <sub>1</sub> (aquatic)		0.52/(0.46-0.58)	0.48/ (0.42-0.54)	0.58/ (0.49-0.65)	0.77/ (0.58-0.88)	0.20/ (0.17-0.23)
C <sub>2</sub> (mixed, terrestrial - aquatic)		0.51/(0.35-0.58)	0.49/ (0.42-0.60)	0.46/ (0.18-0.75)	0.54/ (0.21-0.95)	0.26/ (0.16-0.47)

Table 3. Parameters of the group composition of asphaltenes in oils (according to the PMR and elemental analysis). Saturation – the proportion of carbon in saturated structures; aromaticity – the proportion of aromatic carbon; substitution – the proportion of aromatic peripheral carbon in which hydrogen is replaced by saturated structures; condensation – the proportion of carbon in the condensation cores of aromatic structures; naphthenic content – the proportion of carbon in cycloaliphatic saturated structures

away from the aromatic cores ( $CCH_3^{\beta\gamma}$  and  $C(CH_2+CH)^{\beta\gamma}$ , respectively); substituents located in the  $\alpha$ -position to the aromatic rings ( $C^\alpha$ )).

## Conclusion

Analysis of the elemental composition of asphaltenes in biodegraded and non-biodegraded oils of different genotypes reveals an increase in the  $(H/C)_{at}$  ratio and oxygen content of asphaltenes in biodegraded oils, which may be caused by the oxidation of various structural blocks of asphaltene complexes during microbial oxidation of crude oils.

A comparative analysis of the compositional and structural parameters of asphaltenes obtained by the PMR method reveals differences in biodegraded oils as a function of their genetic type. These data were used to identify at least two structural types of asphaltenes in the studied biodegraded oils from the shallow Cenomanian pools of West Siberia. Moderately biodegraded Novoaganskaya oils (terrestrial-aquatic genotype) differ from non-degraded ones of the same genotype by an increase in aromaticity and a decrease in the saturation of asphaltenes. Such changes in the group composition of asphaltenes may be indicative of the redistribution of structural groups of asphaltenes due to the microbial oxidation of oils. The high saturation

of asphaltenes in the severely biodegraded Gubkinskaya and Novoportovskaya oils and, at the same time, the high substitution of aromatic structures in the asphaltenes from Gubkinskaya oil may be due to the formation of new asphaltene complexes with the increasing degree of biodegradation of hydrocarbon components in these oils.

## Acknowledgements

This work was supported by the Russian Foundation for Basic Research Project No. 18-05-00786.

The authors are grateful to the reviewer for valuable critical comments and recommendations which have been very helpful in improving the work.

## References

- Borisova, L.S. (2012). Introduction to the geochemistry of high-molecular components of petroleum: Textbook. Novosibirsk: NGU, 90 p. (In Russ.)
- Borisova, L.S. (2009). Geochemistry of oil asphaltenes of Western Siberia. *Geologia nefi i gaza = Oil and gas geology*, 1, pp. 76-80. (In Russ.)
- Brown J.K., Ladner W.R., Sheppard N. (1960). A study of the hydrogen distribution in coal-like materials by high resolution nuclear magnetic resonance spectroscopy. 1: The measurement and interpretation of the spectra. *Fuel*, 39(1), pp. 79-86.
- Filatov D.A., Krivtsov E.B., Sviridenko N.N., Golovko A.K., Altunina L.K. (2017). Biogenic oxidation of the high-viscosity oil of the Ashal'chinskoe field and its hetero compounds. *Neftekhimiya = Petroleum chemistry*, 57(4), pp. 386-393. (In Russ.)
- Fursenko E.A., Borisova L.S. (2006). The role of biodegradation processes in the formation of oil and condensate composition in Lower Cretaceous deposits of Western Siberia. *Geologia, geofizika i razrabotka*

*neftyanikh mestorozhdenii = Geology, Geophysics and Development of Oil and Gas Fields*, 4, pp. 44-51. (In Russ.)

Golovko A.K., Gorbunova L.V., Kam'yanov V.F. (2010). The regularities in the structural group composition of high molecular heteroatomic petroleum components. *Geologia i geofizika = Russian Geology and Geophysics*, 51(3), pp. 364-374. <https://doi.org/10.1016/j.rgg.2010.02.005> (In Russ.)

Goncharov I.V. (1987). *Geochemistry of West Siberia oils*. Moscow: Nedra, 181 p. (In Russ.)

Gordadze, G.N., Giruts M.V., Koshelev V.N., Yusupova T.N. (2015). Distribution features of biomarker hydrocarbons in asphaltene thermolysis products of different fractional compositions (using as an example oils from carbonate deposits of Tatarstan oilfields). *Neftekhimiya = Petroleum chemistry*, 55(1), pp. 22-31. <https://doi.org/10.1134/S0965544115010053> (In Russ.)

Kashirtsev V.A. (2003). Organic geochemistry of naphthides in eastern Siberian Platform. Yakutsk: SO RAN publ., 160 p. (In Russ.)

Kontorovich A.E., Peters K.E., Moldowan J.M., Andrushevich V.T., et al. (1991). Biomarker hydrocarbons in oils of the Middle Ob region. *Geologia i geofizika = Russian Geology and Geophysics*, 10, pp. 3-34. (In Russ.)

Kontorovich A.E. (1973). Rational complex of modern methods of analysis in organic geochemistry. *Modern methods of analysis in organic geochemistry*. Novosibirsk: SNIIGiMS, 100 p. (In Russ.)

Kontorovich A.E., Stasova O.F. (1964). To the oil geochemistry of the West Siberian lowland. *Geologia i geofizika = Russian Geology and Geophysics*, 2, pp. 13-24. (In Russ.)

Kurbasky G.P. (1987). *Geochemistry of Tatarstan oils*. Moscow: Nauka, 167 p. (In Russ.)

Liao Y., Geng A., Huang H. (2009). The influence of biodegradation on resins and asphaltenes in the Liaohe Basin. *Organic Geochemistry*, 40, pp. 312-320. <https://doi.org/10.1016/j.orggeochem.2008.12.006>

Meredith W., Snape C.E., Carr A.D., Nytoft H.P., Love G.D. (2008). The occurrence of unusual hopanes in hydropyrolysates generated from severely biodegraded oil seep asphaltenes. *Organic Geochemistry*, 39(8), pp. 1243-1248. <https://doi.org/10.1016/j.orggeochem.2008.01.022>

Mullins O.C., Sheu E.Y., Hammami A., Marshall A.G. (2007). *Asphaltene. Heavy Oils. And Petroeconomics*. New York: Springer, 669 p. <https://doi.org/10.1007/0-387-68903-6>

Petrov A.I. (1984). *Oil hydrocarbons*. Moscow: Nauka, 263 p. (In Russ.)

Peters, K.E., Kontorovich A.E., Huiozinga B.J., Moldowan J.M., Lee C.Y. (1994) Multiple Oil Families in the West Siberian Basin. *AAPG Bulletin*, 78, pp. 893-899.

Peters K.E., Walters C.C., Moldowan J.M. (2005). *The biomarker guide*. V.2. 2<sup>nd</sup> ed. New York: Cambridge University Press, 1155 p.

Philippi G.T. (1977). On the depth, time and mechanism of original the heavy to mediumgravity naphthenic crude oils. *Geochim. et Cosmochim. Acta*,

41(1), pp. 33-52. [https://doi.org/10.1016/0016-7037\(77\)90185-5](https://doi.org/10.1016/0016-7037(77)90185-5)

Rozanova E.P., Kuznetsov S.I. (1974). *Microflora of Oil Deposits*. Moscow: Nauka, 197 p. (In Russ.)

Silva T.F., Azevedo A.A., Rangel M.D., Fontes R.A., Aquino Neto F.R. (2008). Effect of biodegradation on biomarkers released from asphaltenes. *Org. Geochem.*, 39(8), pp. 1249-1257. <https://doi.org/10.1016/j.orggeochem.2008.03.015>

Snowdon L.R., Volkman J.K., Zhang Z.R., Tao G.L., Liu P. (2016). The organic geochemistry of asphaltenes and occluded biomarkers. *Organic Geochemistry*, 91, pp. 3-15. <https://doi.org/10.1016/j.orggeochem.2015.11.005>

Uspensky V.A., Radchenko O.A. (1947). On the genesis of oil types. Moscow: Gostoptekhizdat, 80 p. (In Russ.)

Vassoevich N.B., Amosov G.A. (1953). Alteration of oils in the Earth's crust. *Geologicheskii sbornik NITO neftyanikov VNIGRI*, 2. (In Russ.)

## About the Authors

*Lyubov S. Borisova* – PhD (Geology and Mineralogy), Associate Professor, Senior Researcher

Novosibirsk State University

Trofimuk Institute of Petroleum Geology and Geophysics of Siberian Branch of Russian Academy of Sciences

3, Ak. Koptyug ave., Novosibirsk, 630090, Russian Federation

*Elena A. Fursenko* – PhD (Geology and Mineralogy), Senior Researcher

Novosibirsk State University

Trofimuk Institute of Petroleum Geology and Geophysics of Siberian Branch of Russian Academy of Sciences

3, Ak. Koptyug ave., Novosibirsk, 630090, Russian Federation

*Manuscript received 1 February 2018;*

*Accepted 10 September 2018;*

*Published 30 November 2018*



# Analysis of the composition and properties of heavy oils in situ by Low Field NMR relaxation method

V.Ya. Volkov<sup>1,2\*</sup>, B.V. Sakharov<sup>1,3</sup>, N.M. Khasanova<sup>1</sup>, D.K. Nurgaliev<sup>1</sup>

<sup>1</sup>Kazan Federal University, Kazan, Russian Federation

<sup>2</sup>MIREA – Russian Technological University, Moscow, Russian Federation

<sup>3</sup>State Research Center for Applied Microbiology and Biotechnology, Obolensk, Russian Federation

**Abstract.** For the analysis of heavy oils, the method of simultaneous measurement of the free induction decay (FID) together with the decay of the echo signal in the Carr-Purcell-Meiboom-Gill (CPMG) pulse program was used. The measurements were carried out on a «Chromatek-Proton 20M» NMR analyzer operating at a frequency of 20 MHz. A special control program was created on the NMR analyzer that automatically tunes and measures the full FID curve, then switches to measuring the decay of the echo amplitude by the CPMG pulse sequence, and then the investigation ends with a joint processing of all the experimental data. This method makes it possible to measure the amplitudes of NMR signals and the relaxation times T2 of protons of heavy oil components in situ, including asphaltenes, without any perturbations in the analyzed system. Under the influence of paramagnetic centers located in asphaltenes, the amplitude-relaxation characteristics of oil protons are divided into 7 groups associated with solid asphaltenes in crystalline and amorphous states, resins with high and low density, aromatic and saturated compounds. The NMR amplitudes of these fractions correlate well with the group composition of heavy oils as determined by gravitational-chromatographic SARA method. The combined FID + CPMG method can be recommended for determining the SARA composition and other properties of oil in situ. The behavior of fractions of heavy oil in the temperature range (-15°C ÷ +60°C) was investigated by SARA-NMR method. For the first time in situ, it has been shown that resins participate in the formation of asphaltenes in a closed volume when the oil is cooled from a stable state at room temperature, and vice versa, asphaltenes are disaggregated by heating with the release of resins.

The SARA-NMR method is promising for the on-line monitoring of the production, transportation and processing of heavy oil in real conditions of temperature, pressure and dissolved gases. However, the design of the NMR sensor must be adapted to industrial applications. The possibilities of designing NMR probes on process pipelines of larger diameter than in laboratory instruments can be extended taking into account the procedure proposed for correcting the inhomogeneity of the magnetic field in the probed volume based on the FID signal of the liquid oil fraction.

**Keywords:** LF-NMR, vanadyl, SARA, asphaltenes, resins, saturated, aromatic compounds

**Recommended citation:** Volkov V.Ya., Sakharov B.V., Khasanova N.M., Nurgaliev D.K. (2018). Analysis of the composition and properties of heavy oils in situ by Low Field NMR relaxation method. *Georesursy = Georesources*, 20(4), Part 1, pp. 308-323. DOI: <https://doi.org/10.18599/grs.2018.4.308-323>

## Introduction

As the reserves of conventional oil in the world continue to decline, more attention is being paid to improving the technology of extraction, transportation and processing of heavy oils and bitumen, the projected reserves of which can ensure the future of the oil industry for many decades. However, high viscosity and high density of heavy oils and natural bitumen create serious obstacles along this path (Akbarzade et al., 2007; Yang et al., 2008; Yashchenko et al., 2012).

Traditional methods of analyzing crude oil are laborious, usually associated with the extraction of the analyzed components, which destroys the informational integrity (nativity) of the research object and, to a large extent, devalues the results obtained. In addition, they take a long time and require the use of toxic organic solvents. Analytical technologies based on nuclear magnetic resonance (NMR) have attracted special attention from oil industry workers because they are fast and non-destructive methods that can be used to analyze dense and opaque samples, such as crude oil, with little or no additional training (Yang et al., 2008; Maqbool et al., 2011; Silva et al., 2011). Particularly keen interest in the possibilities of the NMR method for the study of samples in the initial state (in situ) increased after

\*Corresponding author: Vladimir Ya. Volkov  
E-mail: [volkovobolensk@mail.ru](mailto:volkovobolensk@mail.ru)

© 2018 The Authors. Published by Georesursy LLC  
This is an open access article under the CC BY 4.0 license  
(<https://creativecommons.org/licenses/by/4.0/>)

NMR logging tools became commercially available at the beginning of the 1990s. NMR measurements of fluid properties that were performed previously only in the laboratories now have been used in well conditions (Coates et al., 2001; Dunn et al., 2002; Akkurt et al., 2008-2009). At the same time, the needs for ground-based laboratory NMR research have only increased to use results for correctly interpretation a log data.

The so-called NMR methods in low magnetic fields (Low Field NMR, LF NMR) have contributed the most to this information. Low fields are conventionally considered fields from hundredths of the Tesla to  $\approx 1$  Tl (Mitchell et al., 2014). Resonance frequencies for protons in such fields lie in the range from hundreds of kHz to  $\approx 42.5$  MHz. Most small-sized laboratory NMR relaxometers operate at these frequencies, relatively cheap and reliable enough for field use (Maran-II 2.0MHz, Maran Ultra 23MHz, NMR Analyzer mq10 10MHz, Minispec mq20 20MHz, Proton 20M 15÷20÷25MHz, etc.).

When NMR is registered, the amplitudes of the proton signal of hydrogen-containing molecules of oil, water and dissolved gases and rates of signal decay after the radio pulses are measured. The relaxation times of the components in the analyzed samples are determined from the rate of the amplitude damping at different sections of the relaxation curve. The initial amplitude of the NMR signal is directly proportional to the number of protons, and it can be correlated with the volume or mass of substances in the measurement domain. The relaxation time depends on the mobility of molecules in the sample. When the viscosity increases, or the movement of molecules containing hydrogen is limited in space, for example, by pore sizes, then relaxation takes place faster.

On this basis, methods have been developed for the simultaneous determination of the physicochemical properties of oil of interest to the petroleum industry, such as viscosity, density in API degrees and the relative hydrogen index (RHI). Comparison of the NMR data and the results of standard measurements showed good results, confirmed by high correlation coefficients ( $R^2 > 0.96$ ). Moreover, by times of transverse relaxation, it was possible to predict the kinematic viscosity of anonymous crude oil samples in the range  $21 \div 1892 \text{ mm}^2\text{s}^{-1}$ , and also the API density between  $17^\circ$  and  $29.4^\circ$ , without any preliminary preparation of the samples. In addition, the oil was identified in connection with their origin. This observation makes it possible to justify a new methodology for obtaining a “chemical signature” of crude oil from various deposits (Barbosa et al., 2013; Muhammad et al., 2014). Some features of the relationship between viscosity and NMR relaxation times were found in oil dispersed systems (Kashaev, 2017).

In the study of heavy oils and bitumen, the situation becomes more complicated. With an increase in the viscosity and molecular weight of hydrocarbons, their spin-spin NMR relaxation time  $T_2$  is greatly reduced to such an extent that the apparatus used does not allow lossless recording of signals from large and slow-moving asphaltene aggregates and other solid-phase components, for example paraffin. When the viscosity of bitumen exceeds 100000 cP, the relaxation decay of big hydrocarbons is partially or completely not detected either by logging tools or by laboratory NMR methods at comparable resonance frequencies. As a result, the quantity of long-chain and / or aggregated hydrocarbons is reduce, which underestimates the reserves of heavy oil and bitumen.

To obtain the missing information Yang et al. (Yang et al., 2008) heated the samples analyzed and studied their NMR characteristics at elevated temperatures when the viscosity decreased significantly. This approach was used to correct the initial amplitude of the FID by measuring the relaxation time  $T_2$  of bitumen at different temperatures in the range ( $8 \div 90^\circ\text{C}$ ) using the Carr-Purcell-Meiboom-Gill pulse sequence (CPMG). Then, the true hydrocarbon content and water saturation were determined.

Back in 2001, to increase the mobility of heavy oil molecules and, thus, to shift their relaxation times to the measured range, Mirotchnik with co-authors (Mirotchnik et al., 2001a) added an equal amount of solvent to the crude oil. Hexane, tetrahydrofuran, trichlorethylene, toluene, kerosene and n-pentadecane were used as the solvent. It was shown that the spectrum of transverse relaxation times ( $T_2$ ) of oil components can be divided into ranges (or frames) in the interval from  $5 \cdot 10^{-2}$  to 3 seconds. For conventional oils, frames can be represented as follows. The slowest relaxation frame corresponds to C4-C15 saturated compounds, then aromatic hydrocarbons, olefins, waxes, resins, asphaltenes, in descending order of relaxation time. For heavy oils and bitumen samples, the frames can be arranged in the following order. The fastest relaxation frame represents asphaltenes, the second shortest relaxation frame represents resins, and the subsequent slower frame is responsible for saturated compounds. The slowest frame characterizes aromatic compounds.

Comparison of the obtained data with the results of an independent analysis of the same samples by the traditional SARA method had a good agreement between them. The NMR method turned out to be suitable for analyzing the group composition in oil-saturated, uncemented sandstones even in the presence of relict water (Mirotchnik et al., 2001b). Besides, the duration of NMR analysis turned out to be about an order of magnitude less than of the chromatographic method of SARA (tens of minutes versus several hours).

Unfortunately, the addition of a solvent destroys the informational “virginity” of the samples. The main advantage of the NMR method, non-invasiveness, is practically lost. Despite the fact that extraction of components from the sample does not take place in this method and all the components of the oil remain in the mixture, however, the relationships between them undoubtedly change significantly under the influence of the introduced solvent. As a result, the method is not suitable for the analysis of crude and, especially, “live” oil in the unperturbed state “as is” (in situ). It is possible that a good coincidence of NMR data with the results of chromatographic SARA analysis in this case is explained by the fact that both methods work with “dead” samples partially or completely destroyed by the introduction of the same type of solvents. Thus, the task of creating a non-invasive analysis of the composition and properties of heavy oils in situ continues to remain relevant to the present.

In a number of cases, the necessary information can be obtained indirectly by analyzing the effect of asphaltenes on the NMR-characteristics of lighter oil fractions. Mutina et al. (Mutina et al., 2008) showed that asphaltenes act as relaxing contrast agents on surrounding substances without affecting their diffusion coefficient  $D$ . This is explained by the presence of free radicals and paramagnetic centers of vanadyl in asphaltenes. Prunelet et al. in time of flocculation study by NMR find out that the relaxation rate of the solvent molecules increases linearly with the concentration of asphaltenes (Prunelet et al., 2004).

Zielinski et al. (Zielinski et al., 2010; Zielinski et al., 2011) investigated the aggregation of asphaltenes in model solutions and crude oil by the LFNMR method at two frequencies of 2 and 5 MHz, when no own signal of solid asphaltenes was detected. However, under the influence of the paramagnetism of asphaltenes, spin-spin relaxation of protons in solutions was observed to be directly proportional to the intrinsic proton relaxation rate in hydrocarbon molecules. In other words, the longer the hydrocarbon chain, the faster it relaxes under the influence of dissolved asphaltenes. In addition, the efficiency of asphaltene clusters as relaxation agents increased with their size. These results were interpreted from the point of view of the theoretical model, which explains the enhancement of relaxation in the aggregation of asphaltenes due to entanglement of the hydrocarbon motion of the solvent in asphaltene clusters and subsequent limitation of rotational mobility and diffusion within clusters. Comparing the longitudinal and transverse relaxation rates, the authors were able to estimate in crude oil. This model is confirmed by other physical methods, including solid-state techniques and multidimensional NMR experiments in high fields, and continues to

improve, exerting a great influence on the research and deciphering of new experimental data (Korb et al., 2013; Stapf et al., 2014; Vorapalawut et al., 2015).

A little over 10 years ago, Shkalikov et al. for the first time (Shkalikov et al., 2006; Shkalikov et al., 2008), when studying oil by the solid-echo method at 19.8 MHz, recorded components with short spin-spin relaxation times ( $9.8 \div 31.2 \mu\text{s}$ ) and the form of the signal of free induction (FID), characteristic for solids. It was found that these signals are due to the presence in the oil of asphaltenes and/or resins in the glassy state, or paraffins in the crystalline phase, depending on the temperature of the sample. On this basis, a method has been developed for determining the content of paraffins and asphaltenes in petroleum, which involves processing two of the three parallel samples with solvents and removing asphaltenes from one of them. By the ratio of the amplitudes of the FID of protons of the solid and liquid phases in these samples, the authors judged the unknown quantities (Nikolin et al., 2008). Unfortunately, the non-invasiveness of the method is lost in this case.

Later, the authors developed a technique for determining the content of liquid-phase and solid-state components in a mixture of hydrocarbons only from the temperature dependence of the fraction of the solid-phase component in the total NMR signal without affecting the composition of the sample (Nikolin et al., 2010). It was shown that each oil fraction has its own temperature range for the existence of a solid component in the NMR signal, which makes it possible to obtain quantitative information on the content of asphaltenes, resins and paraffins in oil. However, the state of the mixture under analysis changes very substantially, since measurements are made over a wide temperature range from  $-150$  to  $+150^\circ\text{C}$ . The phase transitions observed in this temperature range were explained by the melting of solid phases of asphaltenes, resins and paraffins upon heating and their solidification upon cooling. Meanwhile, resins can participate in the formation of the asphaltene aggregates and complicate the picture. The nature of these transitions and, in general, the effect of temperature on the interaction between the components of oil systems is precisely the subject of the close interest of oil industry workers. It is uncontrolled asphaltene deposition with pressure and temperature changes that causes blockage of pores in the oil reservoir, obliteration of pipelines and other problems that arise during the production, transportation and subsequent processing of heavy oils. Unfortunately, these processes in situ have not been investigated to date.

At the same time, Trezza et al. (Trezza et al., 2006) demonstrated the potential of low-field NMR at 20 MHz to obtain detailed information on the phase state and composition of multicomponent lipid systems used in food technology. Combining the CPMG series with



the measurement of FID after a single 90° pulse, the authors were able in one experiment to obtain data sufficient to describe a system with contributions from the liquid, semisolid and solid phases, including lipid crystals in various polymorphic states.

In our works (Sakharov et al., 2015, Volkov et al., 2016, 2017; Khasanova et al., 2017) presents the results of the application of such a pulsed FID-CPMG program with some modifications for the investigation of crude heavy oils. The envelopes of the signals of the spin echo of oil protons, recorded in the interval from 0.1 ms to several seconds, are described by the sum of exponentials whose amplitudes ( $A_i$ ) allow estimating the content of liquid-phase components, and the relaxation times ( $T_{2i}$ ) – characterize the interaction of molecules of liquid oil fractions with each other and with solid phase of asphaltenes. The FIDs after the 90° pulse have a complex shape largely determined, as is well known, by the inhomogeneity of the magnetic field in the sample volume. At the initial section in the interval from 10 to 50÷100  $\mu$ s, when the influence of the field inhomogeneity does not yet significantly affect the damping of the transverse magnetization of the protons, the shape of the FID is described by the sum of the Gaussian and exponential functions, which is characteristic of solid crystalline or amorphous bodies, including asphaltenes (Shkalikov et al., 2008). The rest of the FID to 2÷3 ms is described by the product of exponents by a function describing the inhomogeneity of the magnetic field in the sensor coil. This function is individual for each instrument and requires further analysis and accounting when processing data or compensation in preparation for measurements. Contributions to this part of the FID are from viscous oil components with relaxation times from hundreds of microseconds to milliseconds (mostly resins).

These results were discussed at Russian and international conferences both on magnetic resonance (Sakharov et al., 2015, Volkov et al., 2016a), and on topical problems of the oil and gas industry (Volkov et al., 2016b, 2017; Khasanova et al. 2017) and aroused great interest of the participants. The purpose of this article is to provide an in-depth understanding of the methodological features, existing and potential capabilities of the above methodology for non-contact (for personnel) and non-invasive for oil analysis in the natural state (“as is”, in situ).

## Materials and methods

The sample of crude oil from different wells of the Ashalchinsky field of the Volga-Ural oil and gas bearing basin, characterized by asphaltene content (7.7%, well No.2127 and 5.8%, well No.2270) was the subject of the study. Average composition of Ashalchinsky oils: light hydrocarbons – 57.5%, resins – 35.6%, asphaltenes – 6.8%. Five samples were prepared

from the selected oils: No. 1 (well 2127) and No. 2 (well 2270). To obtain samples No. 3 and No. 4 with a lower content of asphaltenes, the deasphalted (DA) residue (maltene) was added to the crude oil from well No.2270 with a petroleum/maltene ratios of 1: 1 [(oil 2270 + 1DA) = samples No. 3]; and ratios 1: 2 [(oil 2270 + 2DA) = samples No.4]. The deasphalted residue (DA2270) was sample No. 5. The content of asphaltenes was checked by hexane precipitation in accordance with the standard procedure (Akbarzade et al., 2007). Oil samples were placed in ampules with a diameter of 4 mm (EPR) and 10 mm (NMR) and sealed with rubber stoppers. The spectrometer CMS-8400 (ADANI, Belarus) X-band (with a frequency of 9.4 GHz) was used to record the EPR spectra.

NMR measurements were made on a Proton 20M NMR analyzer, manufactured by CJSC SKB Chromatec, Russia (<http://www.chromatec.ru>). The device is designed in the form of two blocks: a magnetic unit and a control unit. The resonance frequency for protons is 20 MHz. Dead time of the NMR receiver signals: no more than 10 microseconds. The phase of filling the high-frequency pulses is set independently on the 4 channels 0°, 90°, 180° and 270°. Signals of FID and echo in the CPMG series were obtained in phase-sensitive mode. Subsequent quadrature detection provided an increase in the signal-to-noise ratio by a factor of  $\sqrt{2}$  and the independence of the result from the possible drift of the phase of the frequency base oscillator. To reduce the influence of inhomogeneities the static  $B_0$  and high-frequency  $B_1$  magnetic fields on the accuracy of setting 180° pulses in the detectable volume, the sensor was placed in the most homogeneous part of the magnetic gap (the FID half-life time of the Glycerin was  $t_{1/2} \geq 1.6$  ms) and sample filled the ampoule no more than 80% ( $\leq 1.1$  cm) from the height of the high-frequency coil. The effectiveness of these measures was evaluated by checking the differences between the amplitudes of the first odd and even echo signals in the CPMG series.

Thermostabilization of the magnet at 40°C provided the instability of a constant magnetic field no worse than  $5.10^{-6}$  per hour. The device automatically adjusts resonant conditions based on the phase detection of the free-induction signal of a standard sample, usually glycerin, or the FID of the test substance if it has a sufficiently intense slow component. All the oil samples studied in this study met this requirement. Thus, the resonant conditions in the process of measuring and accumulating NMR signals (FID and echo) were maintained with accuracy not much different from the accuracy of the stabilization of spectrometers equipped with separate NMR magnetic field stabilizers.

The experimental results were obtained under the following measurement conditions. The duration of the 90° pulse was 2.4  $\mu$ s, the 180° pulse was 4.7  $\mu$ s. The

FID after the 90° pulse was recorded in the interval  $11 \div 2000 \mu\text{s}$  with a sampling step of  $0.5 \mu\text{s}$  with the passband width of the receiver  $\Delta f_1 = 1 \text{ MHz}$ , 100 accumulations ( $N_1$ ) were used with a repetition period of 1 second. Immediately after this, the receiver band automatically decreased to  $\Delta f_2 = 100 \text{ kHz}$  and the echo measurement program in the Carr-Purcell-Meiboom-Gill series (CPMG) was activated (Fig. 1). In this case, the signal-to-noise ratio increases by a factor of 10, which makes it possible to reduce the number of accumulations by an order of magnitude and, thus, to shorten the measurement time. The narrowing of the band did not distort the shape of the relaxation curve, since the rate of change in the amplitudes of the echo signals is an order of magnitude smaller than the rate of change of the FID.

The number of 180° pulses in the CPMG series was  $n = 1000$ , the interval  $2\tau$  between them and, correspondingly, the echo signals was 50, 100, usually 200  $\mu\text{s}$ . Taking into account the duration of the CPMG pulse series, the cycle repetition period was set to not less than 1.5 s, the number of accumulations  $N_2$  varied from 9 to 25 or 36, depending on the need to extract the signals of the minor components. Before the measurements, the samples were kept in a water thermostat at a specified temperature for at least an hour. The results were processed using a specially designed multi-stage fitting program based on the Solver Excel software package. Previously, all wishes were fulfilled regarding the subtraction of the background signal, the maximum sample volume, and the correction of the inhomogeneity of the constant magnetic field  $B_0$ , which were proposed (Trezza et al., 2006) to improve the accuracy of the analysis, with some additional modifications.

### Accounting of the inhomogeneity of the magnetic field and processing of the results

The evaluation and correction of inhomogeneity of  $B_0$  in our work was carried out without using a separate ampule with triolein, in contrast to the way it was done in the work cited above (Trezza et al., 2006). The inhomogeneity of the magnetic field was determined directly in the volume of the sample under analysis in the form of a part of the FID at  $t \geq 200 \mu\text{s}$ ,

generated by maltene with long transverse relaxation times. In an ideally homogeneous magnetic field, the envelope of the amplitudes of the echo signals in the CPMG series must coincide with the relaxation decay of the transverse magnetization of the nuclei (FID). As is known, this impulse program was specially created to eliminate the influence of inhomogeneity, which is always present in the magnets of real devices (Carr, Purcell, 1954). In most commercial NMR relaxometers, the duration of the FID of homogeneous liquids does not exceed  $1 \div 3$  milliseconds, while the actual time of their spin-spin relaxation  $T_2$  is usually much greater. Thus, the duration and shape of the FID of such liquids is almost completely determined by the magnitude and nature of the inhomogeneity of the magnetic field in the volume of the ampule occupied by sample. The relaxation contribution to the “inhomogeneous” form of the FID can be eliminated by dividing by an exponential with the corresponding exponent  $T_2$ . In our case, when the sample is a macroscopically homogeneous mixture of asphaltenes and liquid maltenes with different relaxation times, the shape of the FID is described by the equation:

$$FID(t, T_2, T_{2g}^*) = F(t, T_{2g}^*) \times \text{fit}[CPMG(t)], \quad (1)$$

where  $F(t, T_{2g}^*)$  is the factor that describes the “inhomogeneous” form of the FID, determined by the interference of Larmor frequencies associated only with the deviations of the magnetic field in different parts of the sample from the resonance value  $w_0 = \gamma B_0$ , and the relaxation contribution is represented by the envelope of the amplitudes of the maltene echo signals ( $\text{fit}[CPMG]$ ). In this decay, the signal of asphaltenes is practically absent, since the first echo is measured at  $2\tau = 200 \mu\text{s}$ , and the typical time  $T_2$  of asphaltenes does not exceed 50  $\mu\text{s}$ .

As follows from equation (1), the form of the function describing the shape of the FID in an inhomogeneous magnetic field, can be determined from the formula:

$$F(t, T_{2g}^*) = \text{fit} \left[ \frac{FID(t, T_2, T_{2g}^*)}{\text{fit}[CPMG(t)]} \right]^{t^2}, \quad (2)$$

where the index (\*) at  $T_2$  indicates that the decay of nuclear magnetization is due to the dephasing of spin

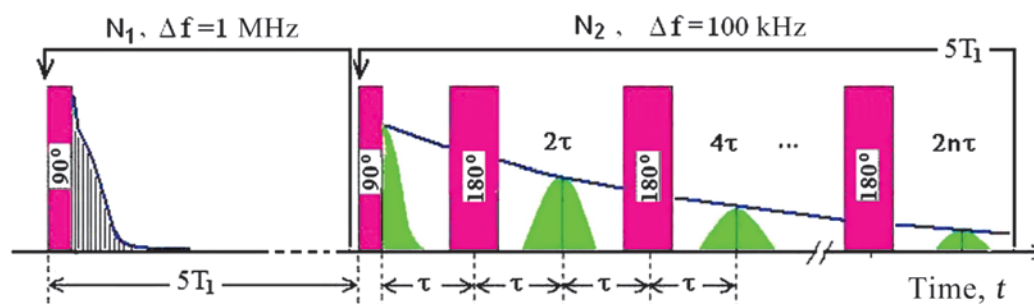


Fig. 1. Scheme of the combined impulse sequence FID + CPMG

packets in an inhomogeneous magnetic field, and borders:  $t_1 = 200 \mu\text{s}$ ,  $t_2 = 2000 \mu\text{s}$ , are of the interval in which the fitting of the experimental array of points was carried out to determine the function  $F(t, T_{2g}^*)$ . The shape of this function, describing the inhomogeneity of the magnetic field in our instrument, is described with good accuracy by the product of the ordinary and Gaussian exponentials:

$$F(t, T_{2g}^*) = (\exp(-t/T_{2gr})^2) \times \exp(-t/T_{2gl}). \quad (3)$$

At the same time, it is natural to expect that the effect of this function extends on the interval  $0 \div 200 \mu\text{s}$  (Fig. 2) missed at the fitting, which allows us to clarify the parameters of the solid-phase part of the FID. This kind of inhomogeneity of the constant magnetic field in the sample is probably related to the cylindrical shape of the ampule and its location in the gap of a permanent magnet with axial symmetry of the field in the XY plane and a linear gradient along the OZ axis. Thus, the corrected form of the  $FID^{cor}(t)$  is described by the equation:

$$FID^{cor}(t) = \frac{FID(t, T_2, T_{2g}^*)}{\exp(-t/T_{2gr})^2 \times \exp(-t/T_{2gl})}. \quad (4)$$

Graphically, the result is shown in Fig. 2, where the product Gauss\*exp (eq. 3) is prolonged to an interval from  $t = 200$  to  $t = 0 \mu\text{s}$ , which allows correction of the entire FID, including the section containing the signal of asphaltenes. This figure is specially presented in the form of two parts to clearly show the sequence of actions during the correction (Fig. 2A), and also to demonstrate the almost complete coincidence of the  $FID^{cor}(t)$  with the envelope of the amplitudes of the echo signals in the zone of their intersection  $t_1 < t < t_2$  (Fig. 2B). Note that the signal-to-noise ratio for  $FID^{cor}(t)$ , as you move away from the origin, deteriorates due to the division of the  $FID(t)$  on the function decreasing with time (eq. 4).

Let us once again pay attention to the fact that under such an approach the influence of the inhomogeneity of the magnetic field is corrected directly in the volume

occupied by a particular sample in an ampule whose diameter and filling height will be automatically reflected in the parameters of the function of the FID form (eq. 2,3, Fig. 2). This softens the requirements for the use of calibrated ampules and the precise positioning of the sample in the NMR analyzer magnet gap. As a consequence, the accuracy of measurements increases substantially throughout the entire length of the FID, and not only at its initial site, as in (Majumdar et al., 2017). A large number of FID digitization points in the analyzed interval from 10 to 2000 microseconds (3880 pieces) significantly supplement one thousand amplitudes of echo signals, that improve the statistical characteristics of the components decomposition from the total relaxation decay of the transverse magnetization and, thereby, increases their reliability. This is especially important for the determination of minor components with short relaxation times, the amplitude of which is a few percent on the background of strong signals of slowly relaxing fractions, whose content is an order of magnitude larger.

## Experimental results and discussion

As follows from the review of the literature, the main influence on the relaxation of protons in heavy oil is determined by the dipole interaction of protons with stable radicals located on the molecules of asphaltenes. The samples of the Ashalchinsky oil prepared for the study also have signals of free radicals (R) and paramagnetic centers of the vanadyl-porphyrin complex  $VO^{2+}$  (Fig. 3).

The connection between EPR signals and asphaltenes is confirmed by their decrease if dilution of crude oil with maltene, however, this dependence is nonlinear. The explanation is the presence of a small number of the same radicals in the resin molecules. Thus, in the deasphalted sample No. 5, the EPR amplitude of the vanadyl-porphyrin signal is about 15% of the signal in the initial oil (Fig. 3c). Later it turned out that one-third

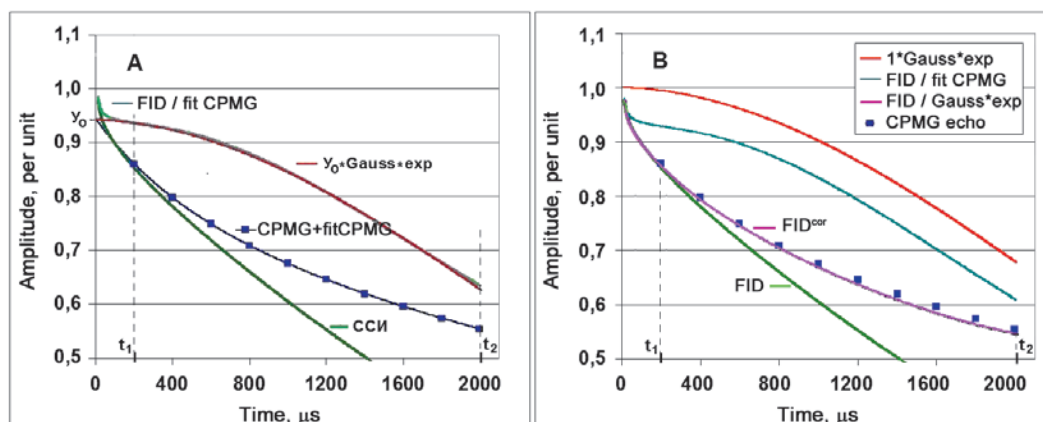


Fig. 2. A) Experimental definition of the function describing the shape of the FID in an inhomogeneous magnetic field; B) Obtaining the corrected  $FID^{cor}(t)$  by point-wise dividing the experimental values of the FID into values of the form function at the same instants ( $FID/Gauss*exp$ )



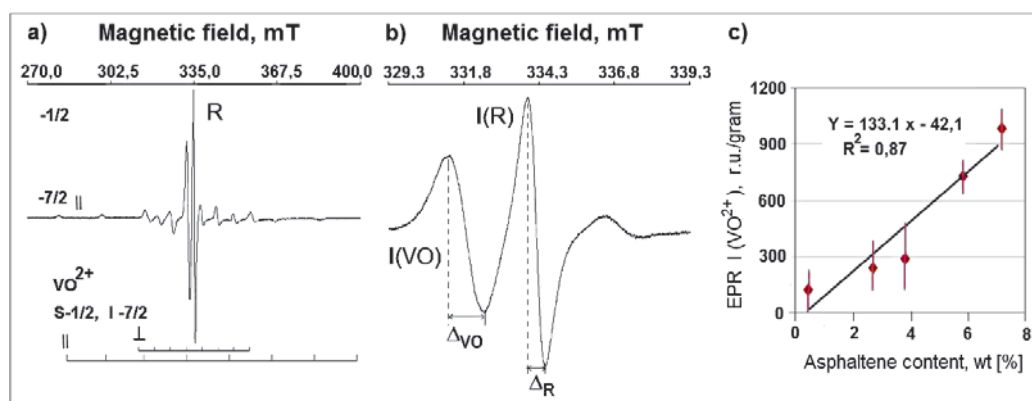


Fig. 3. The EPR spectrum (a) of vanadyl-porphyrin  $\text{VO}^{2+}\text{-P}$   $\{S = 1/2, I = 7/2 (^51\text{V})\}$  and (b) the free radical  $R$  ( $S = 1/2$ ) in the Ashalchinsky crude oil. The structure of super-hyperfine splitting is shown schematically for the direction of the magnetic field along (//) and perpendicular to ( $\perp$ ) the axis of the V-O direction; (c) Correlation of the vanadil EPR signal with the amount of asphaltenes

of this signal can refer to asphaltenes, which condensed some time after sample preparation and were detected by NMR. Since the content of resins and asphaltenes in the samples is known, it is possible to estimate the number of paramagnetic centers in these fractions per unit mass. In the resins of the investigated Ashalchinsky oils it is approximately 30–100 times less than in asphaltenes. These facts were taken into account later in the planning and interpretation of experiments.

Figure 4A shows the experimental decays of the transverse magnetization of two crude heavy oil samples differing in the content of asphaltenes (7.7% and 5.8%, respectively), and one sample of deasphalted oil (maltene). The top line with dots is the experimental decay envelope of the nuclear spin echo amplitudes of the maltene (CPMG), which characterizes the shape of the relaxation curve (FID) of a homogeneous liquid in an ideally homogeneous magnetic field. It can be clearly seen that the real FID form of maltenes is significantly distorted by the inhomogeneity of the static magnetic field in the sample. In addition, FID is reduced due

to the influence of paramagnetism of asphaltenes, and, the faster, the more content of asphaltenes in sample (compare 2270 and 2127). This decrease can be separated from the influence of the magnet field inhomogeneity on the basis of taking into account the FID form of the maltene, as shown in the Materials and Methods section, and to determine the true values of the NMR signal amplitudes and the transverse relaxation times of petroleum protons.

Fig. 4B in the semilogarithmic coordinate system shows the result of the preliminary decomposition into components of the FID signal of crude oil (well No. 2270) with an asphaltenes content of about 5.8%. As expected, the FID shape at  $t > 200$  microseconds is well approximated by eq. (3) with the following values of the parameters characterizing the field inhomogeneity:  $T_{2gr} = 2.01$  ms and  $T_{2gl} = 5.95$  ms. After subtracting this part of the FID related to the liquid maltene from the total free induction signal, two other components are separated in the remainder: (1) the exponential with the relaxation time  $T_{2d'} = 416$  microseconds, as it later turned

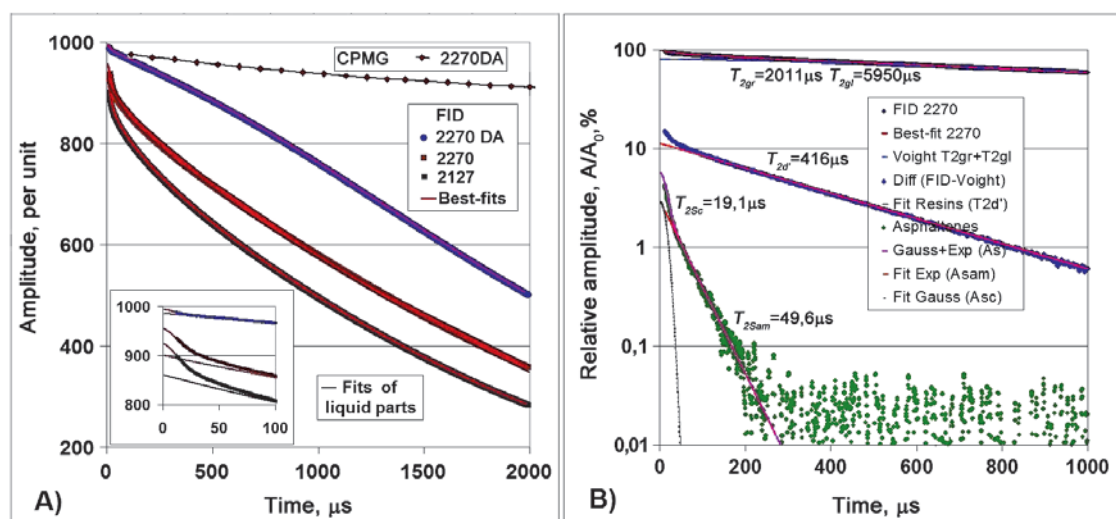


Fig. 4. A) FID's of heavy oil samples (2127, 2270), FID and CPMG of the maltene (2270DA), on the inset: the initial sections of the FID with fitting lines; B) Scheme of graphical FID decomposition of the 2270 crude oil into components on the basis of the model described by eq. (5)

out, related to the high-viscosity fraction of the resins, and (2) the solid phase related to asphaltenes, which is described by the sum of Gaussian ( $T_{2sc} = 19.1 \mu s$ ) and the usual exponent ( $T_{2sam} = 49.6 \mu s$ ).

Completely the FID form is well approximated by the set of functions entering into equation (5):

$$A(t) = A_{s0} \times [(1 - f_{sam}) \times (\exp(-t/T_{2sc}))^2 + f_{sam} \times \exp((-t/T_{2sam}))] + A_{d'} \times (\exp(-t/T_{2d'})) + A_{lm} \times (\exp(-t/T_{2gr})) \times \exp(-t/T_{2gl}) \quad (5)$$

where  $A_{s0}$ ,  $A_{d'}$  and  $A_{lm}$  – true amplitudes (at  $t = 0$ ) of the mathematically extracted components by fitting,  $T_{2sc}$ ,  $T_{2sam}$  – transverse relaxation times characterizing crystalline (Sc) and amorphous (Sam) constituting the solid phase (S – solid) with total amplitude  $A_{s0}$ , and  $f_{sam}$  is the fraction of the amorphous part of the solid phase.  $A_{lm}$  is the amplitude of liquid maltene (Im – liquid maltene) without the contribution of the amplitude of high-viscosity  $A_{d'}$  resins. For the convenience of approximation and analysis of the results obtained, the “solid” part of formula (5) is assembled into one term in square brackets. The results of the fitting are shown in the drawings with thin red lines inside the experimental curves. The relative fraction of the components in the NMR signal of all protons in the sample is determined by dividing by  $A_0$  the function of the fitting (5) at  $t = 0$ , which must coincide with the sum of the amplitudes ( $A_{s0} + A_{d'} + A_{lm}$ ). (Sakharov et al., 2015; Volkov et al., 2016a, b).

Fig. 5 shows FID of asphaltenes in dry powder form, extracted from oil 2270, and a fragment of FID of this oil relating to asphaltenes in crude oil (in the natural environment), normalized to the maximum amplitude of the solid-phase fraction described as the function Gauss + exp. The fastest relaxation times are close to each other (15.5 and 19.1  $\mu s$ ) and belong to the hard asphaltene core, since the shape of the relaxation curve

is described by the Gaussian function typical for solids. The relaxation times of the exponential parts of the FID differ by almost three times (17.2 and 49.6  $\mu s$ ), and the greater time relates to asphaltenes in crude oil. This is consistent with the current knowledge of the existence of asphaltene molecules in crude heavy oil, which combine into hard nanoaggregates of 8-10 molecules, and when the concentration is increased, into larger clusters consisting of stacked nanoaggregates and a fairly loose porous environment of asphaltene and resins molecules, in which the molecular mobility is substantially higher than in the nucleus (the modified model of Jena, Mullins et al., 2012).

In dry asphaltene powder mobility of molecules around the core is low ( $T_2 = 17,2 \mu s$ ) due to lack of the liquid phase and the close to the mobility in the nucleus ( $T_2 = 15,5 \mu s$ ). However, due to the disorder of the porous structure around core (amorphous) of the relaxation decay shape remains exponential at 40°C and higher temperatures. When the temperature is lowered to room temperature and lower, in our experiments to -15°C, it gradually assumes a Gaussian form, that is, the rigidity of the system rises up to the level close to typical solids. We note that the fraction of the exponential (amorphous) part of the FID in crude oil is one third larger ( $f_{sam} = 0.49$ ) than in the dry powder ( $f_{sam} = 0.31$ ). The explanation is that the porous structure of asphaltenes in oil is impregnated with maltene and large resin molecules lose mobility due to spatial limitations and increase in adhesion time with “pore walls”. As a result, the amplitude increases by an amount proportional to the mass of the absorbed molecules, and the relaxation time of protons of asphaltenes and resins in the porous environment of the nucleus is averaged at about 45-50  $\mu s$  (at +40°C). This is consistent with the well-known fact of the isolation of resins from asphaltene precipitate at additional purification of asphaltenes by solvents.

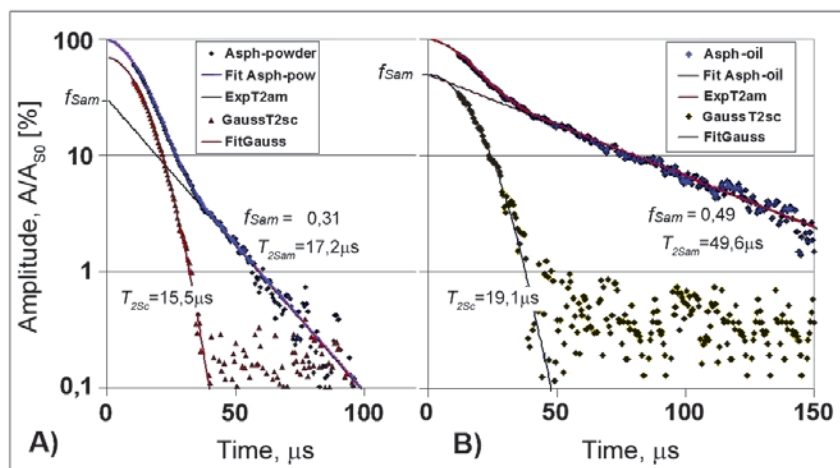


Fig. 5. A) The FID of dry powder of asphaltenes extracted from crude oil 2270, and B) a fragment of the FID from Fig. 4, relating to asphaltenes in crude oil 2270. Solid lines are the results of approximating the experimental curves by part of equation (5) in square brackets

Furthermore, recently high-field NMR techniques with magic angle spinning have experimentally confirmed that there are two domains in the asphaltene clusters: rigid central core consisting of stacked aggregates and substantially smaller proportion of peripheral movable alkyl side chains. (Majumdar et al., 2017). Apparently, it is these chains that participate in the formation of a viscoelastic network between the clusters, ensuring the stability of the colloidal crude oil system at high concentrations of asphaltenes in the natural state (Akbarzade et al., 2007).

Figure 6 shows the results of simultaneous measurement of FID and echo signals in the CPMG series of the same sample of crude oil with an asphaltenes content of 5.8%. The envelope of the echo signals of the CPMG series (the top line in Fig. 6B) is best described by the sum of 4 exponents (eq. 6) (Sakharov et al., 2015; Volkov et al., 2016):

$$A_{CPMG}(t) = A_d \times (\exp(-t/T_{2d}) + A_c \times \exp(-t/T_{2c}) + A_b \times \exp(-t/T_{2b}) + A_a \times \exp(-t/T_{2a})) \quad (6)$$

These exponents are represented in the figure by tangential straight lines that have slopes determined by the transverse relaxation times of the protons  $T_{2i}$  of the corresponding fractions of the maltene. The indices  $i = a, b, c, d$  are arranged in order of increasing relaxation rates  $1/T_{2i}$ . Tangents intersect the y-axis (abscissa) at points that characterize the fraction of protons (in percent) of these maltene in the total signal of oil protons, including asphaltene protons, since the amplitudes of the echo signals are normalized to the maximum amplitude of the FID at  $t = 0$ .

Figure 6A shows the result of approximating the FID of the same sample by the formula (5), the dark triangles show the amplitudes of the echo signals transferred from the right side of the figure. It can be seen that after taking

into account the inhomogeneity of the magnetic field the liquid-phase part of the  $FID^{cor}$  practically coincides with the envelope of the echo signals, and their amplitudes at  $t = 0$  are equal within the measurement error. In turn, the amplitudes and relaxation times of the fastest component CPMG ( $A_d, T_{2d}$ ) and the intermediate component of the FID ( $A_d, T_{2d}$ ), calculated from the results of the fitting of FID and CPMG, also practically do not differ from each other (Table 1). Firstly, this confirms the adequacy of the procedure for compensating for the inhomogeneity of the field. Secondly, it allows us to more accurately determine the parameters of the intermediate ( $d'$ ) component according to the FID data, when the number of points in the CPMG series pertaining to this component decreases to several units, which is observed with a higher content of asphaltenes in oil.

Note that with decreasing the amount of asphaltenes, when the time  $T_{2d}$  increases to 1 ms or more, the accuracy of its measurement by the FID decreases due to the deterioration of the signal-to-noise ratio. In this case, the measurement is preferably performed by the CPMG method. Thus, the combined sequence of pulses FID + CPMG provides the possibility of analyzing samples with relaxation times from 10  $\mu$ s to many seconds without any losses and omissions on the time scale. This makes it possible to observe all the components of heavy oil from light fractions to resins and asphaltenes without resorting to heating (Yang et al., 2008) or the use of solvents (Mirotchnik et al., 2001a, 2001b) to increase the mobility of molecules, as in the works cited above. Thus, a tool for the analysis of heavy oils in situ appears which does not have any noticeable effect on the state of the object under study.

Below are the results of using this tool to analyze the group composition of heavy oils. Figure 7 shows the experimental FID and relaxation decays of the echo

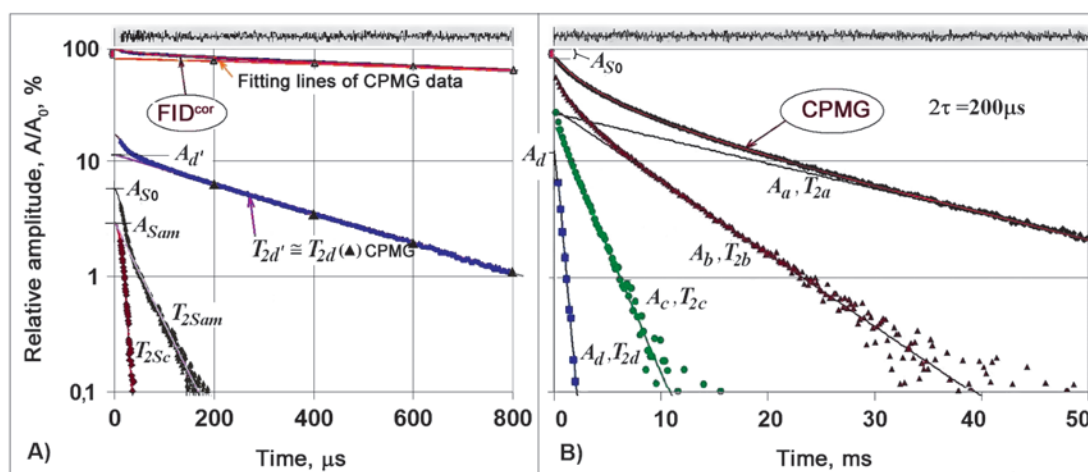


Fig. 6. The results of approximation (fitting): A) FID, after correction of magnetic field inhomogeneity, and B) envelope amplitudes of signals of nuclear spin echo of protons in CPMG series of crude oil sample of Ashalchinsky field (2270). Noisy lines at the top characterize the accuracy of the approximation – these are the differences between the experimental points and the fitting lines multiplied by factor 5. The amplitudes of the echo signals are normalized, as well as the FID points, to the value  $A_0$  of the function of the FID fitting (eq. 5) at  $t = 0$



No	$C_{asph}$	$A_{S0}$	$T_{2Sc}$	$f_{Sam}$	$T_{2Sam}$	$A_d'$	$A_d$	$T_{2d}'$	$T_{2d}$	$A_c$	$T_{2c}$	$A_b$	$T_{2b}$	$A_a$	$T_{2a}$
	%	%	$\mu s$	part	$\mu s$	%	%	ms	ms	%	ms	%	ms	%	ms
1	2	3	4	5	6	7	8	9	10	11	12	13	14	15	16
1	7,7	7,2	19,7	0,5	49,7	13,9	14,1	351	0,37	27,6	1,7	32	5,2	19,1	12,3
2	5,8	6	19,1	0,5	49,6	11,4	11,6	416	0,41	24,8	2,1	30,7	7,3	26,9	20,3
3	3,8	3,7	17,4	0,53	58,2	10,7	11,5	648	0,62	21,9	2,7	32,5	9,8	30,4	30,2
4	2,7	2,4	17,9	0,51	50,1	n/d	13,3	n/d	0,85	25,2	4,2	33,4	15,4	25,7	44,4
5	0,4	0,7	15,9	n/d	44,6	n/d	13,7	n/d	1,74	25,5	8	32,6	29,8	27,5	81,7
Average values		6,6 <sup>1,2</sup>	17,6		50,6		12,5			24,4		32,3		24,1	
	Asphaltenes					Alcohol-benzen resins				Benzene resins		Saturated		Aromatic	
SARA <sup>1,2</sup>	<6,8 %>					<35,6 %>						<32,4%>		<25,2%>	
SARA*	7,5%					13,3%				24,2%		54,4%			
No1	Anmr - Asara				-5,9%	-6,0%				-14,0%		1,2%		24,2%	
No2	Asara				11,8%	12,8%				-2,5%		5,2%		-6,7%	

Table 1. The results of the relaxation curves analysis (Fig. 7) of heavy oils with different content of asphaltenes

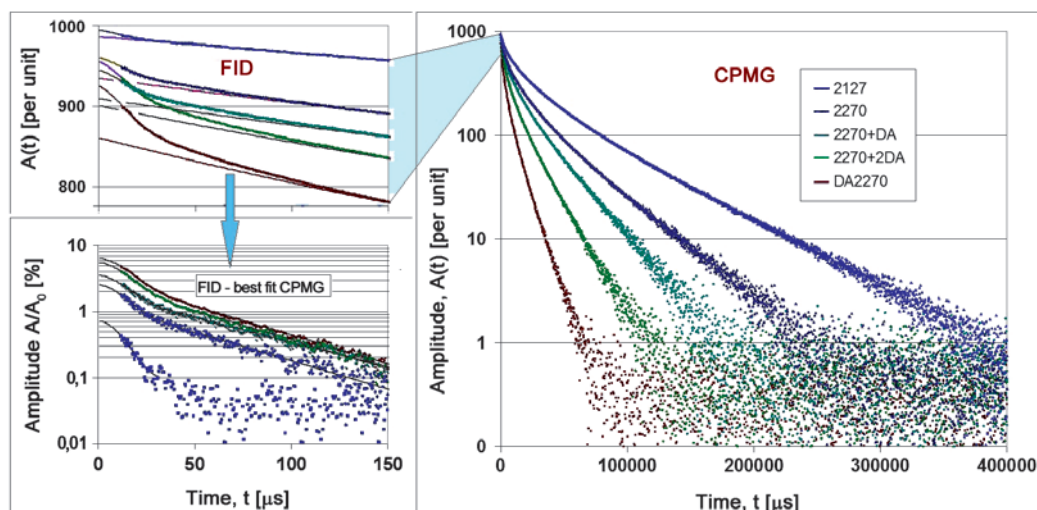


Fig. 7. Transverse magnetization decays (FID and CPMG) of the crude oils (2127, 2270), maltene (DA2270), and samples obtained by mixing oil and maltene in the ratio 1:1 (2270 + DA) and 1:2 (2270 + 2DA)

signals of samples with different asphaltene content obtained in one of the three series of experiments using a combined pulse train (Fig. 1), and in Table 1 the results of approximation of the experimental data by equations (5) and (6). As was proved above, the microsecond relaxation region from 10 to 100 microseconds unambiguously refers to protons of asphaltenes, minus the amplitude of maltenes. The results obtained by precipitation of asphaltenes with hexane and NMR data (the second and third columns of Table 1) correlate well with each other and are related to each other by a linear dependence with a slope close to unity and a coefficient  $R^2 > 0.98$ .

The components with the longest relaxation times (with the index “a”), according to Mirotnik et al. (2001a), should refer to aromatic compounds, the following – with shorter  $T_2$  (subscript “b”) characterize the saturated compounds, and components with times in the intermediate zone from hundreds of microseconds to several milliseconds (indices “c” and “d”) should be viscous resins.

When analyzing the group composition of oil, the standard SARA method determines the total resin

content, while the NMR method clearly registers two components with fairly short relaxation times from 350  $\mu s$  to 8 ms. The sum of the amplitudes of these components, expressed as a percentage of the total amplitude of the oil signal, practically coincides with the percentage of resins (%) in the SARA analysis of the samples. The explanation is that the resins are well divided into two fractions by two kinds of solvents, benzene and a mixture of ethyl alcohol and benzene. Apparently, the NMR method, sensitive to the peculiarities of intermolecular interactions, fixes this readiness of different properties of resin fractions to react differently to the introduction of solvents into the system. The isolated resins are called “benzene resins” (BR) or “low-density resins” and “alcohol-benzene” (ABR) or “high-density resins”.

Let us pass to the analysis of information represented by the spin-spin relaxation times of protons of heavy oil fractions in situ. The relaxation time of  $T_{2sc}$  protons in the asphaltene core are the shortest ( $18.0 \pm 1.3 \mu s$ ) and practically does not change in samples with different asphaltenes content (Table 1). As noted above, this

is due to the rigid lattice of solid asphaltenes and the rapid averaging of the nuclear magnetization of the protons around the paramagnetic vanadyl-porphyrin complex due to direct spin-spin interaction. In the amorphous part of aggregates of asphaltenes, the lattice is less ordered and, in addition, the molecules of mobile fractions penetrate into it, so that  $T_{2\text{Sam}}$  is noticeably larger than the proton  $T_{2\text{Sc}}$  of the crystalline nucleus ( $\sim 2.5$  times), but also varies little with the concentration of asphaltenes ( $50,0 \pm 4.1 \mu\text{s}$ ). It can be safely assumed that the nearest environment of asphaltenes is the same in all samples No.1 to No.5 for all asphaltene particles, despite the differences in their quantity. This is natural, since the composition of the maltene in the samples is practically the same, and the particles are distributed uniformly in the samples and do not form large aggregates (sediment).

In contrast, the relaxation times of protons of liquid fractions strongly depend on the content of asphaltenes in the samples. The relaxation rates  $1/T_{2i}$ , calculated from the data in Table 1, increase in proportion to the concentration of asphaltenes with high correlation coefficients close to unity (Fig. 8). Judging by their slope, the paramagnetism of asphaltenes exerts the greatest influence on closely spaced high-density resins (the “d” index) and has a much weaker effect on the more distant low density resins (“c”), as well as on saturated (“b”) and aromatic (“a”) compounds.

The increase in the proton relaxation rate of all fractions is due to an increase in the number of paramagnetic particles per unit volume of the sample. It would seem that protons of highly mobile light-fraction molecules must quickly exchange magnetization with paramagnetic centers of asphaltenes and should have shorter relaxation times than viscous slow-moving resins, but this is not observed.

In addition, Fig. 8 clearly shows that the spin-spin systems of protons of different fractions are sufficiently isolated from each other, so that their relaxation times are not averaged to one common time for all protons. Consequently, the molecules of the fractions are not

distributed uniformly as in an ideal solution, but form microphases bound in the volume, exchanging by particles so slowly that their relaxation times are determined separately. Analysis of the porous model of asphaltenes (Zielinski et al., 2010) suggests that the lifetime of the resins in contact with asphaltenes is large enough to make it difficult to access of light fractions to the surface of the asphaltenes. As a result, the relaxing effect of paramagnetic centers of asphaltenes is transmitted through spin-spin systems of resins to protons of saturated and aromatic compounds with velocities that depend on the size of molecules and the local viscosity.

This weakening is characterized by the coefficients of the slope of the straight lines on (Fig. 8). It is likely that the very existence of such microphases, with developed boundaries and surface tension forces, is the basis for the stability of heavy oils with both large and small amounts of asphaltenes prone to aggregation. It is not by chance that the equilibrium in such a complex structured system is very sensitive to the influence of many external and internal factors and can be investigated only by methods that do not introduce additional perturbations in time of analytic process.

### Determination of the SARA composition

The NMR amplitudes of asphaltenes, resins, saturated and aromatic compounds presented in Table 1 vary simbarically with the results of the SARA analysis. Figure 9 shows a histogram that clearly indicates the degree of proximity of these data, as well as a graph illustrating the statistical evaluation of this correlation. The slope of the straight line on the chart is almost equal to 1 and the correlation coefficient  $R^2 = 0.94$  indicates a high degree of reliability of the revealed relationship. However, absolute discrepancies between NMR and SARA estimates of the content of fractions in this case vary in a fairly wide range from 5 to 25%, averaging about 15% (Table 1). In this connection, the question arises whether SARA can be a reference test for NMR and other methods of analyzing oils.

The method of determining the group composition, based on the precipitation of the asphaltene fraction using with an excess of alkane solvent and the subsequent chromatographic separation of maltene into resins, saturated and aromatic compounds, was widely used and was repeatedly certified by the American Society for Testing Materials (ASTM D3279-07, ASTM D412409-2012 / GOST 32269-2013). Nevertheless, this method has been widely criticized because of the low accuracy, the length of the analysis, the large amount of oil and solvents required, the difficulty of automating the process (Kharrat et al., 2007; Bissada et al., 2016). Thus, simultaneous testing of samples of the same oil in four certified laboratories revealed significant

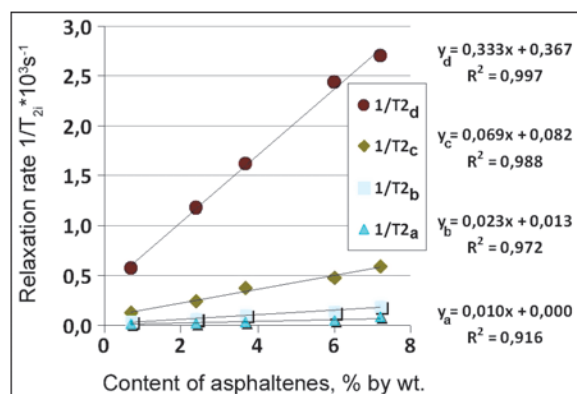


Fig. 8. Dependences of the spin-spin relaxation rates of liquid fractions on the content of asphaltenes in oil

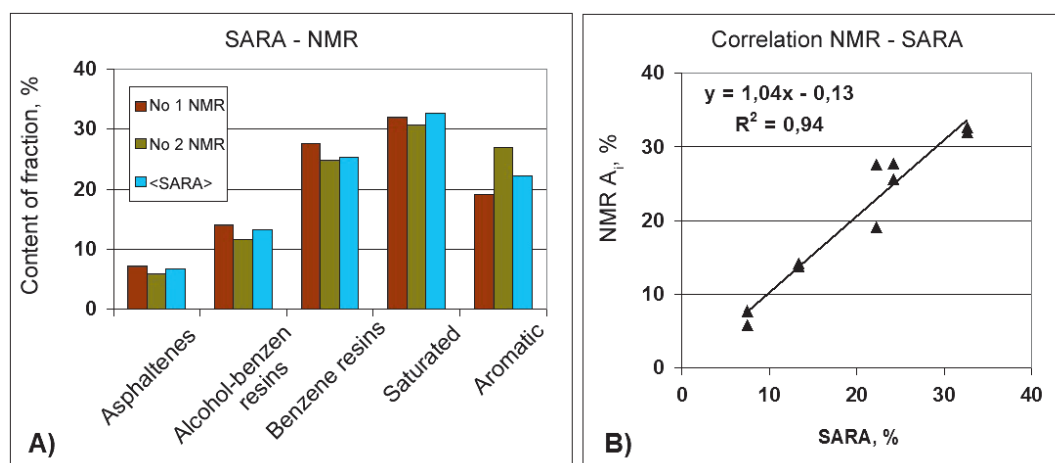


Fig. 9. A) Group composition of Ashalchinsky oil according to NMR and standard SARA analysis; B) Statistical evaluation of the correlation of these data with each other

differences in the results of the analyzes. The laboratory data differed by 2-10% for resins and asphaltenes, for 12-28% for aromatic, and reached 40-60% for saturated compounds. Moreover, repeated chromatography of the isolated components revealed significant impurities of neighboring fractions in them. For example, up to 69% of asphaltenes and aromatic compounds were contained in the resins, and almost 26% of aromatic compounds, resins and asphaltenes were found in saturated compounds (Bissada et al., 2016).

It has been repeatedly noted in the literature that the amount of precipitated asphaltenes depends on the type of alkanes and the sequence of their application (Shkalikov et al., 2010; Achugasim et al., 2015). Therefore, the result is specific for the solvent/oil system and may not coincide with the actual content of asphaltenes in the original oil. It is generally accepted that even in small quantities, asphaltenes are an essential component that contributes significantly to the harmony of the interaction of the phases of crude oil. The removal of asphaltenes disrupts the very delicate balance that exists between fractions in crude oil, and a strictly structured system turns into a mixture far from the properties of the original oil. It is no accident, to date, methods for predicting the stability of crude oil based on SARA analysis are of low efficiency and need further development (Guzmán et al., 2017).

Thus, on the formal side of the problem under discussion, the SARA chromatographic method can not serve as a standard test for metrological certification of the proposed NMR method for determining the group composition of oils. It is necessary to search for a stable natural standard and/or to develop an artificial test of the composition and methodology of certification, which is necessary for the application of this express method in industrial laboratories responsible for the economic result of enterprises. In the meantime, until the problem of the official recognition of the SARA-NMR analysis method is being solved, there

is nothing to prevent the use of certified measuring instruments, the NMR analyzer, and the founded correlation for research purposes. Moreover, in the list of tasks that are of interest to the solution, non-invasive methods are needed to solving practically all the actual problems of the oil industry.

### Effect of temperature on SARA composition

It is believed that the main causes of uncontrolled asphaltene deposition are changes in pressure, temperature and composition in the extraction, storage, transportation and refining of oil. However, as noted above, it is not yet possible to create a method for confidently predicting such events (Guzmán et al., 2017). In the article (Shadman et al., 2017), the authors concluded that to determine the onset of asphaltene precipitation, it is necessary to know the mechanism of precipitate formation. Zielinski et al. (2010) noted that aggregation of asphaltenes strongly depends on the properties of the solvent and the presence of polar molecules, such as resins, and underscored the need for reliable methods that would allow observing asphaltenes in their natural surroundings-in natural oil.

In our studies, we used the NMR relaxation method presented here to analyze the interactions of oil fractions in situ without extraction of asphaltenes (Volkov et al., 2017; Khasanova et al., 2017). Figure 10 shows the experimental results of the effect of temperature on the relaxation decays of protons of heavy oil during heating and cooling in sealed ampoules. Before carrying out the measurements, the samples were kept in thermostats at a specified temperature for at least two hours.

When the ampoules are heated to 30°C, 40°C, 50°C and 60°C, the total amplitude  $A_0$ , which is the sum of the signals of all the protons in the sample, decreases according to the Curie law, while the relative amplitudes ( $A_i/A_0$ ) of the fractions depend only on their quantity at a given temperature. When heated from room temperature to +60°C, the relative amplitude ( $A_s/A_0$ ),



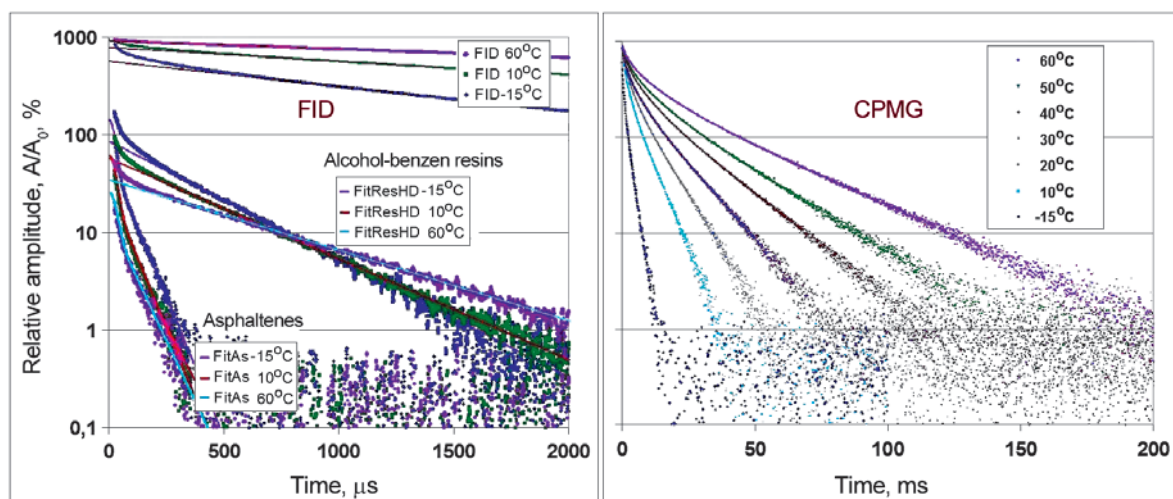


Fig. 10. Decays of the transverse magnetization (FID and CPMG) of protons of crude oil (well 2127) in situ at different temperatures

reflecting the content of all asphaltenes, decreases, the relative amplitudes of benzene resins ( $A_c/A_0$ ) increase, but in alcohol-benzene resins ( $A_d/A_0$ ), aromatic ( $A_b/A_0$ ) and saturated ( $A_a/A_0$ ) components of the amplitude practically do not change (Fig. 11). The times of spin-spin relaxation of protons of all fractions increase monotonically.

When the samples are cooled to 12°C, 10°C, 4°C, 0°C and -15°C, the amplitude of asphaltenes increases with the simultaneous decrease in the amplitudes of the BR and ABR resins, and the number of light fractions remains practically unchanged. The times of relaxation of  $T_{2i}$  decrease monotonically. In these experiments, the observed changes were completely reversible, after the samples returned to a temperature of +20°C, their state is described by the indices ( $A_i$ ,  $T_{2i}$ ), which are close to the initial values within the limits of measurement errors.

Thus, for the first time in situ, direct experimental confirmation has been obtained of the statement that resins are a potential source for the formation of asphaltenes in aggregation and precipitation processes, and asphaltenes in turn are a source of resins, for example, in refining heavy oils and bitumen. If there are enough thermostats, this experience can be performed within one working day. At the same time, the possibility of multiple repetition of measurements remains, since the samples are returned to storage in thermostats in an unchanged state. This allows not only to check the results, but also to improve the accuracy of measurements by improving the signal-to-noise ratio when adding digital data and their statistical processing.

Let's pay attention to the linear dependences of the relaxation times  $T_{2i}$  of the components on the reciprocal temperature (Fig. 12), which allow us to determine the activation energies of the relaxation processes in crude oil. This parameter can be useful for assessing the stability of oils in various conditions.

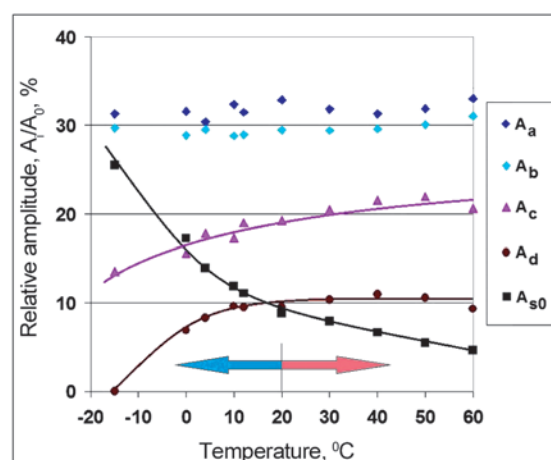


Fig. 11. Temperature dependences of the NMR amplitude of SARA protons of heavy oil fractions upon cooling from room temperature to -15°C and heating to +60°C

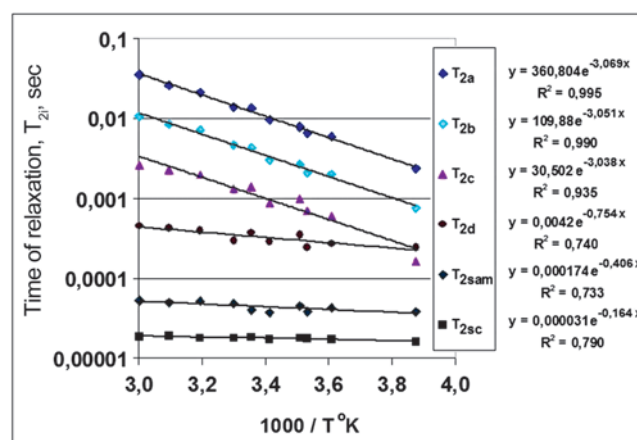


Fig. 12. Temperature dependences and activation energies of spin-spin relaxation of SARA protons of heavy oil fractions upon cooling from room temperature to -15°C and heating to +60°C

For comparison, the study of reversibility of precipitation of asphaltenes in crude oil by the gravity-chromatographic method of SARA (Abedini et al., 2011) at 25°C, 40°C, 50°C and 60°C required more than a day for each point both at increase in and with a decrease in temperature. To obtain the result, it was necessary to create conditions for maintaining the temperature for a long time in the laboratory, where more than fifteen operations are performed. They include the preparation of a large number of samples, accurate dosing and weighing of reagents, holding at a given temperature, continuous mixing for complete extraction, centrifugation, washing for complete discoloration of the solvent, etc. As a result of the analysis, the samples are destroyed. To exclude possible accidents and increase the accuracy of the measurements, the authors processed three samples at each temperature. As a result, this experience can last up to two weeks. It is no accident that the methods of magnetic radiospectroscopy (NMR, EPR) are increasingly used for non-invasive analysis in the oil industry.

## Conclusion

Despite the identified shortcomings (Bissada et al., 2016), the standard gravimetric chromatography method SARA (ASTM 2012. D412409) is widely used to analyze the group composition of oils. The density and viscosity of the oil, the relative hydrogen index RHI, the acid number and many other factors that affect the economic efficiency of the technological processes at each stage of the creation of the surplus value from the development of the fields to the production, transportation and refining of oil depend on the amount and ratio of the fractions. The results of this analysis are associated with an assessment of the compatibility and, as a consequence, the stability of mixtures of crude oils, which allows foreseeing the problems of sedimentation during their further storage and transportation, although the effectiveness of such predictions is recognized as low (Guzmán et al., 2017).

The SARA-NMR method presented above is a good alternative to the procedures recommended by ASTM for analyzing the group composition of heavy oils. On the accuracy of determining the content of individual SARA components, the NMR method is not inferior to ASTM methods, and the reproducibility is potentially higher, since it is performed automatically, without the use of chemical reagents and any other interference in the state of the samples. If necessary, the absolute accuracy of measurements can be increased in 3÷5 times due to an increase in the accumulation time of data. The resolving power in the amplitude of the proton signal is  $\approx 3$  mg H<sub>2</sub>O under standard measurement conditions (see the section “Materials and Methods”), which is 0.5% with a sample weight of 600 mg. Thus, the absolute content of asphaltenes in crude oil of about 5% can be determined

with a relative accuracy of not worse than 10%, and with the accumulation of data may be improved to 2÷3%.

The accuracy of the measurements is provided not only by the stability of the electronic systems of the instrument, but also by the fundamental features of the NMR method: the amplitude of the signal is strictly proportional to the number of protons in the sample, regardless of the phase state of the substance in which the protons are stay: solid, liquid or gaseous. Since the content of the components is determined with respect to the content of all the protons in the sample, the accuracy in significant limits does not depend on the volume (weight) of the sample within the sensor coil and on the possible drift of the gain of the NMR receiver of the relaxometer during long signal accumulation.

The main advantage of the proposed method is its non-invasiveness. This quality provides adequate information corresponding to the real properties of the object of research. NMR data accurately reflect the true composition and nature of the interaction of components in the analyzed samples, in contrast to the results of chemical analysis, since the use of solvents violates the physical-chemical and information structure of the original oil. There is an opportunity to receive detailed information on the processes occurring inside the crude, and potentially “live” oil under such conditions by temperature, pressure, the presence of dissolved gases, etc., which exist in reality.

Unfortunately, the realization of this perspective of the method application in full is impossible on the usual NMR instruments without solving the problem of sampling with preservation and maintenance of natural conditions during the analysis. However, innovative development of low-field NMR sensors has already been developed to measure the relaxation and diffusion times in liquids, including oil, at very high pressures (up to 2500 atm) and high temperatures (up to 175°C) (Freedman et al., 2014). A cylindrical magnet with a diameter of 9 cm and a length of 20 cm had an aperture along the axis of 6.6 cm in diameter, in the middle part of which the magnetic field provided a resonance frequency for protons of 2.18 MHz. The signal-to-noise ratio of the new sensor is more than 15 times higher than that of existing commercial systems, i.e. data can be obtained more than 200 times faster than it was possible before.

Such high technical characteristics make it possible to predict that soon NMR sensors will be created on process pipelines, or on their branches of sufficiently large diameter, for on-line monitoring of various technological processes in the oil industry. Only non-contact methods in the course of actual operation can provide true information on complex and delicate processes in “live” oil, analyzed as close as possible to the wellhead, and then through the stages of de-gasification, dehydration, mixing, transportation up to distillation and

manufacturing of many types of commodity products. The objective information will enable to optimize the technological processes of extraction and processing of hard-to-recover hydrocarbon reserves, and the installed equipment will enter the automated digital system of industry management.

## Acknowledgments

*This work was funded by a Russian government subsidy to support the Kazan Federal University's Competitive Growth Program among world-class academic centers and universities.*

*The authors are grateful to the reviewer Dr. Oliver C. Mullins for his critical comments and questions, that made it possible to more clearly express the results presented in the manuscript.*

## References

- Abedini A., Siavash A., Torabi F., Saki Y., Dinarvand N. (2011). Mechanism of the reversibility of asphaltene precipitation in crude oil. *J. Petrol. Sci. and Eng.*, 78, pp. 316-320.
- Achugasim O., Ekpo I.E. (2015). Precipitation of Heavy Organics (Asphaltenes) from Crude Oil Residue Using Binary Mixtures of n-Alkanes. *Advances in Chemical Engineering and Science*, 5, pp. 96-101. <http://www.scrip.org/journal/aces> <http://dx.doi.org/10.4236/aces.2015.51010>
- Akbarzade K., Allenson S., Krik D. et al. (Summer 2007). Asfalteny: problemy i perspektivy [Asphaltenes: problems and perspectives]. *Neftegazovoye obozreniye = Oil and gas review*, pp. 28-53. (In Russ.)
- Akkurt Ridwan, Bakman G. Nate, Chen Kao Ming, and et.al. (Winter 2008-2009). Novyye vozmozhnosti yadernomagnitnogo karotazha [New opportunities for nuclear magnetic logging]. *Neftegazovoye obozreniye = Oil and gas review*, 20(4), pp. 4-27. (In Russ.)
- Barbosa L.L., Sad C.M.S., Morgan V.G., et al. (2013). Time-domain proton nuclear magnetic resonance and chemometrics for identification and classification of Brazilian petroleum. *Energy Fuels*, 27, pp. 6560-6566. <https://doi.org/10.1021/ef4015313>
- Bissada K.K. (Adry), Jingqiang Tan, Ewa Szymczyk, Mike Darnell, Mei Mei (2016). Group-type characterization of crude oil and bitumen. Part I: Enhanced separation and quantification of saturates, aromatics, resins and asphaltenes (SARA). *Organic Geochemistry*, 95, pp. 21-28. <https://doi.org/10.1016/j.orggeochem.2016.02.007>
- Carr H.Y. and Purcell E.M. (1954). Effects of Diffusion on Free Precession in Nuclear Magnetic Resonance Experiments. *Phys. Rev.*, 94, pp. 630-638. <https://doi.org/10.1103/PhysRev.94.630>
- Coates G.R., Xiao L., Prammer M.G. (2001). Karotazh YAMR. Printsipy i primeneniye [NMR Logging: Principles of Applications]. Houston: Halliburton Energy Services Publ., 342 c.
- Dunn K.-J., Bergman D.J., Latorraca G.A. (2002). Nuclear Magnetic Resonance Petrophysical and Logging Applications. New York: Pergamon.
- Freedman R., Anand V., Grant B., Ganesan K., Tabrizi P., Torres R., Catina D., Ryan D., Borman C., Krueckl C. (2014). A compact high-performance low-field NMR apparatus for measurements on fluids at very high pressures and temperatures. *Rev Sci Instrum*, Feb. 85(2), 025102. doi: 10.1063/1.4863857.
- Gutowsky H.S., Roger Ray B. and Rutledge R.L. (1958). Carbonaceous free radicals in crude petroleum. *J. Chem. Phys.*, 28, pp. 744-745. <https://doi.org/10.1063/1.1744250>
- Guzmán Roque, Ancheyta Jorge, Trejo Fernando, Rodríguez Silvano (2017). Methods for determining asphaltene stability in crude oils. *Fuel*, 188, pp. 530-543. <https://doi.org/10.1016/j.fuel.2016.10.012>
- Jewell D.M., Weber J.H., Bunger J.W., Plancher H., Latham D.R. (1972). Ion-exchange, coordination, and adsorption chromatographic separation of heavy-end petroleum distillates. *Analytical Chemistry*, 44, pp. 1391-1395. <https://doi.org/10.1021/ac60316a003>
- Kashaev R.S. (2018). Viscosity Correlations with Nuclear (Proton) Magnetic Resonance Relaxation in Oil Disperse Systems. *Applied Magnetic Resonance*, 49(3), pp. 1-7. <https://doi.org/10.1007/s00723-018-0977-2>
- Kayukova G.P., Kiyamova A.M., Romanov G.V. et al. (2008). Technological qualities of natural bitumen of Tatarstan, depending on the chemical and geochemical characteristics of their composition. *Neftyanoye khozyaystvo = Oil industry*, 1, pp. 22-27. (In Russ.)
- Kharrat, A.M., Zacharia, J., Cherian, V.J., Anyatonwu, A. (2007). Issues with comparing SARA methodologies. *Energy & Fuels*, 21, pp. 3618-3621. <https://doi.org/10.1021/ef700393a>
- Khasanova Nailia, Sakharov Boris, Volkov Vladimir, Nourgaliev Danis (2017). Low-field NMR method for analysis of heavy oils without extraction of asphaltenes. In Book: "New methods and technologies in petroleum geology". 17th Int. Multidiscip. Scientific GeoConference SGEM 2017. Vienna, Austria, 17(14), pp. 297-315.
- Korb Jean-Pierre, Louis-Joseph Alain, and Benamsili Lyès (2013). Probing Structure and Dynamics of Bulk and Confined Crude Oils by Multiscale NMR Spectroscopy, Diffusometry, and Relaxometry. *J. Phys. Chem. B*, 117, pp. 7002-7014. <https://doi.org/10.1021/jp311910t>
- Majumdar Rudraksha Dutta, Montina Tony, Mullins Oliver C., Hazendonk Paul (2017). Insights into asphaltene aggregate structure using ultrafast MAS solid-state <sup>1</sup>H-NMR spectroscopy. *Fuel*, April 193, pp. 359-368. <https://doi.org/10.1016/j.fuel.2016.12.082>
- Maqbool Tabish H., Srikratiwong Perapat and Fogler Scott (2011). Effect of Temperature on the Precipitation Kinetics of Asphaltenes. *Energy Fuels*, 25(2), pp. 694-700. <https://doi.org/10.1021/ef101112r>
- Marc Jones, Spencer E. Taylor (2015). NMR relaxometry and diffusometry in characterizing structural, interfacial and colloidal properties of heavy oils and oil sands. *Advances in Colloid and Interface Science*, 224, pp. 33-45. <http://dx.doi.org/10.1016/j.cis.2015.07.007>
- Mirotnichik K., Kantzas A., Starosud A., Aikman M. (2001a). A New method for group analysis of petroleum fractions in unconsolidated porous media. *J. Can Pet Technol.*, 40, pp. 38-44. <https://doi.org/10.2118/01-07-02>
- Mirotnichik K.D., Allsopp K., Kantzas A., Curwen D., Badry R. (2001b). Low-field NMR method for bitumen sands characterization: a new approach. *SPE Reserv Eval Eng.*, 4, pp. 88-96. <https://doi.org/10.2118/71208-PA>
- Mitchell J., Gladden L.F., Chandrasekera T.C., Fordham E.J. (2014). Low-field permanent magnets for industrial process and quality control. *Progress in Nuclear Magnetic Resonance Spectroscopy*, 76, pp. 1-60. <https://doi.org/10.1016/j.pnmrs.2013.09.001>
- Morgan V.G., Barbosa L.L., Lacerda V.Jr., et al. (2014). Evaluation of the Physicochemical Properties of the Postsalt Crude Oil for Low-Field NMR. *Ind. Eng. Chem. Res.*, 53, pp. 8881-8889. <https://doi.org/10.1021/ie500761v>
- Muhammad Asif, Azeredo Rodrigo Bagueira de Vasconcellos (2014). <sup>1</sup>H NMR spectroscopy and low-field relaxometry for predicting viscosity and API gravity of Brazilian crude oils – A comparative study. *Fuel*, 130, pp. 126-134. <https://doi.org/10.1016/j.fuel.2014.04.026>
- Mullins Oliver C., Sabbah Hassan, Eyssautier Joëlle and et al. (2012). Advances in Asphaltene Science and the Yen-Mullins Model. *Energy Fuels*, 26(7), pp. 3986-4003. <https://doi.org/10.1021/ef300185p>
- Mutina A.R., Hürlimann M.D. (2008). Correlation of transverse and rotational diffusion coefficient: A probe of chemical composition in hydrocarbon oils. *J. Phys. Chem. A*, 112, 3291-3301. <https://doi.org/10.1021/jp710254d>
- Nikolin I.V., Safonov S.S., Skirda V.D., Shkalikov N.V. (2008). Sposob opredeleniya soderzhaniya parafinov i asfal'tenov v nef'ti [Method for determining the content of paraffins and asphaltenes in oil]. Patent RF No. 2333476 (In Russ.)
- Nikolin I.V., Shkalikov N.V., Skirda V.D. (2010). Sposob opredeleniya soderzhaniya zhidkofaznykh i tverdotel'nykh komponent v smesi uglevodorodov [Method for determining the content of liquid-phase and solid-state components in a mixture of hydrocarbons]. Patent RF No. 2383884 (In Russ.)
- NMR analyzer «Chromatek-Proton 20M» <http://www.chromatec.ru/products/main/nmr/proton20m/>
- Prunelet Alexandre, Fleury Marc, Cohen-Addad Jean-Pierre (2004). Detection of asphaltene flocculation using NMR relaxometry. *C. R. Chimie*, 7, pp. 283-289. <https://doi.org/10.1016/j.crci.2003.11.011>
- Silva Sandra L., Silva Artur M.S., Ribeiro Jorge C., et al. (2011). Chromatographic and spectroscopic analysis of heavy crude oil mixtures with emphasis in nuclear magnetic resonance spectroscopy: A review. *Analytica Chimica Acta*, 707(1-2), 30, pp. 18-37. <https://doi.org/10.1016/j.aca.2011.09.010>
- Sakharov B.V., Khasanova N.M., Volkov V.Ya. (2015). Joint measurement and combined processing of SI and echo signals in the CPMG series for the evaluation of the component composition of heavy oils. Sb.tezisev VI Vseros. konf.: «Novyye dostizheniya YAMR v strukturnykh issledovaniyakh» [Proc. VI All-Russian Conf. «New NMR achievements in structural research»]. Kazan, pp. 67-68. (In Russ.)
- Shadman Mohammad Mahdi, Dehaghani Amir Hossein Saeedi, Badizad



Mohammad Hasan (2017). How much do you know about the methods for determining onset of asphaltene precipitation? *Petroleum*, 3, pp. 287-291. <https://doi.org/10.1016/j.petlm.2016.08.011>

Shkalikov N.V. (2010). Issledovaniye tyazhelykh neftey i ikh komponent metodom YAMR [Investigation of heavy oils and their components by NMR]. *Diss. kand. fiz.-mat. nauk.* [Cand. phys. and math. sci. diss.] Kazan. (In Russ.)

Shkalikov N.V., Skirda V.D., Arkhipov R.V. (2006). Solid-like Component in the Spin-Spin NMR-Relaxation of Heavy Oils. *Magnetic Resonance in Solids. Electronic Journal*, 8(1), pp. 38-42. <http://mrsej.ksu>.

Shkalikov N.V., Ganeeva Yu M., Yusupova T. N., Skirda V.D. (2008). The characterization of asphaltenes by <sup>1</sup>H NMR relaxation method: microsecond range of spin-spin relaxation times. *Magnetic Resonance in Solids. Electronic Journal*, 10(1), pp. 38-42. <http://mrsej.ksu>

Stapf Siegfried, Ordikhani-Seyedlar Amin, Ryan Nina, Mattea Carlos, Kausik Ravinath, Freed Denise E., Song Yi-Qiao, and Hürlimann Martin D. (2014). Probing Maltene –Asphaltene Interaction in Crude Oil by Means of NMR Relaxation. *Energy Fuels*, 28, pp. 2395-2401. <https://doi.org/10.1021/ef4024788>

Takeshi Yamanobe, Hiroki Uehara, and Masaki Kakiage (2010). Practical NMR Analysis of Morphology and Structure of Polymers. *Annual Reports on NMR Spectroscopy*, 70, pp. 203-239. [https://doi.org/10.1016/S0066-4103\(10\)70003-X](https://doi.org/10.1016/S0066-4103(10)70003-X)

Trezza E., Haiduc A.M., Goudappel G.J. W. and van Duynhoven J. P. M. (2006). Rapid phase-compositional assessment of lipid-based food products by time domain NMR. *Magn. Reson. Chem.*, 44, pp.1023-1030. <https://doi.org/10.1002/mrc.1893>

Volkov V.Ya., Sakharov B.V., Khasanova N.M. (2016a). Investigation of heavy oils by NMR relaxation in low fields. *Sb.tezisev mezhd. simp. «Magnitnyy rezonans: ot fundamental'nykh issledovaniy k prakticheskim prilozheniyam»*. [Proc. International symposium "Magnetic resonance: from fundamental research to practical applications"]. Kazan, pp. 59-60. (In Russ.)

Volkov V.Ya., Sakharov B.V., Khasanova N.M. (2016b). SARA-YAMR method gruppovogo analiza neftey in situ. [SARA-NMR method for group analysis of oils in situ]. Kazan: Ikhlas Publ., v.1, pp. 97-100. (In Russ.)

Volkov V.Ya., Sakharov B.V., Khasanova N.M. (2017). Monitoring the properties of crude heavy oils using magnetic radiospectroscopy. *Mater. nauchno-prakt. konfer.«Gorizonta'nyye skvazhiny i GRP v povyshenii effektivnosti razrabotki neftyanykh mestorozhdeniy»* [Proc. Sci. and Pract. Conf. "Horizontal wells and fracturing in increasing the efficiency of oil fields development"]. Kazan: SLOVO Publ., pp. 149-152. (In Russ.)

Vorapalawut Nopparat, Nicot Benjamin, Louis-Joseph Alain and Korb Jean-Pierre (2015). Probing dynamics and interaction of maltenes with asphaltene aggregates in crude oils by multiscale NMR. *Energy Fuels*, 29(8), pp. 4911-4920. <https://doi.org/10.1021/acs.energyfuels.5b01142>

Yang Z., Hirasaki G.J. NMR measurement of bitumen at different temperatures. (2008). *J. Magn. Reson.*, 192(2), pp. 280-293. <https://doi.org/10.1016/j.jmr.2008.03.007>

Yashchenko I.G. (2012). Tyazhelyye vanadiyenosnyye nefti Rossii [Heavy vanadium-bearing oils in Russia]. *Izvestiya Tomskogo politekhnicheskogo universiteta = Proceedings of Tomsk Polytechnic University*, 321(1), pp. 105-111. (In Russ.)

Zielinski L., Saha I., Freed D.E., and Hürlimann M.D. (2010). Probing Asphaltene Aggregation in Native Crude Oils with Low-Field NMR. *Langmuir*, 26(7), pp. 5014-5021. <https://doi.org/10.1021/la904309k>

Zielinski, L.; Hürlimann, M. D. (2011). Nuclear Magnetic Resonance Dispersion of Distributions as a Probe of Aggregation in Crude Oils. *Energy Fuels*, 25(11), pp. 5090-5099. <https://doi.org/10.1021/ef200883r>

## About the Authors

**Vladimir Ya. Volkov** – DSc (Chemistry), Professor  
Kazan (Volga region) Federal University  
MIREA – Russian Technological University  
78, Vernadsky Ave., Moscow, 119454, Russian Federation

**Boris V. Sakharov** – Researcher  
Kazan (Volga region) Federal University  
State Research Center for Applied Microbiology and Biotechnology  
Obolensk, Serpukhov district, Moscow region, 142279, Russian Federation

**Nailia M. Khasanova** – PhD (Phys. and math.), Associate Professor, Researcher, Institute of Geology and Petroleum Technologies,  
Kazan (Volga region) Federal University  
4/5, Kremlevskaya st., Kazan, 420008, Russian Federation

**Danis K. Nurgaliev** – Professor, DSc (Geology and Mineralogy), Vice-Rector for Research  
Kazan (Volga region) Federal University  
4/5, Kremlevskaya st., Kazan, 420008, Russian Federation

Manuscript received 25 April 2018;

Accepted 13 August 2018; Published 30 November 2018

## SHORT COMMUNICATION

DOI: <https://doi.org/10.18599/grs.2018.4.324-330>

## Study of the lithological characteristics of Domanic deposits of the Pervomayskoe field

A.A. Takhauov\*, A.A. Titov

Tatar Geological Exploration Department Tatneft PJSC, Kazan, Russian Federation

**Abstract.** The paper presents the results of studying rocks of the domanic horizon of the Pervomayskoe oil field represented by core material of the well 467D. In tectonic terms, this well, like the entire Pervomayskoe field, is confined to the axial part of the Kama-Kinel deflection system on the territory of the North-Tatar arch. Administratively, the Pervomayskoe deposit is located on the territories of the Elabuga, Mendeleevsky and Tukaevsky districts of the Republic of Tatarstan. To study the core material presented, different studies were conducted, including a macroscopic description of the core; comparison of the studied rocks with well logging data; optical microscopic analysis; X-ray analysis; determination of reservoir properties of rocks; study of organic matter by the Rock-Eval pyrolysis method.

Based on the analysis, it was found that the domanic horizon is composed of rocks containing carbonate and siliceous minerals to varying degrees, occasionally including minor mixtures of other minerals. The section of rocks is characterized by a sharp change in the lithological composition with a thickness of interlayers of several centimeters. According to Rock-Eval data, carbonate-siliceous interlayers have a high content of organic matter. Organic matter in Domanic deposits is characterized as immature and is found in rocks in the form of kerogen.

**Keywords:** hydrocarbons, Domanic deposits, domanicites, shale, shale oil, core, Pervomayskoe field; Republic of Tatarstan

**Recommended citation:** Takhauov A.A., Titov A.A. (2018). Study of the lithological characteristics of Domanic deposits of the Pervomayskoe field. *Georesursy = Georesources*, 20(4), Part 1, pp. 324-330. DOI: <https://doi.org/10.18599/grs.2018.4.324-330>

The potential of unconventional sources of oil and gas is currently one of the most pressing issues of the modern gas and oil industry. Nowadays, the main interests of exploration and production are hydrocarbon deposits confined to highly porous reservoirs of predominantly intergranular porosity. However, the reserves of “conventional” hydrocarbons are unfortunately gradually being depleted. This is why further prospects for the development of the oil and gas industry are increasingly associated with the prospection and exploration of objects associated with reservoirs with complex lithologic and petrophysical characteristics, also called “unconventional” reservoirs.

One of the best-known unconventional sources of hydrocarbons is shale oil and gas, produced mainly in the United States of America. It is considered that according to lithological and geochemical characteristics as well as reservoir potential, shale strata developed in the United States are analogous to the Bazhenov deposits of the West Siberian Plate and their analogues in other

regions. For the territory of the Volga-Ural oil and gas region, domanic deposits offer the best perspectives for the production of “unconventional” hydrocarbons.

According to current research, the domanic deposits, or domanicites, are rocks of the domanic horizon of the Upper Frasnian Upper Devonian substage. Their distinctive feature is a high content of organic matter: from 5 to 20%. The overlying sediments from the Mendymsky to the Trans-Volga horizons of the Upper Devonian are called domanicoids (Korolyuk et al., 1984). They contain a lesser amount of organic matter: from 0.5 to 5%. Domanikits and domanicoids differ slightly in their lithologic composition: domanicoids are generally low-permeability, massive, layered carbonate rocks whereas Domanikits are massive, sometimes shaly, layered carbonate-siliceous and siliceous-carbonate rocks with very low permeability. Because of the type of organic matter, its maturity and thermodynamic conditions, domanic deposits in the territory of the oil and gas regions in Tatarstan are considered promising for oil generation.

According to the latest estimates, the resources of “unconventional” oil in the domanic sediments of Tatarstan range from 4.5 billion tons (Dyny J.R., 2005) to 14.6 billion tons (according to the data of the Academy

\*Corresponding author: Artur A. Takhauov  
E-mail: [takhauov@gmail.com](mailto:takhauov@gmail.com)

© 2018 The Authors. Published by Georesursy LLC  
This is an open access article under the CC BY 4.0 license  
(<https://creativecommons.org/licenses/by/4.0/>)

of Sciences of the Republic of Tatarstan). They are currently being developed as a pilot by Tatneft PJSC. Oil production is also carried out in the Republic of Tatarstan from deposits of domanic sediments discovered many years ago during exploration campaigns for oil. The development of these deposits is carried out by methods used for conventional reservoirs, since these deposits are associated with linear zones of increased fracturing of rocks confined to regional faults (Khisamov et al., 2010). In other words, the type of porosity in the domanic rocks, to which these deposits are confined, is fractured, with a significant relationship between porosity and permeability, which is typical of «conventional» reservoirs. However, in most cases, fracturing of the domanic deposits in Tatarstan is rare, therefore they are usually referred to as “unconventional” reservoirs and require their own set of development methods. According to the world experience in developing such deposits, this set of methods used most often includes drilling horizontal wells and conducting multi-stage hydraulic fracturing to increase the permeability of rocks.

Having this information in mind, the domanic deposits of Tatarstan are undoubtedly a current topic for research. The object of the study was the core material from well 467D of the Pervomayskoe field, which is located on the territory of the Republic of

Tatarstan and tectonically located in the axial zone of the Kama-Kinel deflection system on the territory of the North-Tatar arch. This territory is characterized by an average thickness of mendym-domanikovy deposits from 60 to 80 meters (Fig. 1).

The set of studies carried out included: macroscopic core description, comparison of the core with well logging data, optical microscopic analysis, X-ray analysis, determination of reservoir properties, rock pyrolysis using the Rock-Eval method.

The aim of the work conducted was to prepare a preliminary assessment of the domanic deposits of the Pervomayskoe field as an “unconventional” reservoir with a possibility of containing hydrocarbons.

The core material from well 467D was selected at depths of 1662.2-1684.4 m. This interval represents the rocks of the lower part of the domanic horizon, which lies in this well at depths of 1644.5-1682.4 m (Fig. 2) and the top of the Sargayevsky horizon, present at depths of 1682.4-1691.4 m. The choice of the interval for sampling was justified with a more intense saturation of the organic content of the core samples from this part of the section. According to well logging data, this part of the domanic horizon is characterized by increased radioactivity, which is associated with a high content of organic matter, adsorption of uranium salts, as well as lower resistance values, which indicates the absence of oil in these rocks.

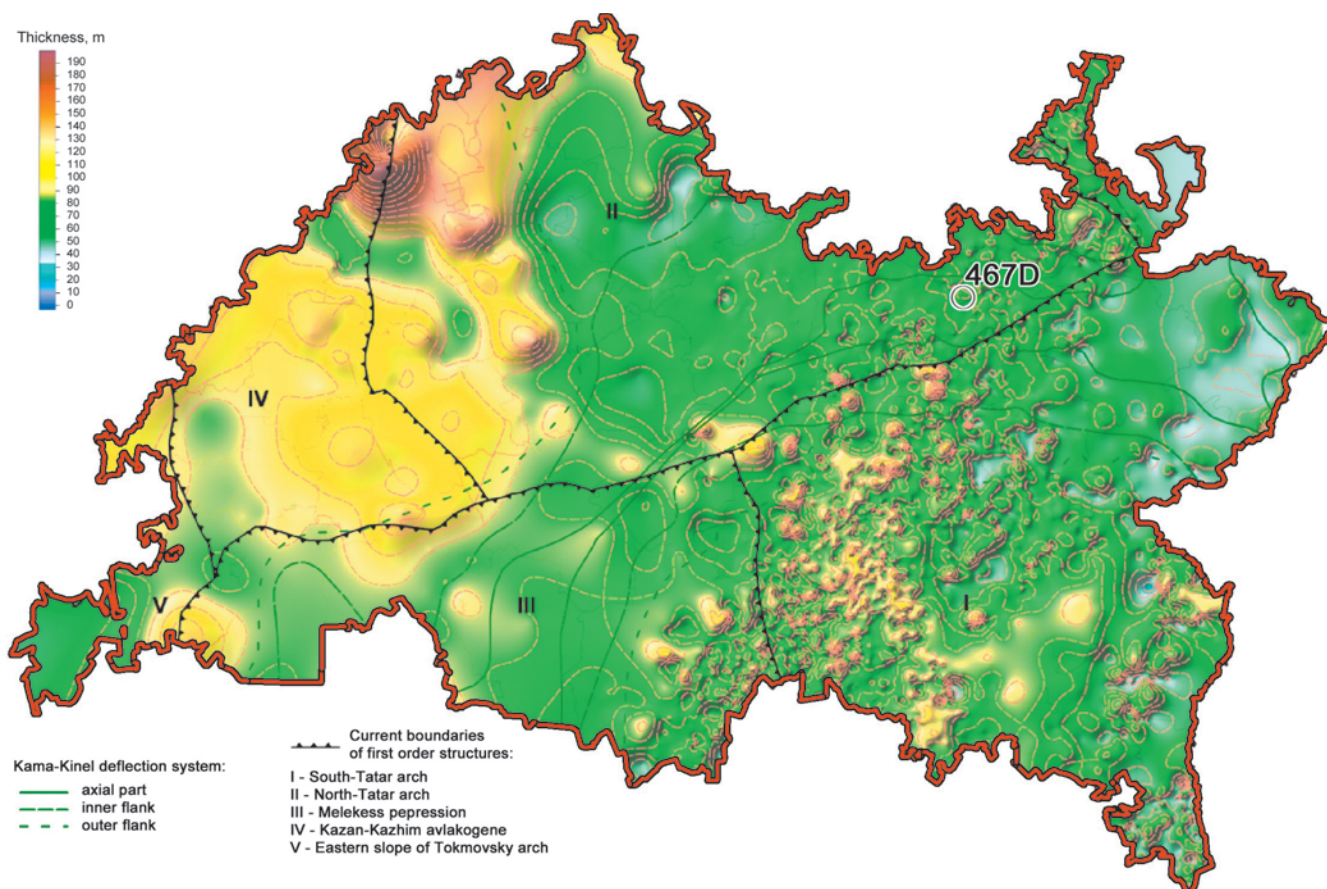


Fig. 1. Map of Mendym-domanic deposits of the Upper Devonian according to deep drilling data on the territory of the Republic of Tatarstan



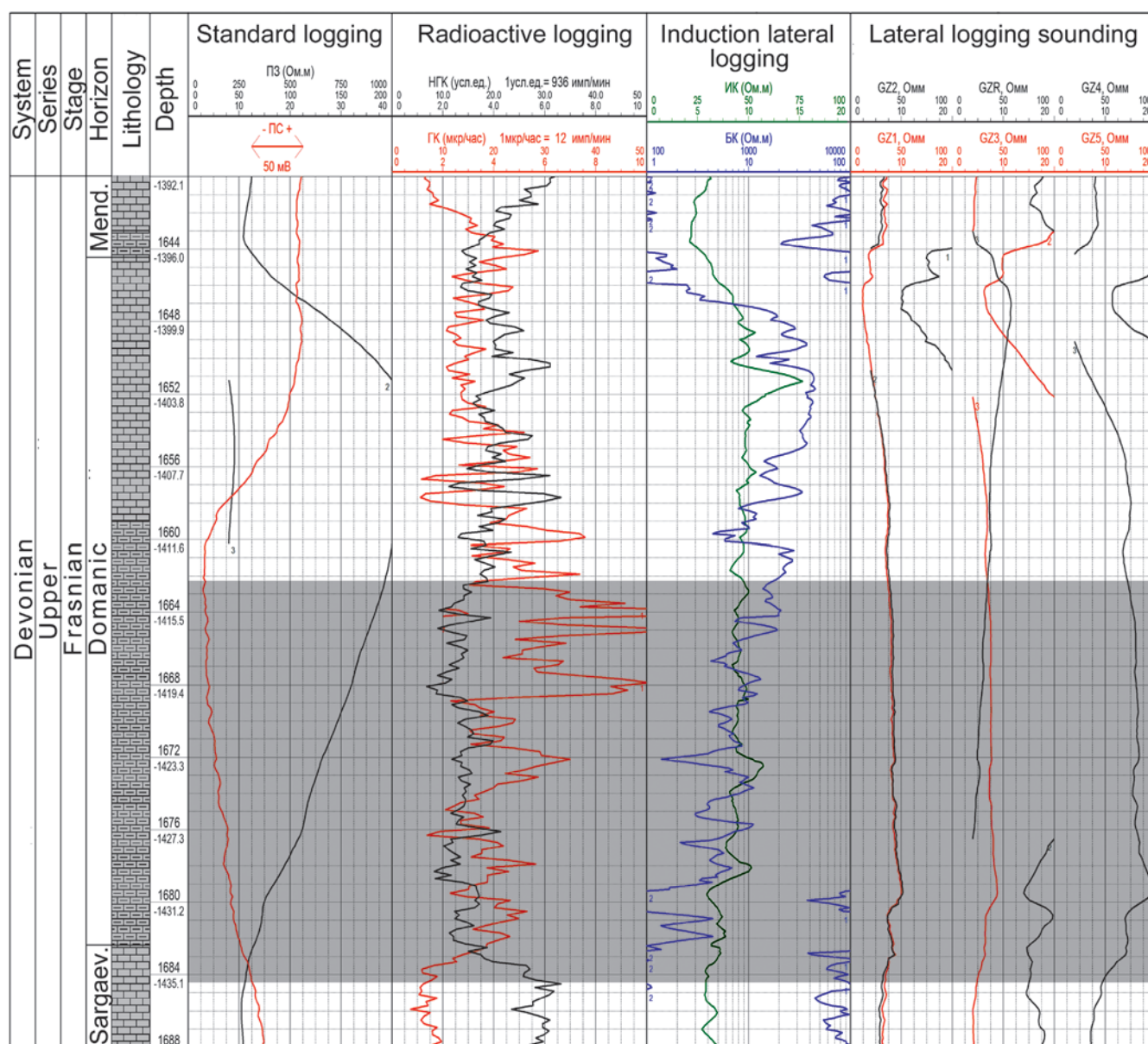


Fig. 2. Well logging data in the interval of occurrence of the domanic horizon in the 467D well (The selection of core material for the study is shown in color)

Based on the macroscopic description of the core of the domanic horizon, the rocks are predominantly carbonate-siliceous and siliceous-carbonate, sometimes carbonate, with a cryptocrystalline structure, laminated, shaly and sometimes with a massive texture, intensely saturated with organic matter. Carbonates are chemogenic and organogenic. In the samples, horizontal and wavy layering are found, as well as rewashing and redeposition of sediments. Horizontal stratification is characteristic of carbonate-siliceous rocks (Fig. 3a), non-horizontal, and wavy - of siliceous-carbonate rocks (Fig. 3b).

Optical microscopic and X-ray analyses made it possible to clarify the mineralogical composition of the domanic rocks: silica, calcite, rarely dolomite, clay minerals are rarely found and are in minor proportions.

The study of petrographic thin sections in transmitted light was carried out using a Polam L-211M microscope with a USB2.0 YW500 digital camera.

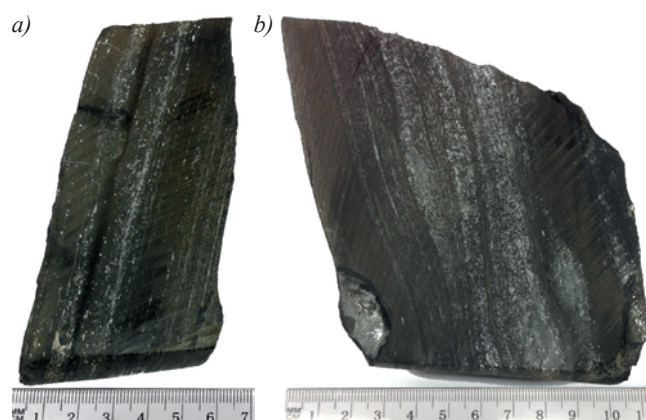


Fig. 3. Stratification of rocks: a) horizontal layering of carbonate-siliceous rock; well 467D, Pervomayskoe field, sample no.20, depth – 1679.4 m; b) wavy layering of siliceous-carbonate rock; well 467D, Pervomayskoe field, sample no.11, depth – 1672.5 m

Studying thin sections, it was discovered that the texture of the rocks is predominantly thin and medium-layered, sometimes shaly, massive, patchy, breccia-like. The interlacing of fine-grained limestone with a carbonate-siliceous rock is quite common. The thickness of the interlayers varies from tenths to several millimetres. Remains of radiolarians and phytoplankton were found.

X-ray analysis was performed on a D2 Phaser diffractometer (Bruker, Germany) for measuring powder preparations in Brega-Brentano geometry (3-40°) using monochromatic CuK  $\alpha$ -radiation, in scan mode with a step of 0.02° with a speed of 1°/min. The voltage of the X-ray tube was 30 kV, and the current strength was 30 mA. Diffraction patterns were identified by comparing with reference diffractograms from the international PDF-2 ICDD database. On each diffractogram, the diffraction reflections of the minerals present in the sample are shown in a determined colour in a bar-graph.

Confronting macroscopic, optical microscopic and X-ray data, the following lithogenetic types of rocks can be distinguished: organogenic-detrital limestone, granular limestone, siliceous-carbonate and carbonate-siliceous rocks, silicites. These rocks are interbedded, the thickness of the interlayers ranges from several to tens of centimetres.

Some interlayers consist of almost completely siliceous rocks with an insignificant content of calcite and microcline (Fig. 4). In these rocks, there is a higher

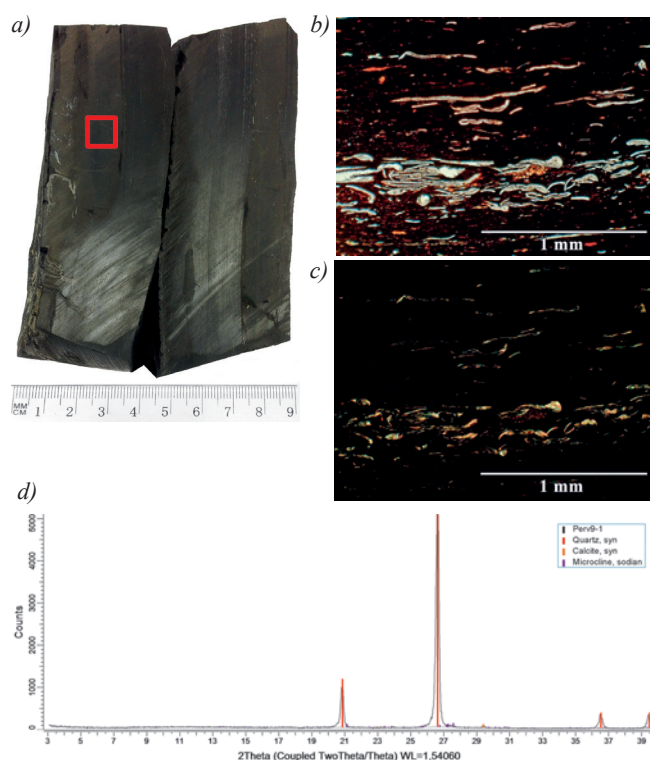


Fig. 4. The carbonate-siliceous rock sample studied: a) photograph of the sample; well 467D, Pervomayskoe field, sample no.9, depth – 1670.4 m; b) photograph of a thin section in parallel nicols; c) a photo of a thin section in crossed nicols; d) diffractogram

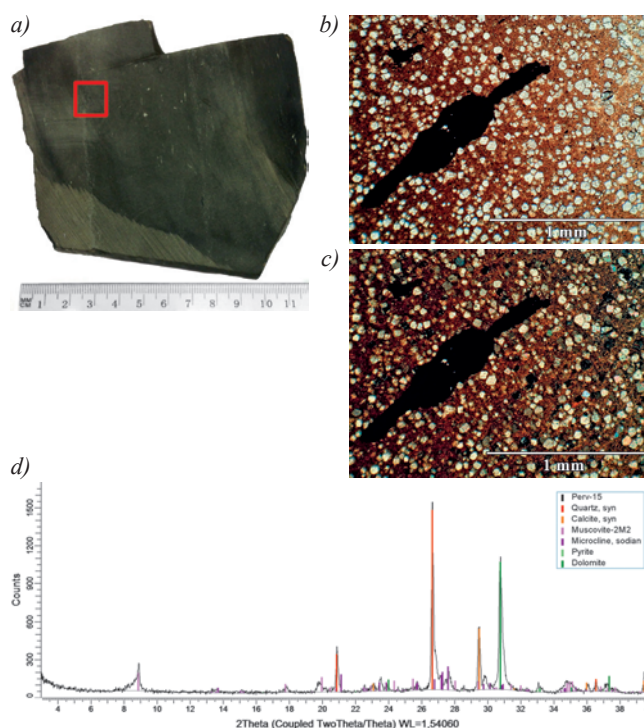


Fig. 5. The carbonate-siliceous rock sample studied: a) photograph of the sample; well 467D, Pervomayskoe field, sample no.15, depth – 1675.5 m; b) photograph of a thin section in parallel nicols; c) a photo of a thin section in crossed nicols; d) diffractogram

content of organic matter (kerogen). In thin section remains of ostracod and tentaculite are observed, which are mainly deposited in thin interlayers parallel to the stratification of the rock.

In other layers, a decrease in the silica content and an increase in the carbonate minerals content (calcite, dolomite) is observed (Fig. 5). These rocks contain a higher percentage of impurities of other minerals (pyrite, microcline, muscovite, etc.) and a significantly smaller amount of organic residues and, consequently, a smaller amount of organic matter.

There are interlayers in which silica is found in much smaller quantities than carbonates (calcite) (Fig. 6). Calcite in these rocks is predominantly organogenic. A large amount of organic residues occurring parallel to the layering is observed. The content of organic matter (kerogen) in these interlayers is rather high.

Carbonate interlayers were also present with a complete absence or very low content of silica (Fig. 7). A large amount of organic residues is observed even if organic matter in carbonates is practically absent, or is present in small amounts in layers with a mixture of silica.

All the distinguished lithogenetic types of rocks are deposited by interbedding, and no regularities were observed in the sequence of their intercalation. A characteristic feature of this section is a sharp change in the lithological composition and content of organic matter (Fig. 8), while the thickness of the layers is



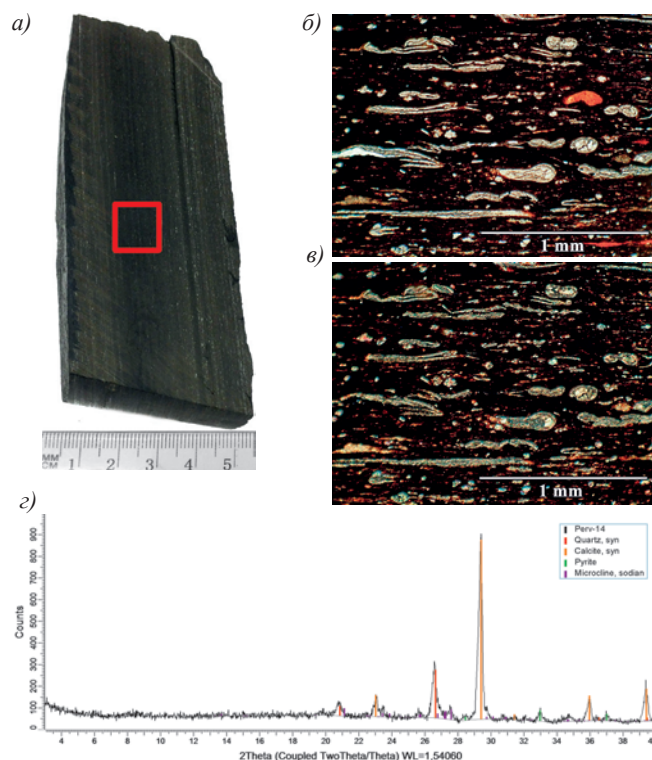


Fig. 6. The carbonate-siliceous rock sample studied: a) photograph of the sample; well 467D, Pervomayskoe field, sample no.14, depth – 1674.4 m; b) photograph of a thin section in parallel nicols; c) a photo of a thin section in crossed nicols; d) diffractogram

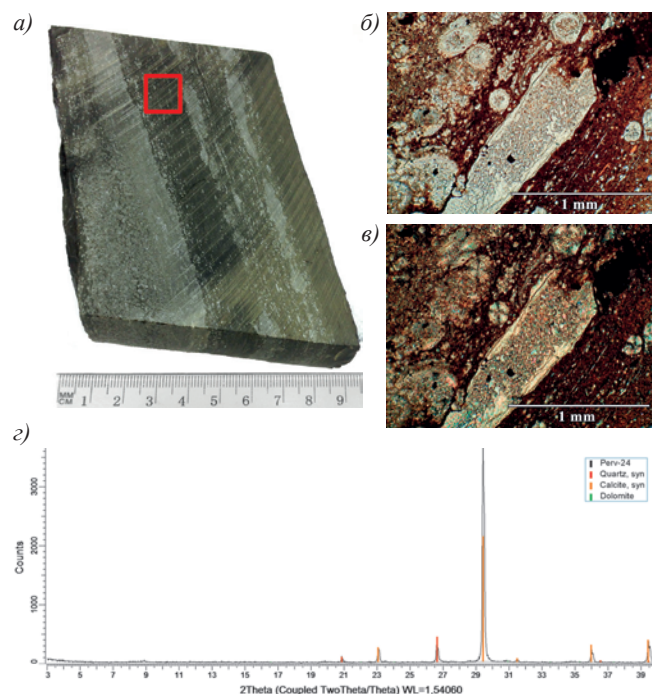


Fig. 7. The carbonate-siliceous rock sample studied: a) photograph of the sample; well 467D, Pervomayskoe field, sample no.24, depth – 1683.9 m; b) photograph of a thin section in parallel nicols; c) a photo of a thin section in crossed nicols; d) diffractogram

only a few centimetres. The content of organic matter is directly related to the presence of silica in the rock. The exceptions are the interlayers with a low content

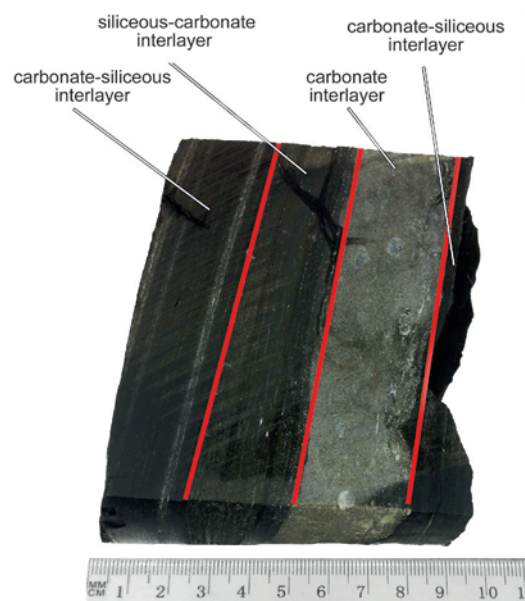


Fig. 8. Interbedding of different lithological types of rocks; well 467D, Pervomayskoe field, sample no.5, depth – 1666.5 m

of organic residues and a high content of impurities of other minerals, such as dolomite, pyrite, muscovite, microcline. In these interlayers, the organic content is characterized by lower values.

Subsequently, the reservoir properties of rocks were investigated. The open porosity was determined by saturating the samples under vacuum with a model of produced water (NaCl solution with a density of 1.16 g/cm<sup>3</sup>) and their weighing before and after saturation (Preobrazhensky Method).

The permeability of rocks was determined by testing samples of cylindrical shape for gas permeability to nitrogen on the GK-5 device.

As a result of measurements, it was determined that the rocks of the domanic horizon have very low porosity and permeability (Table 1). The permeability value was only obtained for sample no.1, granular limestone.

No. of sample	Depth, m	Open porosity, %	Permeability to gas, 10 <sup>-3</sup> μm <sup>2</sup>
1	1662,20	0,68	0,46
2	1663,40	0,38	0
3	1664,70	0,40	0
7	1668,30	0,10	0
9	1670,40	0,88	-
14	1674,40	0,34	0
15	1675,50	0,26	0
16	1676,60	0,55	-
17	1677,20	0,59	-
18	1677,80	0,65	-
19	1678,70	1,20	-
20	1679,40	0,73	-

Table 1. Reservoir properties of rocks



In other samples, the permeability value was so small that it could not be measured and assumed to be zero. The presence of increased permeability in limestones relative to other rocks indicates a better communication between the pores, which is characteristic of traditional reservoirs, but most of the section studied is practically impermeable. Low values of open porosity also allow us to consider the studied rocks as “unconventional” reservoirs, which are characterized by closed porosity.

To determine the type as well as the amount of organic matter in the rocks, the Rock-Eval pyrolysis method was used. For the analysis, a HAWK Resource Workstation pyrolyzer manufactured by WildCat Technologies was used.

The results of Rock-Eval confirmed the dependence of the content of organic matter on the silica content (Table 2): in high-silica rocks (samples 3, 4, 8, 9, 14) the organic content is from 16.43 to 26.22%; in limestone (samples 1, 18, 24) – from 1.15 to 2.58%; in



siliceous-carbonate dolomitic rocks with a low content of organic residues (samples 15, 16, 21, 22) the content of dispersed organic matter varies from 1.40 to 4.89; in the remaining interlayers, predominantly represented by carbonate-siliceous rocks, the organic content varies from 4.09 to 10.70%. Organic matter in the studied rocks is in the form of kerogen (parameter S2>S1) and is immature ( $T_{max} < 435^{\circ}\text{C}$ ). Kerogen is considered to be type II (HI value varies from 300 to 600), which is characterized by predominant generation of oil.

### Conclusion and Discussion

Based on the analysis of the lithological composition and organic matter of the domanic sediments of the 467D well of the Pervomayskoe field, the following conclusions can be noted:

1) The studied rocks are composed of carbonate and siliceous minerals with minor mixtures of pyrite and microcline.

Sample	Depth <i>m</i>	S0	S1 «Free oil» mg HC/g of rock	S2 Kerogen, mg HC/g of rock	S3 mg CO <sub>2</sub> /g of rock	TOC Total Organic Carbon, wt %	Tmax Maturity °C	HI Index of hydrogen, mg HC/g TOC
1	1662,2		0,06	1,47	0,17	1,15	432	127
2	1663,4		0,24	29,93	0,30	5,79	432	517
3	1664,7		0,73	115,83	0,56	20,49	433	565
4	1665,8		0,74	87,40	0,39	16,43	429	531
5	1666,6		0,47	56,83	0,33	10,70	432	531
6	1667,5		0,20	23,39	0,17	4,48	431	522
7	1668,3		0,31	39,93	0,23	7,81	431	511
8	1669,5		0,73	98,43	0,47	17,84	432	551
9	1670,4		0,85	101,10	0,53	18,46	432	547
10	1671,6		0,34	43,29	0,24	8,00	431	540
11	1672,5		0,30	30,27	0,36	5,80	431	522
12	1673,3	0,17	0,20	19,58	0,31	4,95	430	395
13	1673,4		0,29	32,36	0,25	6,09	431	531
14	1674,4		0,89	171,72	0,73	26,22	430	654
15	1675,5		0,14	4,52	0,45	1,40	437	322
16	1676,6		0,20	24,89	0,56	4,89	436	508
17	1677,2		0,37	43,33	0,33	7,63	433	567
18	1677,8		0,12	10,75	0,17	2,29	431	469
19	1678,7		0,19	21,39	0,20	4,09	431	523
20	1679,4		0,47	54,79	0,35	9,62	430	569
21	1680,5		0,13	12,50	0,09	2,58	431	484
22	1681,6	0,11	0,12	7,07	0,25	1,87	431	377
23	1682,4		0,19	24,23	0,26	4,39	430	552
24	1683,9		0,12	10,86	0,37	2,43	436	445
25	1684,4		0,16	20,56	0,32	3,51	429	585

 - high-silica rocks, silicite  
 - siliceous-carbonate dolomite rocks


 - limestone  
 - carbonate-siliceous rocks

Table 2. The results of pyrolysis using the Rock-Eval method for the core of well 467D

2) Lithogenetic types of rocks were identified: limestones, organogenic-detrital, granular limestones, siliceous-carbonate and carbonate-siliceous rocks, silicites.

3) In the section is observed an interbedding of rocks without a definite dependence with interbedding thickness of several centimetres, which indicates sharp changes in the conditions of sedimentation.

4) It was established that the content of organic matter is higher in carbonate-siliceous rocks, smaller in siliceous-carbonate rocks, and practically absent in carbonate rocks. Thus, there is a direct dependence of the organic content on the silica content in the rock.

5) Organic matter in the Domanic sediments is characterized as immature and is found in the rocks in the form of kerogen. Kerogen is of type II.

According to preliminary estimates, based on studies of the 467D well, it can be said that the deposits of the domanic horizon of the Pervomayskoe field are extremely heterogeneous in terms of lithological composition and organic matter content. Domanicites are dense, mostly silicified rocks, with no fractures and porosity visible under the microscope. The porosity values do not exceed 1.2%, the permeability values in the majority of the section are close to zero. The average content of organic matter in the section of rocks is rather high and amounts to 7.96%, which is typical of the domanicites of the Volga-Ural oil and gas region. The data obtained indicate that the Pervomayskoe domanic deposits are reservoirs of «unconventional» type. In case of their development, it is necessary to use the methods used to develop shale deposits (“shale oil”) and deposits

in low-permeability reservoirs (“tight oil”) – drilling horizontal wells and carrying out multi-stage hydraulic fracturing. It is also necessary to use a technology that allows the development of immature organic matter (“oil shale”). Such technologies exist nowadays, but are at the stage of experimental research (ICP Shell, Chevron CRUSH, ExxonMobil ElectroFrac).

## References

- Dyni J.R. (2005). *Geology and Resources of Some World Oil-Shale Deposits*. Scientific Investigations Report 2005-5294. 42 p.
- Khislamov R.S., Gubaydullin A.A., Bazarevskaya V.G., Yudinsev E.A. (2010). *Geologiya karbonatnykh slozhno postroyennykh kollektorov devona i karbona Tatarstana* [Geology of carbonate complexly constructed Devonian and Carboniferous reservoirs of Tatarstan]. Kazan: Fen, 283 p. (In Russ.)
- Korolyuk I.K., Letavin A.I., Mkrchyan O.M., Khachatryan R.O. et al. (1984). *Strukturno-formatsionnyye kriterii prognoza neftegazonosnosti* [Structural and formational criteria for predicting oil and gas content]. *Teoreticheskiye osnovy poiskov, razvedki i razrabotki mestorozhdeniy nefiti i gaza* [Theoretical foundations of search, exploration and development of oil and gas fields]. Moscow: Nauka, pp. 47-62. (In Russ.)

## About the Authors

**Artur A. Takhauov** – Geologist, Tatar Geological Exploration Department Tatneft PJSC  
23/25, Chernyshevsky st., Kazan, 420111, Russian Federation

**Arsen A. Titov** – Geophysicist, Tatar Geological Exploration Department Tatneft PJSC  
23/25, Chernyshevsky st., Kazan, 420111, Russian Federation

*Manuscript received 28 February 2018;  
Accepted 13 September 2018;  
Published 30 November 2018*

## SHORT COMMUNICATION

DOI: <https://doi.org/10.18599/grs.2018.4.331-335>

## Types of reservoirs of the Ufa stage of the Republic of Tatarstan. Genesis and reservoir properties

*R.F. Vafin<sup>1</sup>, R.R. Khaziev<sup>2\*</sup>, L.Z. Anisimova<sup>2</sup>, K.Yu. Koluzaeva<sup>2</sup>*<sup>1</sup>Kazan (Volga Region) Federal University, Kazan, Russian Federation<sup>2</sup>Institute for Environmental Problems and Subsoil Use of Tatarstan Academy of Sciences, Russia, Kazan

**Abstract.** In this paper, we studied core material from well No. 15 of the extra-viscous oil field, geographically located within the western border of the South Tatar arch. Under laboratory conditions, reservoir properties (porosity, permeability), oil saturation and particle size distribution of Sheshmin sandstones were measured. It was established that the terrigenous reservoir belongs to class I and II according to the classification of A.A. Hanin, with high permeability. In addition, in well No. 15, a downward trend was identified in reservoir properties downstream of the section, the reason for which is probably the migration of underlying formation waters from carbonate sediments of Sakmar age. By analyzing the grain size data distribution, the reservoir is represented by well-sorted fine-grained sandstone with a dominant fraction of 0.1-0.25 mm (about 65% of the entire sample); paleodynamic analysis was carried out using the Passega diagram; It was established that the formation of the reservoir took place under conditions of gradation suspension (P-Q-R area in the diagram), in the lower parts of fast river flows, directly at the bottom. The findings are consistent with data from previous researchers. According to the study of the cores of other wells, maps of changes in reservoir properties have also been constructed, which highlighted reservoir zones with high reservoir properties – the central parts of the North and South Uplifts.

**Keywords:** extra-viscous oil field, reservoir properties, grain size data distribution, classification of A.A. Hanin, Passega diagram

**Recommended citation:** Vafin R.F., Khaziev R.R., Anisimova L.Z., Koluzaeva K.Yu. (2018). Types of reservoirs of the Ufa stage of the Republic of Tatarstan. Genesis and reservoir properties. *Georesursy = Georesources*, 20(4), Part 1, pp. 331-335. DOI: <https://doi.org/10.18599/grs.2018.4.331-335>

The key alternative to the light oil reserves of the Devonian complex are deposits of extra-viscous oils (EVO), concentrated in the Ufa and Kazan deposits in the south-eastern part of the Republic of Tatarstan (RT). Ufa sediments are of greater interest for the following reasons: 1) biggest part (about 60%) of EVO reserves (Vafin et al., 2010) are concentrated in sediments of the Sheshminskaya package of the Ufa stage; 2) Kazan deposits are made up of carbonates, which are hard to develop; 3) Currently existing technologies for the development of reserves, such as SAGD, CHOPS, VAPEX (Nikolin, 2007), are more effective in terrigenous sediments than in carbonates. It should be noted that the RT has accumulated considerable experience in the development of EVO deposits using thermal-steam formation treatment methods (Muslimov, 2009).

The origin and characteristics of the formation of the Ufa have been studied by geologists since the

1970s (Sementovsky, 1973; Troepolsky, 1976; Gusev, 1996; Badamshin, 1995; Geology of Tatarstan, 2003; Syurin, 2017). Most scientists are inclined to believe that Ufa sediments are deltaic deposits and partly coastal-marine; The main source of drift was igneous sediments of the Ural (Krinari, 1998). In order to identify the paleodynamic situation and assess the reservoir productivity, the samples of core material from well no.15 of the EVO field in the south-eastern part of the RT were investigated (in agreement with the users of the subsoil, the name of the field is not disclosed; the names of the elements have been changed; the numbering of the wells is arbitrary).

The EVO field is located in the Cheremshansky district of the Republic of Tatarstan, in which there are 2 local uplifts – the Northern and the Southern (Fig. 1). Both uplifts have a brachymorphic structure with an amplitude of 15-18 m (Table 1, Fig. 2). The effective oil-saturated reservoir thickness in the deposits increases from the periphery to the center. The maximum net thickness observed in well no. 5 on the South Rise is 22 m. The OWC is set at minus 63 m according to the results of probing the formation of a near field (NF) and the results of exploration drilling.

\*Corresponding author: Radmir R. Khasiev  
E-mail: [radmir361@mail.ru](mailto:radmir361@mail.ru)

© 2018 The Authors. Published by Georesursy LLC  
This is an open access article under the CC BY 4.0 license  
(<https://creativecommons.org/licenses/by/4.0/>)



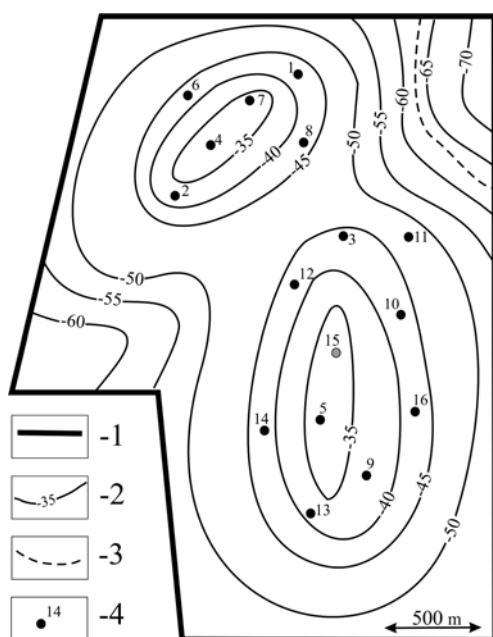


Fig. 1 Structural map of the top of the Sheshminsky horizon of the EVO field. Legend: 1 – licensed area limit; 2 – iso-gypsum on the top of the sand package; 3 – internal contour of oil; 4 – wells

Reservoir	Size (km km)	Effective oil-saturated reservoir thickness (m)	Number of wells, entered the reservoir
Nothern	1,5 0,7	11-19	6
Southern	2 1,1	11-22	10

Table 1. The parameters of the deposits of the EVO field

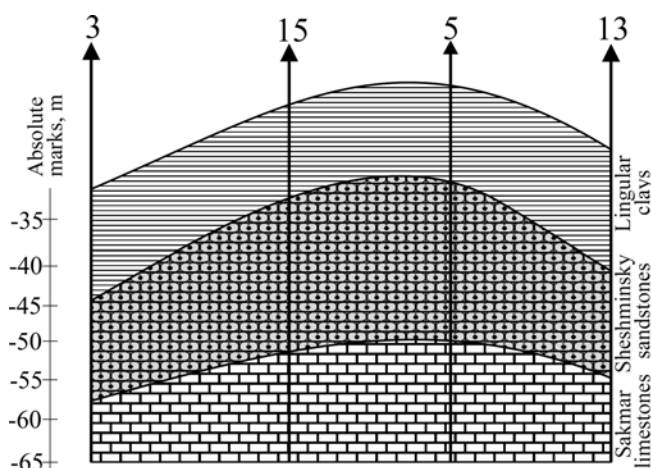


Fig. 2 Geological profile along the line of wells 3-15-5-13. South Deposit. Conventions of lithology – Fig. 3

The object of the study of the group of authors was core material of well no. 15, drilled on the southern uplift of the EVO field. The total effective oil-saturated thickness of the Sheshminskaya package according to macro-descriptions of the core in the studied well no. 15 is 20 m. The core sampling interval covers the overlying package of “lingular clays”, the entire thickness of the reservoir and part of the underlying sediments of the Sakmar age.

According to the results of the macroscopic description of the core material, the productive layer is represented by fine-grained sandstones with varying degrees of saturation of EVO (Fig. 3, 4). The texture of the saturation of rocks is mostly continuous, even if small areas (from 0.1 to 0.5 m) are observed with patches with a banded and oblique texture of saturation (Fig. 4).

The authors selected 10 samples for research with an average sampling step of 2 m (Fig. 3) for carrying out the following laboratory analyzes: a study of reservoir properties, grain size distribution. All samples before the study were pre-extracted with the determination of the percentage of viscous oil.

During sample preparation, part of the samples was rejected for various reasons (sample destruction, insufficient degree of extraction, etc.). Full information on the studies performed is shown in Table 2.

According to the study of the reservoir properties, the reservoir has rather high values of porosity and

System	Series	Stage	Horizon	Depth, m	Lithology	Cutoff point	Macro description
Permian	Lower	Ufimian	Sheshminian	155			Clays, dark-grey with light shade, firm, with subconchoidal fracture, calcareous, with burrow, with Lingula test, pyrites-bearing
				160		← 1	Sandstones, in the range of light-brown to dark-brown, moderately and well cemented, fine-grained, calcareous, indistinctly laminated, uniform intensive bitumen saturated
				165		← 2	
				170		← 3	
				175		← 4	
				180		← 5	
						← 6	
						← 7	
						← 8	
						← 9	
						← 10	
Permian	Lower	Ufimian	Sheshminian	185			Limestones, from light-grey, firm, with single brachiopods tests, oriented inside the core; limestones cavernous in places, non-uniform spotted bitumen saturated

Fig. 3 Litho-stratigraphic section, built according to the macroscopic description of the cores of well no. 15

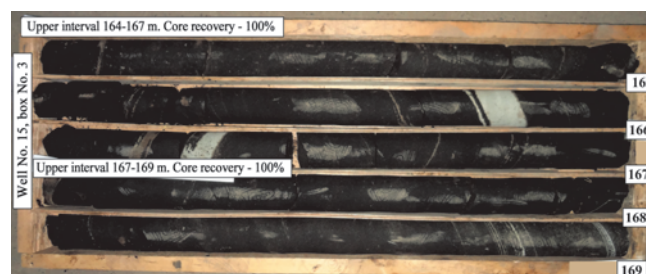


Fig. 4 Photo of the box no. 3 of the well 15. The photograph clearly shows a continuous and oblique striated texture of oil saturation

Sample (No.)	Reservoir properties	Grain size distribution
1	+	+
2	-	+
3	+	+
4	+	-
5	+	+
6	-	+
7	+	+
8	+	+
9	+	+
10	-	+

Table 2. Full information on research samples no. 1-10 with laboratory methods of analysis

permeability, and according to the classification of A.A. Khanin (Gimatutdinov, 2005) belongs to the I and II type reservoirs (Table 3). A trend of deterioration of reservoir properties can be noted: with an increase in the depth of the sand package, porosity, permeability and oil saturation decrease (Uspenskii, Vafin, 2016). Most likely, there is a process of formation of secondary calcite in the pore space of the reservoir during the migration of highly mineralized formation waters from the underlying sediments of Sakmar age. A similar phenomenon is noted in the work (Vedenina et al., 2018) where the EVO field was investigated for changes in the reservoir properties across the section and by area.

According to the particle size analysis, the biggest proportion in all samples falls on the interval of 0.1-0.25 mm (Table 4, fig. 5), which characterizes the reservoir as fine-grained sandstone.

According to the data of particle size distribution, the parameters (Nedolivko et al., 2011) of Md and C were calculated for the reconstruction of the sedimentary

No. sample	K <sub>p</sub> (%)	K <sub>pe</sub> (μm <sup>2</sup> )	K <sub>s</sub> (%)	Type reservoirs
1	13	1,56	19	I
3	15,6	0,99	45	II
4	22	1,22	51	I
5	18	1,71	60	I
7	12,4	0,66	41	II
8	13,75	0,37	/	III
9	11,86	0,22	28,6	III

Table 3. Laboratory data of reservoir properties of well n° 15 indicating the classes of reservoirs according to A.A. Khanin (Gimatutdinov et al., 2005)

No. sample	>0,8	0,4-0,8	0,25-0,4	0,1-0,25	0,063-0,1	0,01-0,063	<0,01	Total %
1	0	10,21	11,71	58,09	6,51	5,31	8,17	100
2	0	12,65	10,63	50,5	12,53	5,71	7,98	100
3	0	1,63	5,46	51,69	28,86	5,54	6,68	100
5	0	3,91	7,66	81,62	1,68	1,07	4,06	100
6	0	4,33	7,6	69,83	11,34	2,8	4,1	100
7	0	2,38	8,63	79,99	1,9	1,72	5,38	100
8	0	5,17	4,56	62,38	19,84	4,54	3,51	100
9	0	3,47	2,68	72,85	3,95	4,51	12,54	100
10	0	1,62	2,53	59,04	10,9	15,23	10,68	100

Table 4. Data of particle size distribution of samples

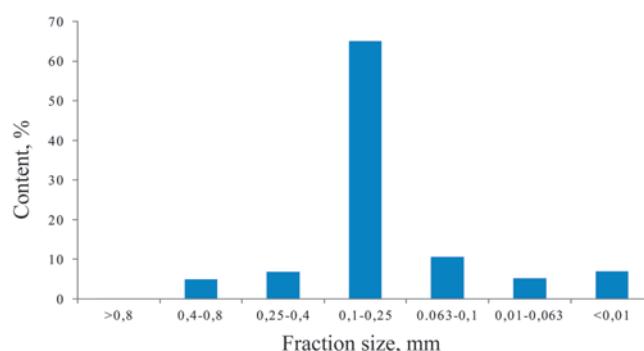


Fig. 5 The average histogram of the particle size distribution of the productive formation of well 15

paleodynamic environment; and Q3 and Q1 – to determine the degree of sorting  $So$  ( $So = \sqrt{\frac{Q3}{Q1}}$ ).

As can be seen from table 5, all the rock samples studied have a good degree of sorting of sandy material, which probably indicates sedimentation in a calm paleodynamic setting. For reconstruction, the Passegga paleodynamic diagram was used. Figure 6 shows that the scatter plot distribution lies on the P-Q-R area corresponding to the field of gradation suspension formed in the lower parts of fast river flows, directly at the bottom. The obtained data is consistent with the findings of previous researchers. Such a method of paleodynamic analysis is applicable both on sedimentary deposits of the territory of the Republic of Tatarstan and the West Siberian OGB (Khaziev et al., 2017), where, according to the paleodynamic analysis, the Jurassic stratum Y1-1 within the Ety-Purovsky arch has a similar origin with the Ufa package of RT.

To study the patterns of distribution of reservoir properties of rocks in the field, we used tabular data from the reservoir properties research at other wells. A total of 579 samples were examined using tabular data (including samples from well 15). For each well, weighted average reservoir properties values were calculated for the Sheshminsky horizon section (Table 6).

With the data of table 6, maps of porosity and permeability on the territory were constructed using the Surfer 8.0 software package (Maltsev et al., 2014) and using interpolation methods (Kriging, Radial Basic Function, Nearest neighbor). As the results of the

No. samp.	Md (μm)	C (μm)	Q3 (μm)	Q1 (μm)	So	Degree of sorting
1	150	520	170	90	1,37	Good
2	130	510	160	80	1,41	Good
3	90	450	130	75	1,31	Good
5	120	490	160	100	1,26	Good
6	125	500	170	90	1,36	Good
7	130	510	170	110	1,24	Good
8	140	500	160	100	1,26	Good
9	100	460	120	75	1,26	Good
10	80	500	140	75	1,36	Good

Table 5. Design parameters for the reconstruction of the situation of sedimentation

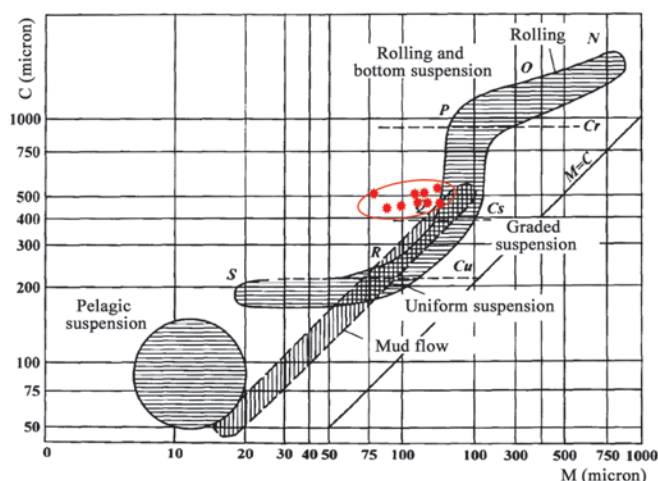


Fig. 6 Passega diagram with scatter plot distribution

No. of well	K <sub>p</sub> (%)	K <sub>pe</sub> (μm <sup>2</sup> )
1	0,11	0,371
2	0,13	0,182
3	0,12	0,230
4	0,13	0,571
5	0,14	0,432
6	0,09	0,196
7	0,14	0,532
8	0,09	0,346
9	0,11	0,429
10	0,08	0,299
11	0,07	0,139
12	0,09	0,372
13	0,11	0,411
14	0,09	0,363
15	0,14	0,677
16	0,11	0,292

Table 6. Weighted average values of reservoir properties by wells. (The weighted average reservoir properties value for well no. 15 is calculated considering previous core studies (in total 123 samples))

construction showed, the most optimal method, based on a small data array, is Radial Basic Function. Maps are constructed with this method (Fig. 7).

Using the constructed maps (Fig. 7), it was found that the most favorable areas are the central parts of the Northern and Southern uplifts. At this location, reservoirs of classes I and II with high permeability are present (from 0.45 to 0.6 μm<sup>2</sup>).

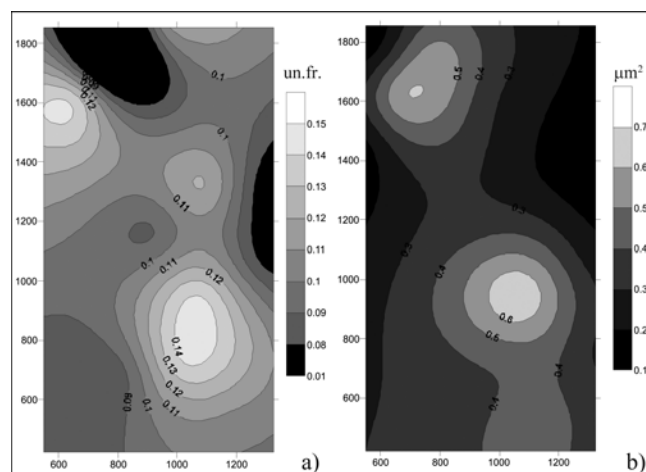


Fig. 7 Maps of porosity (a) and permeability (b) of the field

## Conclusion

This work has shown the following conclusions:

The reservoir on the territory of the field belongs to class 1 and 2 according to the classification of A.A. Hanin

The tendency of deterioration of reservoir properties going down through the section was underlined, the reason most likely being the migration of underlying formation waters from sediments of Sakmar age;

According to the grain size composition, the reservoir is represented by well-sorted fine-grained sandstone with a dominant fraction of 0.1-0.25 mm (65% of the entire sample);

Paleodynamic analysis was performed using the Passega diagram; It was established that the reservoir was formed under conditions of gradation suspension (P-Q-R region in the diagram), in the lower parts of fast river flows, directly at the bottom. The findings are consistent with data from previous researchers.

Distribution maps of reservoir properties in the field were constructed, revealing that the deterioration of reservoir properties goes from the central part to the periphery.

## Acknowledgments

The authors are grateful to the reviewer for valuable critical comments and recommendations which have been very helpful in improving the manuscript.

## References

- Badamshin E.E. (1995). Geology and investigation of oil and bitumen complexes. Kazan: KGU publ., 105 p. (In Russ.)
- Burov B.V., Esaulova N.K., Gubareva V.S. (2003). Geology of Tatarstan: Stratigraphy and tectonics. Moscow: GEOS, 403 p. (In Russ.)
- Gimatdinov S.K., Shirkovsky A.I. (2005). Physics of oil and gas reservoir. Moscow: Nedra, 311 p. (In Russ.)
- Gusev A.K. (1996). Tatarian stage. In book: Stratotypes and reference sections of the upper Permian of the Volga region and Kama. Kazan: EcoCentre, 539 p. (In Russ.)
- Khaziev R.R., Andreeva E.E., Arefiev Yu.M., Baranova A.G., Valeeva S.E., Anisimova L.Z., Goryntseva K.Yu. (2017). Lithological and Mineralogical Characteristics and Forming Conditions of the Jurassic Sediments on the West



Siberian basin. *Georesursy = Georesources*, 19(4-2), pp. 364-367. DOI: <https://doi.org/10.18599/grs.19.4.9>

Krinari G.A. (1998). Paleogeography of the Tatarian basin in the area of parastratotype using lithological and mineralogical data. *Proc. Int. Simp.: "Upper Permian stratotypes of the Volga region"*. Moscow: GEOS, pp. 80-84. (In Russ.)

Maltsev K.A., Mukharamova S.S. (2014). Building models of spatial variables (using Surfer package). Kazan: Kazan State University, 103 p. (In Russ.)

Nedolivko N.M., Ezhova A.V. (2011). Petrographic studies of terrigenous and carbonate reservoir rocks. Tomsk: Tomsk Polytechnic University, 172 p. (In Russ.)

Nikolin I.V. (2007). Methods of development of heavy oils and natural bitumen. *Mat. Vseros. seminara: Nauka – fundament resheniya tekhnologicheskikh problem razvitiya Rossii* [Proc. All-Russ. Sem.: Science – Basement of solving technological problems of Russia's development], pp. 55-68. (In Russ.)

Surin A.A. (2017). Conceptual approach to geological 3D-modeling of deposits of super-viscous oil (SVN) of the sheshminsky horizon of the Republic of Tatarstan. *Science. Technique. Technology*. <http://id-yug.com/images/id-yug/Bulatov/2017/1/PDF/2017-V1-168-172.pdf> (In Russ.)

Sementovsky Yu.V. (1973). Conditions of forming mineral deposits in the late Permian era in the East of the Russian platform. Kazan: Tatar book publishing house, 255 p. (In Russ.)

Troepol'skii V.I. (1976). Permian bitumens of Tatarstan. Kazan: KSU, 223 p. (In Russ.)

Uspensky B.V., Vafin R.F., Morozov V.P. (2016). Characteristics of reservoir properties of rocks of Ashalchinsk pack and their dependence on conditions of formation. *Oil economy*, 7, pp. 69-71. (In Russ.)

Vafin R.F., Nikolaev A.G., Valeeva R.D. (2010). Reservoirs of ultra-viscous oils of the Ufa sediments Bolshe-Kamesky field. *Uchenye Zapiski Kazanskogo Universiteta. Seriya Estestvennye Nauki*, 152(1), pp. 216-225. (In Russ.)

Vedenina N.G., Baranova A.G., Garifullina V.V., Khaziev R.R., Vafin R.F. (2018). Particle size distribution and collection properties of the field of superviscous oil in the territory of the Republic of Tatarstan. *Georesursy = Georesources*, Special issue, pp. 62-67. (In Russ.)

## About the Authors

*Rustem F. Vafin* – Senior lecturer, Department of Oil and Gas Geology, Kazan (Volga Region) Federal University

4/5, Kremlevskaya st., Kazan, 420008, Russian Federation

*Radmir R. Khaziev* – Researcher, Laboratory of Geological and Environmental Modeling, Institute for Environmental Problems and Subsoil Use of Tatarstan Academy of Sciences

28, Daurskaya st., Kazan, 420059, Russian Federation

*Liliya Z. Anisimova* – Researcher, Laboratory of Geological and Environmental Modeling, Institute for Environmental Problems and Subsoil Use of Tatarstan Academy of Sciences

28, Daurskaya st., Kazan, 420059, Russian Federation

*Kseniya Yu. Koluzaeva* – Junior Researcher, Laboratory of Geological and Environmental Modeling, Institute for Environmental Problems and Subsoil Use of Tatarstan Academy of Sciences

28, Daurskaya st., Kazan, 420059, Russian Federation

*Manuscript received 20 April 2018;*

*Accepted 5 September 2018;*

*Published 30 November 2018*

## ORIGINAL RESEARCH ARTICLE

DOI: <https://doi.org/10.18599/grs.2018.4.336-343>

## Simulation of composition changes in reservoirs with large hydrocarbon columns and temperature gradient

A.V. Yashin<sup>1,2\*</sup>, I.M. Indrupskiy<sup>1,2</sup>, O.A. Lobanova<sup>1</sup><sup>1</sup>Oil and Gas Research Institute of the Russian Academy of Sciences, Moscow, Russian Federation<sup>2</sup>Gubkin Russian State University of Oil and Gas (National Research University), Moscow, Russian Federation

**Abstract.** This paper compares three methods for calculation of initial composition variation with depth in hydrocarbon reservoirs: considering thermal diffusion, considering temperature gradient without thermal diffusion effects; and by gravity forces only. Newton method-based numerical algorithm was implemented for solution of thermodynamic equations to evaluate pressure and hydrocarbon composition. Test calculations are performed for main gas-condensate reservoir of Vuktylskoye field with a gas column of 1350 m.

The results obtained with the numerical algorithm indicate that gravity segregation impact is the strongest for all the cases considered. Concentration decreases with depth for low molecular weight components and increases for high molecular weight components. The higher molecular weight of the component, the stronger variation of its concentration with depth. Initial reservoir pressure also changes accordingly.

However, thermal diffusion also has a significant influence on variation of hydrocarbon composition with depth and initial reservoir pressure. For the test case considered, thermal diffusion magnifies the impact of gravity and results in strongly nonlinear dependencies of component concentrations on depth. When thermal gradient is taken into account without thermal diffusion effects, the results are only slightly different from those with the isothermal gravity segregation calculations.

None of the calculation methods were successful in matching estimates of initial composition variation with depth obtained from well exploitation data. Physical mechanisms governing variation of composition within the main reservoir of the Vuktylskoye field require additional investigation. Despite the long history of the reservoir development, this problem was previously studied based only on field development data.

**Keywords:** hydrocarbon mixture, geothermal gradient, thermal diffusion, component composition, initial composition, gas condensate reservoir, Vuktylskoye field

**Recommended citation:** Yashin A.V., Indrupskiy I.M., Lobanova O.A. (2018). Simulation of composition changes in reservoirs with large hydrocarbon columns and temperature gradient. *Georesursy = Georesources*, 20(4), Part 1, pp. 336-343. DOI: <https://doi.org/10.18599/grs.2018.4.336-343>

### Introduction

Hydrocarbon reservoirs with large oil or gas columns are characterized by significant changes in reservoir pressure and temperature with depth. As a result, the initial composition of the reservoir fluid also changes significantly with depth.

The distribution of components in depth in massive hydrocarbon reservoirs is greatly influenced by gravitational forces. Initial composition of the fluid in such reservoirs is formed in such a way that the concentration of light components decreases in the direction from the top to the bottom, while concentration of heavy components increases on the contrary. Accordingly, the content of

condensate in the reservoir gas increases and the solution-gas content in oil decreases.

In 1954, A.Y. Namiot made calculations for mixtures modeling oils of different composition (Namiot, 1954). It was concluded that gravity forces have a significant impact on the composition of oils containing significant amounts of heavy hydrocarbons and dissolved gas. In case of reservoirs consisting mainly of light hydrocarbons, the composition varies slightly with depth. Subsequently, the mathematical apparatus for calculating changes in multicomponent mixtures composition under the influence of gravity has been widely developed and applied (Whitson, Belery, 1994; Brusilovskii, 2002).

The method of calculating gravitational distribution of pressure and composition by reservoir depth is based on the assumption of the system thermodynamic equilibrium in the gravity field. This state of the system can be achieved at a constant system temperature throughout the entire volume.

\*Corresponding author: Anton V. Yashin  
E-mail: [antm-yashin@yandex.ru](mailto:antm-yashin@yandex.ru)

© 2018 The Authors. Published by Georesursy LLC  
This is an open access article under the CC BY 4.0 license  
(<https://creativecommons.org/licenses/by/4.0/>)





Successive approximation of the variables is performed by solving at each step the system of equations  $JS=F$  obtained by linearizing the equations of system (6). The matrix  $J$  and the vectors  $S$ ,  $F$  have the following form:

$$J = \begin{pmatrix} \frac{\partial \Phi_1}{\partial p} & \frac{\partial \Phi_1}{\partial y_2} & \dots & \frac{\partial \Phi_1}{\partial y_N} \\ \dots & \dots & \dots & \dots \\ \frac{\partial \Phi_N}{\partial p} & \frac{\partial \Phi_N}{\partial y_2} & \dots & \frac{\partial \Phi_N}{\partial y_N} \end{pmatrix}; \quad S = \begin{pmatrix} p^{m+1} - p^m \\ y_2^{m+1} - y_2^m \\ \dots \\ y_N^{m+1} - y_N^m \end{pmatrix};$$

$$F = \begin{pmatrix} -\Phi_1^m \\ -\Phi_2^m \\ \dots \\ -\Phi_N^m \end{pmatrix} \quad (7)$$

where  $m = 0, 1, 2, \dots$  is the iteration number.

The components of the matrix  $J$  are calculated as follows:

$$\frac{\partial \Phi_i}{\partial p} = \frac{\partial \ln f_i}{\partial p}, \quad i = 1, \dots, N; \quad (8)$$

$$\frac{\partial \Phi_i}{\partial y_j} = \frac{\partial \ln f_i}{\partial y_j} - \frac{\partial \ln f_i}{\partial y_1}, \quad i = 1, \dots, N, j = 2, \dots, N. \quad (9)$$

The apparatus of cubic equations of state is used for calculation of fugacities and their derivatives (Brusilovskii, 2002).

Within the approximate approach, it is possible to take into account temperature changes with depth in the system (4). For this, hydrocarbon column is divided into a number of small intervals and the temperature is considered constant within each interval. The difference in temperatures between the intervals should be taken into account when calculating fugacities; however, thermodynamic equilibrium conditions (1) are considered approximately valid. However, such a calculation neglects the heat transfer and the accompanying mass transfer of components caused by thermal diffusion.

### Equation of state

The following Peng-Robinson cubic equation of state was applied to calculate the fugacities in this work:

$$Z^3 - (1 - B)Z^2 + (A - 3B^2)Z - (AB - B^2 - B^3) = 0. \quad (10)$$

For a given equation of state, the fugacities are calculated by the following formula:

$$\ln f_i = \ln(y_i p) + \frac{B_i}{B}(Z - 1) - \ln(Z - B) +$$

$$+ \frac{A}{2\sqrt{2}B} \left( \frac{B_i}{B} - \frac{2}{A} \sum_{j=1}^N y_j A_{ij} \right) \ln \left[ \frac{Z + (1 + \sqrt{2})B}{Z + (1 - \sqrt{2})B} \right], \quad (11)$$

where

$$Z = \frac{pv}{RT}, \quad (12)$$

$$A = \sum_{i=1}^N \sum_{j=1}^N y_i y_j A_{ij}, \quad (13)$$

$$B = \sum_{i=1}^N y_i B_i, \quad (14)$$

$$A_{ij} = (1 - k_{ij}) \sqrt{A_i A_j}, \quad (15)$$

$$A_i = \frac{a_i p}{R^2 T^2}, \quad (16)$$

$$B_i = \frac{b_i p}{RT}, \quad (17)$$

$$a_i = 0.45724 \frac{(RT_{ci})^2}{p_{ci}} \alpha, \quad (18)$$

$$b_i = 0.07780 \frac{RT_{ci}}{p_{ci}}, \quad (19)$$

$$\alpha = (1 + m * (1 - \sqrt{T_r}))^2, \quad (20)$$

$$T_r = \frac{T}{T_{ci}}, \quad (21)$$

$$m = 0.03796 + 1.485 * w_i - 0.1644 * w_i^2 +$$

$$+ 0.01667 * w_i^3 \quad (w_i > 0.4), \quad (22)$$

$$m = 0.37464 + 1.54226 * w_i -$$

$$- 0.26992 * w_i^2 \quad (w_i \leq 0.4), \quad (23)$$

where  $Z$  is the compressibility factor;  $p$  is the reservoir pressure;  $T$  is the reservoir temperature;  $R$  is the universal gas constant;  $T_r$  is the reduced temperature;  $T_{ci}$  is the critical temperature of the component;  $p_{ci}$  is critical component pressure;  $w_i$  is acentric factor;  $y_i$  is the mole concentration of the component in the mixture.

### Thermal diffusion

The temperature gradient makes a significant contribution to the change in the composition of the hydrocarbon mixture. Taking into account the vertical temperature gradient leads, as a rule, to a stronger dependence of the initial composition on the depth than can be explained only by gravitational forces.

The effect of thermal diffusion on the distribution of the reservoir components is described using nonequilibrium thermodynamical models. Different approaches to considering the effect of thermal diffusion have been proposed by such authors as Belery and Da Silva (Belery, Da Silva, 1990), Haase (Haase, 1990), Kempers (Kempers, 1989), Whitson (Whitson, Belery, 1994), etc.

Pedersen and Lindeloff (Pedersen, Lindeloff, 2003) proposed the following relationships to calculate the compositional change with depth in reservoirs under the influence of gravity and thermal diffusion:

$$RT_2 \ln f_i(p, \vec{y})|_{h_2} = RT_1 \ln f_i(p, \vec{y})|_{h_1} + M_i g(h_1 - h_2) - M_i \left( \frac{H}{M} - \frac{\widetilde{H}_i}{M_i} \right) \frac{\Delta T}{T}, \quad i = 1, \dots, N, \quad (24)$$

where  $\widetilde{H}_i$  is the absolute partial molar enthalpy of  $i$ -th component,  $H$  is the absolute molar enthalpy of the mixture,  $M$  is the average molecular weight of the mixture,  $\Delta T$  is the temperature difference between the depths  $h_2$  and  $h_1$ ,  $T_1$  is the temperature at the depth  $h_1$ ,  $T_2$  is the temperature at the depth  $h_2$ . Relation (24) corresponds to the nonequilibrium stationary state of the system in a gravitational and geothermal field.

The authors (Pedersen, Lindeloff, 2003) suggested that the change in component composition under stationary conditions and influence of the temperature gradient is determined by the specific enthalpy of each component. Components with a higher enthalpy than the average for the mixture tend to a warmer zone. Under typical reservoir conditions, high molecular weight components will have a higher specific enthalpy than low molecular weight ones. This corresponds to actual observations showing that the change in component composition with depth in reservoirs with a positive vertical temperature gradient is higher than can be explained only by the gravitational effect.

The partial molar enthalpy of  $i$ -th component in a mixture at temperature  $T$  can be represented by the following expression:

$$\widetilde{H}_i(T) = H_{i0}^{ig} + (H_i^{ig}(T) - H_{i0}^{ig}) + \widetilde{H}_i^{res}, \quad (25)$$

where  $H_i^{ig}(T)$  is the partial molar enthalpy of  $i$ -th component in the ideal-gas state at temperatures  $T$  and 273.15 K, respectively,  $\widetilde{H}_i^{res}$  – is the partial residual molar enthalpy:

$$\widetilde{H}_i^{res} = -RT^2 \frac{\partial \ln \varphi_i}{\partial T}, \quad (26)$$

where  $\varphi$  is the fugacity coefficient of the  $i$ -th component.

Enthalpy of the  $i$ -th component in an ideal-gas state at a temperature of 273.15 K can be determined by the following formula:

$$\frac{H_i^{ig}(273.15K)}{R} = -134.2 + 8.367 * M_i, \quad (27)$$

and at temperature  $T$ , it can be determined from the following thermodynamic relation:

$$H_i^{ig}(T) - H_i^{ig}(273.15K) = \int_{273.15K}^T C_{P,i}^{id} dT, \quad (28)$$

where the heat capacity of an ideal gas is determined by the correlation with temperature:

$$C_{P,i}^{id} = C_{1,i}T + C_{2,i}T^2 + C_{3,i}T^3 + C_{4,i}T^4, \quad (29)$$

where the coefficients  $C_{1,i}$ - $C_{4,i}$  are tabulated for  $C_1$ - $C_5$  components of the mixture (Reid, Prausnitz, Poling, 1987). For  $C_{6+}$  components, the coefficients are calculated using Kesler-Lee empirical formulas (Kesler, Lee, 1976).

## Vuktylskoye field

Based on the described model, calculation were performed for changes in the initial composition with depth for the main gas-condensate reservoir of the Vuktylskoye field with a large gas column (Tables 1-3). Fig. 1 shows the changes in the initial component composition of the gas-condensate mixture with the reservoir depth according to the data of (Dolgushin, 2007). The plots shown were obtained from actual data analysis of wells completed in the reservoir at various depths. Fig. 2 shows the change in the initial reservoir pressure and temperature over the depth of the reservoir. It is interesting to compare the dependences of the initial composition and pressure on the depth according to Fig. 1-2 and obtained by mathematical modeling. The latter are necessary as initial conditions for forecast simulations on a multicomponent 3D reservoir flow model.

	Constant temperature	Interval temperatures	Thermal diffusion
N <sub>2</sub>	5.45201	5.46618	6.09901
2	0.03593	0.03571	0.03625
C <sub>1</sub>	79.22680	79.31150	80.15020
C <sub>2</sub>	7.76406	7.72844	7.28671
C <sub>3</sub>	2.82648	2.80510	2.57673
iC <sub>4</sub>	0.33319	0.33012	0.30394
nC <sub>4</sub>	0.58375	0.57766	0.51958
iC <sub>5</sub>	0.10752	0.10618	0.09520
nC <sub>5</sub>	0.09297	0.09175	0.08075
C <sub>6+(1)</sub>	1.25377	1.23458	0.91920
C <sub>6+(2)</sub>	1.68256	1.68550	1.51376
C <sub>6+(3)</sub>	0.55714	0.54645	0.37851
C <sub>6+(4)</sub>	0.07829	0.07547	0.03763
C <sub>6+(5)</sub>	0.00534	0.00513	0.00244
C <sub>6+(6)</sub>	0.00021	0.00020	0.00011
P	33.04260	32.93150	33.02160

Table 1. Calculated component composition (molar fractions of the components in the mixture) at a depth of 2000 m

	Constant temperature	Interval temperatures	Thermal diffusion
N <sub>2</sub>	5.28145	5.28555	5.62076
2	0.03791	0.03784	0.03805
C <sub>1</sub>	77.43990	77.46610	78.24030
C <sub>2</sub>	8.13089	8.12082	7.86716
C <sub>3</sub>	3.11116	3.10486	2.95724
iC <sub>4</sub>	0.38162	0.38069	0.36201
nC <sub>4</sub>	0.67508	0.67320	0.63203
iC <sub>5</sub>	0.12954	0.12912	0.12066
nC <sub>5</sub>	0.11273	0.11233	0.10392
C <sub>6+(1)</sub>	1.58503	1.57859	1.33152
C <sub>6+(2)</sub>	2.09588	2.09788	1.94260
C <sub>6+(3)</sub>	0.84917	0.84494	0.67343
C <sub>6+(4)</sub>	0.15536	0.15387	0.10148
C <sub>6+(5)</sub>	0.01359	0.01345	0.00838
C <sub>6+(6)</sub>	0.00075	0.00074	0.00047
P	34.50070	34.47140	34.50690

Table 2. Calculated component composition (molar fractions of the components in the mixture) at a depth of 2500 m

	Constant temperature	Interval temperatures	Thermal diffusion
N <sub>2</sub>	4.68992	4.69193	4.18694
2	0.04139	0.04135	0.04100
C <sub>1</sub>	71.89110	71.90820	68.45650
C <sub>2</sub>	8.93229	8.92625	9.25570
C <sub>3</sub>	3.81971	3.81585	4.12125
iC <sub>4</sub>	0.50947	0.50890	0.56036
nC <sub>4</sub>	0.92533	0.92411	1.03742
iC <sub>5</sub>	0.19383	0.19354	0.22240
nC <sub>5</sub>	0.17162	0.17134	0.19968
C <sub>6+(1)</sub>	2.64608	2.64113	3.38334
C <sub>6+(2)</sub>	3.24845	3.25410	3.75229
C <sub>6+(3)</sub>	2.11299	2.10898	3.10978
C <sub>6+(4)</sub>	0.69862	0.69576	1.37629
C <sub>6+(5)</sub>	0.10599	0.10547	0.25513
C <sub>6+(6)</sub>	0.01317	0.01305	0.04189
P	37.34190	37.32690	37.38680

Table 3. Calculated component composition (molar fractions of the components in the mixture) at a depth of 3350 m

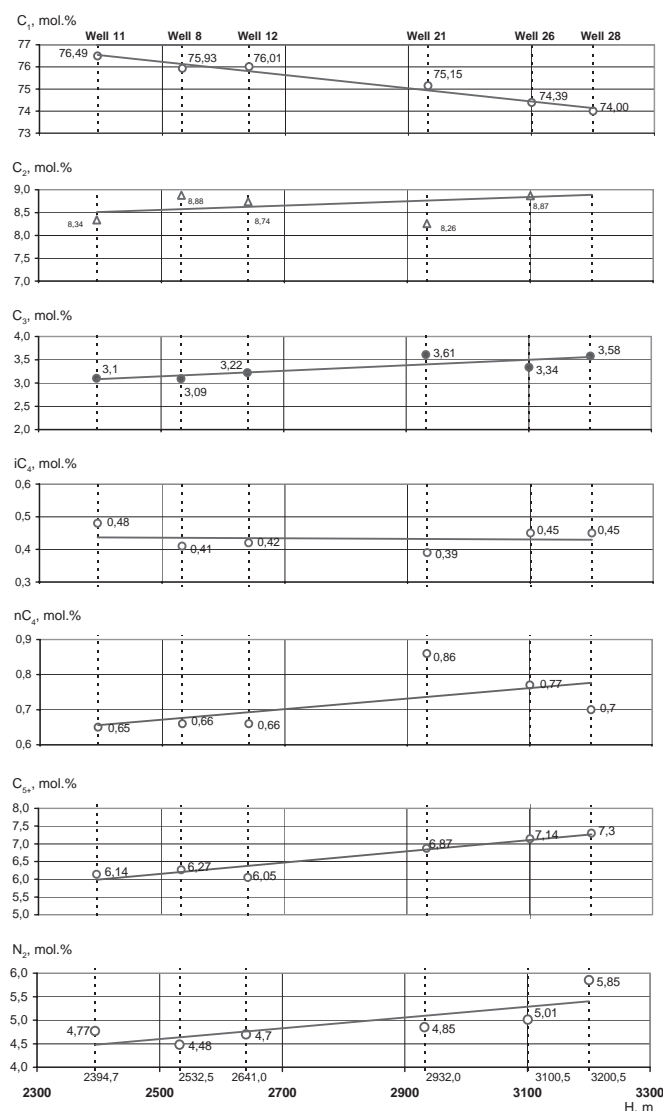


Fig. 1. Changes in the content of  $C_1$ ,  $C_2$ ,  $C_3$ ,  $iC_4$ ,  $nC_4$ ,  $C_{5+}$ ,  $N_2$  reservoir gas components within the vertical reservoir section for the initial conditions of the Vuktylskoye field (Dolgushin, 2007)

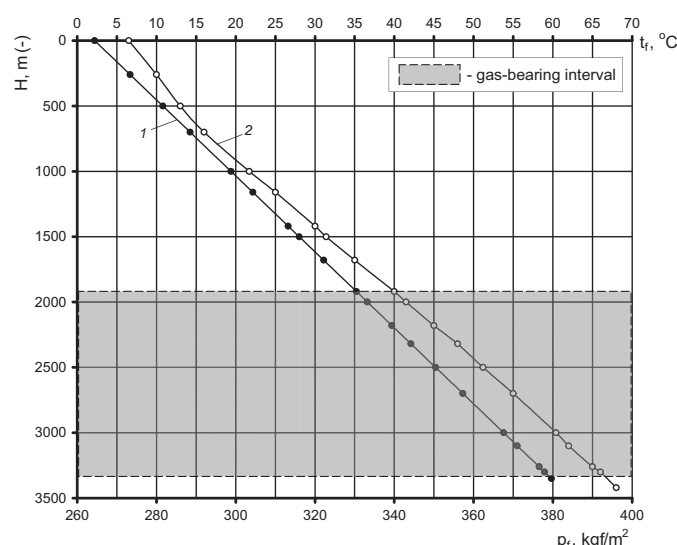


Fig. 2. Dependence of the initial values of reservoir pressure (1) and temperature (2) on the depth for the Vuktylskoye field (Dolgushin, 2007)

The model of the gas-condensate mixture was adopted according to the latest development design document (Supplement to the field development plan ..., 2014) and is represented by hydrocarbon components (methane, ethane, propane, butane, pentane and six fractions), as well as nitrogen and carbon dioxide (Table 4). At a depth of 3000 m, the initial composition of the mixture is known, the temperature of the reservoir is 334 K, the reservoir pressure is 36.1 MPa. Geothermal gradient equals to 0.019°C/m. Physical properties of hydrocarbon fractions are presented in Table 5. The goal is to recalculate the pressure and composition from the initial depth of 3000 m to a depth of 2000 m (upper level of the reservoir), 2500 m and 3350 m (gas-liquid contact).

Components	Mole fraction, %	Molar mass, kg/kmol	P, MPa	, K	dT, °C/m
N <sub>2</sub>	5.01	28.01	36.1	334	0.019
2	0.04	44.01			
C <sub>1</sub>	74.85	16.04			
C <sub>2</sub>	8.56	30.07			
C <sub>3</sub>	3.47	44.1			
iC <sub>4</sub>	0.45	58.12			
nC <sub>4</sub>	0.8	58.12			
iC <sub>5</sub>	0.16	72.15			
nC <sub>5</sub>	0.14	72.15			
C <sub>6+(1)</sub>	2.08	85.02			
C <sub>6+(2)</sub>	2.67	110.46			
C <sub>6+(3)</sub>	1.38	157.95			
C <sub>6+(4)</sub>	0.35	231.22			
C <sub>6+(5)</sub>	0.0404	338.18			
C <sub>6+(6)</sub>	0.0034	500			

Table 4. Model of gas condensate mixture and input data at a depth of 3000 m (Supplement to the field development plan ..., 2014)



Fraction	Density, g/cm <sup>3</sup>	Critical temperatur., T <sub>c</sub> , K	Critical pressure P <sub>c</sub> , MPa	Acentric factor	Molar concentration of the component in the mixture z	M, g/mol	Boiling temperature, T <sub>b</sub> , K
6+(1)	0.664	504.9	3.060	0.2923	0.02082	85.0188	339.126
6+(2)	0.708	570.4	2.505	-0.2581	0.02668	110.457	399.174
6+(3)	0.750	646.6	1.941	0.3433	0.01381	157.954	474.645
6+(4)	0.787	732.4	1.382	0.8143	0.003451	231.218	569.612
6+(5)	0.821	818.6	0.946	1.0015	4.04·10 <sup>-4</sup>	338.184	673.787
6+(6)	0.854	904.8	0.645	1.2589	3.36·10 <sup>-5</sup>	500	783.105

Table 5. Physical properties of fractions (Supplement to the field development plan ..., 2014)

The calculations were carried out using the following three methods:

- 1) Gravity method – the equation (1),
- 2) Taking into account the interval temperature change, but without thermal diffusion,
- 3) Taking into account thermal diffusion – the equation (24).

### Calculation results

Fig. 3-10 show some calculation results. The depth changes of pressure and initial concentrations of gas-condensate mixture individual components are given for the main reservoir of the Vuktylskoye field. Fig. 9 corresponds to the group of C<sub>5+</sub> hydrocarbons, i.e. the sum of pentanes and all C<sub>6+</sub> fractions.

The concentration of light components (nitrogen and methane) decreases with depth (Fig. 3-4), while the concentration of heavier hydrocarbons starting with ethane increases with depth (Fig. 5-9). The higher the molecular weight of the component, the more its content increases with depth. Initial reservoir pressure changes consistently (Fig. 10). These features are associated with the influence of the gravitational field and are predominant in all variants of calculations.

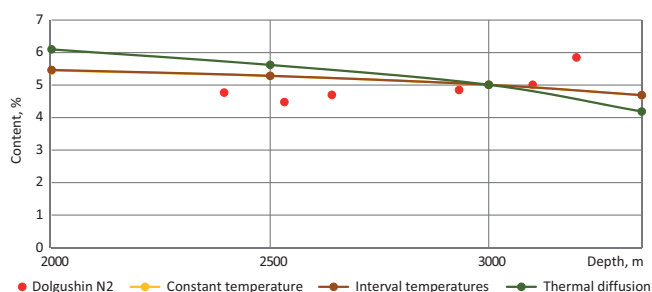


Fig. 3. Change in nitrogen content with depth

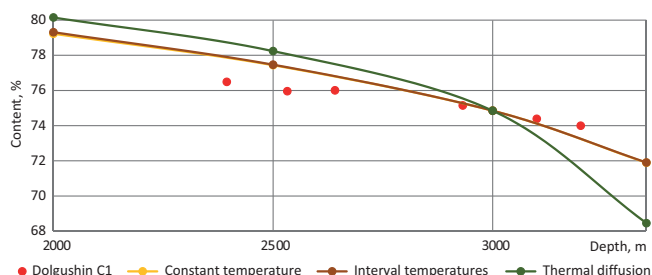


Fig. 4. Change in methane content with depth

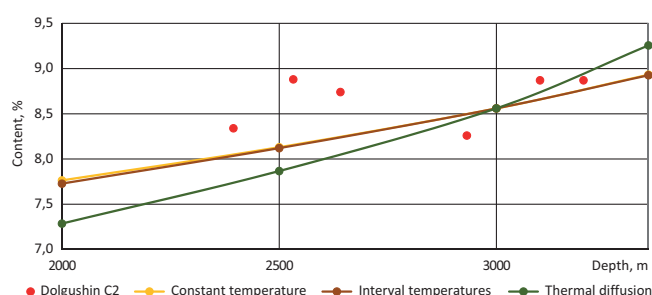


Fig. 5. Change in ethane content with depth

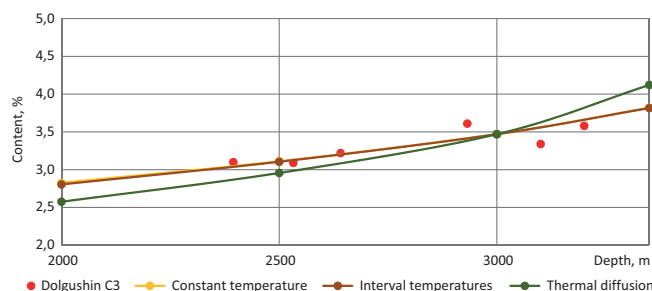


Fig. 6. Change in propane content with depth

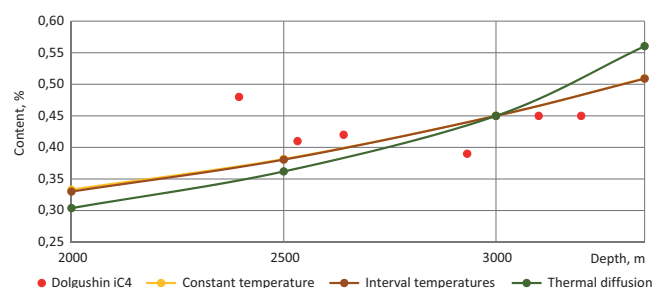


Fig. 7. Change in iso-butane content with depth

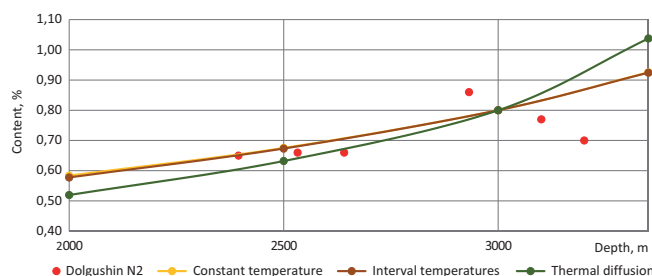


Fig. 8. Change in normal-butane content with depth

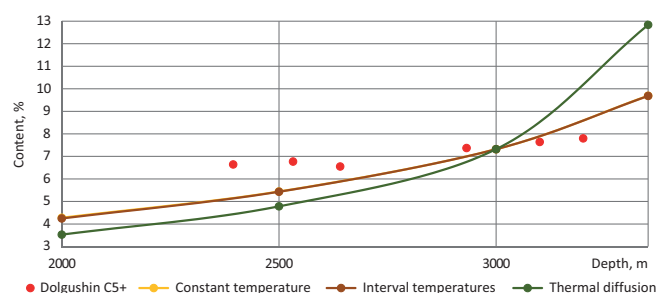


Fig. 9. Change in content of group of components  $C_{5+}$  with depth

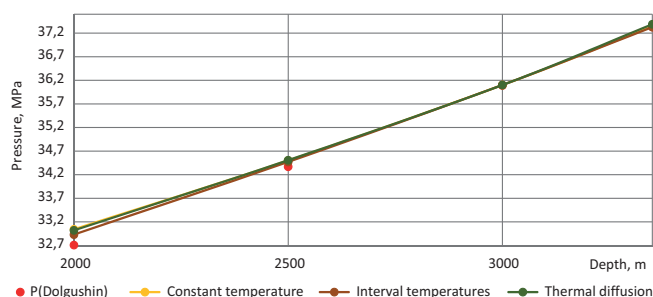


Fig. 10. Change in initial reservoir pressure with depth

From Fig. 3-10, it can be seen that when taking into account the temperature variation, the obtained composition distribution with depth is only slightly different from the isothermal case. This result confirms the conclusions of the work (Whitson, Belery, 1994).

Also from Fig. 3-10, it follows that the effect of thermal diffusion is essential and enhances the gravitational field influence for the described hydrocarbon system. A similar result was obtained in (Pedersen, Hjerstad, 2006) for another reservoir, where it was shown to match the actual data. The same method to account for thermal diffusion was used. However, this conclusion should not be absolutized, since a number of other authors indicate that thermal diffusion can reduce the influence of the gravitational field. In any case, it is characteristic that the composition changes with depth taking into account thermal diffusion become essentially nonlinear.

From Fig. 3-6, it can be seen that the data calculated by the gravitational method of the composition distribution and the interval-wise temperature consideration do not agree well with the actual data presented by N.V. Dolgushin (Dolgushin, 2007). Accounting for the effect of thermal diffusion also does not give a satisfactory approximation, and for a number of components it makes bigger the observed deviation.

Thus, the physical mechanisms causing the initial distribution of the component composition with depth for the Vuktylskoye field require further analysis. In particular, it is advisable to take into account the possible effect of the residual liquid hydrocarbon phase, the effect of the adopted component model

of the mixture and to try other models for describing thermal diffusion.

On the other hand, it should be taken into account that information on the distribution of the composition according to well data (Dolgushin, 2007) is also not the result of direct measurements. It is obtained by analyzing and averaging the well performance data with significant (hundreds of meters) production intervals in a heterogeneous reservoir. It is also important that N.V. Dolgushin made some assumptions regarding the possibility of relying on data on the well production composition at certain dates as an estimate of the initial distribution.

## Conclusions

The paper considers mathematical modeling of changes in the initial component composition of hydrocarbon mixtures with depth in massive reservoirs under the influence of natural physical fields (gravitational and geothermal).

Numerical algorithms have been implemented to calculate the distribution of hydrocarbon mixture components over depth in the gravitational field under isothermal conditions, or taking into account interval temperature variation and thermal diffusion.

The results of comparative calculations for the main gas-condensate reservoir mixture of the Vuktylskoye field showed that thermal diffusion has a significant effect on the distribution of components, as well as the initial reservoir pressure. In the case under consideration, thermal diffusion magnifies the influence of the gravitational field and leads to pronounced non-linear dependencies for the components concentrations.

Satisfactory agreement of the calculations results with the component composition distribution according to well operation data was not achieved for any of the algorithms. The physical mechanisms determining the distribution of the initial composition within the reservoir volume of the Vuktylskoye field require further analysis.

## References

- Belery P., Da Silva F.V. (1990). Gravity and thermal diffusion in hydrocarbon reservoirs. Paper presented at the Third Chalk Research Program, June 11-12, Copenhagen, Denmark.
- Brusilovskii A.I. (2002) Fazovye prirashcheniya pri razrabotke mestorozhdenii nefi i gaza [Phase transitions in the development of oil and gas fields]. Moscow: Graal Publ., 575 p. (In Russ.)
- Dolgushin N.V. (2007) Metodologiya izucheniya gazokondensatnoi kharakteristiki neftegazokondensatnykh mestorozhdenii s vysokim soderzhaniem kondensata i bol'shim etazhom gazonosnosti [Methodology for studying gas-condensate characteristics of oil and gas-condensate fields with a high content of condensate and a large gas columns]. *Diss. doktora tekhnicheskikh nauk* [Dr. tech. sci. diss.]. Ukhta: SEVERNIPIGAZ, 400 p. (In Russ.)
- Supplement to the field development plan of the Vuktylskoye oil-, gas- and condensate field (2014). Report. Ukhta: Gazprom VNIIGAZ (In Russ.)

Haase R. (1990). Thermodynamics of irreversible processes. New York: Dover.

Kempers L.J.T.M. (1989). A thermodynamic theory of the Soret effect in a multicomponent liquid. *The Journal of Chemical Physics*, 90(11), pp. 6541-6548. <https://doi.org/10.1063/1.456321>

Kesler M.G., Lee B.I. (1976). Improve prediction of enthalpy of fractions. Hydrocarbon processing 55, pp. 153-158.

Namiot A.Yu. (1954) Razlichie svoystv nefi v predelakh neftenosnoi zalezhi. Issledovaniya v oblasti fiziki plasta [Differences in the properties of oil within an oil deposit. Studies in the reservoir physics]. *Tr. VNII*, 3, pp. 41-60. (In Russ.)

Pedersen K.S., Hjermsstad H.P. (2006). Modeling of large hydrocarbon compositional gradient. *SPE paper 101275 presented at the 2006 Abu Dhabi International Petroleum Exhibition and Conference*, Abu Dhabi, U.A.E. <https://doi.org/10.2118/101275-MS>

Pedersen K.S., Lindeloff N. (2003). Simulations of compositional gradients in hydrocarbon reservoirs under the influence of a temperature gradient. *SPE paper 84364 presented at the SPE ATCE*, Denver, USA. <https://doi.org/10.2118/84364-MS>

Reid R.C., Prausnitz J.M., Poling B.E. (1987). The properties of gases and liquids. New York: McGrawHill.

Whitson C.H., Belery P. (1994). Compositional gradients in petroleum reservoirs. *Paper presented at University of Tulsa Centennial Petroleum Engineering Symposium*, Tulsa, Oklahoma, USA. <https://doi.org/10.2118/28000-MS>

## About the Authors

*Anton V. Yashin* – Engineer, MSc student  
Gubkin Russian State University of Oil and Gas  
(National Research University)

Oil and Gas Research Institute of the Russian Academy  
of Sciences

3, Gubkin st., Moscow, 119333, Russian Federation

*Ilya M. Indrupskiy* – DSc (Engineering), Professor,  
Head of Laboratory

Gubkin Russian State University of Oil and Gas  
(National Research University)

Oil and Gas Research Institute of the Russian Academy  
of Sciences

3, Gubkin st., Moscow, 119333, Russian Federation

*Olga A. Lobanova* – PhD (Engineering), Researcher  
Oil and Gas Research Institute of the Russian Academy  
of Sciences

3, Gubkin st., Moscow, 119333, Russian Federation

*Manuscript received 29 March 2018;*

*Accepted 27 September 2018;*

*Published 30 November 2018*





# The safe operations modes substantiation for water source wellbores of the Vadelypskoye deposit

A.V. Seryakov<sup>1\*</sup>, M.Yu. Podberezheny<sup>2</sup>, O.B. Bocharov<sup>1</sup>, M.A. Azamatov<sup>2</sup>

<sup>1</sup>Novosibirsk Technology Center Baker Hughes JSC, Novosibirsk, Russian Federation

<sup>2</sup>Salym Petroleum Development N.V., Moscow, Russian Federation

**Abstract.** The sand production problem for the water sources wellbores at the Vadelypskoye oilfield that is located in Hanty-Mansy region of Russia is considered. The serious issue during field operations is the open wellbore wall destruction even if low drawdown rates (4-6 bar) are applied to the water-bearing pay at one kilometer depth.

Petrophysical analysis of high permeable (0.6-2.5 D) sandstones of water-bearing pay is presented. The effectiveness of the sands prevention methods used at the deposit is discussed and the practical recommendations for drilling and operations are given.

To identify the conditions of safe fluid extraction the three-dimensional poroelastic software was used for modeling of the vertical borehole section located in the water saturated sandstone. We consider the mudcake is stripped and disappeared due to the wellbore technological operations but the plugging zone persisted. The colmatage zone was taken into account in the modeling as the radial area with reduced relative to formation permeability. Along with this, the axial sandstone permeability is non-uniform and assigned according to the core data.

Different horizontal stresses ratios and values are considered in the simulations. The medium-clogged and high-clogged damage zone influence on the formation effective stresses was studied for minimal and maximal drawdown values. It was established that the most stable borehole relative to the draw-down is located in the homogeneous horizontal stress field within the medium-clogged damage zone.

Special attention was given to the damage zone permeability and thickness influence on the wellbore wall failure while pumping. It was determined that rock failure is more possible when the thin and low-permeable colmatage zone is built in formation. The near-wellbore zone colmatage effect on rock destruction can be definitely seen for conditions of equal horizontal stresses but decreases when horizontal loads are unequal. The analysis of different in-situ conditions showed that the difference between horizontal stresses has more effect on destruction than colmatage zone parameters changes.

The water-pumping admissible drawdown pressure ranges are specified for each horizontal stresses regime and the recommendations were given for sanding screen characteristics. For wellbore planning at the Vadelypskoye deposit the preferable drill mud composition was described that will contribute to subsequent safe water pumping.

**Keywords:** sand production, water sources wellbores, destruction, poroelastic modelling, high permeable sandstone, colmatage zone

**Recommended citation:** Seryakov A.V., Podberezheny M.Yu., Bocharov O.B., Azamatov M.A. (2018). The safe operations modes substantiation for water source wellbores of the Vadelypskoye deposit. *Georesursy = Georesources*, 20(4), Part 1, pp. 344-354. DOI: <https://doi.org/10.18599/grs.2018.4.344-354>

## Introduction

One of the problems occurring hydrocarbon displacement by water is formation failure while water production from weak sandy sediments. Apart from damaging the equipment, sand production causes data transfer problems due to the hydrodynamic telemetry channel clogging while drilling. Therefore determining

of the critical parameters and events that prevent sand production is a main issue.

At the Vadelypskoye oil field water production is performed from the upper (relative to oil reservoirs) layers mainly composed of highly permeable sandstones (600-2500 mD). What raises a red flag is that sand production starts at relatively low-pressure drawdown changing within 4-6 bar.

This paper presents the petrophysical characteristics of the water-saturated sandbody. It discusses the effectiveness of the methods that prevent sand particles from getting into the lifted water. It also presents the

\*Corresponding author: Alexander V. Seryakov  
E-mail: [Alexander.Seryakov@bakerhughes.com](mailto:Alexander.Seryakov@bakerhughes.com)

© 2018 The Authors. Published by Georesurs LLC  
This is an open access article under the CC BY 4.0 license  
(<https://creativecommons.org/licenses/by/4.0/>)

results of 3D numerical geomechanical modeling of the water-supply sections of the sandbody that have become a basis for determining safe pressure-drop ranges to minimize formation failure. In addition, the article gives recommendations on the composition of drilling muds to reduce sand production at the Vadelypskoye oil field.

### Description of the oil field

The Salym oil fields are located 120 km from Surgut in Khanty-Mansi Autonomous Area and operated by the Salym Petroleum Company (SPD). The Vadelypskoye field borders on West Salym and Upper Salym fields (Fig. 1). The field's geological structure composed of a Paleozoic folded basement, an intermediate complex and the terrigenous sandy-argillaceous sediments and

a Mesozoic-Cenozoic platform mantle. Its commercial oil inflow comes from the Cherkashin and the Achimov units.

To maintain the sufficient formation pressure necessary for efficient oil displacement the company uses water flooding, in particular, injecting the Aptian-Albian heterolitics (Uvat formation) underground waters, whose average mineralization (17 g/l) is similar to the one of oil reservoir water. The issues of application of formation pressure maintenance (FPM) systems at the field is maintaining the stability of the walls of uncased water-supply wells and sanding during water lift from the Uvat formation, whose average thickness is about 290 m. Most of the formation (85%) is permeable sediments (Fig. 2) with the water reservoirs mainly formed of

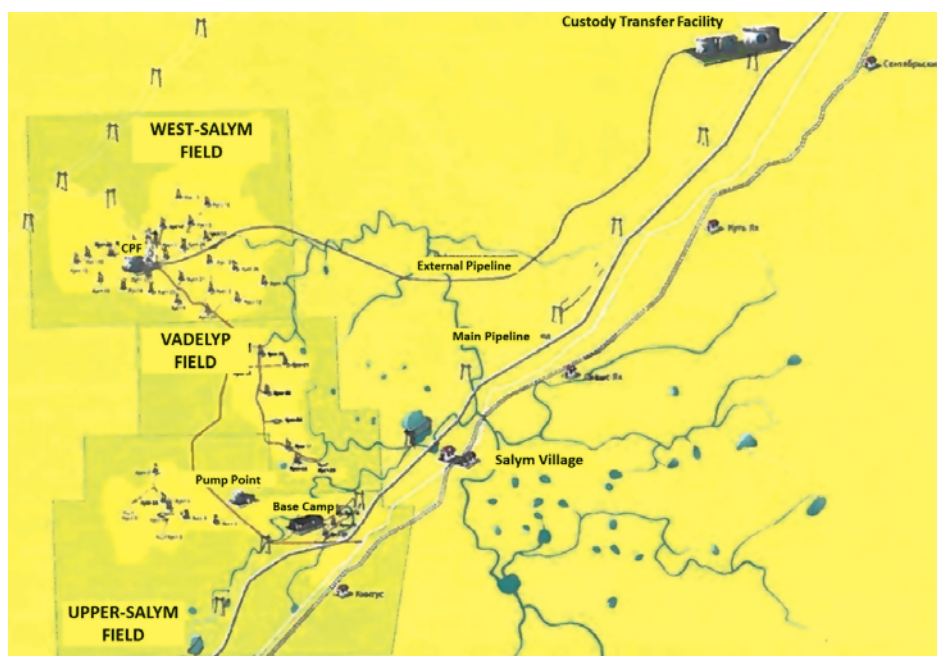


Fig. 1. Map of the Salym oil fields

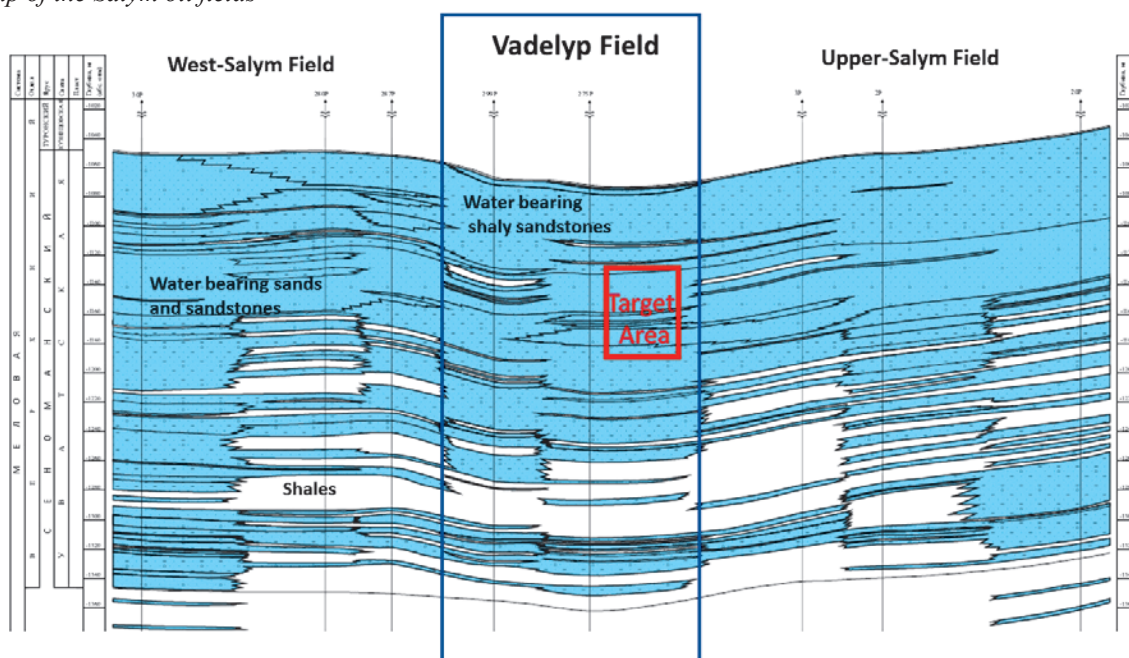


Fig. 2. The Aptian-Albian heterolitics of the Salym oil fields. The red box marks the location of the hole

siltstone (55%); sand and silt rocks, and sandstone present in 30% and 16 % respectively.

Petrophysical analysis of a core from the water-saturated layer of the Uvat formation, taken at the depth of about 1 km showed the presence of thin carbonate interlayers in the sandstone as well as the presence of siltstone (Fig. 3).

Most of the volume in the studied interval was sandstone to be a consolidated, but relatively fragile rock that being drilled produces high amounts of suspended particles, which trouble data transfer while drilling.

### Methods to prevent sand production

Traditionally sand production and falling of the macrofractal pieces of rock in a well is prevented by installation of different protective devices that reduce the well-head erosion and downhole equipment damage in operation. Selecting a proper protective system requires an R&D study to maximize the effectiveness of the protection.

At the Vadelypskoye oil field, they install suspended wire-wrapped sand screens with different cell sizes. It has been confirmed that the cells of 0.2 mm (200  $\mu\text{m}$ ) the concentration of transported particles is 75 mg/l. In this case, the main part of the sediment is grains of 60-100  $\mu\text{m}$  as shown in Table 1.

Field measurements and analysis of the volume ratio of transported sand particles have shown that sand screen with the cells of 0.1 mm (Fig. 4) reduces particle concentration 7 times to 10 mg/l.

Reducing the cell size to 0.05 mm has resulted in complete clogging of the screen and water lift

Grain size, $\mu\text{m}$	Portion in the sample, %
7.5-20	5
20-60	25
60-100	60
>100	10

Table 1. Sand particle size distribution

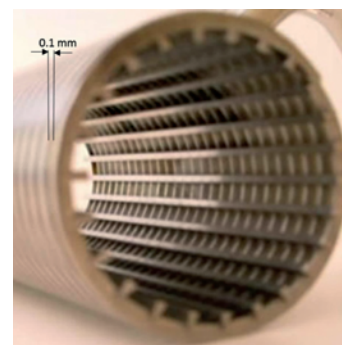


Fig. 4. Wire-wrapped sand screen with the cell width of 0.1 mm

termination, so optimal formation – fluid filtration occurs through the cells of 0.1 mm in size.

### Logging and petrophysical core analysis data

The water-bearing level of the well we considered in our study was located within the depths of 1247-1257 m. Within this interval, the SibBurMash Company performed an isolated coring procedure. The core samples were fixed in transportation cases with a polymer composition to prevent their possible damage while moving to the laboratory. After the coring, the Kogalymneftegeofizika (KNGF) Company ran a combo wireline logging tool including gamma (GR), microlog (MPZ, MGZ), caliper, density (RHOZ), neutron (TNPH), five-probe induction (AE10-90) and acoustic logging (VP) devices. The results of the described procedures can be seen in Fig. 5.

In the laboratory of Coretest Services Company, the core was measured and a standard set of analyses was

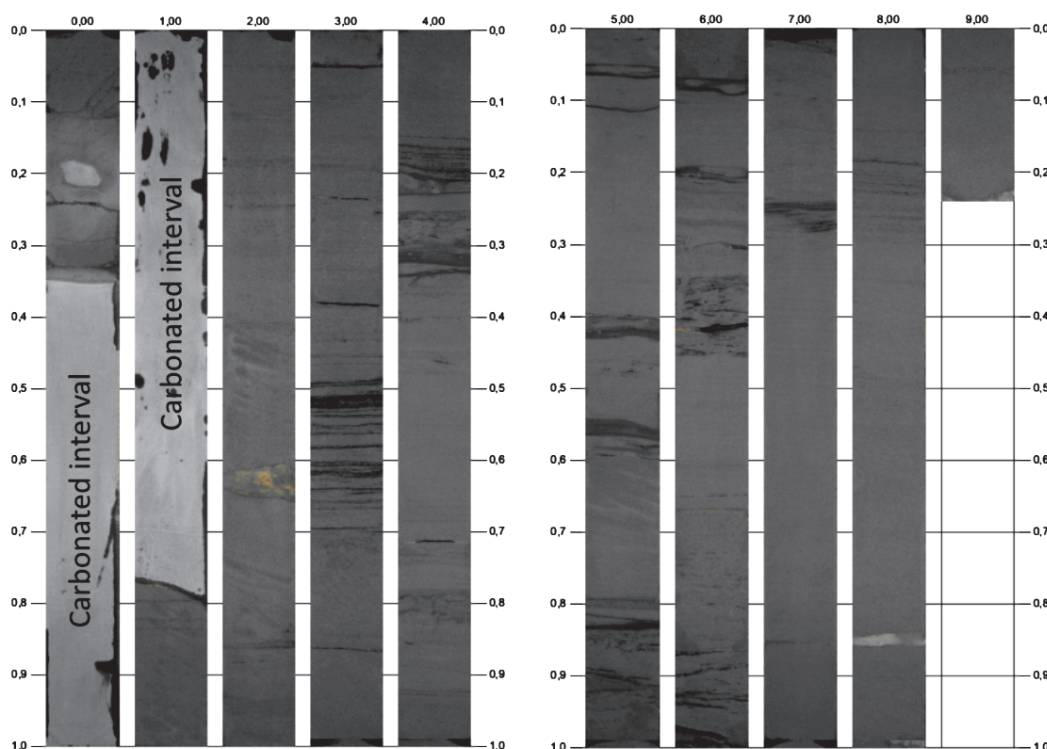


Fig. 3. Day-light photograph of one-meter sections of the core extracted from the water-bearing layer of the Uvat formation



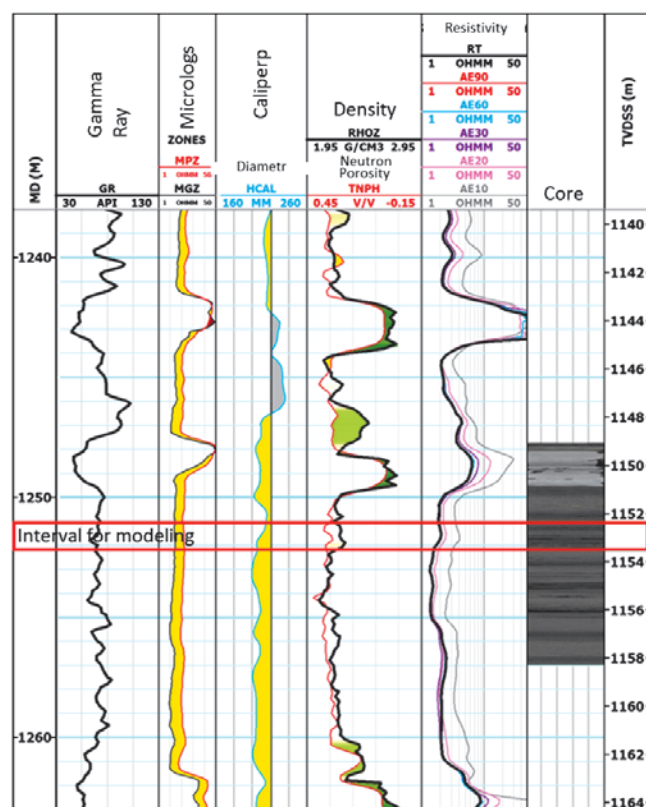


Fig. 5. Logging and coring results. The red box marks the interval selected for modeling

performed including studying the core's granulometric composition and geomechanical tests for formation conditions to determine steady and dynamic elasticity moduli, and breakdown moduli.

The tests demonstrated the core's average porosity to be 33% and permeability – 875 mD. The reservoir's minimum porosity value was 17% and permeability – 0.4 mD. Measurements of the porosity  $\phi$  and permeability  $k$  showed a very good match with the regional (West Siberia) trend:  $\text{Log}_{10}(k) = 21.36 \cdot \phi - 4.15$  (Fig. 6).

Thin-section analysis demonstrated the rock within the indicated interval to be fine-grained sandstone with finely cemented quartz grains of subrounded shape. The

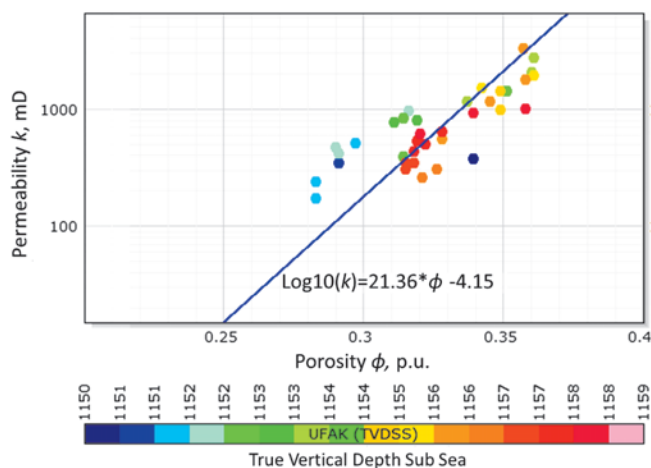


Fig. 6. Porosity vs. permeability. The color legend marks the absolute depth in meters

grains, as a rule, do not have clear orientation and their disposition is chaotic. Measuring orthogonal S-waves (VS1, VS2) in a water-saturated core also revealed no anisotropy (Fig. 7) and confirmed the rock structure as appropriate for isotropic description at micro-, meso- and macrolevels.

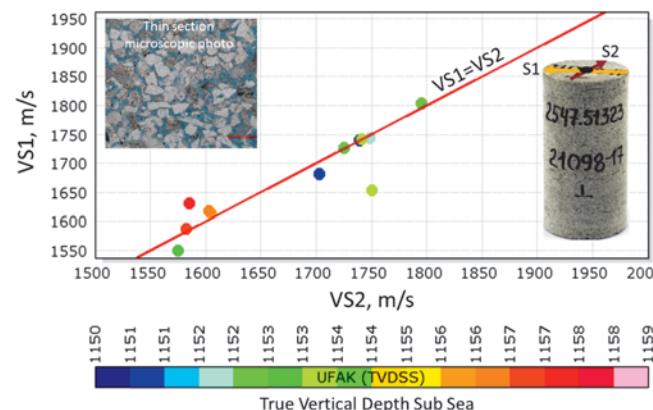


Fig. 7. Measured orthogonal S-wave velocities and the thin section demonstrate the rock's isotropy. The color legend marks absolute depths in meters

### Porous medium deformation model

To develop a strategy for drilling and operation of water-supply wells that have no casing within the productive interval, 3D geomechanical modeling of the water-supply layers was performed.

The joint changes of stresses and pore pressure in a formation is described with the quasi-static Biot model (Biot, 1941; Biot, Willis, 1957), whose equation system includes equilibrium equations for the total stress tensor  $\sigma_{ij}$ :

$$\sigma_{ij,j} = g_i \quad (1)$$

The comma in the equation indexes denotes a corresponding coordinate derivative,  $\vec{g} = (0, 0, \rho g)$ .

The momentum conservation equation with the Darcy law results in the equation for pore pressure  $p$ :

$$\frac{1}{M} \frac{\partial p}{\partial t} - \frac{k}{\mu} \Delta p + \alpha \frac{\partial e}{\partial t} = 0, \quad (2)$$

where  $e$  denotes the volumetric deformation,  $M$  – the Biot modulus,  $k$  – the medium permeability,  $\mu$  – the fluid viscosity,  $\alpha$  – the Biot-Willis coefficient.

The physical ratios between total stresses, deformations and pore pressure are expressed through generalized Hook's law. In assumption of isotropic medium, these ratios are written as:

$$\sigma_{ij} = 2G\varepsilon_{ij} + \lambda e\delta_{ij} - \alpha p, \quad (3)$$

where  $G$  denotes the shear modulus,  $\lambda$  – the Lamé parameter,  $\varepsilon_{ij}$  – deformation tensor components. As the destruction criterion, the model relies upon The Mohr-Coulomb failure criterion, which means a failure is initiated when the value of equivalent stress function  $\sigma_e$

determined from equation (4) exceeds the unconfined compressive strength (UCS):

$$\sigma_e = \sigma'_1 - \sigma'_3 \operatorname{ctg} \psi, \quad (4)$$

where  $\sigma'_1$ ,  $\sigma'_3$  denote the minimum and maximum main effective stress,  $\operatorname{ctg} \psi = (1 + \sin \varphi) / (1 - \sin \varphi)$ ,  $\varphi$  – the inner friction angle.

The equation system (1)-(3) is solved in 3D space using the finite – element method (Zienkiewicz, 1971; Wang, 2000). Hexagons are used to discrete the continuous medium. The basic functions are determined for the hexagon's apexes and are bilinear, while the shape functions are quadratic, which allows one to describe a well's surface. The numerical algorithm to solve poroelastic problem conjugates the solution for the pore pressure and for displacement through iterations at each time step until a given accuracy for determined parameters is achieved (Manakov, 2012).

The finite-element algorithm has been implemented in the Geofluid 3D software package that also includes a mesh generator, a solver and a post processor.

### Input modeling parameters

For modeling purposes, we selected a one -meter interval (1252.55-1253.55 m) of an uncased well with the radius of  $r_b = 0.11$  m and the formation permeability  $k$  changing in accord with the permeability profile (Table 2).

Within the selected borehole interval cores were taken perpendicular to the bedding at the depths of 1252.34, 1252.56 and 1253.06 meters. The core samples were studied in a laboratory to determine the porosity  $\phi$  and the static elastic modules (Young modulus  $E$ , Poisson's ratio and UCS) that were obtained from a triaxial compression test for the reservoir conditions.

The computation domain was a one-meter vertical formation section around a well, surrounded by a

mesh (Fig. 8). The rock's poroelastic properties were considered constant for the whole section apart from the permeability  $k$ , whose values changed in accordance with Table 2.

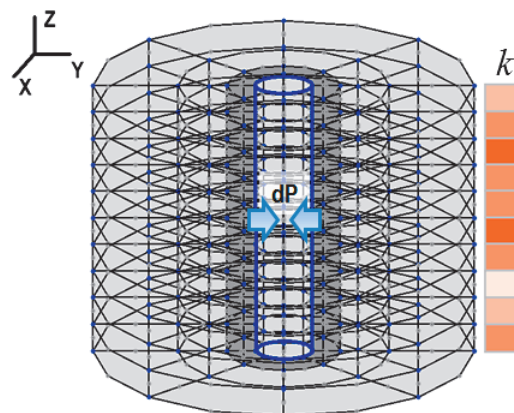


Fig. 8. Computation domain

The obtained logging and coring data were used to determine the input parameters of modelled interval presented in Fig. 9. For the Vadelypskoye – field rock the shear modulus values is  $G = E/2(1+\nu) = 2.07$  GPa, and the Biot-Willis coefficient  $\alpha = 0.95$ . The granule compressibility of the rock matrix was selected to be  $K'_s = 36$  GPa, which is a characteristic compressibility value for sandstones (Wang, 2000); and fluid compressibility  $K'_f = 2.3$  GPa for water. Using the formula derived from the poroelasticity equations (Bocharov, Seryakov, 2016):

$$K_u B = \frac{K'_s}{\phi(c_f / \delta - 1)} = \frac{K'_s}{\phi(K'_s / K_f - 1)}, \quad (5)$$

where the porosity  $\phi = 0.34$ , we obtained  $K_u B = 7.23$  GPa and derived the Biot parameter  $M = K_u B / \alpha = 7.64$  GPa.

A pressure drop (dP) being a difference between formation and borehole pressures was set on the borehole wall. In case of water pumping this parameter becomes negative, but here in the article, we are going to use its positive values and to underline that we are dealing with a pressure drawdown scenario. In order to account for a mud damaged zone or a colmatation zone, the formation permeability along the radial coordinate was considered heterogeneous. The colmatation zone was marked as a shaded area around the well (Fig. 10).

The caliper measurements performed in 8 hours after penetration had shown a presence of mudcake whose thickness varied from 10 to 15 mm. Since the studied sandstone was of highly-permeable type, the creation of a damaged zone did not cause any doubts. When modeling water pumping we assumed that all the mudcake was washed out while drillstring tripping, so only a colmatation zone with the thickness  $h_d$ , and reduced, relative to the formation, permeability  $k_d$  was accounted for (Fig. 3). It was apparent that the near-wellbore zone contamination degree characterized by

Depth, m	$k$ , mD
1252.55	1992.86
1252.60	1027.21
1252.65	1222.66
1252.75	1244.95
1252.80	2110.56
1252.85	1513.01
1252.90	1530.42
1252.95	1444.12
1253.00	2053.87
1253.05	1740.98
1253.10	1152.60
1253.15	811.16
1253.20	1539.87
1253.25	0.39
1253.30	1705.04

Table 2. Permeability profile of water-saturated interval

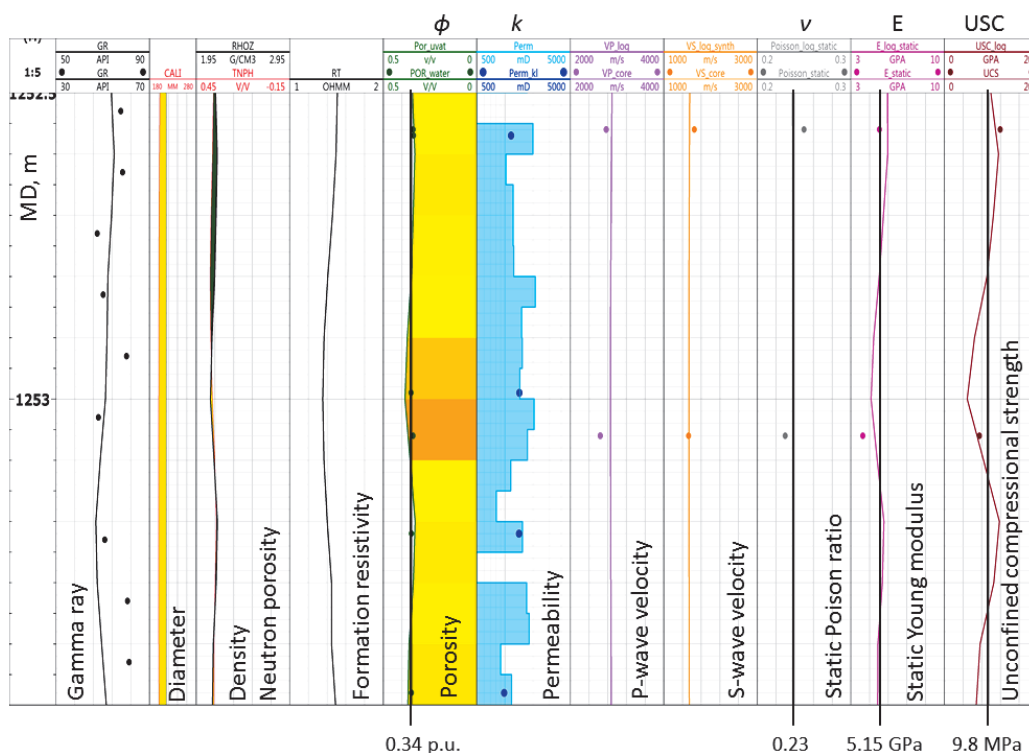


Fig. 9. Logging data and interpretation results; coring and the average parameter values used in the modeling

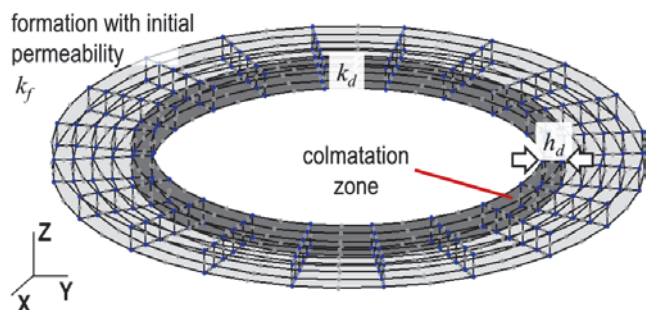


Fig. 10. Near-well area schematic. The colmatation zone has thickness  $h_d$  and permeability  $k_d$  that is the fraction of the total formation permeability  $k$  at the given depth

the parameters  $k_d$  and  $h_d$  would play important role in the distribution of pore pressure and, consequently, effective stresses around the well. In order to forecast the well's behavior, its stability parameters had been calculated for different experimentally confirmed near-well parameters (Podbereznyy et al., 2017). For the computations parameter  $h_d$  was varied from 2 to 30 mm, parameter  $k_d$  was varied from 0.1 to 0.0001 of the formation permeability beyond the colmatation zone  $k$ .

Now, let us consider initial geomechanical conditions around the well. The pore pressure  $p$  in the formation was 12.3 MPa, which was confirmed by field data and corresponds to hydrostatic. The vertical stress  $S_v$  calculated from gamma-gamma density logging data was 23 MPa for the given depth. The estimations of the minimum horizontal stress  $S_{hmin}$  were within the range of 15-17.5 MPa, which was confirmed

by DFIT data. As for the maximum horizontal stress  $S_{Hmax}$ , downhole measurements showed it could be as equal to the minimum or inline from it by the value up to 1 MPa.

One of the most important parameter for borehole wall stability modeling is UCS. Considering the parameter's distribution within the 1252.55-1253.55 m interval, a conclusion was made that its lowest value would correspond to the highly – permeable sublayer at the depth of 1253 m where the highest porosity level (34%) increased the probability of matrix damage and sanding.

According to the results of laboratory core studies (Fig. 11), the UCS and porosity correlated as  $UCS = 277 \cdot e^{-10 \cdot \phi}$ , which corresponds to the data provided by Chang et al, 2006. Considering the assessment data, in our study we had decided to use the value  $UCS = 9.8$  MPa to determine breakdown in the highly-permeable interval.

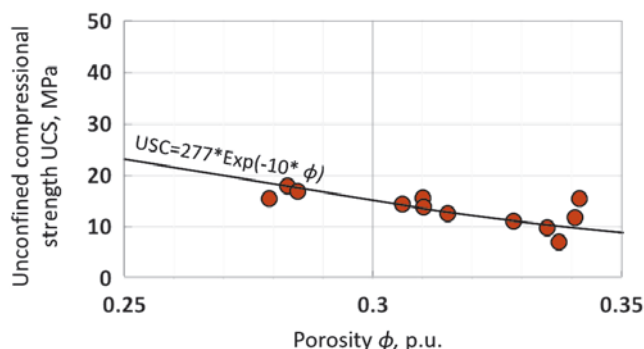


Fig. 11. UCS vs. porosity



## Results of the modeling

Here it should be underlined one more time that the main objective of the modeling was determining of safe water pumping modes within previously described ranges for minimum and maximum horizontal stresses, in dependence of pump-off pressure and near-well contamination degree.

### A. Downhole conditions and admissible pressure drawdown

First hand, we studied the effect the horizontal stresses and pressure drawdown degree had on sand production. To determine the main regularities of the stress state in computations for different colmatation zones some extreme values were selected:  $0.2k$  that is often used in commercial packages (GMI SFIB User's manual, 2008) and  $0.001k$ , where  $k$  denotes formation permeability. For the maximum horizontal stress  $S_{Hmax}$  and minimum  $S_{Hmin}$  the following options were considered:

1(A): when the stresses were equal  $S_{Hmax} = S_{Hmin}$  with the extreme stress values  $S_{Hmin} = 15$  MPa and  $S_{Hmax} = 17.5$  MPa studied;

2(A): when  $S_{Hmax} = S_{Hmin} + 1$  MPa with the boundary stress values  $S_{Hmin} = 15$  MPa,  $S_{Hmax} = 16$  MPa;  $S_{Hmin} = 7.5$  MPa,  $S_{Hmax} = 18.5$  MPa studied.

During modeling, the boundary  $dP$  values of 4 and 6 bar were used.

At the preliminary stage of the computations, it was found out that the stress function value  $\sigma_e$  (equation 4) changes insignificantly along the well's trajectory. The qualitative representation of this phenomenon can be seen in Fig. 12 (a) demonstrating a 2D distribution pattern of  $\sigma_e$  where on z-axis is plotted the relative depth  $h$  whose zero value corresponds to the upper sandstone boundary of 1252.5 m.

For detailed estimation of  $\sigma_e$  it was more convenient to consider 1D depth-related plot presented in Fig. 12 (b). Modeling was performed for the following

conditions:  $S_{Hmax} = S_{Hmin} = 15$  MPa,  $dP = 4$  bar and 5-mm radius of the damaged zone with the permeability equal to 0.001 of the formation permeability. As you can see the measurement of  $\sigma_e$  can be described with a linear function, except for an interval at the relative depth of  $h = 0.7$  m. Comparing this deviation with the permeability distribution given in Fig. 12 (c) one can see the presence of a low-permeable carbonate interlayer. However, this deviation amplitude is less than 1%, while from a solid interlayer one usually expects a significant UCS increase. For that reason, when estimating the rock failure, we regarded an interval at the relative depth of 0.5 m where maximum porosity, permeability and UCS were reached.

### Variant 1(A). Results obtained for equal stresses $S_{Hmax} = S_{Hmin}$ .

It was established that at the pressure drop of 4 bar rock failure occurs only when  $S_{Hmax} = S_{Hmin} = 15$  MPa in low-permeable colmatation zone, in other words, when  $k_d = 0.001k$ . In this case, the maximum  $\sigma_e$  value of 9.92 MPa was registered not on the well contour but at the distance of about 2 mm from its walls. This change of the function  $\sigma_e$  was of regular character and revealed itself in the low-permeable colmatation zones. We will touch on this effect in more detail in the part describing the effect  $k_d$  and  $h_d$  have on well stability. When increasing the horizontal stresses up to

$S_{Hmax}, S_{Hmin}$ , MPa	dP, bar	$\sigma_e$ for $k_d = 0.2k$	$\sigma_e$ for $k_d = 0.001k$	$\sigma_e$ for $h_d = 0$
15	4	9.59	9.92	9.58
15	6	9.68	10.35	9.66
17.5	4	9.62	9.76	9.57
17.5	6	9.9	10.1	9.84

Table 3. The maximum values of  $\sigma_e$  (MPa) in the near-well area for homogeneous horizontal stresses

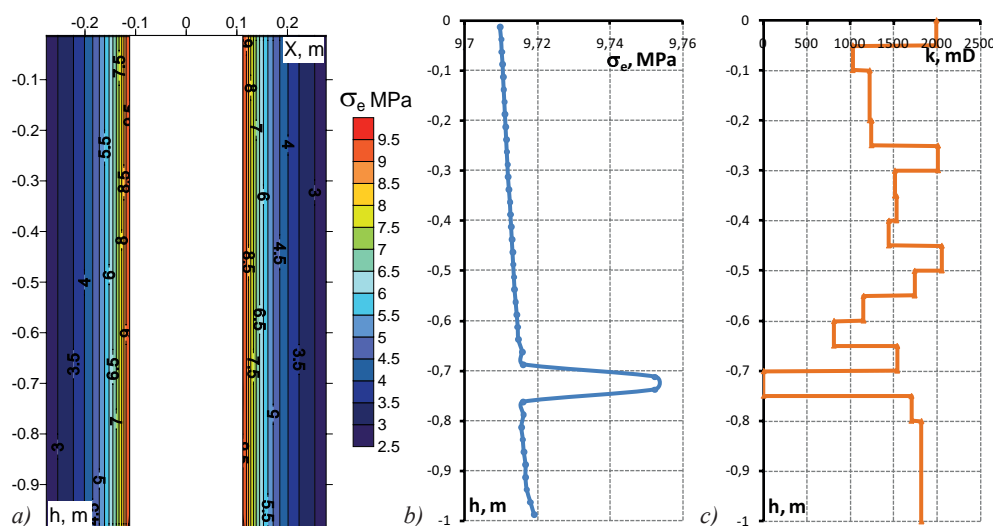


Fig. 12. Stress function ( $\sigma_e$ ) distribution along the well: 2D spectral pattern (a); 1D depth-related plot (b); formation permeability (c)

$S_{Hmax} = S_{Hmin} = 17.5$  MPa, the failure occurs neither at  $k_d = 0.001k$  nor at  $k_d = 0.2k$ .

When water lift was performed at the pressure drawdown of 6 bar, the well remained intact only at  $S_{Hmax} = S_{Hmin} = 15$  MPa and  $k_d = 0.2k$ , while all the other combinations were unsafe. For more detail turn to Table 3, whose first two columns contain downhole conditions, and the other three – corresponding  $\sigma_e$  values.

In order to obtain a reference value for  $\sigma_e$  we calculated such water-lift variations that had no colmatation zone. The values of equivalent stress  $\sigma_e^0$  for this case can be found in the utmost-right column of Tab. 3. Comparison  $\sigma_e^0$  against the other calculated variants showed that the stress-state function in the colmatation zone with the permeability reduced down to 20% of the formation's has little difference from the values obtained for a water extraction from noncontaminated formation. This effect has been observed for the indicated low-pressure drawdown and initial stress ratio ranges in the formation. The modeling also demonstrated that the safest pump-off technique was pumping from a noncontaminated formation, which was impossible in presence of highly-permeable sandstones.

The colmatation zone with the permeability of 0.1% of the formation's was the reason for a more abrupt pressure drop in the contaminated area and increased near-well effective stresses.

The isolines and spectral diagrams of  $\sigma_e$  distribution in XY plane at the relative depth of 0.5 m for a case of homogeneous horizontal stress can be seen in Fig. 13.

*Variant 2(A).* As the deformation theory predicts, in a heterogeneous field of the horizontal loads  $S_{Hmax} > S_{Hmin}$ , the maximum concentration of shear stresses went in the direction of the minimum stress  $S_{Hmin}$ .

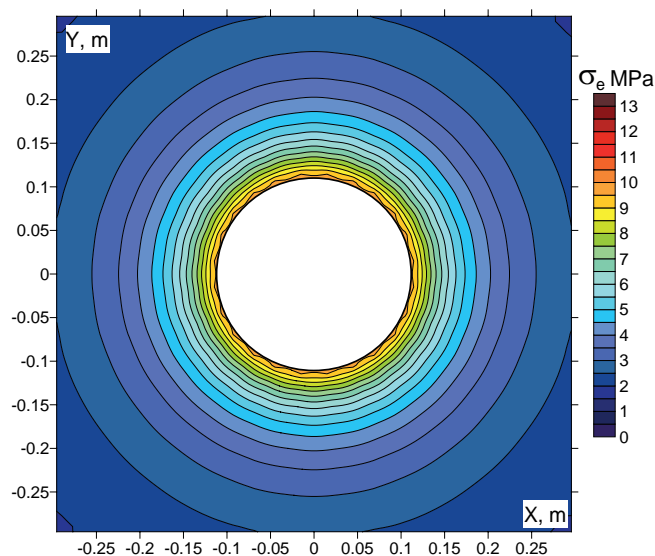


Fig. 13. Stress function  $\sigma_e$  distribution in the near-wellbore area calculated for  $S_{Hmax} = S_{Hmin} = 15$  MPa, 4-bar pressure drop and colmatation zone  $k_d = 0.001k$ . The horizontal section goes through an interlayer with highest permeability

The  $\sigma_e$  values obtained for all the colmatation zone permeabilities and pressure drops exceeded the UCS value. Therefore, in the case of heterogeneous horizontal stresses, even with a slight difference the sand production begins. The numerical values of  $\sigma_e$  for the different initial conditions can be found in Table 4. Its last column contains the maximum values of  $\sigma_e^0$  with no colmatation zone.

$S_{Hmin}$ , MPa	$S_{Hmax}$ , MPa	dP, bar	$\sigma_e$ for $k_d = 0.2k$	$\sigma_e$ for $k_d = 0.001k$	$\sigma_e$ for $h_d = 0$
15	16	4	9.9	10.04	9.9
15	16	6	9.99	10.47	10
17.5	18.55	4	12.52	12.65	12.59
17.5	18.55	6	12.79	12.99	12.86

Table 4. The maximum values of  $\sigma_e$  (MPa) in the near-well area for heterogeneous horizontal stresses

Analysis of the obtained values showed that the presence of a colmatation zone with the permeability of 20% of the formation's even insignificantly reduce the level of equivalent stress in absence of rock breakdown. On the other hand, the low-permeable colmatation zone (0.1% of the formation's) increased the  $\sigma_e$  values. Comparing the  $\sigma_e$  values for the noncontaminated formation with their analogs from Table 3, we concluded that the horizontal-stress heterogeneity had a greater effect on a failure possibility than the colmatation zone parameters.

In Fig. 14 you can see the  $\sigma_e$  parameter distribution for the pressure drop of 4 bars and the borehole conditions  $S_{Hmax} = 18.55$  MPa,  $S_{Hmin} = 17.5$  MPa.

Generalizing the results obtained for homogeneous and heterogenous horizontal stress it can be concluded

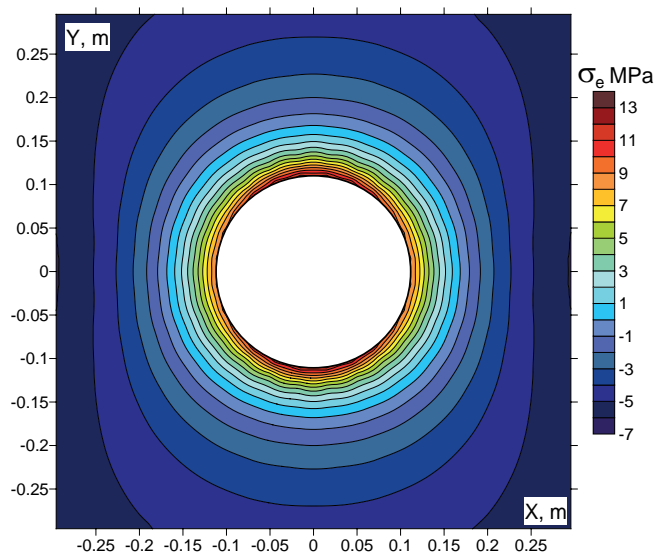


Fig. 14. Stress distribution ( $\sigma_e$ ) in the near-wellbore area, calculated for the pressure drop of 4 bar, the borehole conditions  $S_{Hmax} = 18.55$  MPa,  $S_{Hmin} = 17.5$  MPa, and the colmatation zone permeability  $k_d = 0.001k$

that a failure probability increases with increase in the amplitude and a difference between the horizontal stresses, with increase in pressure drawdown, and with reduction in the colmatation-zone permeability.

### B. Invaded zone parameters and their effect on sand production

For further analysis of the colmatation zone effect on sandstone destruction during water pumping, we performed a series of computations with changing  $k_d$  (permeability) and  $h_d$  (width). The pressure drop was selected to be 4 bar and 2 variants of horizontal pressures were considered:

$$1(B): S_{Hmax} = S_{Hmin} = 16 \text{ MPa};$$

$$2(B): S_{Hmax} = 18.55 \text{ MPa}, S_{Hmin} = 17.5 \text{ MPa}.$$

For the colmatation zone width  $h_d$  the following values were set: 2, 5, 7, 10 and 30 mm. The colmatation zone permeability  $k_d$  varied from 10% to 0.01% of the formation's, that means that the coefficient  $\gamma$  in the ratio  $k_d = \gamma k$  was 0.1, 0.01, 0.001 and 0.0001.

*Variant 1(B).* In the homogeneous field of horizontal stresses, a computation in absence of the colmatation zone gave  $\sigma_e^0 = 9.558 \text{ MPa}$ . For analysis of the computations with colmatation zone taken into account it was convenient to consider the deviation function  $\Delta\sigma_e = (\sigma_e - \sigma_e^0)/\sigma_e^0$  from the  $\sigma_e^0$  reference value. The modeling demonstrated that the maximum level of equivalent stress was achieved in presence of a very small and low-permeable colmatation zone densely packed with drilling-mud particles. Under these conditions, water pumping induces a significant gradient of effective stresses that results in a breakdown. The  $\Delta\sigma_e$  deviation distribution in dependence on the parameters of  $h_d$  and the reduction factor  $\gamma$  can be seen in Fig. 15.

Here it should be noted that a maximum stress value for the impermeable colmatation zone (0.1 and 0.01%) was obtained not on the borehole's wall, but in

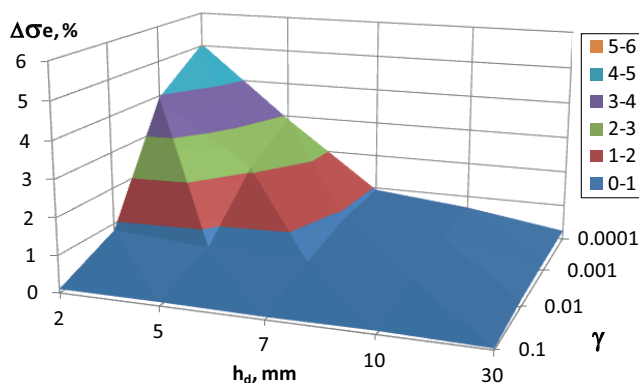


Fig. 15. Deviation of the maximum values of equivalent stresses in the near-wellbore area in the homogeneous field of horizontal stresses  $S_{Hmax} = S_{Hmin} = 16 \text{ MPa}$  in dependence on the width  $h_d$  and the colmatation zone permeability  $k_d$ . The parameter  $\gamma$  is a quantitative characteristic of permeability reduction when compared to the uninvaded formation ( $k_d = \gamma k$ )

the formation at the distance of 1-2 mm from the well contour. This can be seen in the  $\sigma_e$  distribution diagrams built for the colmatation zone thickness of 2 and 5 mm (Fig. 16). So, if while water extraction UCS values are exceeded, rock failure is most likely to occur in the zone of 1-2 mm from the borehole wall.

In general, the modeling demonstrated that the invaded zone had a little effect on the stresses' degree in the pore matrix while water lift. Their highest increase (5%) was observed when a low-permeable and low-extended colmatation zone was formed.

*Variant 2(B).* In case of no colmatation zone, the maximum value of the equivalent stress  $\sigma_e^0$  equal to 10.4841 MPa was obtained on the well contour in the direction of minimum horizontal stress. Therefore, the borehole conditions with  $S_{Hmax} = 18.55 \text{ MPa}$  and  $S_{Hmin} = 17.5 \text{ MPa}$  are unsafe.

As the modeling shown the presence of invaded zone for heterogeneous horizontal stresses led to insignificant increase of  $\sigma_e$ , whose maximum deviation reached 2.3%. The graphical representation of the  $\Delta\sigma_e$  function in variables ( $h_d, \gamma$ ) can be seen in Fig. 17. The diagram is a qualitative replica of the surface derived for  $S_{Hmax} = S_{Hmin} = 16 \text{ MPa}$ .

Comparing the  $\sigma_e^0$  values for different horizontal stress ratios against variation  $\Delta\sigma_e$  for the  $S_{Hmax} > S_{Hmin}$  case, we came to a conclusion that stress heterogeneity had a greater effect on rock failure than the colmatation zone.

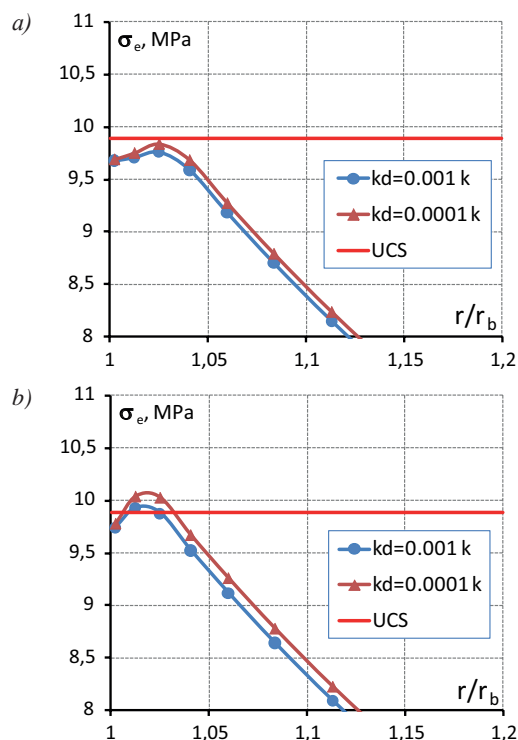


Fig. 16. The  $\sigma_e$  function distribution in the near-well area for  $h_d = 5 \text{ mm}$  (a) and  $h_d = 2 \text{ mm}$  (b), horizontal stresses  $S_{Hmax} = S_{Hmin} = 16 \text{ MPa}$ ,  $dP = 4 \text{ bar}$ , relative section depth  $h = 0.5 \text{ m}$ , and well radius  $r_b = 0.11 \text{ m}$



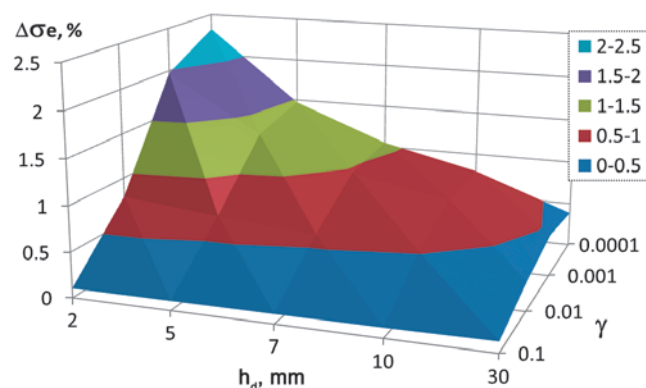


Fig. 17. Deviation function built for  $S_{Hmax} = 18.55$  MPa,  $S_{Hmin} = 17.5$  MPa in the dependence on the colmatation zone width  $h_d$  and the permeability reduction factor  $\gamma$

## Conclusions

Generalizing of the results obtained for the Vadelypskoye oil field has brought us to the following conclusions:

1. The modeling has confirmed sand production during water pumping from the reservoir at the pressure drawdown of 4-6 bar.

2. In the presence of homogeneous horizontal stresses, the following operation modes can be considered as safe:

- pressure drop down to 6 bar is acceptable at the horizontal stresses of 15 MPa and in the presence of a moderately contaminated (10-20% of formation's permeability) near-wellbore area;

- pressure drop down to 4 bar is acceptable at the horizontal stresses of 17 MPa and in the presence of a moderately contaminated near-wellbore area.

3. Under the borehole conditions when the maximum horizontal stress exceeds the minimum one by 1.05 MPa for cases  $S_{Hmin} = 15$  MPa,  $S_{Hmax} = 16$  MPa; and  $S_{Hmin} = 17.5$  MPa,  $S_{Hmax} = 18.55$  MPa in the presence of a moderately contaminated near-wellbore area, sanding begins at the pressure drawdown of 4 bar.

4. The effect of near-well contamination degree and its width on equivalent stress increasing is most apparent in the presence of homogeneous horizontal stresses and may reach up to 6% of the equivalent stress level calculated for water extraction from a noncontaminated formation.

5. Highly-impermeable colmatation zones of 2-5 mm in length produce a high pore pressure gradient while water lift that causes cylindrical pieces (1-2 mm) to scale off from borehole walls. This effect can be observed in the presence of homogeneous horizontal stresses.

6. Changing of the colmatation- zone parameters in a field of horizontal stresses may increase the equivalent stress up to 2.5% relative to the one calculated for water pumping from a noncontaminated formation.

7. Analysis of transition from homogeneous horizontal stresses to heterogenous ones with account for a destruction function for the near-well area demonstrates that the equivalent stress is more sensitive to a difference between horizontal stresses rather than to colmatation zone parameters.

## Recommendations for drilling and operation of water-supply wells at the field

The obtained results have enabled us to formulate the following recommendations:

1. Use sand screens with the cell diameter of 0.1 mm.

2. When penetrating a target horizon use a drill mud whose particles are bigger than the pore size to prevent damage zone formation.

3. Use a drilling mud with low concentration of suspended particle to form a permeable colmatation zone. This drilling mode provides a non-increasing of the equivalent stress on the wall under subsequent water pumping.

4. If using suspensions is critical for preventing mud from entering into inferior oil-saturated layers, we recommend using fine-dispersed fractions to form an extended colmatation zone, which, however, may complicate water extraction.

5. Produce water from a formation with the heterogenous horizontal stresses of about 15 MPa, apply the pressure drawdown of no more than 6 bar.

6. Produce water from a formation with the heterogenous horizontal stresses of about 17 MPa, apply the pressure drawdown of no more than 4 bar.

7. Pay special attention to determining actual horizontal stresses in the formation, since the amount of maximum horizontal stress exceeding over the minimum one has a more significant effect on rock failure while water extraction than colmatation zone formation while drilling.

## References

- Biot M.A. (1941). General Theory of Three-Dimensional Consolidation. *Journal of Applied Physics*, 12(2), pp. 155-161. <https://doi.org/10.1063/1.1712886>
- Biot M.A., Willis D.G. (1957). The Elastic Coefficients of the Theory of Consolidation. *Journal of Applied Mechanics*, 24, pp. 594-601.
- Bocharov O.B., Serjakov A.V. (2016). Modelirovanie neharakternogo razrusheniya produktivnykh sloev peschanika pri burenii [Simulation of uncharacteristic destruction of sandstone productive layers during drilling]. *Fizicheskaya Mezomehanika = Physical Mesomechanics Journal*, 19(6), pp. 86-93. (In Russ.)
- Chang C., Zoback M. D. and Khaksar A. (2006). Empirical relations between rock strength and physical properties in sedimentary rocks. *Journal of Petroleum Science and Engineering*, 51, pp. 223-237. <https://doi.org/10.1016/j.petrol.2006.01.003>
- Fjær E., Holt R.M., Horsrud P., Raaen A.M. and Risnes R. (1992). Petroleum Related Rock Mechanics. *Developments in Petroleum Science*, 33, 337 p.
- GMI SFIB User's manual (2008). GeoMechanics International, Inc., 295 p.
- Manakov A.V., Rudjak V.Ja. (2012). Algoritm sovместного modelirovaniya fil'tracionnykh i geomechanicheskikh processov v priskvazhinnoj zone [Algorithm for joint modeling of filtration and geomechanical processes in the near-wellbore]

zone]. *Sibirskiy zhurnal industrialnoy matematiki = Siberian Journal of Industrial Mathematics*, 15, 1(49), pp. 53-65. (In Russ.)

Podberezheny M., Polushkin S., Makarov A. (2017). Novel Approach for Evaluation of Petrophysical Parameters from Time-lapse Induction Logging-While-Drilling Measurements in Deviated and Horizontal Wells. *Proceedings of the SPE Russian Petroleum Technology Conference*, Moscow, Russia. SPE-187911-MS. <https://doi.org/10.2118/187911-MS>

Wang H.F. (2000). *Theory of Linear Poroelasticity with Applications to Geomechanics and Hydrology*. Princeton: Princeton University Press, 287 p.

Zienkiewicz O. (1975). *Metod konechnykh elementov v tekhnike* [The finite element method in engineering science]. Moscow: Mir, 544 p. (In Russ.)

### About the Authors

*Alexander V. Seryakov* – Researcher, PhD (Engineering)

Novosibirsk Technology Center Baker Hughes JSC  
4A, Kutateladze st., Novosibirsk, 630090, Russian Federation

E-mail: [Alexander.Seryakov@bakerhughes.com](mailto:Alexander.Seryakov@bakerhughes.com)

*Maxim Yu. Podberezheny* – Chief petrophysicist, PhD (Physics and Mathematics)

Salym Petroleum Development NV  
31, Novinsky boul., Moscow, 123242, Russian Federation

*Oleg B. Bocharov* – PhD (Physics and Mathematics), Deputy Director

Novosibirsk Technology Center Baker Hughes JSC  
4A, Kutateladze st., Novosibirsk, 630090, Russian Federation

*Marat A. Azamatov* – Head of the Department, Master of Physics, MSc Petroleum Engineering

Salym Petroleum Development NV  
31, Novinsky boul., Moscow, 123242, Russian Federation

*Manuscript received 31 July 2018;*

*Accepted 26 September 2018;*

*Published 30 November 2018*



## SHORT COMMUNICATION

DOI: <https://doi.org/10.18599/grs.2018.4.355-358>

## Evaluation of mineral and organic inhibitor effects on bentonite clay

*F.V. Degtjarjov**Production association "Belorusneft" BelNIPIneft, Gomel, Republic of Belarus**E-mail: f.degtjarev@beloil.by*

**Abstract.** The supra-salt complex of the oilfield of the Republic of Belarus is represented by high-colloidal multicolored clay deposits with layers of unstable sandstones and aleurolites evenly distributed throughout the section. Drilling of intervals which are represented by clay sediments is accompanied by complications caused by swelling of clays – stuck, tightening, sticking clay on the drilling tool. Swelling occurs during drilling of high-colloidal clays. As a result of the action of the drilling mud and its filtrate, the clay swells, narrowing the trunk and reducing the stability of the walls of well. For the prevention or maximum reduction of the intensity of the swelling the drilling mud must have a high inhibitory ability. Such properties are attached by special reagents-inhibitors, which are the main component of the inhibiting drilling fluid. The creation of such drilling fluid is advisable to start with the choice of the reagent-inhibitor.

This article provides a comparison of the inhibitory effect of the two reagents specific to organic (Polyekol) and inorganic (potassium chloride) compounds. To assess the effectiveness of these reagents, the indicator of moisturizing ability was used. In the experiment, the highest efficiency demonstrated organic reagent-inhibitor Polyekol at a concentration of 2%, and the inorganic reagent-inhibitor potassium chloride resulted in cracking of samples. The results obtained during the comparison of these reagents will form the basis for the development of an inhibiting drilling mud for drilling of the supra-salt deposits of the Pripyat trough.

**Keywords:** clay, swelling, complications, wellbore stability, reagents-inhibitors, drilling mud, indicator of moisturizing ability

**Recommended citation:** Degtjarjov F.V. (2018). Evaluation of mineral and organic inhibitor effects on bentonite clay. *Georesursy = Georesources*, 20(4), Part 1, pp. 355-358. DOI: <https://doi.org/10.18599/grs.2018.4.355-358>

The supra-salt complex of the oilfield of the Republic of Belarus is represented by high-colloidal multicolored clay deposits with layers of unstable sandstones and aleurolites evenly distributed throughout the section. When drilling oil wells, the swelling of clay rocks can cause a large number of complications, such as drilling tool sticking, cavern formation, sloughing hole, borehole enlargement and keyseating, oleaginization, loss of circulation (Sereda, Soloviev, 1974). Swelling occurs during the drilling through high colloidal clays. As a result of the washing fluid and its filtrate activity, the clay swells narrowing the borehole and reducing the stability of the borehole walls. To prevent or minimize the intensity of swelling, the drilling fluid should have high inhibition properties. Such properties can be achieved by use of special inhibitor reagents, which are the main component of the inhibitory drilling mud. Creation of such a drilling fluid is advisable to start with the selection of inhibitor reagent.

As an inhibitor reagent can be used a substance of both organic and inorganic nature, and their mixture. Currently, there are a huge number of such reagents available on the market. This article compares the inhibitory effect of two reagents related to organic (Polyecol) and inorganic (potassium chloride) compounds. The results obtained during the comparison of these reagents will form the basis for further development of an inhibiting drilling fluid, which can be used to drill over-salt sediments of the Pripyat trough.

The use of potassium chloride while drilling as an inhibitor of clay sediments in the territory of the Republic of Belarus has many years of experience. This reagent is included in the formulation of many drilling fluids as a clay-swelling inhibitor. However, with the development of production technologies and the creation of new research methods, a huge number of new inhibitor reagents belonging to other classes of chemicals have appeared. Therefore, in order to select the most effective reagent, it is necessary to conduct comparative tests.

The differences of inhibitor reagents belonging to different classes of chemical compounds are related to their structure, hydration principle and the action



mechanism they have on clay minerals. To select the most effective inhibitor, it is necessary to accurately represent both the structure of clay minerals and the mechanism of their hydration.

According to the articles (Biletskij, Kasenov, Sushko, 2013), clay microstructure is represented by elementary plate packs with a small (fraction of micrometers) thickness and a relatively very large surface. It corresponds to a high surface energy manifested in the form of a negative electric charge. Negatively charged plates repel each other combining into packets using positive metal ions. The higher the positive charge (valence) of metals, the stronger the connection of elementary plates in the package. For example, sodium and calcium clays can be identified by the type of metal predominating in them, and the second one (containing bivalent  $\text{Ca}^{2+}$ ) dissolve worse than the first one (containing monovalent  $\text{Na}^+$ ).

During the drilling of clay rocks, the drilling fluid or its water filtrate rushes through fractures and pores into the borehole walls and comes into contact with the clay structures. It is known that the  $\text{H}_2\text{O}$  water molecule has an elongated shape, with a positive hydrogen ion concentrated at one end (the pole of the «dipole»), and a negative oxygen ion at the other. In the course of Brownian motion with clay packages, the dipoles with their positive side stick to the negatively charged surface of the plates. The surface of the elementary plates is completely «seated» by equally oriented dipoles of water i.e. covered with a «hydrated shell». With a high charge of plate, the hydration shell can thicken building on itself all new layers of water dipoles. Hydration shells moving apart the plates in the package overcoming the retention effect of metal ions. At the macroscopic extent, the hydrated shells thickening results in an increase in the volume («swelling») of clay adjacent to the well. Shear fractures appear between the swelling layer making up the borehole walls and the main «dry» rock causing collapses of the swollen material, which then accumulates in the narrowed sections of the wellbore (Biletskij, Kasenov, Sushko, 2013).

The use of inhibiting drilling muds has been recognized as the most effective method to prevent borehole walls instability. Such solutions transform easily-dissolved clay in the near-wellbore zone into difficult-to-dissolve clay. Such drilling muds necessarily contain an inhibitor reagent. The action of such reagents is based on cations adsorption on the clay surface and osmotic pressure. Osmotic pressure results from the fact that the flushing fluid has a higher concentration of cations, compared to the rock, stimulating the flow of water from the rock into the drilling fluid and, as a result, reducing the hydration of the rock (Egorova, 2010).

Inorganic compounds, in particular sodium and potassium chlorides, are widely used to reduce the

penetration of water into the space between the layers of clay minerals. These compounds undergo electrolytic dissociation into positive and negative ions in solution. Positive ions neutralize the negative charge of the elementary clay plates. Their hydrated shells are thinned down to complete dissolution. The plates are connected to each other reducing the occupied volume. With the help of inhibitors, it is possible to prevent swelling of clay borehole walls, cavern formation and the associated complications (Biletskij, Kasenov, Sushko, 2013).

Organic inhibitors are considered relatively expensive. For this reason, they are commonly used in tandem with inorganic salts of sodium and potassium, herewith causing synergistic effect (Masalida, 2017). In this paper, we compared effectiveness of the following inorganic and organic reagents and their mixtures as clay swelling inhibitors:

1. Polycel (SPC «Policell») is a complex action organic reagent designed to improve the inhibiting, lubricating and anti-wear properties of process liquids used in drilling and well workover operations. The main active ingredient is ethylene glycol ethers.

2. Potassium chloride is an inorganic clay and shales inhibitor commonly used to drill clay sediments in concentrations from 1 to 10%.

The indicator of wetting ability ( $P_0$ , cm/h) (Uljasheva, 2008; Koshelev, Gvozdt et al., 2015; Sulakshin, Chubik, 2011), is used for the purpose of a scientifically based selection of reagents for inhibiting drilling solution used in drilling of clay sediments (Povzhik, Degtyarev, 2017).

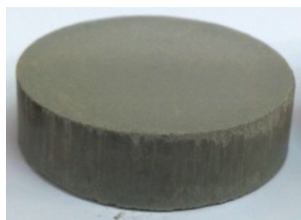
Preparation and the experiments consisted in pressing under pressure of 40.0 MPa dried to a moisture content of 8-10% and crushed to a size of 20-200 microns of a model clay material (Fig. 1), preliminary weighing and aging of compressed tablets in test media for 1 hour followed by measuring the weight of the moistened samples.

PBMV bentonite was used as a model clay material. This material contains at least 70% of the montmorillonite mineral (Grim, 1956), which due to its layered structure gives bentonite strong swelling properties in case of its contact with water. In addition, PBMV bentonite is modified with sodium carbonate. This process replaces the exchange cation in the interlayer space of the clay mineral with sodium, causing further increase in its reactivity (Bortnikov, 2012).

Thus, PBMV bentonite has both high ability to swell, and the constancy of the composition, which allows it to be used as a model for determining reagents inhibiting properties. It should be noted that the use of a single modeled clay material is necessary to eliminate the data unreliability associated with the difference in the compositions and properties of different clays.

The inhibitory effect of a drilling mud largely depends on its rheological properties. The biopolymer system

Fig. 1. Pressed bentonite mud powder sample



characterized by the highest values of conventional and plastic viscosity, static and dynamic shear stress, demonstrates the best effect on stabilizing the clay sample (Saltykov, 2008; Zamulin, 2015; Kister, 1972). In this regard, a structurant xanthan gum (MHF80PLUS Zibo Hailan Chemical Co., Ltd.) was used to simulate the rheological characteristics of the drilling fluid under the experimental conditions (Povzhik, Dobrodeeva, Degtyarev, 2017).

A 0.25% solution of xanthan biopolymer was prepared and treated with inhibitors at concentrations of 1 and 2% for Polyeacol and 2.5 and 5% for KCl, as well as their mixtures. A 0.25% xanthan biopolymer solution without additives was used as a reference solution. Compressed tablets were aged in the test media for 1 hour. All experiments were conducted in three repetitions; Figure 2 shows the averaged experimental results.

According to Figure 2, in solutions with KCl in any of the studied concentrations occurs an increase in the current rate of moistening of the samples by 1.57-1.79 times as compared with the reference solution. The identified strong cracking of the compressed tablet (Fig. 3A, B) may indicate the absence of an inhibitory effect in the experimental conditions.

The increase in the moistening rate during the experiment, i.e. the absorption of water by a clay sample in a solution of an inorganic inhibitor (in this case KCl), is due to the fact that the clay does not contain filtrate in its pores. This makes the inhibitory effect of osmotic pressure impossible, while the adsorption of potassium cations on the clay surface plays a minor role in this experiment. Initially, the clay becomes saturated with liquid with its further swelling, and since the solution is also enriched with cations, then its reactivity increases. As a result, the clay sample hydration rate also increases (Masalida, 2017). It was noted that water absorption

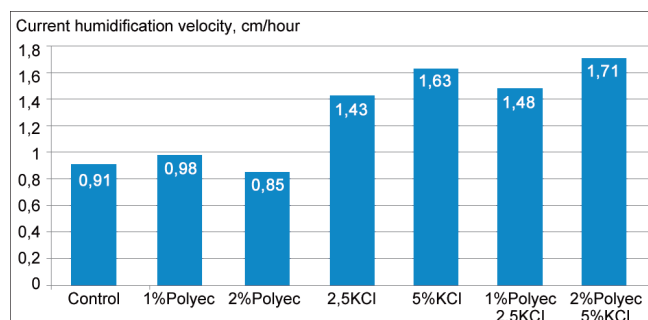


Fig. 2. Current compressed samples moistening rate

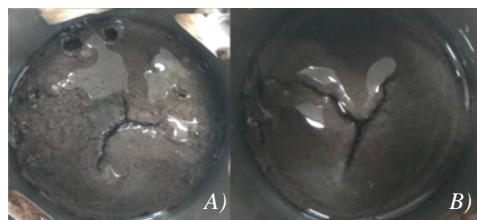


Fig. 3. Pressed samples after 1 hour in a 0.25% solution of xanthan biopolymer with a KCl content of 2.5% (A) and 5% (B)

intensity depends on the concentration of metal cations. When using solutions unsaturated with salts, an increase in the clay sample occurs gradually (in a 2.5% solution of potassium chloride, the sample moistening rate increases 1.57 times as compared with the reference solution), unlike in case of more concentrated solutions (in a 5% solution of potassium chloride sample moistening increases 1.79 times compared with the reference solution).

The best results were obtained in a solution with a Polyeacol content of 2% causing decrease in the sample moistening rate by 6.6% (Fig. 4A, B). After being in Polyeacol solutions, the compressed tablets have small cracks and more friable surface than after being in potassium chloride solutions. The effectiveness of Polyeacol under experimental conditions is explained by the fact that, as a surfactant, it forms stronger hydrogen bonds with the clay mineral thus displacing water from the interlayer space.

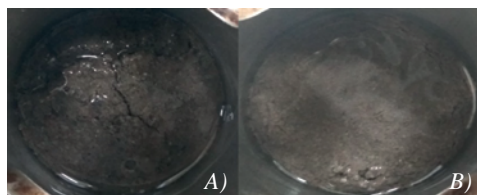


Fig. 4. Pressed samples after 1 hour in a 0.25% solution of xanthan biopolymer with a Polyeacol content of 1% (A) and 2% (B)

## Conclusions

Inorganic inhibitor solutions (in this case, KCl) in contact with a dry clay sample cause its disruption, since the studied clay does not contain filtrate in its pores. The clay is initially saturated with liquid, and the sample is cracked due to the wedging pressure.

A biopolymer base (xanthan gum at a concentration of not less than 0.25%) with Polyeacol organic inhibitor (concentration of 1.5-2%) is well suited to stabilize clay sediments. Under the experimental conditions, there is no synergistic effect from the use of inorganic and organic inhibitors.

These studies allow us to determine the direction of further studies on creating an inhibiting drilling mud formulation for drilling oversalt sediments of the Pripyat trough.

## References

- Bileckij M.T., Kasenov A.K., Sushko S.M. (2013). The practice of inhibiting drilling muds application for the purpose of preventing geological aggravations while penetrating bulging clays. *Vestnik Kazanskogo nacional'nogo tekhnicheskogo universiteta imeni K.I. Satpaeva* [Bulletin of the Satpayev Kazakh National Technical University], 3(97), pp. 16-22. (In Russ.)
- Bortnikov S.V. (2012). Activation of alkaline-earth bentonite by sodium carbonate. *Al'manah sovremennoy nauki i obrazovaniya* [Almanac of modern science and education], 2(57), pp. 61-63. (In Russ.)
- Egorova E.V. (2010). Razrabotka ingibiruyushchego burovogo rastvora dlya bureniya v glinistykh otlozheniyakh [Development of inhibitory drilling mud for drilling in clay sediments]. *Avtoref. dis. kand. tehn. nauk* [Abstract Cand. tech. sci. diss.]. Astrahan, 194 p. (In Russ.)
- Grim R.E. (1956). Clay mineralogy. Moscow: Foreign Literature Publ., 457 p. (In Russ.)
- Kister Je.G. (1972). Chemical treatment of drilling muds. Moscow: Nedra Publ., 392 p.
- Koshelev V.N., Gvozdz' M.S., Rastegaev B.A., Ul'shin V.A., Fatkullin T.G. (2015). The choice of a solution for drilling up clay rocks. *Burenie i nef't' = Drilling and oil*, 9, pp. 27-32. (In Russ.)
- Masalida I.V. (2017). Study of the inhibiting properties of organic and inorganic reagents in polymer-clay drilling mud. *Problemy geologii i osvoeniya nedr: trudy XXI Mezhd. simpoziuma im. ak. M.A. Usova* [Problems of geology and subsoil development: Proc. XXI Int. Symp. named after ac. M.A. Usov]. Tomsk: TPU publ., v.2, pp. 506-508. (In Russ.)
- Povzhik P.P., Dobrodeyeva I.V., Degtyarev F.V. (2017). The study of physico-chemical properties of clay-containing samples with the aim of selecting reagents-inhibitors of clay hydration. *Oborudovaniye i tekhnologii dlya neftegazovogo kompleksa = Equipment and technologies for oil and gas complex*, 4, pp. 21-24. (In Russ.)
- Povzhik P.P., Degtyarev F.V. (2017). Laboratory testing of clays inhibitors and selecting of the optimal reagent for troubleproof drilling of supra-salt part of the Pripyat trough. *Oborudovaniye i tekhnologii dlya neftegazovogo kompleksa = Equipment and technologies for oil and gas complex*, 6, pp. 4-8. (In Russ.)
- Saltykov V.V. (2008). The theory and practice of opening high clay terrigenous reservoirs for oil and gas with biopolymer solutions. *Avtoref. dis. dokt. tehn. nauk* [Abstract Dr. tech. sci. diss.]. Tyumen, 43 p. (In Russ.)
- Sereda N.G., Solov'ev E.M. (1974). Drilling of oil and gas wells. Moscow: Nedra Publ., 455 p. (In Russ.)
- Sulakshin S.S., Chubik P.S. (2011). The destruction of rocks during exploration. Tomsk: TPU publ., 367 p. (In Russ.)
- Uljasheva N.M. (2008). Tekhnologiya burovyykh zhidkostey [Technology of drilling muds]. Uhta: UGTU, 164 p. (In Russ.)
- Zamulin P.V. (2015) Types of drilling muds. The development of polymer-containing drilling muds, their features and advantages over the other solutions. *Sovremennye problemy gidrogeologii, inzhenernoj geologii i gidrogeojekologii Evrazii: materialy Vserossijskoj konferencii* [Modern problems of hydrogeology, engineering geology and hydrogeoecology of Eurasia: Proc. All-Russian Conf.]. Tomsk: TPU publ., pp. 591-596. (In Russ.)

## About the Author

**Filipp V. Degtjarjov** – PhD student, Engineer, Drilling Fluids Service  
Production association “Belorusneft” BelNIPIneft  
15b, Knizhnaya st., Gomel, 246003, Republic of Belarus

Manuscript received 10 July 2018;

Accepted 17 October 2018;

Published 30 November 2018



## SHORT COMMUNICATION

DOI: <https://doi.org/10.18599/grs.2018.4.359-364>

## Gas removal efficiency from a well

A.A. Isaev\*, R.Sh. Takhautdinov, V.I. Malykhin, A.A. Sharifullin  
Sheshmaoil Management Company LLC, Almet'yevsk, Russian Federation

**Abstract.** The set of equipment for evacuation of wells by pumping gas out from the annulus of the well was developed to study the effect of gas on the characteristics of pumps, increase the pump's feed rate, to reduce gas ingress into the pump and reduce wear of rod screw pumps. The influence of vacuum and pressure increase in the annulus on the dynamic level of the well was studied. The necessity of gas removal from the annular space and bottomhole well zone was substantiated.

**Keywords:** set of equipment for evacuating of wells, cavity pump installation, wear of elastomer

**Recommended citation:** Isaev A.A., Takhautdinov R.Sh., Malykhin V.I., Sharifullin A.A. (2018). Gas removal efficiency from a well. *Georesursy = Georesources*, 20(4), Part 1, pp. 359-364. DOI: <https://doi.org/10.18599/grs.2018.4.359-364>

During the operation of wells, a fluid along with gas comes out of a formation, the fluid gets degassed, consequently the part of the gas enters the pump, and the other part, separated from the fluid, enters the annulus. The liberation of gas proceeds due to the bottomhole pressure depletion when wells are operated under the saturation pressure. Bottomhole pressure depletion leads to an increase in differential pressure and the inflow of oil from the formation into the well. When a well is operated under a reservoir pressure ( $P_r$ ) above the saturation pressure ( $P_{sat}$ ), the gas in the formation will remain in a dissolved state, which facilitates reduction of oil viscosity and increase in mobility of well production within the reservoir (Isaev, 2017).

During oil production, reservoir energy is expended to overcome the hydraulic resistance, adhesive, capillary and other forces. In the reservoir, the fluid flows in capillaries of variable cross-section, the drops of oil or gas surrounded by water get deformed in a narrowing capillary, wherein the radii of curvature of front and rear parts are different, the latter is very wide compared with the tapered front part. In this case, the capillary pressure becomes infinitely large, and this phenomenon is called the Jamin effect. The Jamin effect is the occurrence of additional back pressure in a porous medium due to the fact that the pore channel is a structure of capillaries of variable radii and shapes (Gimatudinov, 1971). The influence of the Jamin effect is widely considered by drillers during completion of producing formations when it is necessary, using the Jamin effect, to take

into account such an indicator as drilling mud spurt loss and its clogging properties; it is important to prevent uncontrolled negative impact on the bottomhole formation zone (Andaeva et al., 2013).

Due to vacuuming, the Jamin effect is reduced. Fig. 1 shows the direct Jamin effect, where in the well 1 with the oil reservoir 2, occurs the release of dissolved gas from oil, wherein the movement of fluids in porous media becomes easier.

Experience with operation of wells in the presence of gas in the annulus of wells shows a degradation of the dynamometer chart completeness, a decrease in the delivery rate and operating efficiency of the pumps, a decrease in flow rates and a dynamic level.

As it has been noted, the creation of a vacuum allows the gas to be removed from the fluid in the annulus. Research has established that during evacuation, the chemical analysis of oil changes: it is determined by measuring the gas factor, the values of which were thus zero; thereby, it is possible to completely abandon the gas anchors, since no gas enters the pump during evacuation. Before evacuation the average gas factor values were 24 m<sup>3</sup>/t. Measurements of free and dissolved gas were performed using the UZGF unit (gas factor measurement unit), developed by employees of the Department for Innovations and Examination of the Sheshmaoil Management Company. The unit is certified, the method for measuring the gas factor has been agreed and approved by Nefteavtomatika JSC.

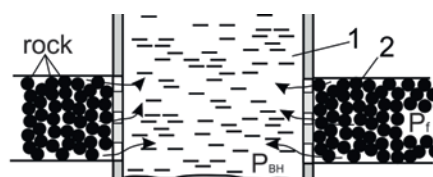


Fig. 1. Gas flow from the oil formation to the well

\*Corresponding author: Anatoly A. Isaev  
E-mail: [isaev@shoil.tatais.ru](mailto:isaev@shoil.tatais.ru)

Due to the operation of a well with intake pressure ( $P_{in}$ ) below the saturation pressure, the elastomer material of the screw pump is saturated with aggressive gases. This caused 44.6% of all the repairs with screw pump units (PCP units) at Sheshmaoil Management Company (Isaev, 2016). The analysis of the PCP units' sucker rod partings showed that during the operation under  $P_{sat} > P_{in}$ , 77% of the rod breaks occurred (Isaev, Arkhipov, 2015). Reducing the dynamic level lower than  $H_{sus} - H_{dyn} < 100$  m. leads to wear of the elastomer, the pump starts to work in conditions of dry friction, thereby not providing the necessary cooling and lubrication of the pump, which leads to overheating of the elastomer, resulting in an elastomer increasing in size and rupturing. Such facts were recorded on 202 implemented PCP units at Sheshmaoil Management Company LLC (66.8% of the total). As can be seen, the operation of the PCP units is strongly influenced by the value of the fluid level above the screw pump and the saturation pressure. Therefore, it is necessary to strive for increase of the level in the annulus, which is made possible by removing the gas from above the fluid level.

Evacuation will eliminate the saturation pressure, because gas in the «reservoir-bottomhole-pump intake» system is absent, especially at low levels of fluids in the well, and the removal of gas from the reservoir, under certain conditions, will allow increasing the mobility of the reservoir production due to the release by the gas of its occupied space.

Various devices are used to reduce the gas pressure in the annulus of wells: wellhead backpressure valves; bypass valves installed on tubing; compressors installed on conventional pumping unit or wellhead fittings (Sevastyanov et al., 2014; Technology of Gas Withdrawal..., 2012; Molchanova, Topolnikov, 2007; Mak-Koi, 2004). Such devices depend on the gas pressure in the annulus and the pressure in the manifold line.

The primary objective was to develop a device that allows to pump the gas out, regardless of the pressure in the annulus, this can be achieved by pumping gas out with a compressor of a certain capacity. The second objective was to pump the gas to a pressure line with a pressure at the outlet of the compressors not lower than the wellhead pressure. The most suitable device for pumping the gas out and pumping it over was a piston compressor. When pumping gas out the compressor allows to create a vacuum, that is, negative pressure. The complex for pumping gas from the annulus of the well and pumping it into the product gathering system (KOGS), shown in Fig. 2 was developed, certified and patented in the Department for Innovations and Examination of the Sheshmaoil Management Company. The technology of creating a vacuum in the annulus of the well, providing a negative pressure of up to



Fig. 2. Set of equipment for gas extraction from wells (KOGS)

0.085 MPa, has been used in 6 fields of Sheshmaoil Management Company. The maximum capacity of the KOGS compressor is 0.95 Nm<sup>3</sup>/min., the maximum operating pressure at the outlet is 2.5 MPa. The KOGS dimensions are small – 4.2 m<sup>2</sup>.

The schematic diagram of the KOGS unit is shown in Fig. 3. A three-stage compressor consists of a 1st stage compressor head, which operates in a single-stage compressor mode with pistons of different diameters, performs a 1st gas compression stage, and a 2nd and 3rd stage compressor head, which is a two-stage compressor with pistons of different diameter which performs 2nd and 3rd compression stages. Both heads and two electric motors are mounted to them on plates welded to the condensate-gathering tank (CGT). The unit is equipped with an external oil tank (EOT) with an oil level sensor (LS1) to monitor the critically low oil level, to visually monitor the oil level in the lubrication systems of the compressor heads. The condensate-gathering tank (CGT) is a steel vessel with convex elliptical bottoms and four holders. A condensate level sensor (LS2) and a condensate drain valve (KR2) are provided to control the level and drain of condensate from the tank (CGT). The heating system, which includes the RIZUR heater, provides cabin heating with the doors closed and at an external temperature below +10°C in addition to the compressor heads, refrigerators (X1, X2). The ventilation system, which includes the VGO2 fan, provides, if necessary, forced ventilation of the unit's cabin.

The KOGS unit is equipped with electrically driven ball valves (K1 and K2), respectively, at the inlet and outlet of the unit, a back pressure valve (OK1) at the outlet of the unit, safety relief valves (KP1, KP2, KP3), respectively, on the compressor stage and its outlet, a back pressure valve (OK2), safety relief valve of KPS type and ball valve (KR5) in the off- gas gathering system, ball valves (KR1 and KR6), respectively, at the inlet and outlet of the unit, gas valves (KR3, KR4) in gas pipelines, for activation bypass line at the beginning of the compressor start-up.

The unit is equipped with pressure gauges (MN1 and MN2) and pressure sensors (PT1 and PT2) to control

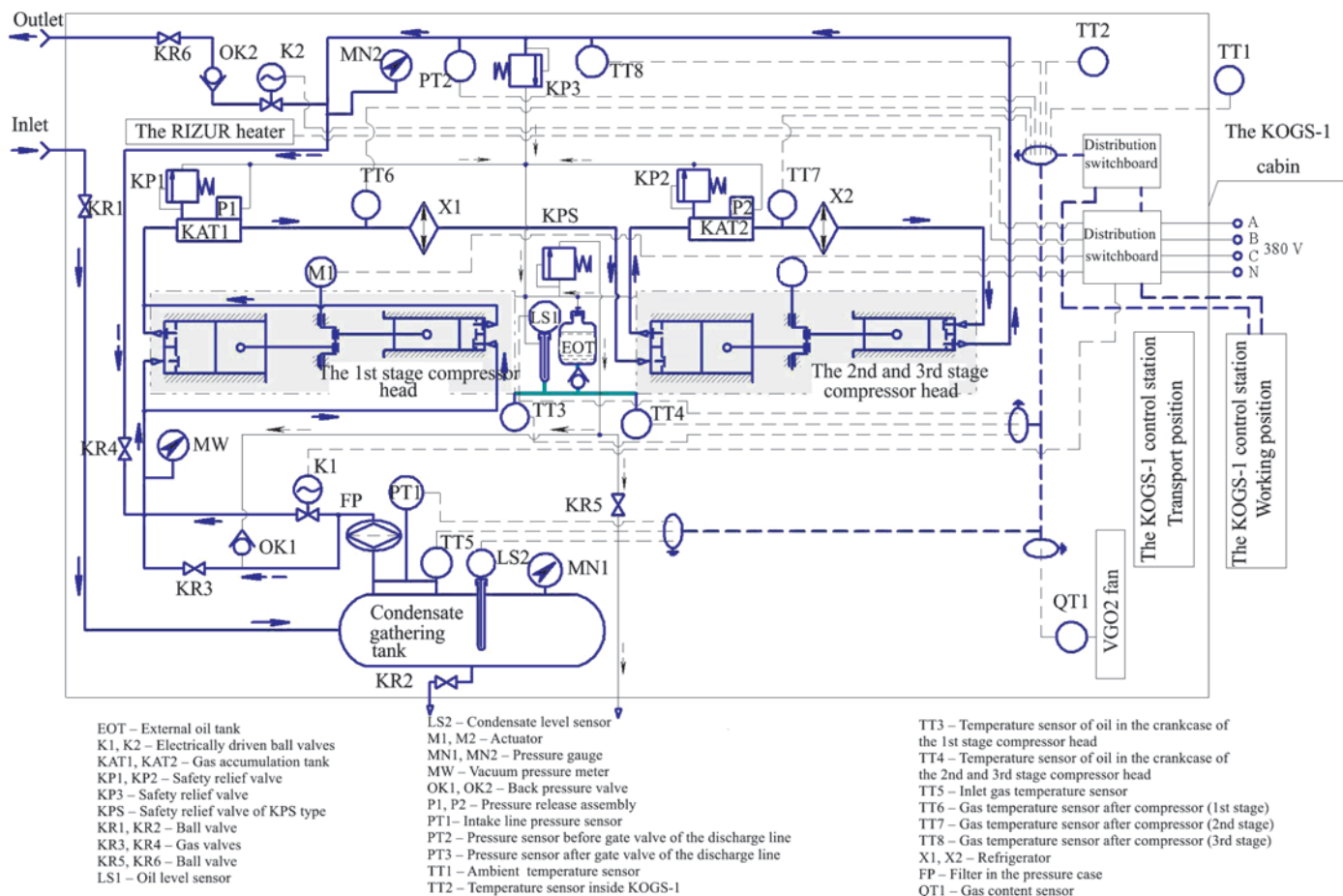


Fig. 3. Schematic diagram of the KOGS unit

the pressure at the inlet and outlet of the unit, a vacuum pressure meter (MW) to control the magnitude of the vacuum at the intake of the unit, temperature sensors (TT1 and TT2) to monitor the temperature outside and inside the unit's cabin, temperature sensors (TT3 and TT4) to monitor the temperature of the oil in the crankcase of the compressor head of the 1st stage, as well as of the 2nd and 3rd stages, temperature sensors (TT5, TT6, TT7 and TT8) to control the inlet gas temperature after the 1st, 2nd and 3rd stages of the compressor, respectively. A gas content sensor (QT1) is installed in the unit's cabin to control the gas content.

The pipelines interconnect the elements of the unit and have an entrance to the annulus of the well and an exit to the production gathering system of a well. A filter is installed in the pressure case (FN) at the outlet of the condensate-gathering tank.

The control station, which is located in the cabin of the unit in the transport position, and in the working position extends to a safe distance, consists of components that allow to carry out safe unit operation in automatic mode.

The KOGS unit works as follows (Fig. 3). The unit is started by simultaneous starting of electric motors of both compressor heads. Gas from the annulus of the well through the unit's entrance enters the condensate-gathering tank (CGT) and, after passing through the filter in the pressure case (FP), enters the cylinders of

the first compression stage, where it is pre-compressed, then via the pipeline and through the refrigerator it enters the second stage, and finally reaches the third stage of compression. The compressed gas is supplied to the product gathering system through the unit's outlet via the pressure line and further through the injection to the line and gas injection control nodes (Fig. 4). KOGS units work 45 minutes on average, then gas is accumulated for 161 minutes.

The use of KOGS increases the production of gas, which is used to heat the oil during its treatment at the oil gathering and treatment facilities. According to the gas meter readings at the DNS-6a and UPSV-567 facilities

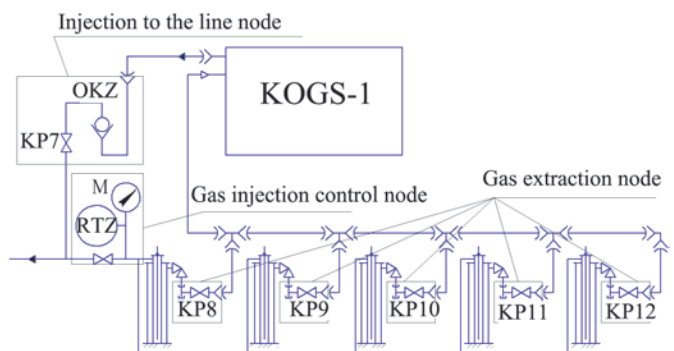


Fig. 4. Layout of a KOGS unit connection in a well cluster: KP7, KP8, KP9, KP10, KP11, KP12 – ball valve, OKZ – check valve, PTZ – pressure sensor, M – pressure gauge



of Sheshmaoil, the volume of additional gas production averages 120 m<sup>3</sup>/day for one KOGS unit. An important advantage of KOGS units is the elimination of emissions of harmful substances (gas) into the atmosphere.

The positive side of KOGS unit application was the reduction of wear of the screw pump's elastomer. Under favorable conditions of wells operation by PCP units ( $P_{\text{sat}} < P_{\text{in}}$ ) the average value of wear degree of the elastomer is 29.5%, i.e. natural wear of the screw pump's elastomer takes place. The degree of wear of the elastomer was determined by the following method: screw pump bench test reports were analyzed before and after the tripping out, then the flow rates at a pressure head of 1000 m have been compared (Isaev, 2018).

The degree of the elastomer wear during the operation of the screw pump up to 21 million rotations and  $P_{\text{sat}} > P_{\text{in}}$  corresponds to the wear degree of the elastomer under favorable conditions. A further increase in the number of rotor rotations in conjunction with the condition  $P_{\text{sat}} > P_{\text{in}}$  leads to even greater wear of the elastomer, thus it is necessary to maintain a dynamic level above the screw pump: one of the solutions is to pump the gas from the annulus of the well (Isaev, 2018). Field experiments with evacuation of annular gas were carried out at 16 wells with the PCP units at the Dachny, Krasnooktyabrsk, Severny and Letny fields (the Republic of Tatarstan). After repair works on these wells and pumps removal, bench tests of screw pumps were carried out to determine the degree of wear of the screw pumps. The wear rate of the elastomer during operation of screw pump with KOGS unit was 24% (Fig. 5), thereby gas evacuation from the annulus of the well allows reduction of pump wear and increases the exploratory work of PCP units (Fig. 6).

The greatest effect of using KOGS units can be achieved under maximum pressure in the annulus ( $P_{\text{an}}$ ) and minimum difference between formation and the bottomhole pressures ( $P_{\text{f}} - P_{\text{BH}}$ ) (Tronov, 2002; Isaev, 2017). According to the efficiency criterion  $K_{\text{eff}}$ , 3/4 of the wells, which are subject to evacuation, have a flow rate above 2 m<sup>3</sup>/day. Regardless of the flow rate, the criterion  $K_{\text{eff}}$  does not exceed 35% (Isaev, 2018).

The introduction of KOGS units on wells leads to an increase in the dynamic level with a subsequent increase in the flow efficiency of the pump and oil production. Wide experience in the effective operation of KOGS, in

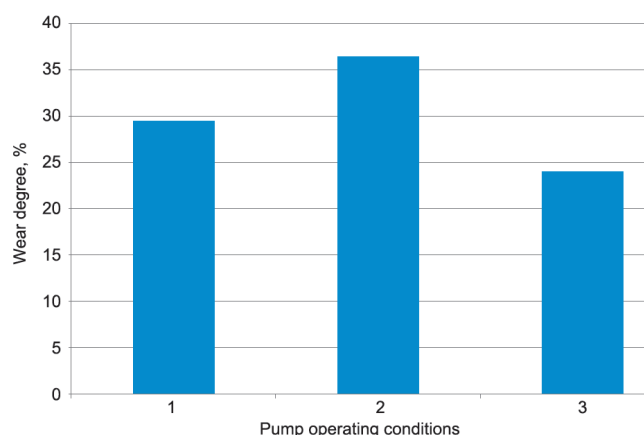


Fig. 5. The wear degree of PCP unit depending on the operating conditions: 1 – favorable, 2 – at  $P_{\text{sat}} > P_{\text{in}}$ , 3 – with use of KOGS

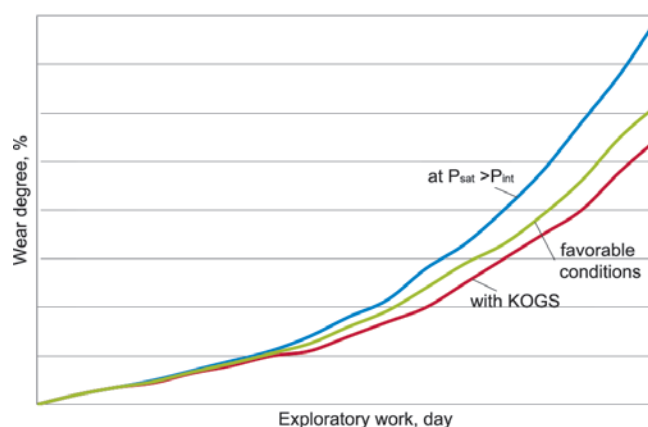


Fig. 6. The dependence of the wear degree on the exploratory work and operating conditions of PCP units

the selection of wells has been accumulated for 8 years of pilot field operation with KOGS units on 424 wells at Sheshmaoil Management Company. The creation of a vacuum can lead to the absence of gas in the pumped-out fluid and its zero metering by the flowmeters, therefore the minimum pressure for starting the KOGS was taken 0.05-0.1 MPa on these wells. A significant increase in oil viscosity was not detected during vacuuming; only 5 wells recorded an increase in viscosity from 120 to 180 MPa·s on average. The increase in completion of a dynamometer chart when evacuating equals 40% on average (Fig. 7).

The following comparative experiment with measurements of dynamic level and unit's flow rate was conducted on wells 9708 and 9302 of the

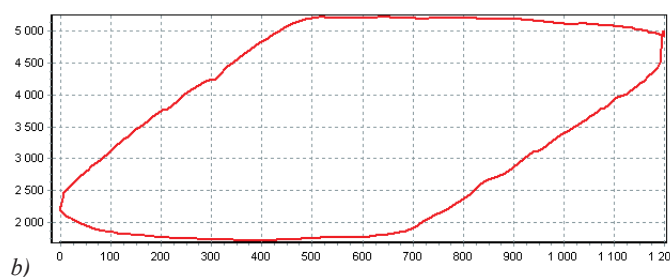
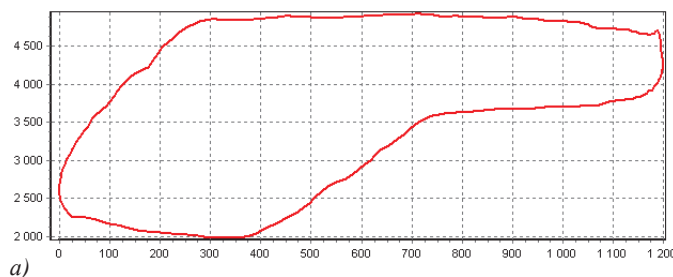


Fig. 7. Dynamometer chart for well no. 3737 before (a) and after (b) evacuation

Krasnooktyabrsky field (Table 1). At first, the annular space was evacuated by the KOGS units in continuous mode with pressure from minus 0.05 MPa to 0 MPa, and in periodic mode. Periodic vacuuming mode includes first creating a vacuum up to minus 0.05 MPa, then opening the casing valve to equalize the pressure in the annulus with the atmospheric one, followed by an increase in pressure to 0.2 MPa. This process was repeated 4 times. The subsequent analysis showed that the increase in the dynamic level during the described periodic pressure in comparison with the constant vacuum is 2.4%, the fluid flow rate increases by an additional 6-7%. It is planned to conduct additional comparative field experiments with constant and periodic evacuation on wells with different physical and chemical properties of production and geological operating conditions.

All KOGS units are equipped with a BS-21-UVS-2 control station, designed for automatic (based on pressure) and local control of the KOGS units. Under the automatic control mode, the station provides operation of the KOGS unit using signals from pressure sensors installed on the intake and discharge lines. Under the local control mode, the unit is turned on and off with control buttons located on the front side of the station. The unit's data is transmitted to the dispatcher's automated workstation (AWS) in real time mode regardless of the the control station's operation mode. In automatic mode, the station provides the ability to start / stop the unit from the dispatcher's automated workplace. The control station provides remote control and change in the basic working conditions of KOGS unit. In addition to the control station, the automation complex for KOGS includes two non-direct-acting electromagnetic flange valves, one check valve, one DTS125L air temperature sensor, one Metran-75

pressure sensor and two Metran-55-Ex pressure sensors. Table 2 shows the technical characteristics of the BS-21-UVS-2 control station.

When KOGS is operated, the power of the electric motors (compressors (12 kW\*h), heater (1.5 kW\*h), air fan (0.3 kW\*h), heating of the suction and pressure hoses (5 kW\*h), electric drive of two valves (0.2 kW\*h)) adds up to 19 kW\*h. In the warm season, the heating and the furnace are turned off. Given the average KOGS load of 31.7%, the energy consumption of electric motors will be 91 kW\*h/day.

During the implementation of KOGS a total of 12,702 tons of oil were additionally produced (Fig. 8). As of 01.09.2018 45 KOGS units are in operation (24 in Sheshmaoil LLC, 17 in Ideloil LLC and Geotech LLC operates 4 units) connected to 194 oil wells. After optimization of all wells, the predicted additional oil production for 2018 is 18,000 tons.

With a discounted payback period of 1.09 years, the profitability index of the discounted costs is 1.35.

### Summary

1. Studies of the well's annular space evacuation revealed an improvement in the condition of oil inflow to the well; an increase in operating efficiency and delivery rate of pump; additional production of petroleum gas and oil; decrease in wear of screw pumps and increase in an exploratory work of PCP units; and the elimination of harmful emissions into the atmosphere.

2. Evacuation allows to reset the gas factor, because gas does not flow into the pump during the evacuation.

3. A set of equipment for evacuation of wells has been developed to create vacuum in the annulus of the well and subsequent gas transfer into the manifold.

	Well number	Operational date of KOGS	Pump-setting depth, m	Perforation interval, m	dyn/ annul before evacuation	dyn with constant vacuum	dyn with periodic vacuum
1	9708	11.08.2017	837	839-842	807/7,4	719	701
2	9302	27.07.2017	970	978-982, 989-994	876/3,3	823	804

Table 1. The main properties of wells no. 9708 and 9302

	Technical properties	Value
1	Common power of the station, V	3 380 ±38
2	Nominal frequency, hz	50±1
3	Station power, no more than, kW	20
4	Capacity, no more than, mm	800 600 250
5	Weight, no more than, kg	40
6	Protection level	IP54

Table 2. Technical properties of the Control Station BS-21-UVS-2

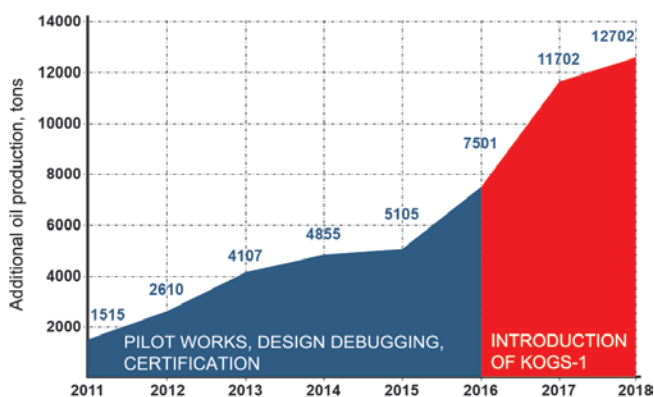


Fig. 8. Additional production from the introduction of KOGS (as of 01.04.2018)

4. Additional oil production during the implementation of KOGS since 2010 amounted to 12,702 tons.

5. The pay-back period of the KOGS introduction on wells is 1.09 years.

### Acknowledgments

*The authors are grateful to the reviewer for valuable critical comments and recommendations which have been very helpful in improving the manuscript.*

### References

- Andaeva E.A., Sidorov L.S., Sidorov Yu.L. (2013). Effekt Zhamena kak faktor uvelicheniya produktivnosti skvazhin [Jamen effect as a factor of wells productivity increase]. *Stroitel'stvo neftyanykh i gazovykh skvazhin na sushe i na more* [Construction of oil and gas wells on land and at sea], 5, pp. 26-30. (In Russ.)
- Gimatudinov Sh.K. (1971). Fizika neftyanogo i gazovogo plasta [Physics of oil and gas reservoir]. 2nd ed. Moscow: Nedra Publ., 312 p. (In Russ.)
- Isaev A.A. (2016). Razrabotka shtangovykh lopatok dlya vintovykh nasosnykh ustanovok pri ekspluatatsii oslozhnennykh skvazhin [Development of rod blades for screw pumping units during operation of complicated wells]. *Diss. kand. tekhn. nauk* [Cand. tech. sci. diss.]. Ufa, 126 p. (In Russ.)
- Isaev A.A., Arkhipov K.I. (2015). Vliyaniye uslovii ekspluatatsii na obryvnost' kolonny nasosnykh shtang [The influence of operating conditions on the breakage of the column of pump rods]. *Uchenye zapiski Al'met'evskogo gosudarstvennogo neftyanogo instituta*, VXIII, 1, pp. 192-196. (In Russ.)
- Isaev A.A., Takhautdinov R.Sh., Malykhin V.I., Sharifullin A.A. (2017). Razrabotka avtomatizirovannogo kompleksa po otboru gaza iz skvazhin [Development of the Automated System for Gas Extraction from Wells]. *Neft'. Gaz. Novatsii* [Oil. Gas. Innovations], 12, pp. 65-72. (In Russ.)
- Mak-Koi Ch. (2004). Rabotayushchii ot balansira stanka-kachalki gazovyi kompressor polezen v razlichnykh promyslovykh operatsiyakh [The gas compressor working from the balance of the pumping unit is useful in various field operations]. *Neftegazovye tekhnologii* [Oil and gas technologies], 3, pp. 44-46. (In Russ.)
- Molchanova V.A., Topol'nikov A.S. (2007). Issledovanie effektivnosti ustroystva dlya otkachki gaza iz zatrubnogo prostranstva [Investigation of the effectiveness of the device for pumping gas from the annulus]. *Neftepromyslovoe delo* [Oilfield business], 10, pp. 27-33. (In Russ.)
- Sevast'yanov A.V., Ivanov A.A., Fatkullin A.S. (2014). Tekhnologiya otvoda gaza iz zatrubnogo prostranstva neftyanykh skvazhin [Technology

of gas removal from oil wells annular area]. *Neftepromyslovoe delo* [Oilfield business], 9, pp. 54-55. (In Russ.)

Technology of Gas Withdrawal from the Annular Space of Producing Wells. (2012). Production and service company Yugson-Service. *Neftegazovaya vertical = Oil and gas vertical*, 6, pp. 12-14. (In Russ.)

Tronov V.P. (2002). Separatsiya gaza i sokrashchenie poter' nefti [Gas separation and reduced oil loss]. Kazan: Fen, 408 p. (In Russ.)

### About the Authors

**Anatoliy A. Isaev** – PhD (Engineering), Leading Engineer of the Department for Innovations and Examination

Sheshmaoil Management company LLC

P.O. 8, box 192, Almet'yevsk, 423458, Russian Federation

Phone: +7 8553 39 39 95, e-mail: isaev@shoil.tatais.ru

**Rustem Sh. Takhautdinov** – General Director

Sheshmaoil Management company LLC

P.O. 8, box 192, Almet'yevsk, 423458, Russian Federation

**Vladimir I. Malykhin** – Chief Specialist for Innovation Activities

Sheshmaoil Management company LLC

P.O. 8, box 192, Almet'yevsk, 423458, Russian Federation

**Almaz A. Sharifullin** – PhD (Engineering), Head of the Department for Innovations and Examination

Sheshmaoil Management company LLC

P.O. 8, box 192, Almet'yevsk, 423458, Russian Federation

*Manuscript received 8 May 2018;*

*Accepted 25 September 2018;*

*Published 30 November 2018*



SCIENTIFIC AND TECHNICAL JOURNAL

# GEORESOURCES

ISSN 1608-5043 (Print)

ISSN 1608-5078 (Online)

V.20. No.4. 2018

Part 2

[www.geors.ru](http://www.geors.ru)

Main topic:

## THERMAL FIELD OF THE EARTH GEOTHERMAL STUDIES



• Heat flow from the Earth interior  
as indicator of deep processes.....366

*B.G. Polyak, M.D. Khutorskoy*

• Postcollisional evolution features of the intracontinental  
structures formed by overthrusting.....377

*O.I. Parphenuk*

GEORESURSY

GEORESOURCES. SCIENTIFIC AND TECHNICAL JOURNAL



# Heat flow from the Earth interior as indicator of deep processes

B.G. Polyak\*, M.D. Khutorskoy

*Geological Institute of the Russian Academy of Sciences, Moscow, Russian Federation*

**Abstract.** The energy aspects of the problem of intraterrestrial heat transfer in various forms are discussed. Endogenous causes of conductive heat flow dispersion – radiogenic heat generation, tectonic movements and magmatism (volcanism), including its latent and open discharge in the form of volcanic and hydrothermal activity are considered. The geological ordering of the heat flow in the continental crust is related to convective discharge of the heat and mass flow from the mantle, marked by the isotopic composition of helium in freely circulating underground fluids. The combined transport of heat and helium, as well as the correlation of He isotopic compositions in volcanic and hydrothermal gases and Sr compositions in young lavas, testify to the silicate nature of the heat and mass flow emanating from the mantle reservoirs of different depths.

**Keywords:** geothermics, heat flow, heat and mass transfer, helium isotopes, magmatism, volcanism

**Recommended citation:** Polyak B.G., Khutorskoy M.D. (2018). Heat flow from the Earth interior as indicator of deep processes. *Georesursy = Georesources*, 20(4), Part 2, pp. 366-376. DOI: <https://doi.org/10.18599/grs.2018.4.366-376>

Thermal field of the Earth among geophysical fields firstly attracted the attention of man. The most violent manifestations of geothermal activity – volcanic eruptions played an important role in the formation of mythological ideas about the structure of the world. Another form of this activity – hot springs since time immemorial have been used for household needs. But as the subject of scientific research the Earth's thermal field also became earlier than all other geophysical fields. Quantitative methods of analysis in geothermics became possible after the invention of the thermometer by Galileo in the early XVII century. Already the first measurements of temperature in mines showed that the temperature in them all year is invariable and that it increases with depth. This peculiarity of the thermal regime in the mines drew the attention of M.V. Lomonosov, who in his treatise “On the free movement of air in the mines noted” (1763-1950) wrote: “...The air in the mines at any time of the whole year retains equal dissolution” (i.e. temperature). The increase in temperature with depth indicated the existence of an upward conductive heat flow (HF), one of the two mechanisms for the removal of intraterrestrial heat.

The value of heat flow density ( $q$ ), according to the fundamental law of J.-B. Fourier, is calculated as the product of the geothermal gradient and thermal conductivity ( $k$ ):  $q = -k(i dT/dx + j dT/dy + k dT/dz)$ .

In real conditions of the existence in the crust of structural and thermophysical inhomogeneities, when the horizontal components of the heat flow are not equal to zero, the deep heat flow will differ somewhat from that measured in vertical wells. This can be taken into account if the configuration of the layers and the thermal conductivity of each of them is known.

But in the overwhelming majority of cases, the approximation of a geothermal gradient only by its vertical component practically does not introduce a noticeable error in the results of observations, since  $dT/dz$  a lot more  $dT/dx$  and  $dT/dy$ . Therefore, without prejudice to the accuracy of the measurements, the HF density is determined by the formula:  $q = -k \cdot grad_z T$  [ $mW/m^2$ ], where  $k$  is the thermal conductivity of rocks, and  $grad_z T = dT/dz$  is the vertical component of the temperature gradient measured in the depth interval opened by the mine workings. Compared with the radius of the planet, this interval is very small, so HF measurements characterize practically its “surface” value at the boundary of the solid Earth –  $q_s$  (more precisely, at the bottom of the heliothermozone, whose temperature is determined by the climatic factor). The current value of this parameter in a particular geographical point reflects the total energy effect of all past and current geological processes and thereby quantitatively limits the range of realistic geotectonic models describing the evolution of the geospheres.

## Tectonic ordering of heat flow

The measured  $q_s$  value may differ from its value in the depth because of near-surface factors disturbing the geothermal field. These factors, as is well known, include

\*Corresponding author: Boris G. Polyak  
E-mail: [polyak@ginras.ru](mailto:polyak@ginras.ru)

© 2018 The Authors. Published by Georesurs LLC  
This is an open access article under the CC BY 4.0 license  
(<https://creativecommons.org/licenses/by/4.0/>)

topography of the Earth surface, the morphology of bodies with different thermal conductivity that form the geological section, the circulation of underground fluids violating the conditions of conductive heat transfer, non-stationary processes of sedimentation and erosion, as well as climatogenic temperature variations introducing geologically short-term perturbations. The data needed to quantify the effects of all these factors are rarely known in their entirety and with sufficient accuracy. But by averaging the results of particular determinations of  $q_s$  within a large homogeneous geoblock (tectonic province), the local opposite-in-sign effects of each the factors that disturb the distribution of conductive heat flow are mutually compensated to some extent. Therefore, regional average (background) estimates  $q_s$  approach the undistorted (depth) value of HF.

Analysis of such average values of  $q_s$  showed that in the continental crust, the HF decreases with age ( $t$ ) of its folding (consolidation) or subsequent tectono-magmatic activation (Polyak, Smirnov, 1966, 1968; Hamza, Verma, 1969). This dependence was repeatedly tested (Sclater, Francheteau, 1970; Čermak, 1976; Kutas et al., 1976; Vitorello, Pollack, 1980; Sclater et al., 1981; and others), having received the name in English-language literature “heat flow – age dependence” (Fig. 1). The time of its manifestation in continental structures covers the Riphean-Phanerozoic stage of their history. But the relationship between heat flow and the age of the oceanic crust is no less real (Sclater, Francheteau, 1970; Smirnov, 1980).

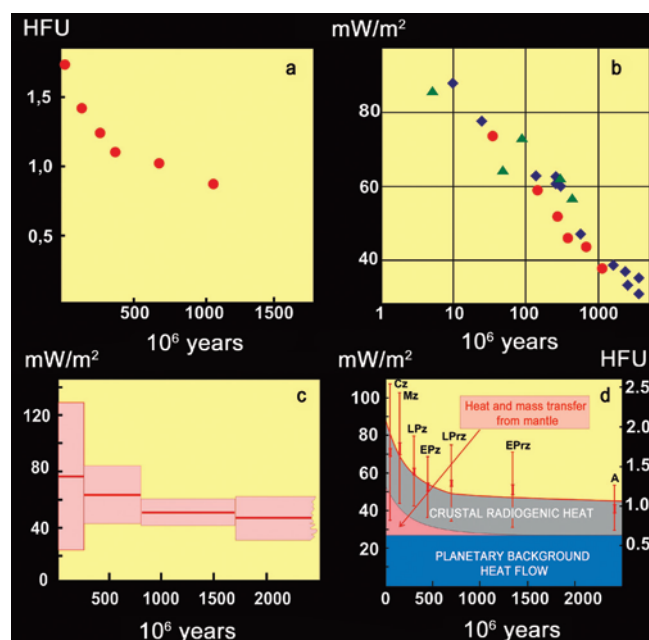


Fig. 1. Relationship of the density of the “surface” heat flow with the age of tectonic-magmatic activity in the continental crust. (a) – (Polyak, Smirnov, 1968), (b) – circles according to (a), rhombuses after (Kutas et al., 1976), triangles after (Čermak et al., 1976), (c) – after (Sclater et al., 1981), (d) – after (Vitorello, Pollack, 1980). 1 HFU is the unit of heat flow,  $1 \cdot 10^6$  cal/cm<sup>2</sup>·s

With the accumulation of data, the general trend in the change of HF in the continental crust was obscured by the dispersion of the particular values of  $q_s$  and the imperfection (convention) of their geochronological reference. However, the existence of a general trend was also supported by another grouping of private estimates of  $q_s$  – by the absolute age of the rocks in the areas of observation (Fig. 1c). In such samples, with a decrease in the spread of the  $q_s$  estimates, their average value, i.e. background HF value decreases as well. As a result, the reality of the relationship between  $q_s$  and  $t$  was confirmed by all later studies, including those using much more empirical  $q_s$  values – 10337 (Pollack et al., 1993) and 19775 (Vieira, Hamza, 2011).

On the continents, the “ $q$ - $t$ ” relationship manifests itself only when analyzing background average  $q_s$  estimates in large geoblocks, indicating the existence of temporary and relatively local heat sources in the depths. However, this relationship only shows how HF is distributed over the surface of the globe but does not explain why it is so distributed. It allows identification of deep heat sources only from the physical side, namely, traditional for geophysics by solving inverse problems, i.e. by selecting the parameters of the source that correspond to the rate of change  $q_s$  – its shape, size, depth, thermal power and time of existence (Kutas, Gordienko, 1972; Smirnov, 1972). The geological nature of the sources remained unknown. They were a priori identified with asthenospheric diapirs, and their energy effect was symbolized by a non-stationary member (Fig. 1d).

The density of the background conductive heat flow observed in the drilled depth interval is the result of a superposition of different endogenous factors, the absolute and relative effects of which are not identical at different hypsometric levels (on the surface of the crust, the Moho section, the lithosphere, etc.) and change over time. They are discussed in the next section.

## Endogenic causes for the heat flow dispersion

### Radioactive heat generation in the lithosphere.

Almost simultaneously with the identification of the “ $q$ - $t$ ” dependence, another connection was found – between the “surface” values of the density of conductive heat flow ( $q_s$ ) and radiogenic heat generation, RHG ( $A_s$ ). The latter parameter reflects the cumulative effect of the decay of long-lived radioactive isotopes of uranium, thorium and potassium in the outcropping and/or drilled rocks. In the energy balance of the Earth, RHG is one of the sources of deep heat, weakening with time, because the half-life of <sup>235</sup>U is  $0.704 \cdot 10^9$  years, <sup>238</sup>U is  $4.468 \cdot 10^9$  years, which is slightly less than the age of the Earth, and <sup>232</sup>Th is  $14.05 \cdot 10^9$  years (Tolstikhin, Kramers, 2008).



The extrapolation of the values of  $A_s$  into the deeper horizons of the crust led to estimates of heat loss at its upper boundary, which exceed the observed values. But the accumulation of empirical material has revealed a decrease in RHG along the depth, as well as its regional differences in the form of correlation dependences having the look  $q_s = A_s \cdot D + q_{red}$  (Roy et al., 1968; Sass et al., 1981; etc.) In these dependencies  $D$  characterizes the rate of  $A_s$  descending along the depth (the lower  $D$  is, the faster this speed is), determining the thickness of the layer in which the overwhelming majority of radiogenic heat is released. The  $q_{red}$  parameter is the so-called “reduced heat flow” coming from below to the bottom of this layer (Khutorskoy, Polyak, 2016; etc.).

When analyzing these dependencies, the negative correlation “ $A_s$ - $t$ ” similar to “ $q$ - $t$ ” relationship, where  $t$  notes the geological age of tectono-magmatic activity (TMA), was observed. The “ $A_s$ - $t$ ” connection became to be considered as a reflection of the regional scale of erosion of the continental crust after its consolidation (stabilization), which removes its upper parts richest with radioelements from the geological section of this geoblock. Although the geothermal effect of this phenomenon is qualitatively indisputable, implying a decrease in  $q_s$ , its quantitative estimates are contradictory. Thus, according to the results of a study of 28 regions of different continents, the  $A_s$  value decreases with increasing age of the last tectonic thermal event (the last phase of TMA), as shown in Fig. 2.

This was attributed to the influence of erosion of the crust, which reduces the geothermal effect of RHG over 1600 million years by half. But the removal of material from the surface into sedimentary basins occurs much faster. With an average erosion rate of 0.5 mm/year, the 10-kilometer layer of the Earth crust will erode over 20 million years, so that the effect of erosion in the Paleozoic and more ancient folded belts in estimating the share of radiogenic heat generation in the structure of HF can be ignored. In addition, erosion of the continental crust can create not only negative anomalies of the background HF, but also positive ones due to the

shortening of the distance between the supposed source of heat and the heliothermozone bottom.

But RHG is capable of determining local positive anomalies of HF. A striking example is the enriched uranium Hercynian granite plutons of the Cornwall peninsula in southwestern England (Table). In them, the density of the ascending conductive heat flow is 104-128 mW/m<sup>2</sup> (Gregory, Durrance, 1987), which is much higher than the average for the UK 55 mW/m<sup>2</sup> (Wheildon et al., 1980).

Cornwall batholiths	Number of HF measurements	Average value of $q$ and average $\pm$ , mW/m <sup>2</sup>	Heat generation, $\mu$ W/m <sup>3</sup>
Carnmenellis	10	115 $\pm$ 7	4,0 $\pm$ 0,5
Bodmin	5	116 $\pm$ 5	4,2 $\pm$ 0,9
Lands End	3	125 $\pm$ 3	5,1 $\pm$ 0,2
Saint Austell	2	126 $\pm$ 0,5	4,2 $\pm$ 0,9
Dartmoor	6	113 $\pm$ 9	5,3 $\pm$ 0,5

Table. Heat flow and heat generation in Cornwall batholiths (Gregory, Durrance, 1987)

In general, despite the long-term study and the undoubted geothermal significance of RHG in rocks, it cannot explain the trend of decreasing background conductive heat flow established in the Phanerozoic folded regions of the continental crust.

### Tectonic movements

After the discovery of the  $q$ - $t$  bond, some geologists assumed that the cause of the increase in heat flow in tectonically mobile belts as compared with stable areas of the crust is its frictional heating during tectonic movements. At the same time, the root causes of these movements themselves and their role in the planetary energy balance were not discussed. But in themselves, tectonic movements need an external source of energy, representing the movement of mountain masses, during which the heat accumulated in them is also transferred.

In young mobile belts, vertical motions create geothermal anomalies of a different signs. Positive anomalies can occur, not counting those caused by friction in the narrow contact zones of the displaced blocks, at relatively rapid erosion of uplifting arrays heated more strongly than their surroundings. Negative anomalies are formed during descending movements, accompanied by the accumulation of sediments and their heating up to temperatures corresponding to the geothermal background at the depth of their subsidence. Subhorizontal movements, which provoke the formation of thrusts in collision situations, also create negative thermal anomalies due to shielding of the deep heat flow by subducting slabs. Tectonogenic geothermal anomalies (except for local frictiogenic) are much longer-lived than those caused by near-surface “distorting” factors. According to (Khutorskoy, 1996), the decrease of  $q_s$  in

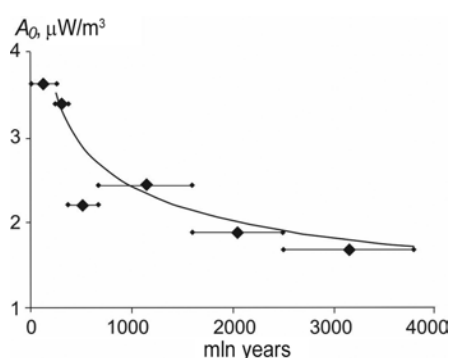


Fig. 2. Radiogenic heat generation ( $A_0$ ) on the surface of the continental crust (Vitarello, Pollack, 1980)

the Pliocene-Quaternary foredeeps and intermontane depressions, downwarping at  $\sim 1$  mm/year, is felt for the first tens of millions of years, while the negative thermal anomalies arising from the thrusting of large plates of the lithosphere in linear folded belts (Ural, Appalachians, etc.), do not have time to fully relax even for hundreds of millions of years (Fig. 3).

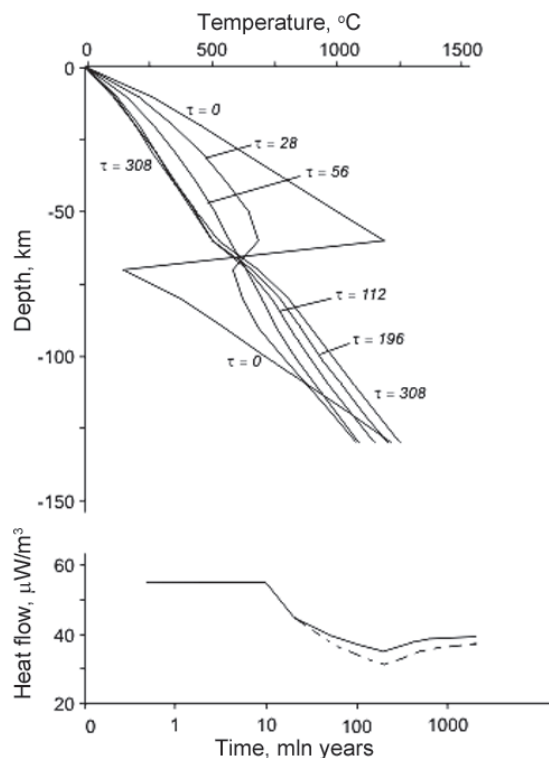


Fig. 3. The change of the geothermal field in the conditions of thrust under the boundary conditions of the second kind at the lower boundary (Khutorskoy, 1996). Above – temperature change after the formation of a thrust in time  $\tau$ ; below – the change in heat flow in time, taking into account (solid line) and excluding (dashed line) heat release at phase transitions

**Magmatism.** This phenomenon is related to the second transport mechanism of deep heat – heat and mass transfer, which, unlike thermal conductivity, consists in the transfer of heat when the heat carrier moves. It is implemented mainly in the convective currents of the mantle. In the crust it accompanies intrusions of deep melts and ascending tectonic movements. As follows from geological observations, in almost any block of the continental crust, tectono-magmatic activity (TMA) was manifested repeatedly. The multistage nature of magmatic activity in a specific geoblock indicates the sequential manifestation of several deep-seated heat impulses in geoblock, each of which influenced the geothermal field. The age of one or another phase of magmatism reflects only the time of the impulse, but does not characterize its power. It is unclear to what extent this power is reflected by the exposure of intrusive bodies – manifestations of latent discharge of deep melts in a given geological epoch, and all the more volumes

of volcanics – traces of open discharge of such melts on the surface of the crust, effaced by subsequent erosion. However, multi-temporal and/or multi-scale mantle pulses responsible for individual phases of magmatic activity in different regions of one tectonic province created different HF values in these regions in the upper horizons of the geological section, i.e. the variance of the private values of  $q_s$ . Accounting for this effect could minimize the dispersion of local values of  $q_s$  attributed to the same stages of geological history and explain their estimates in geoblocks affected by several heat impulses ( $M_1, M_2, \dots$ ) in certain geological epochs ( $t_1, t_2, \dots$ ). The  $q_s$  values should also depend on the morphology and depth of each intrusion and generally reflect the cumulative effect of all consecutive pulses in one area, so quantitative estimates of the geothermal effect of individual pulses are unlikely.

At the same time, the effect of open discharge of the mass flow from the mantle in the form of evacuation of intraterrestrial heat immediately into the atmosphere can be more or less accurately evaluated by mapping the products of volcanism. Such estimates, which differ in different areas, to a certain extent reflect the energy potential of the interior. Considering that “... systems of volcanic areas have a clearly expressed linear structure ... with a length of thousands of kilometers ...” (Luchitskii, 1979, p. 5), for such a comparative analysis it is most objective to use estimates of “linear” productivity of volcanism in  $\text{km}^3/\text{km}\cdot\text{year}$  (or  $\text{t}/\text{km}\cdot\text{year}$ ). In this way, the geoenergetic specifics of various tectonic settings are clearly revealed (Fig. 4).

The same approach to the analysis of the history of individual areas of the region of modern volcanism

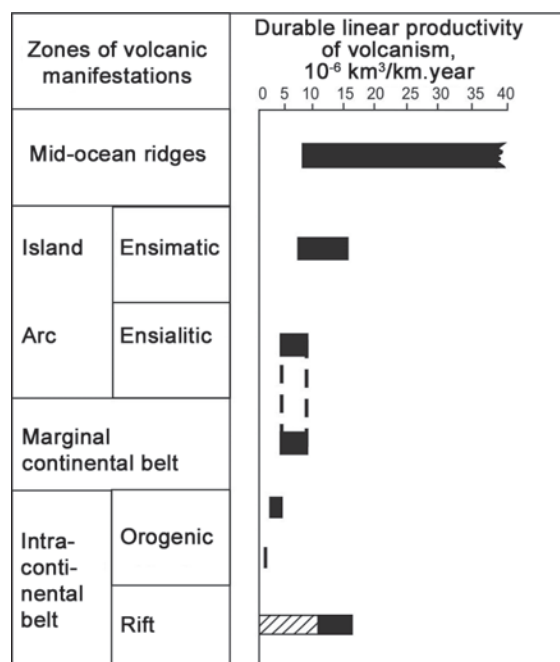


Fig. 4. Linear productivity of volcanism in different tectonic conditions (Polyak, 1988)

allows us to establish both regular variations in the intensity of volcanism over time and its variations along the strike of mobile belts (Fig. 5, 6).

So, Figure 5 shows the inadmissibility of extrapolating data on the productivity of volcanism in a geologically short period (the maximum in Kamchatka during the Holocene) for a much longer period (for example, the Pleistocene period in the same Kamchatka). But the intensity of volcanism is no less variable along the strike of its linear belts in the same stages of their history. For example, in Kamchatka, the total (taking into account the effect in each of the areas of volcanic activity) linear productivity, or thermal power of Quaternary volcanism varies more than three times along the strike of the peninsula. This is clearly seen in Fig. 6. The peak of this power is confined to the segment of the peninsula where the Klyuchevskaya group, the main supplier of volcanism products on the peninsula, is located and practically coincides with the peak of heat outflow by hydrotherms, including the largest Uzon-Geyzernaya hydrothermal system. North of this “high-energy” segment of the peninsula, the maximum frequency of earthquakes in the period 1906-1967 is noted, which indirectly indicates the heterogeneity of the geothermal field along the Kamchatka strike. This segment of the peninsula lies on the strike of the Aleutian arc, and the

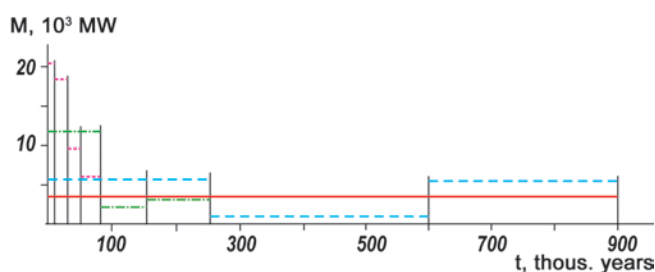


Fig. 5. The thermal power of Kamchatka volcanism in different time-intervals of the Quaternary period (Polyak, Melekestsev, 1979)

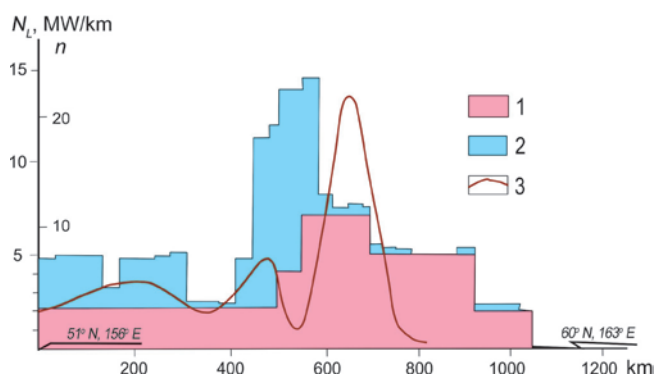


Fig. 6. The distribution of convective loss of the intraterrestrial heat (the effect of open discharge of heat and mass fluids from the depths) along the strike of the Kamchatka peninsula (Polyak, Melekestsev, 1979). 1 – the effect of volcanism, 2 – the effect of discharge of hydrotherms, 3 – the frequency of earthquakes ( $n$ ) in the period 1906-1967 according to (Tokarev, 1970)

oldest segments of the Imperial Range adjoin it, which, in combination, speaks of its geodynamic specificity.

**Hot spots and singularity of HF.** The discovery of a global system of mid-ocean ridges (MOR) gave rise to the concept of plate tectonics. Divergent boundaries of the plates representing most of the spreading zone of the seabed, are distinguished not only by volcanic and hydrothermal activity, but also by the maximum particular values of the density of conductive HF. These values in the axial valleys of MOR (Gulf of California, Red Sea) are much, an order of magnitude or more, higher not only typical of ancient abyssal basins, but also measured in island arcs and marginal mainland mobile belts. The solution of the inverse problem of geothermics in such zones shows that the surface of the fractional melting of the mantle material coincides with the bottom of the oceans. This creates an idea of the singularity of HF in these zones (Lyubimova et al., 1976).

But the values of  $q_s$  are almost as great in the other tectonic settings, for example, in the zones of destruction of the continental crust or in the zones of areal (diffuse) spreading. As shown by field observations (Fig. 7), on

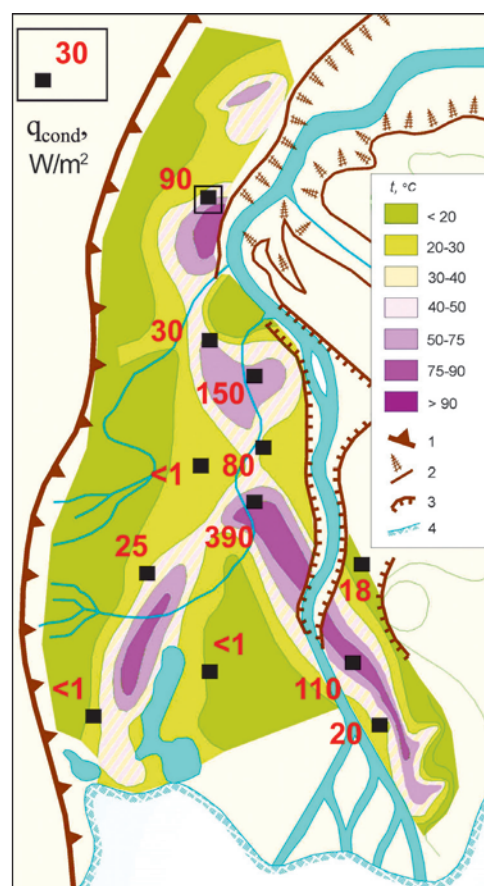


Fig. 7. Temperature variations at a depth of 20 cm and conductive heat flow density ( $W/m^2$ ) on the surface of the Bottom fumarole field in the Lower (northeast) crater of the Mutnovsky volcano (Kamchatka) according to (Muravyev et al., 1983). Measurement points are black squares, the digit beside is the measured  $q_s$  value in  $W/m^2$



land such and even higher  $q_s$  values characterize the sites of high-temperature hydrothermal system discharge and the fumarole fields of active volcanoes, i.e. in the areas where the heliothermozone is pinched out.

Besides the MOR, in the World Ocean there are volcanic ridges of other origin, which are formed when plates move relative to the mantle sites, which are considered to be fixed and called “hot spots” (HS) or “mantle plumes” (MP). The first name does not give an idea of the cause of this phenomenon, since this name is suit for any active volcanic apparatus, around which the deep temperatures gradually decrease. But the latter adequately determines the geodynamic nature of such points (Morgan, 1971) and is therefore preferable. According to modern concepts at such points the melts rise from layer D” on the border of the lower mantle with the outer core (Tolstikhin, Kramers, 2008), forming a chain of volcanic edifices on the ocean floor, as in the Hawaiian-Imperial Ridge – a tectonotype of similar structures (Wilson, 1963; Morgan, 1971).

In the south-eastern end of the Hawaiian Ridge (Fig. 8), volcanoes erupted 5.6-3.8 million years ago (Kauai Island), 3.3-2.2 (Oahu Island), 1.8-1.3 (Molokai Island), <1 – present time (Maui), 0.7 – present time (Hawaii Island). On the southern submerged slope of Hawaii is the currently active volcanic apparatus Loihi Seamount.

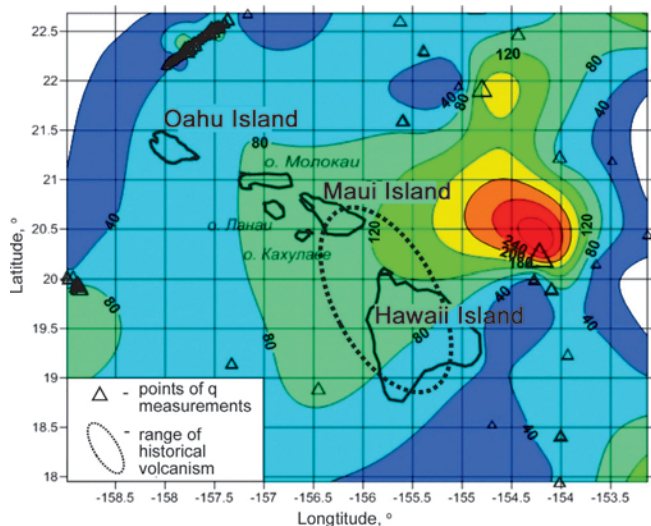


Fig. 8. Density of conductive heat flow and the range of volcanism in historical time in the south-east of the Hawaiian archipelago. Triangles – points of heat flow measurements by (Von Herzen et al., 1989)

In general, the area of recent volcanism extends from Hawaii Island far northwest. It includes not only Haleakala volcano (Maui Island) erupted in 1750, but also underwater volcanoes that erupted in the twentieth century: on the northern slope of Oahu Island (~1906) and in the points with coordinates 21° 39'N – 158° 51'W and (outside Fig. 8) 23° 35'N – 163° 50'W (Gushchenko, 1979).

The connection of mantle plumes with positive anomalies of the heat flow is ambiguous. In the southwest of the Hawaiian Ridge, this connection seems obvious, although in this case the maxima of the HF values are shifted to the northeast relative to the position of active volcanoes (Fig. 8). The latter, however, seems to be the result not so much of a real discrepancy between the material and geothermal traces of the mantle plume discharge, but rather conventional character of HF mapping at limited number and uneven distribution of measurement stations in this part of the Pacific Ocean. But in other places (Yellowstone, Afar) such a relationship is not expressed (probably due to the large influence of various factors distorting the heat flow in the continental crust).

The formation of the seabed as a result of the mantle material discharge is manifested not only in the MOR (axial spreading), but also in almost all back-arc basins, or marginal seas (diffuse spreading). As a rule, these zones are also characterized by an abnormally high heat flow. The geothermal anomaly is most pronounced and well studied in the Tyrrhenian basin (Della Vedova et al., 1984). In different parts of this basin the geodynamic situation is not the same: its western part is characterized by compressive stresses, from Tortonian time up to now whereas the eastern part over the same 11 million years is stretching (Khutorskoy et al., 1986). This eastern part of the Tyrrhenian Sea is a region of high heat flow, large horizontal temperature gradients and submarine basalt volcanism (Fig. 9).

The maximum HF values 515 and 490 mW/m<sup>2</sup> were measured in the rear part of the Aeolian island arc, whereas in this part of Tirrenian Sea the mean HF value is equal 155 mW/m<sup>2</sup>. The thickness of the “thermal” lithosphere in the eastern part of the Tyrrhenian Sea was estimated as 17-23 km (Khutorskoy et al., 1986).

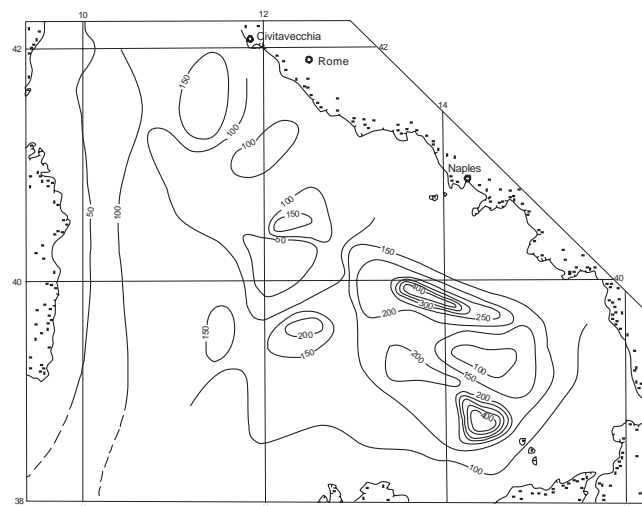


Fig. 9. Map of heat flow in the bottom of the Tyrrhenian Sea. The value of isolines is mW/m<sup>2</sup> (according to data (Della Vedova et al., 1984) with the addition of authors)

The same estimations of the “thermal” lithosphere were obtained in the MOR vicinities.

The high heat flow, basaltic volcanism and low thickness of the lithosphere of the Tyrrhenian basin indicate the introduction of mantle material, which “wedged out” the previously existing blocks. These blocks apparently had a reduced viscosity due to the increase in temperature at their sole and, as a result, did weakly resist the intrusion of the substance. Thus, high heat flow marks areas of ascending advection of mantle material.

Another vivid example of the penetration of mantle material into the upper horizons of the crust is the area of destruction of the continental crust in the north of the Svalbard Plate. In this part of the Barents Sea, the object of our research was the Orly trough (or Støre trough) extending from the archipelago of King Charles in the south to the beginning of the continental slope of the Nansen basin in the north (Fig. 10). The trough is a hollow of meridional strike  $\sim 50$  km wide and almost 200 km long. The height of its sides is up to 400 m, and the bottom lies at depths of 470-520 m and even deeper on the continental slope. In the trough and on its continuation within the continental slope, 28 measurements of heat flow density were carried out from the R/V “Akademik Nikolai Strakhov”. Their results were to be unexpected: the HF values ranged from 300 to 520 mW/m<sup>2</sup> (Khutorskoy et al., 2009). Such values are almost 10 times higher than the level of background heat flow through the bottom of the Barents Sea and are similar to the observed in the axial zones of MOR.

An abnormally high heat flow is observed in the whole Orly trough and in its continuation on the continental slope up to the isobath 1200 m (Fig. 10). Extrapolation of temperatures to the lower half-space shows that subsolidus temperatures can be met at a depth of 6.5-7.0 km below the sea floor in the trough (Fig. 11).

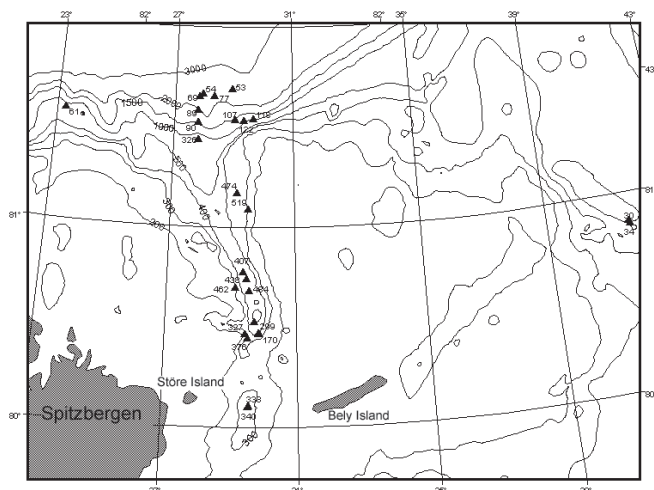


Fig. 10. Heat flow in the Orly (Støre) trough. Values of heat flow are in mW/m<sup>2</sup>. The isobaths were carried out 100, 200, 400, 500, 1000, 2000 and 3000 m

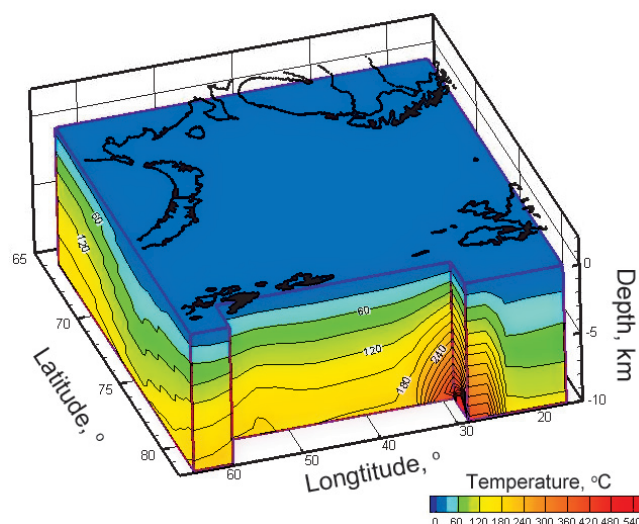


Fig. 11. 3D geothermal model of the Earth's crust of the Barents Sea, view from the north (Khutorskoy et al., 2009)

This suggests the destruction of the continental crust over its entire thickness and the penetration of the hot (mantle?) substance into the basement and, possibly, into the lower layers of the sedimentary cover. At the same time the material signs of discharge of the deep heat and mass flow on the bottom do not found.

The morphology of the trough and especially the geothermal data obtained there for the first time show that this structure has a tectonic nature. Most likely, this is a rift, which has cut the Earth's crust to its full capacity and is now in the active phase of development.

### The material nature of the heat and mass transfer from the depths

So, the conductive heat flow observed in the continental block is formed by a complex superposition of non-stationary processes, different in nature, localization, scale and rate of manifestation.

How realistic is the view explaining the  $q$ - $t$  dependence in the continental crust on the relation between the distribution of the density of conductive heat flow on the continents and the invasion of the asthenosphere diapirs into the lithosphere? Although this view was justified by the fact of volcanic (open) discharge of deep melts in tectonically mobile belts with a conductive HF increased relative to the continental background, it remained quite natural, but an assumption. This hypothesis could be proved only by the detection of direct material (substantial) signs of the presence of mantle derivatives in such zones of high geothermal activity. However, attempts to detect these signs, i.e. juvenile, according to E. Suess (1831-1914), components in the elemental composition of igneous rocks, volcanic emanations, or groundwater were unsuccessful, since the entire set of chemical elements is present both in the mantle and in the crust. The problem was solved only with the help of isotopic studies.

An unequivocal geochemical sign of the presence of juvenile substance in crustal objects turned out to be the isotopic composition of helium in freely circulating underground fluids, since this composition is different in different geospheres due to the presence of genetically different components in terrestrial helium. One of them is radiogenic He, formed in the Earth due to the decay of U and Th; in this helium the ratio between the concentrations of light and heavy isotopes,  $^3\text{He}/^4\text{He} = R_{\text{rad}} \sim (2 \pm 1) \times 10^{-8}$ . The other component arose during the formation of the Universe, is generated by thermonuclear reactions in the depths of the stars and therefore is present in the “solar wind”, which irradiated protoplanetary matter during the formation of the Solar System. It is such a helium, in which the  $R_{\text{SOLAR}} = \sim 1 \times 10^{-4}$  was captured by the Earth during its accretion (Tolstikhin, Kramers, 2008).

As it turned out, traces of solar helium (about 10% of its initial quantity due to constant dissipation into near-Earth space) are still preserved in the Earth's mantle and are present even in today's atmosphere, where  $R_{\text{ATM}} \approx 1.4 \times 10^{-6}$  (Mamyrin, Tolstikhin, 1981) with a very low concentration of He ( $5.24 \times 10^{-4} \%$  vol.). But since  $R_{\text{ATM}} \approx 100 R_{\text{RAD}}$  ( $R_{\text{RAD}}$  is often referred to as  $R_{\text{CRUST}}$ ), the contamination of crustal gases with air helium exaggerates the estimate of R. But the “superatmospheric” values of R in terrestrial gases (and rocks) clearly indicate the presence of solar helium in such objects, which today on Earth could be preserved only in the mantle.

At the present stage of the evolution of the Earth, the maximum values of R in free underground fluids are observed in the products of volcanism both on land and in the World Ocean. In the mid ocean ridges system the R values almost the same in the bottom basalts and submarine hydrotherms (“smokers”), averaging  $^3\text{He}/^4\text{He} = (1.15 \pm 0.1) \times 10^{-5}$  (Marty, Tolstikhin, 1998). This value was taken as the global characteristic for the reservoir of MORB (mid oceanic ridge basalts). But in the areas of mantle plumes (Afar, Yellowstone, etc.) the magnitude of this ratio is even greater, so  $R_{\text{MP=HS}} > R_{\text{MORB}}$ . It reaches its maximum in Iceland. In its north-western peninsula in the gases of one of the thermal springs, the value  $R_{\text{MP}} = 3.45 \times 10^{-5}$  was measured in 1973 (Kononov, Polyak, 1977). Later, in the gases of a neighboring source, an even higher  $R_{\text{MP}}$  value  $> 4.2 \times 10^{-5}$  was measured (Hilton et al., 1998), and also similar ( $3.36 \times 10^{-5}$ ) in the basalts of Iceland (Condomines et al., 1983).

The discovery of traces of solar helium on Earth (Mamyrin et al., 1969; Clarke et al., 1969) occurred almost synchronously with the discovery of the pattern of distribution of conductive heat flow in the continental crust. The obvious importance of this discovery stimulated the rapid development of

regional isotope-helium researches. As a result, it turned out that the distribution of the  $^3\text{He}/^4\text{He}$  ratios in the free underground fluids of the continents showed the same tectonic ordering as the distribution of the background conductive heat flow (Polyak et al., 1979a). This analogy is observed both in regional and pan-regional scales. Europe is one of the largest areal manifestations of the conjugate variability of both parameters (Fig. 12).

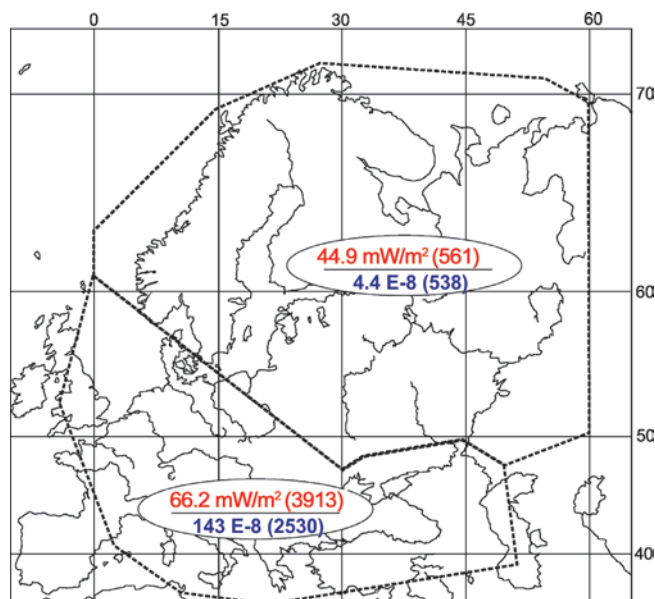


Fig. 12. Average values of conductive heat flow density ( $q$ , mW/m², numerator) and helium isotope composition in underground fluids ( $^3\text{He}/^4\text{He}$ , E-8, denominator) in the “pre-Riphean” and “Phanerozoic” parts of Europe. In brackets – the number of measurements in polygons, limited by a dotted line. The average R values in these samples differ by 30 times, whereas the average  $q$  values are differ only one and a half times

The linear manifestation of the  $^3\text{He}/^4\text{He}$  and  $q$  bond in the Andes mountain chain is just as clear (Fig. 13).

The relationship of the isotopic composition of helium in underground fluids and the background conductive heat flow in the continental crust indicates a common cause of their variations, i.e. intake of deep heat and juvenile substance marked with mantle helium into the crust. Some researchers postulate the possibility of an autonomous flow of volatile from the depths that is not supported by magmatism. However, the carrier of mantle helium is of a different nature, which was revealed by related investigations of the isotopic compositions of He and Sr in the products of volcanic and hydrothermal activity. The investigations showed that there is a close correlation between the values of the  $^3\text{He}/^4\text{He}$  ratios in the gases of the areas of active volcanism and  $^{87}\text{Sr}/^{86}\text{Sr}$  in its solid products. It was discovered after determining the isotopic composition of helium in the gases of volcanoes and hydrotherms in



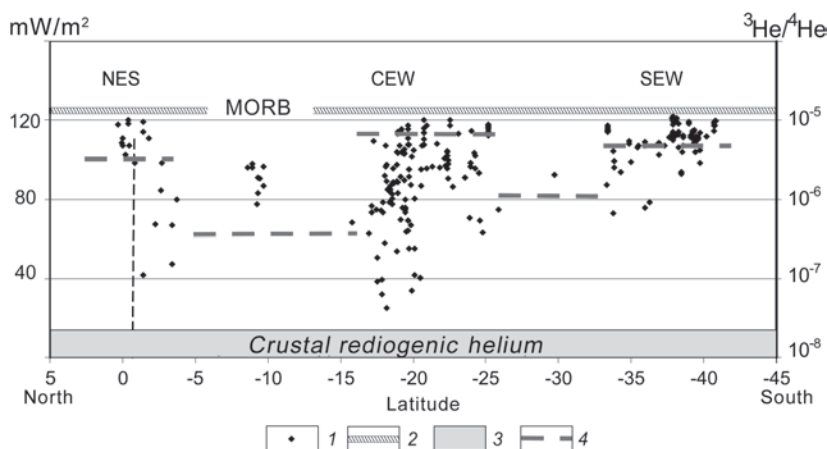


Fig. 13. Relationship between regional conductive heat flow ( $q$ ) and the composition of helium in gases of volcanoes and hydrotherms in the Andean belt by (Newell et al., 2015; Hamza, Muños, 1994). NVZ, CVZ and SVZ are Northern, Central and Southern volcanic zones. 1 –  $^3\text{He}/^4\text{He}$  measurements in the gases of volcanoes and hydrotherms, 2 – He isotopic composition in the MORB reservoir, 3 – the same, in the ancient continental crust, 4 –  $q$  ( $\text{mW}/\text{m}^2$ )

the Apennine peninsula and Sicily Island and comparing it with the composition of strontium in  $\text{N}_2$ -Q volcanites, which are common in the same areas. The participation of the mantle and crustal components is evident in the compositions of both elements (Fig. 14). The proportion

of mantle strontium decreases to the north along the Apennine peninsula and is consistent with an increase in  $\text{K}_2\text{O}$  content in volcanic rocks, thus characterizing the specificity of the Pliocene-Quaternary igneous reservoirs in Italy (Polyak et al., 1979b).

This relationship of He and Sr isotopic compositions in geothermal activity products was confirmed once more in Italy (Parello et al., 2000), and found out in the island arcs of Indonesia (Hilton, Craig, 1989) and other parts of the world. It clearly indicates the transfer of volatile He and Sr into the crust from the mantle by a common carrier agent constituting a silicate substance.

Thus, the “surface” density of conductive heat flow,  $q_s$ , and the isotopic composition of helium in geological objects,  $^3\text{He}/^4\text{He}$ , respectively, characterize both sides of the heat and mass transfer process in the geological environment – its energy (geothermal) and material (geochemical) aspects. These parameters, as two sides of the same coin, are related by the most important common feature: internally caused variability in time. Therefore, a joint analysis of  $q$  and  $^3\text{He}/^4\text{He}$  plays a key role in solving the problems of the evolution of the Earth.

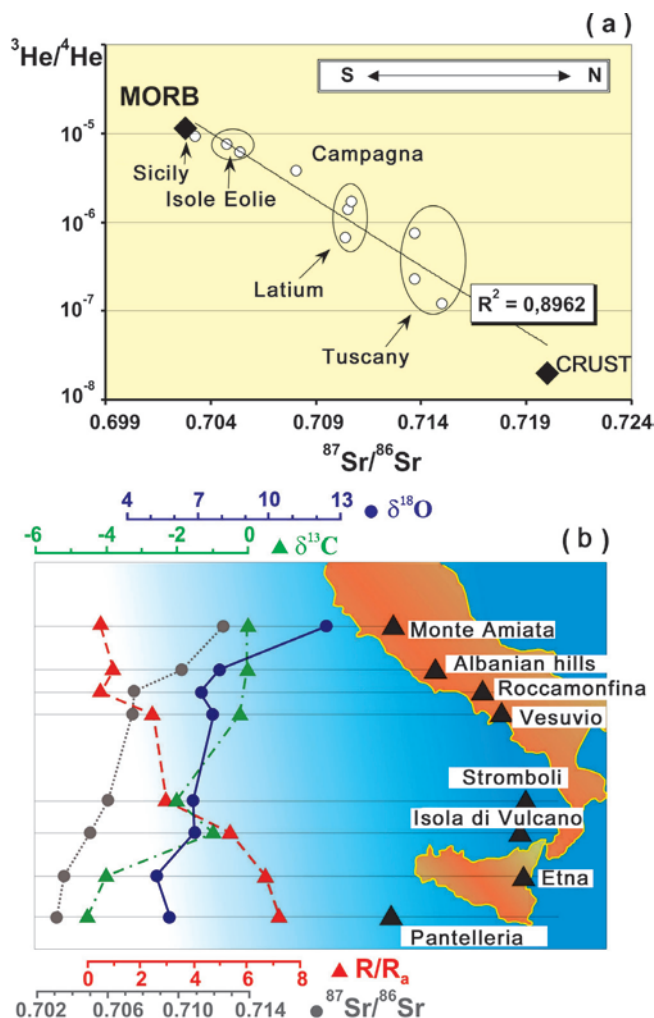


Fig. 14 Relationship of He and Sr isotopic compositions in geothermal activity products in Italy: (a) according to (Polyak et al., 1979b), (b) according to (Parello et al., 2000)

## Acknowledgements

The work was carried out as part of the State Budget Theme No. 0135-2015-0021 with the financial support of the Programs of the Presidium of the Russian Academy of Sciences No. 47 and 49.

## References

- Čermak V. (1976). Heat flow investigation in Czechoslovakia. In: “Geoelectric and Geothermal Studies” (KAPG Geophys. Monogr., A. Adam, ed.). Akad. Kiado. Budapest, 414-424.
- Clarke W.B., Beg M.F., Craig H. (1969). Excess  $^3\text{He}$  in the sea: evidence for terrestrial primordial helium. *Earth Planet. Sci. Lett.*, 6(3), pp. 213-220. [https://doi.org/10.1016/0012-821X\(69\)90093-4](https://doi.org/10.1016/0012-821X(69)90093-4)
- Condomines M., Grönvold K., Hooker P.J. et al. (1983). Helium, oxygen, strontium and neodymium isotope relationships in Icelandic volcanics. *Earth Planet. Sci. Lett.*, 166, pp. 125-136. [https://doi.org/10.1016/0012-821X\(83\)90131-0](https://doi.org/10.1016/0012-821X(83)90131-0)

- Della Vedova B., Pollis G., Foucher I.P., Rehault J.P. (1984). Geothermal structure of the Tyrrhenian. *Sea. Marine Geol.*, 55, pp. 271-289. [https://doi.org/10.1016/0025-3227\(84\)90072-0](https://doi.org/10.1016/0025-3227(84)90072-0)
- Gregory R.G., Durrance E.M. (1987). Helium, radon and hydrothermal circulation associated with the Carmenwallis radiothermal granite of southwest England. *Journ Geophys. Res.*, 92, B12, pp. 12567-12586. <https://doi.org/10.1029/JB092iB12p12567>
- Gushchenko I.I. (1979). Izverzheniya vulkanov mira (katalog) [Eruptions of the world volcanoes (catalog)]. Moscow: Nauka, 475 p. (In Russ.)
- Hamza V.M., Muños M. (1996). Heat flow map of South America. *Geothermics*, 25(6), pp. 599-646. [https://doi.org/10.1016/S0375-6505\(96\)00025-9](https://doi.org/10.1016/S0375-6505(96)00025-9)
- Hamza V.M., Verma R.K. (1969). The relationship of heat flow with the age of basement rocks. *Bull. Volcanol.*, 33(1), pp. 123-152. <https://doi.org/10.1007/BF02596713>
- Hilton D.R., Craig H. (1998). A helium isotope transect along the Indonesian archipelago. *Nature*, 342, pp. 906-908. <https://doi.org/10.1038/342906a0>
- Khutorskoy M.D. (1996). Geotermiya Tsentral'no-Aziatskogo skladchatogo poyasa [Geothermy of the Central Asian fold belt]. Moscow: RUDN Publ., 289 p. (In Russ.)
- Khutorskoy M.D., Gorodnitsky A.M., Gol'mshtok A.Ya. et al. (1986). Teplovoy potok, bazal'tovyi vulkanizm i stroenie litosfery Tirrenskogo moraya [Heat flow, basalt volcanism and the structure of the lithosphere of the Tyrrhenian Sea]. *Geotektonika = Geotectonics*, 5, pp. 116-123. (In Russ.)
- Khutorskoy M.D., Leonov Yu.G., Ermakov A.V., Akhmedzyanov V.R. (2009). Anomal'nyi teplovoy potok i priroda zhelobov v severnoi chasti Sval'bardskoi plity [Abnormal heat flow and nature of gutters in the northern part of the Svalbard Plate]. *Doklady RAN = Proceedings of the Russian Academy of Sciences*, 424(2), pp. 227-233. (In Russ.)
- Khutorskoy M.D., Polyak B.G. (2016). Rol' radiogennoi teplogeneratsii v formirovanii poverkhnostnogo teplovogo potoka [The role of radiogenic heat generation in the formation of surface heat flow]. *Geotektonika = Geotectonics*, 2, pp. 43-61 (In Russ.)
- Kononov V.I., Polyak B.G. (1977). Geotermal'naya aktivnost'. Islandiya i sredinno-okeanicheskii khrebet (glubinnoe stroenie, seismichnost', geotermiya) [Geothermal activity. Iceland and mid-oceanic ridge (deep structure, seismicity, geothermy)]. Moscow: Nauka, pp. 7-82. (In Russ.)
- Kutas R.I., Gordienko V.V. (1972). Teplovoe pole Karpat i nekotorye voprosy geotermii [Thermal field of the Carpathians and some issues of geothermy]. *Tr. MOIP. Otd. geol.*, 46, pp. 75-80. (In Russ.)
- Lomonosov M.V. (1950). O vol'nom dvizhenii vozdukh, v rudnikakh primechennom (Pervye osnovaniya metallurgii ili rudnykh del) [On the free movement of air, in the mines marked (First foundations of metallurgy or ore affairs)]. St.Petersburg: Imperial Academy of Sciences, 1763. *Trudy po fizike i khimii 1738-1746* [Proceedings in physics and chemistry, 1738-1746]. Moscow-Leningrad: USSR Academy of Sciences, pp. 318-319. (In Russ.)
- Luchitskii I.V. (1979). Nekotorye obshchie voprosy global'nykh paleovulkanologicheskikh rekonstruktsii [Some common issues of global paleovulkanological reconstructions]. V kn.: *Global'nye paleovulkanologicheskie rekonstruktsii* [In: Global paleovulkanologic reconstruction]. Novosibirsk: Nauka, pp.4-14. (In Russ.)
- Lyubimova E.A., Nikitina V.N., Tomara G.A. (1976). Teplovyte polya vnutrennikh i okrainnykh morei SSSR (nablyudeniya i teoriya interpretatsii) [Thermal fields of the USSR internal and marginal seas (observations and interpretation theory)]. Moscow: Nauka, 224 p. (In Russ.)
- Mamyrin B.A., Tolstikhin I.N. (1981). Izotopy geliya v prirode [Helium isotopes in nature]. Moscow: Energoizdat, 222 p. (In Russ.)
- Mamyrin B.A., Tolstikhin I.N., Anufriev G.S., Kamenskii I.L. (1969). Anomal'nyi izotopnyi sostav geliya v vulkanicheskikh gazakh [Abnormal isotopic composition of helium in volcanic gases]. *Dokl. AN SSSR* [Report Academy of Sciences of the USSR], V.184, № 5, Pp. 1197-1199.
- Marty B., Tolstikhin I. N. (1998). CO<sub>2</sub> flows from mid-oceanic ridges, arcs and plumes. *Chemical Geology*, 145, pp. 233-248. [https://doi.org/10.1016/S0009-2541\(97\)00145-9](https://doi.org/10.1016/S0009-2541(97)00145-9)
- Morgan W.J. (1971). Convection plumes in the lower mantle. *Nature*, 230, pp. 42-43. <https://doi.org/10.1038/230042a0>
- Muravyev A.V., Polyak B.G., Turkov V.P., Kozlovtsseva S.V. (1983). Povtornaya otsenka teplovoy moshchnosti fumarol'noi deyatel'nosti vulkana Mutnovskogo (Kamchatka) [Re-evaluation of the thermal power of the fumarole activity of the Mutnovsky volcano (Kamchatka)]. *Vulkanologiya i seismologiya = Volcanology and seismology*, 5, pp. 51-63. (In Russ.)
- Newell D.L., Crossey L.Y., Karlstrom K.E., Fisher T.P., Hilton D.R. (2005). Continental-scale links between the mantle and groundwater systems of the western United States: Evidence from travertine springs and regional He isotope data. *GSA Today*, 15(12), pp. 115-157. [https://doi.org/10.1130/1052-5173\(2005\)015\[4:CSLBTM\]2.0.CO;2](https://doi.org/10.1130/1052-5173(2005)015[4:CSLBTM]2.0.CO;2)
- Parello F., Allard P., Alessandro W.F., Jean-Baptiste P., Catani O. (2000). Isotope geochemistry of the Pantelleria volcanic fluids, Sicily Channel rift: a mantle volatile end-member in Southern Europe. *Earth Planet. Sci. Lett.*, 180 (3/4), pp. 325-339. [https://doi.org/10.1016/S0012-821X\(00\)00183-7](https://doi.org/10.1016/S0012-821X(00)00183-7)
- Pollack H.N., Hurter S.J., Johnson J.R. (1993). Heat flow from the Earth interior: analysis of the global data set. *Rev.Geophys.*, 31, pp. 267-280. <https://doi.org/10.1029/93RG01249>
- Polyak B.G. (1988). Teplomassopotok iz mantii v glavnykh strukturakh zemnoi kory [Heat and mass flow from the mantle in the main structures of the Earth's crust]. Moscow: Nauka, 192 p. (In Russ.)
- Polyak B.G., Smirnov Ya.B. (1966). Teplovoy potok na kontinentakh [Heat flow on the continents]. *Doklady AN SSSR = Proceedings of the USSR Academy of Sciences*, 168(1), pp. 170-172. (In Russ.)
- Polyak B.G., Smirnov Ya.B. (1968). Svyaz' glubinnogo teplovogo potoka s tektonicheskim stroeniem kontinentov [The connection of the deep heat flow with the tectonic structure of the continents]. *Geotektonika = Geotectonics*, 4, pp. 3-19. (In Russ.)
- Polyak B.G., Melekestsev I.V. (1979). K otsenke geoenergeticheskogo effekta noveishego vulkanizma ostrovnnykh dug [Evaluation of the geoenery effect of the newest volcanism of island arcs]. *Geotektonika = Geotectonics*, 1, pp. 36-47. (In Russ.)
- Polyak B.G., Tolstikhin I.N., Yakutseni V.P. (1979a). Izotopnyi sostav geliya i teplovoy potok – geokhimicheskii i geofizicheskii aspekty tektonogeneza [The helium isotope composition and heat flow as geochemical and geophysical aspects of tectogenesis]. *Geotektonika = Geotectonics*, 5, pp. 3-23. (In Russ.)
- Polyak B.G., Prasolov E.M., Buachidze G.I. et al. (1979b). Izotopnyi sostav Ne i Ar v termal'nykh flyuidakh Al'piisko-Apenninskogo regiona i ego svyaz' s vulkanizmom [The isotope composition of He and Ar in the thermal fluids of the Alpine-Apennine region and its relationship with volcanism]. *Doklady AN SSSR = Proceedings of the USSR Academy of Sciences*, 247, pp. 1220-1225. (In Russ.)
- Roy R.F., Blackwell D.D., Birch F. (1968). Heat generation of plutonic rocks and continental heat flow provinces. *Earth. Planet. Sci. Lett.*, 5, pp. 1-12. [https://doi.org/10.1016/S0012-821X\(68\)80002-0](https://doi.org/10.1016/S0012-821X(68)80002-0)
- Sass J.H., Blackwell D.D., Chapman D.S., Roy S. (1981). Heat flow of the crust of the United States. Physical properties of rocks and minerals. N.Y.: McGraw-Hill, pp. 503-548.
- Slater J., Francheteau J. (1970). The implication of terrestrial heat flow observations on current tectonics and geochemical models of the crust and upper mantle of the earth. *Geophys. J. Roy. Astr. Soc.*, 20(5), pp. 509-542. <https://doi.org/10.1111/j.1365-246X.1970.tb06089.x>
- Slater J., Parsons B., Jaupart C. (1981). The heat flow through oceanic and continental crust and heat losses from the Earth. *J. Geophys. Res.*, 86, pp. 11535-11552. <https://doi.org/10.1029/JB086iB12p11535>
- Smirnov Ya.B. (1972). Zemnoi teplovoy potok i problemy energetiki geosinklinali [Earth heat flow and energy problems of geosyncline]. *Tr. MOIP. Otd. geol.*, 46, pp. 52-74. (In Russ.)
- Smirnov Ya.B. (1980). Teplovoe pole na territorii SSSR (poyasn. zap. k kartam teplovogo potoka i glubinnnykh temperatur v m-be 1: 10 000 000) [Thermal field on the territory of the USSR (Note to the maps of heat flow and deep temperatures, 1: 10 000 000)]. Moscow: GIN AN SSSR – GUGK SM SSSR, 150 p. (In Russ.)
- Tokarev P.I. (1970). O fokal'nom sloe, seismichnosti i vulkanizme Kurilo-Kamchatskoi zony [On the focal layer, seismicity and volcanism of the Kuril-Kamchatka zone]. *Izv. AN SSSR. Fizika Zemli* [News of the USSR Academy of Sciences. Physics of the Earth], 3, pp. 15-30. (In Russ.)
- Tolstikhin I.N., Kramers J. (2008). The Evolution of Matter from the Big Bang to the Present Day Cambridge University Press. 521 p.
- Vieira F.P., Hamza V.M. (2011). Global heat flow: comparative analysis based on experimental data and theoretical values. *Proc. 12-th Int. Congr. of the Brazilian Geophys. Soc.*, pp. 1-6. <https://doi.org/10.1190/sbgf2011-407>
- Vitarello I., Pollack H. (1980). On the variation of continental heat flow with age and thermal evolution of continents. *J. Geophys. Res.*, 85, pp. 983-995. <https://doi.org/10.1029/JB085iB02p00983>
- Von Herzen R.P., Cordery M.J., Detrick R.S., Fang C. (1989). Heat flow and the thermal origin of hotspot swell: the Hawaiian swell revisited. *J. Geophys. Res.*, 94, pp. 13783-13799. <https://doi.org/10.1029/JB094iB10p13783>
- Wheildon J., Francis M.F., Ellis J.R.L., Thomas-Betts A. (1980). Exploration and interpretation of the SW England geothermal anomaly. *Proceed. 2nd Int. Seminar on Results of EC Geothermal Energy Resources* (A.S. Strub, P.Ungemach, Eds.), Strasbourg, pp. 456-463. [https://doi.org/10.1007/978-94-009-9059-3\\_40](https://doi.org/10.1007/978-94-009-9059-3_40)

**About the Authors**

*Boris G. Polyak* – DSc (Geology and Mineralogy),  
Chief Researcher, Heat and Mass Transfer Laboratory  
Geological Institute of the Russian Academy of  
Sciences  
7, Pyzhevsky lane, Moscow, 119017, Russian  
Federation

*Mikhail D. Khutorskoy* – DSc (Geology and  
Mineralogy), Professor, Head of the Heat and Mass  
Transfer Laboratory  
Geological Institute of the Russian Academy of  
Sciences  
7, Pyzhevsky lane, Moscow, 119017, Russian  
Federation

*Manuscript received 20 July 2018;  
Accepted 16 September 2018;  
Published 30 November 2018*





# Postcollisional evolution features of the intracontinental structures formed by overthrusting

O.I. Parphenuk

Schmidt Institute of Physics of the Earth of the Russian Academy of Sciences, Moscow, Russian Federation

E-mail: [oparfenuk@ifz.ru](mailto:oparfenuk@ifz.ru)

**Abstract.** The investigation of intracontinental collision structures is conducted based on the complex model of the thermal and mechanical evolution of overthrusting process for the rheologically layered lithosphere, which includes brittle upper crust, the lower crust and lithospheric upper mantle with different effective viscosity values. Finite element models with Lagrangian approach were used for the problem simulation. It was shown that thermal evolution of continental orogens essentially results from the geometry and topography due to thrusting and postcollision stage. This work concentrates on the thermal parameters influence on the evolution of collision zones aimed to the study of possibility of granite melt formation. Calculations for mean continental initial temperature distribution lead to the conclusion of possibility of granite melt formation for the case of “wet” granite solidus. The horizon of temperatures higher than “wet” granite solidus appears at the level of 30-40 km, moving upward to the depth 15-20 km at postcollision stage. The early postcollision evolution shows some heat flow increase due to the thickening of the upper crust with maximum heat generation rate. Further history leads to the stable heat flow values because additional loading redistribution resulting from the denudation of surface uplift and corresponding sedimentation is small due to the local erosion in our model. It was shown that surface heat losses after the termination of horizontal shortening depend to a greater extent on radiogenic heat generation rather than thermal conductivity value in the upper crust.

**Keywords:** collision, overthrusting, evolution, heat generation, heat flow value, thermal conductivity, rheology, temperature, solidus

**Recommended citation:** Parphenuk O.I. (2018). Postcollisional evolution features of the intracontinental structures formed by overthrusting. *Georesursy = Georesources*, 20(4), Part 2, pp. 377-385. DOI: <https://doi.org/10.18599/grs.2018.4.377-385>

It is known that vast areas of deeply eroded folded areas of the Earth, for example, ancient shields, are composed mainly (by 70-80%) of granitoids associated with the processes of partial melting and metamorphism in the crust thickened during a collision. Granite-gneiss allochthonous, indicating the tectonic stratification of the continental crust, are described in the Himalayas, the Pamirs, the Caledonides of Norway, Sweden and many other areas (Sokolov, 1999). One of the distinguishing features of the collision areas is the formation of granite melts under partial melting conditions, and in some cases the appearance of a granite layer on the surface as a result of erosion of the mountain uplift. The Early Proterozoic accretion of granite-greenstone and granulite-gneiss terranes joined by collision zones led to the formation of the Siberian craton. On the modern surface of the erosion slice, the collision zones of terranes reflect the level of the middle and lower crust brought to the surface and eroded

at the postcollisional stage when the upper crust, including granitoids, which were melted and intruded into the upper crust, was completely eroded (Rosen, Fedorovskii, 2001).

Early Paleozoic collision systems make it possible to see the granite layer, which appeared at the surface due to the erosion of the mountain uplift and formed the upper crust with a thickness of about 10 km (European variscides). This layer could result from warming up inside the thickened crust during or after the termination of the collision (Gerdes et al., 2000).

## Lapland granulite belt – an example of the early Proterozoic collision orogen

The Baltic shield is the largest projection of the ancient crystalline basement of the East European Platform and is favorable for studying the internal structure of the crystalline crust, since there is no distorting effect of the sedimentary cover. Within the framework of the EGT (European Geotraverse) project, a 500-km POLAR profile was obtained by the method of reflected seismic waves, passing to the north of the Baltic (Fennoscandinavian) shield through several Archean

and Early Proterozoic crustal segments. Figure 1 shows the main tectonic elements of the region with a length of 100×500 km along the POLAR profile: the Lapland part of the Karelian province, the Archean Terranes of Inari and Servaranger, the Early Proterozoic Lapland granulite and Polmak-Pasvik-Pechenga belts. According to modern data, the Lapland granulite belt is a complexly constructed body, pulled in a southwesterly direction to the Karelian province (the northern part of the Karasjok – Kittila greenstone belt) at an angle of 30° (Gaal et al., 1989, Sharov, 1993). Between these tectonic structures there is a relatively narrow tectonic zone – the Tanaelv belt (Tana), bordering the southern and western contacts of the Lapland granulite belt (Perchuk et al., 1999).

Figure 2 gives an idea of the metamorphic zonation along the POLAR profile area and confirms the general tendency of increasing the degree of metamorphism in the direction of thrust and the maximum P-T conditions of metamorphism in the zone of the limiting fault. When crossing the Lapland granulitic belt in the direction of thrust, the equilibrium temperatures increase from 750 to 820°C, and pressures from 6.5 to 7 kbar, showing the metamorphism of higher stages (Gaal et al., 1989).

The rocks of the Lapland granulite belt of the Baltic Shield were pulled in a southwesterly direction to the underlying rocks of the Karelian province, forming the

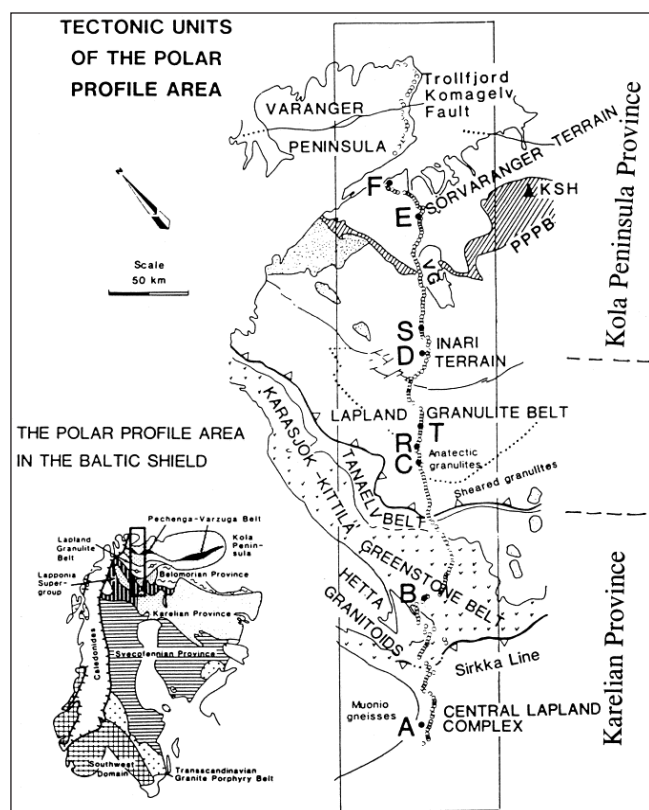


Fig. 1. Tectonic units of the POLAR profile location area (Gaal et al., 1989). Capital Latin letters indicate points of explosions, circles indicate the position of seismographs. PPPB – Polmak-Pasvik-Pechenga belt. SG-3 – the location of the Kola ultra-deep well

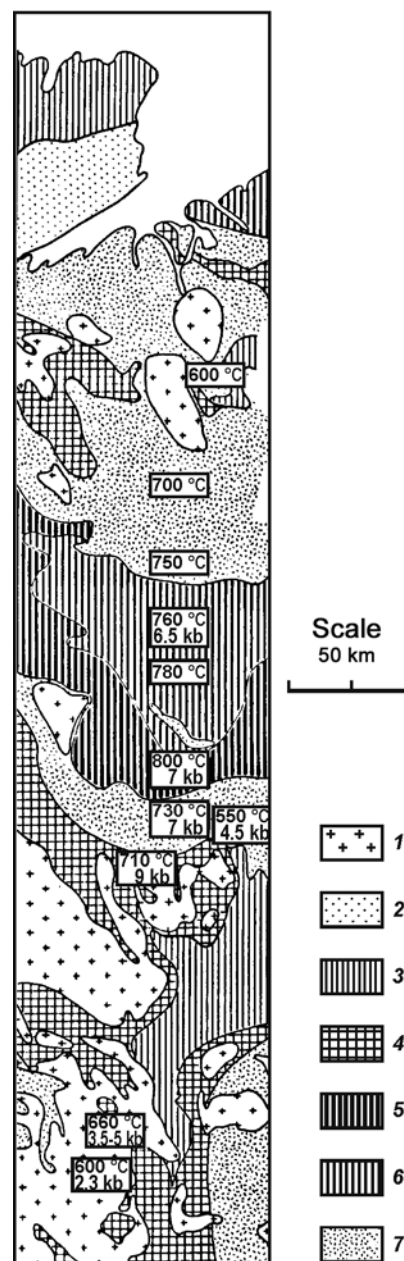


Fig. 2. Metamorphic zonation of the POLAR profile region: 1 – igneous rocks; 2 – very low level; 3 – low level; 4 – medium level; 5 – granulitic facies; 6 – granulitic facies with cordierite; 7 – high stage, migmatites. The numbers in the figure show the P-T estimates of the metamorphism conditions. The position of the region corresponds to Fig. 1 (Tectonophysics, 1989)

tectonic zone of the Tanaelv belt (Tectonophysics, 1989; Barbey et al., 1984). Figure 3 shows a diagram of the crust structure and the isolines of seismic waves velocity. The high-velocity body with seismic velocities of 6.3 to 6.6 km/s in the upper part of the model was created by the Lapland granulite belt, the Tanaelv and Karasjok-Kittila belts. Due to the more extended nature of the thrust, as mentioned above, the anomaly is also more stretched in the horizontal direction and complicated by the processes apparently imposed later. Under the Lapland belt itself, the Moho depth is less than that to

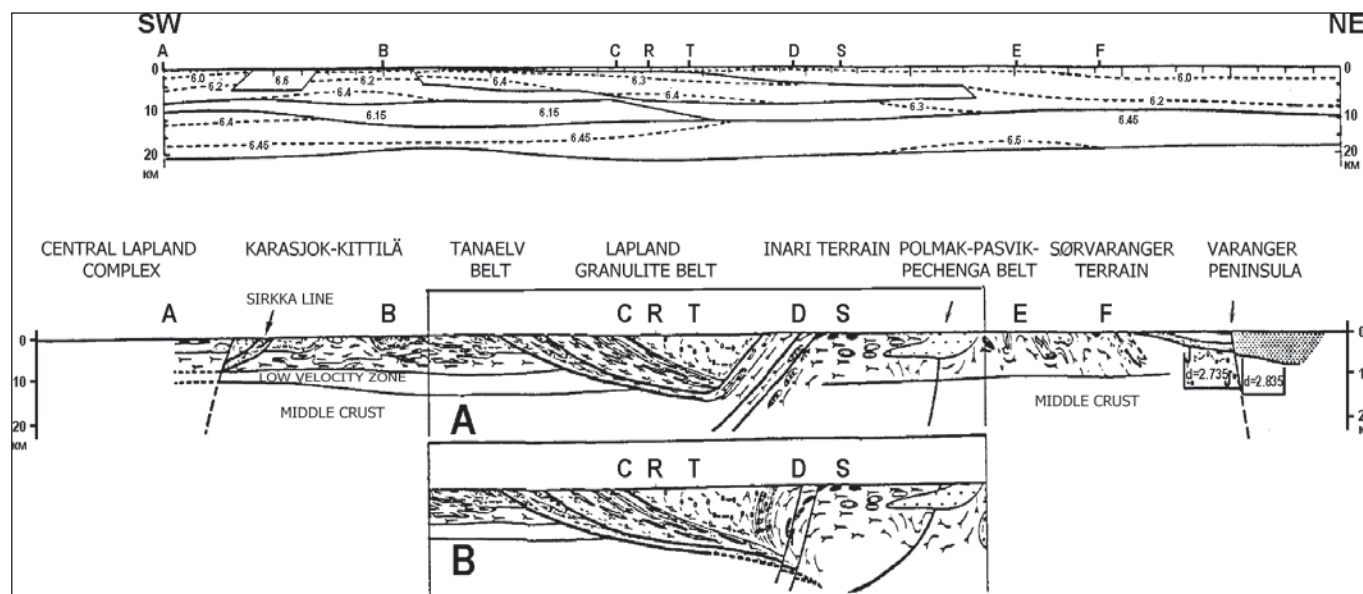


Fig. 3. The upper 20 km of the seismic model and the geological section along the POLAR profile (Gaal et al., 1989). The corresponding designations are shown in Fig. 1

the south and is approximately 40 km with a maximum value of 47 km (Luosto et al., 1989).

This is an example of an ancient intra-collisional structure, in the modern structure of which there is no Moho depression with an increase in the crust thickness in the process of thrusting. There are examples of compressional orogens that have not experienced post-collisional stretching on the lithosphere scale: the roots of the crust are preserved in Appalachians, in the Limpopo belt (South Africa), in some areas of the Grenville front, under the Kapuskasing structural zone (of the Superior province) of Canadian Shield (Mareschal, 1994; Percival, 1990).

### Intracontinental collision model

General features of the structure of the thrust zones in areas of continental collision are the presence of rocks of varying degrees of metamorphism, brought to the surface as a result of erosion and uneven uplift, gravitational and magnetic anomalies, often significant thickening of the crust under the thrust zone and in its vicinity, heterogeneity of the velocity field of seismic waves and complex structural constitution. This is due to the fact that the formation and evolution of the Earth's crust in the vicinity of the fault, along which the thrust and uplift of the upper layer takes place, can in principle be described by one process. During a collision, one continental block advances on another; subsequent uplift and erosion lead to the appearance on the surface of rocks up to the lower crust with an increase in the degree of metamorphism in the direction along the fault surface of the overriding block. The study of collision structures is carried out on the basis of a complex model of thermal and dynamic evolution of the thrust region for the rheologically stratified lithosphere and includes a rigid upper crust,

a lower crust and a lithospheric upper mantle divided into blocks, which differ in effective viscosity values. The problem is solved by the finite-element method using a grid deformed in time (Lagrange method). The horizontal reduction of the crust is accompanied by the thrust along the fracture of the blocks of the upper crust along the inclined zone of disturbances, the appearance of additional stress on the layers lying under this zone, and the erosion of the formed overlying rocks. These processes are compensated by viscous flows at the depths of the lower crust and upper mantle (Parphenuk et al., 1994; Parphenuk, Mareschal, 1998). The advantage of the Lagrange method is the ability to calculate real values of strain rates, values of total and shear stresses and, accordingly, deformation of the Moho boundary, fault zone and surface relief during the redistribution of additional load in the region of thrust during the formation of uplifts and their erosion. The software package for calculating the fields of velocities, stresses and temperatures was developed using the elements of the algorithm presented in the monograph (Reddy, 1984). The modeling of viscous flows at the depths of the lower crust and the lithospheric upper mantle within the framework of the equation of motion and continuity was carried out in the Newtonian rheology approximation for a two-layer incompressible viscous fluid. The problem of the distribution of the velocity field and stress is solved by the finite element method:

$$\begin{cases} \mu_i \nabla^2 \mathbf{u} - \nabla P - \rho_i \mathbf{g} = 0 \\ \nabla \mathbf{u} = 0. \end{cases} \quad (1)$$

Here  $P$  is the pressure,  $\mathbf{u}$  is the velocity vector,  $\rho$  is the density,  $\mu$  is the effective kinematic viscosity ( $\mu = \text{const}$ ),  $\mathbf{g}$  is the acceleration of gravity,  $\nabla$  is the linear differential operator,  $\nabla^2 = \nabla \cdot \nabla$  is the Laplace operator.



Based on the solution of the system of equations (1), calculations are made of the thermal evolution of a region that is deformable in the course of a collision, including the upper crust (with the thrust), enriched with radioactive elements. The energy conservation equation for the case of generalized Lagrangian coordinates is formulated as the heat equation without an inertial term, which is contained in the substantial (full) time derivative:

$$c_i \rho_i \frac{DT}{Dt} = \lambda_i \nabla^2 T + H_i, \quad (2)$$

where  $c$  is the specific heat capacity,  $\rho$  is the density,  $\lambda$  is the coefficient of thermal conductivity,  $H$  is the rate of heat generation. The indices correspond to layers with different thermal properties:  $i = 1$  – the lower crust,  $i = 2$  – the upper mantle,  $i = 3$  – the upper crust. It is assumed that the initial state of the crust and lithosphere is defined as a state of thermal equilibrium at constant surface temperature  $T = 0^\circ\text{C}$  and temperature at the base of the lithosphere  $T = 1160^\circ\text{C}$ . The vertical boundaries are thermally insulated (the heat flow is zero). At the boundaries of layers with different thermophysical properties, the temperature continuity condition is satisfied.

The geometry of the study area, along with the main parameters of the problem and the boundary conditions, is presented in Fig. 4. Calculations of thermal evolution were carried out on a deformed mesh obtained in the process of solving the mechanical problem (1) and completed in the region of the upper crust ( $i = 3$ ). The statement of the problem and the boundary conditions are described in detail in (Parphenuk, Mareschal, 1998; Parphenuk, 2015, 2016).

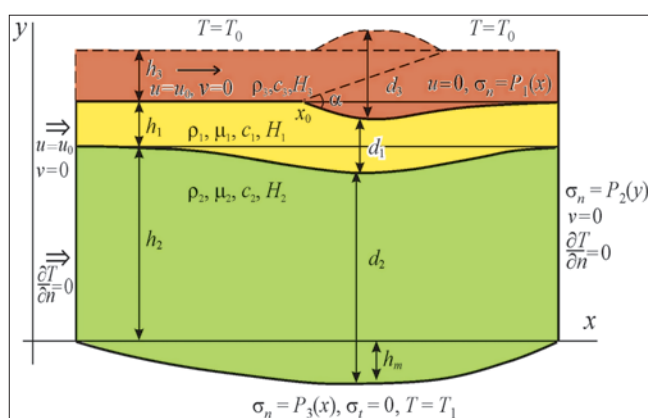


Fig. 4. Geometry of the deformation model for mechanical and thermal problems: the upper crust ( $i = 3$ ) is brown, the lower crust ( $i = 1$ ) is yellow, the lithospheric upper mantle ( $i = 2$ ) is green.  $h_1, h_2, h_3$  are the initial values of the thickness of the lower crust, the upper mantle and the upper crust,  $h_m$  is the deviation of the lower boundary;  $d_1, d_2, d_3$  are the thicknesses of the lower crust, lithospheric mantle and upper crust in the process of deformation,  $u_0$  is the rate of horizontal contraction,  $\alpha$  is the angle of incidence of the fault

### Formation of a collision structure during and after thrusting

The structure of the lithosphere, resulting from the collision thickening of the crust, largely determines the further evolution of the mountain belts that have experienced horizontal compression. As a result of the thrust, the “cold” layer appears under the “hot” layer, and under the effect of an additional load, redistributed during erosion and sedimentation, a gravitationally unstable structure arises. With geologically acceptable strain rates of  $10^{-15}$  to  $10^{-14} \text{ s}^{-1}$  viscous flow at the level of the lower crust and lithospheric upper mantle, the combination of crustal shortening by 70-100 km and additional load during thrust leads to the formation of “roots” of the crust 10-20 km deep 100-200 km. The erosion of the lifted overriding mass brings to the surface plutonic rocks of varying degrees of metamorphism (Parphenuk, 2014). The process of redistributing the load during erosion plays an important role after the end of horizontal compression, preventing the erosion of the formed roots of the crust and the deepening of the upper crust, as it increases the wavelength of the border of the Moho deepening (Parphenuk et al., 1994). The post-collisional stage of evolution is modeled by a change in the boundary conditions after the end of the thrust: in the case of a gravitational instability of the formed structure, the horizontal compression is replaced by stretching and the surface load is redistributed due to ongoing processes of denudation and sedimentation. These processes lead to a reduction of the crustal roots depth (Fig. 5).

The conditions for the formation of crustal roots and the degree of influence of various parameters in the process of advancing plates (the value and contrast of viscosities, the limiting fracture angle, the duration and erosion rate of the uplifts formed) are described in detail in (Parphenuk, 2014; Parphenuk, 2015). In an earlier paper (Parphenuk et al., 1994), estimates were obtained of the possibility of preserving the “roots” of the crust in an environment of gravitational instability of the formed thickening, based on the magnitude of the horizontal extent of the Moho depression. The areas of partial melting, which lead to the formation of collisional granitoids, are largely determined by the geometry and topography of the structures formed in the process of thrust (Jaupart, Provost, 1985).

### Comprehensive analysis of the influence of the thermophysical properties of the Earth's crust on the thermal regime and the dynamics of partial melting zones

In the Earth's crust of recent collisional mountain structures (for example, the Himalayas), there are quasi-steady state melt horizons, marked by geophysical and indirect geological data. They occur at depths of

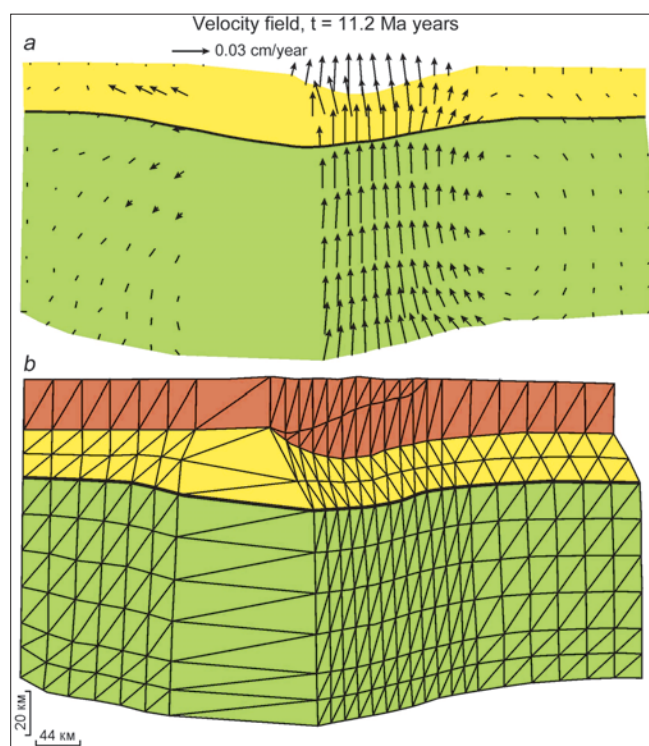


Fig. 5. (a) Distribution of the velocity field of viscous flows in the lower crust and the lithospheric upper mantle at the post-collisional stage (approximately 4 million years after the end of the shortening of 70 km at a rate of 1 cm/year) at an erosion rate of elevated covers of 1 mm/year. The thick line represents the Moho boundary. (b) The geometry of the model, including the upper crust, at the time of completion of the thrust. The effective viscosity is assumed to be  $10^{22}$  Pa·s for the lithospheric upper mantle

10-15 km, have a thickness of about 10 km over a length of 50-250 km, and in physical properties correspond to granite in a state close to the solidus temperature. The possible reason for their appearance is considered to be the melting of the crust substance due to collisional heating during thermal relaxation of the thrust plates (Rosen, Fedorovskii, 2001).

The objective of studying the thermal evolution of collision structures formed by the thrust mechanism is to determine the influence of the values of heat generation and thermal conductivity of the upper crust on the thermal evolution of these areas in connection with the assessment of the possibility of the formation of granite melts. The main source of heating of the continental crust is the heat of decay of long-lived radioactive elements – uranium  $^{235}\text{U}$ ,  $^{238}\text{U}$ , thorium  $^{232}\text{Th}$  and potassium  $^{40}\text{K}$ . The content of these elements is a key parameter for assessing the thermal regime of the continents and the evolution of the mantle substance in the process of crust extraction. Estimates of average concentrations of  $^{235}\text{U}$ ,  $^{238}\text{U}$ ,  $^{232}\text{Th}$  and  $^{40}\text{K}$  differ by almost two times, which leads to average values of the volume heat generation in the range of 0.55-1.31  $\mu\text{W}/\text{m}^3$ . The average surface heat generation for various Archean and Proterozoic geological provinces, obtained by systematic sampling over large areas, yields a spread of

values in an even wider range of 1.01-3.6  $\mu\text{W}/\text{m}^3$  (Jaupart, Mareschal, 2004, 2011).

A detailed study of the distribution of heat flow density and radioactive crust heat generation in provinces of different ages allowed the authors of the work (Jaupart, Mareschal, 2004) to estimate the total heat generation of the Earth's crust: 0.56-0.73  $\mu\text{W}/\text{m}^3$  for the Archean, 0.73-0.90  $\mu\text{W}/\text{m}^3$  for the Proterozoic and 0.95-1.1  $\mu\text{W}/\text{m}^3$  for the Phanerozoic and Paleozoic with a crust thickness of about 40 km. Taking into account the age of the structures and the fact that the lower crust is depleted of radioactive elements, these estimates in the case of the upper crust should be increased assuming the values of the thickness of the upper crust. The influence of the thermophysical parameters of the thrust structure on its evolution is presented for the scenario of crustal shortening with a rate of 0.5 cm/year for 20 million years with erosion and simultaneous sedimentation, which began 5 million years after the onset of thrust. The initial angle of incidence of the fault slipping plane is  $15^\circ$ . The total value of the horizontal shortening is 100 km, the erosion rate is assumed to be 0.5 mm/year, decreasing to 0.25 mm/year at the post-collision stage. Calculations showed that the velocity of thrusting and erosion have a significant effect on the formation of the surface elevation and a weak influence on the topography of the Moho depression – the main cause of the gravitational instability of the thrust structure (Parphenuk, 2015). For thermal calculations, we used the strain history for the effective viscosity of the thickened lower crust of  $10^{22}$  Pa·s and  $10^{23}$  Pa·s of the upper mantle. The main parameters of the calculations are given in Table 1.

This paper discusses options with heat generation 1.5; 2 and 2.5  $\mu\text{W}/\text{m}^3$  in the thickened upper crust (Table 1), which may correspond to the Paleozoic, Proterozoic, and Early Proterozoic settings (when heat generation was ~1.6 times higher than presently). Approximately such values of heat generation are taken in a well-known work (England, Thompson, 1984) for a one-dimensional model of instantaneous thrust.

	Upper crust ( $i = 3$ )	Lower crust ( $i = 1$ )	Upper mantle ( $i = 2$ )
Specific heat capacity ( $c$ , J/kg·K)	$10^3$	$10^3$	$10^3$
Thermal conductivity ( $\lambda$ , W/m·K)	1.5; 2.5; 3.0	3	4
Heat generation rate ( $H$ , $\mu\text{W}/\text{m}^3$ )	1.5; 2.0; 2.5	1.1	0.08
Density ( $\rho$ , kg/m $^3$ )	2750	3000	3300
Effective viscosity ( $\mu$ , Pa·s)	-	$10^{22}$	$10^{23}$
Layer thickness ( $h$ , km)	20	20	80

Table 1. The values of the basic parameters for the mechanical and thermal problems of modeling the evolution of the structure of the intracratonic thrusting (Parphenuk, 2016)

It is assumed that the thermal conductivity of the studied layers of the lithosphere does not depend on pressure and temperature. Analysis of the thermal conductivity of the rocks of the Earth's crust shows that the vast majority of definitions fall in the range of 1.5-3.5 W/m·K except for rocks with a high content of quartz, which have higher values of this parameter (Jaupart, Mareschal, 2011). In addition, most silicate materials are characterized by significant anisotropy, and their thermal conductivity depends on the direction. Increased values of thermal conductivity are measured along the stratification of rocks with values of the anisotropy coefficient in the range 1.1-1.5 (Popov et al., 2008; Jaupart, Mareschal, 2011). In our model calculations, we assume that the thermal conductivities of the three layers and 3 different values for  $\lambda$  of the upper crust are constant (Table 1). A model with an increased thermal conductivity of the upper crust in the direction of the main deformation of the horizontal contraction with anisotropy coefficient 1.2 was also calculated.

Let us consider the influence of two main thermal parameters on the redistribution of deep temperatures and its manifestation in the value of the surface heat flow. Fig. 6 shows a picture of the thermal field for the "normal" value of heat generation at different values of the thermal conductivity coefficient 42 million years after the end of the thrusting.

Calculations with different values of heat generation and thermal conductivity of the upper crust showed the possibility of formation a region of partial melt at depths of 30-40 km at different points in time. For a given set of thermophysical parameters, the maximum temperature range is 590-750°C (from the initial 460°C at a depth of 20 km) and 670-885°C (from the initial 610°C at a depth of 30 km) after a horizontal shortening of 100 km over 20 Ma (Parphenuk, 2016). The further rate of temperature increase during the 42 million years of post-collisional evolution is much smaller, which demonstrates the important role of the initial heating phase during the slow thrust and the formation of a thickened crust. Calculations have shown that with the mid-continental initial temperature, most models provide the possibility of the appearance of a partial melt in conditions of "wet" granite. The zone of excess temperature of the solidus of "wet" granite (Perchuk, 1973) occurs at the level of the lower crust, and after the end of contraction and thrust, the upper boundary of the melting region rises to a depth of 15-20 km. The partial melt zone gradually expands and captures the area in front of the thrust front due to the thickening of the crust and the presence of horizontal heat transfer and covers an area of 150-200 km long at the post-collision stage. The temperature increase can be quite significant (up to 320°C) at a depth of 10-30 km.

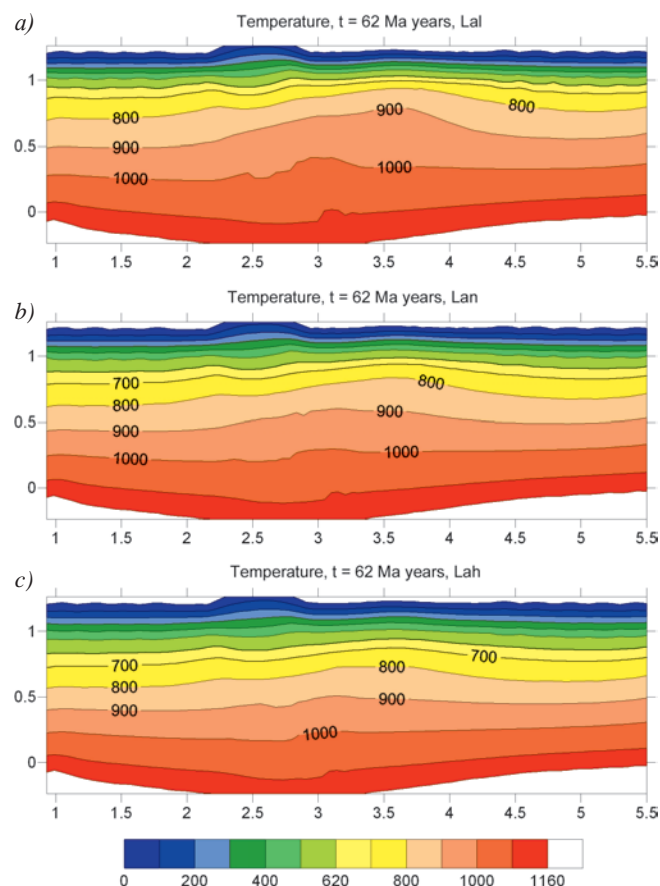


Fig. 6. Temperature distribution for the variant "normal" heat generation rate of  $2.0 \mu\text{W/m}^3$  ( $H_n$ ) for different values of the thermal conductivity of the upper crust: (a)  $\lambda = 2.0 \text{ W/m}\cdot\text{K}$  (Lal – low); (b)  $\lambda = 2.5 \text{ W/m}\cdot\text{K}$  (Lan – normal); (c)  $\lambda = 3.0 \text{ W/m}\cdot\text{K}$  (Lah – high). Vertical and horizontal scales 1: 100 km

The surface manifestation of the deep processes of temperature redistribution is the heat flow density. The results of modeling the thermal field, reflected in the distribution and evolution of the heat flow, are shown in Fig. 7 and 8. The increase in thermal conductivity (Fig. 7a) or the rate of heat generation (Fig. 7b) leads to almost the same distribution of the heat flow density over the thickened crust at the post-collision stage – 42 Ma after the end of the thrusting.

The broken line in fig. 7a shows the heat flow distribution for the case of anisotropy of thermal conductivity with  $\lambda_x = 1.2 \lambda_y$  for the "normal" set of values of thermal parameters (2). The decrease in the vertical heat flow in this case is quite significant – almost 20% of the maximum values, and it is mainly caused by an increase in the heat transfer in the horizontal direction. As in the case of temperature distribution, the maximum values of heat flow are characteristic of the most thickened section of the upper crust (~ 80 km to the right of point  $x_0$ , Fig. 4 – coordinates of the appearance of an additional load).

Figure 8 presents the results of calculations of the evolution of heat flow over the region of the maximum perturbed thermal field (~ 80 km to the right of point  $x_0$



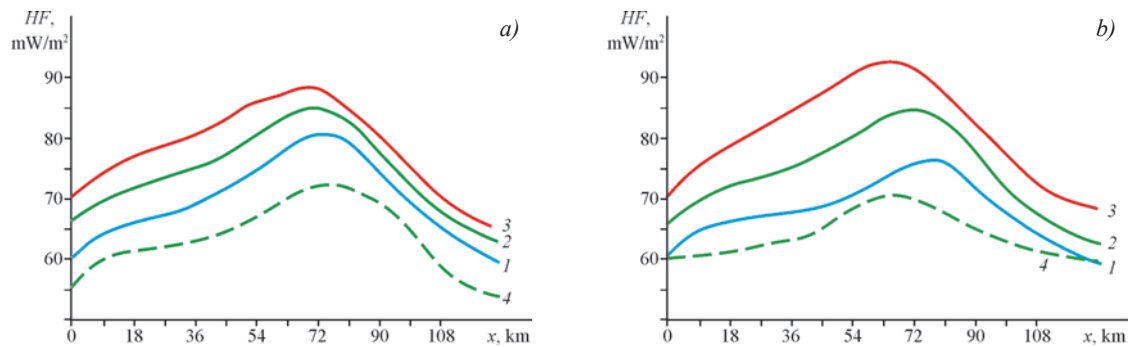


Fig. 7. The distribution of the heat flow density over the uplift (point 0 in the horizontal direction corresponds to the point  $x_0$  in Fig. 4) 42 million years after the end of the horizontal contraction process. (a) Effect of thermal conductivity  $\lambda$ : 1 – 2.0 (low), 2 – 2.5 (normal), 3 – 3.0 (high) W/m·K. The discontinuous curve (4) represents the result for the case of thermal conductivity anisotropy  $\lambda_x = 1.2 \lambda_y$ . (b) Influence of the rate of heat generation of the upper crust  $H$ : 1 – 1.5 (low), 2 – 2.0 (normal), 3 – 2.5 (high)  $\mu\text{W}/\text{m}^3$ . The discontinuous curve (4) represents the distribution of the heat flow at the time of the end of the thrusting ( $t \sim 20$  Ma) for the “normal” model (2)

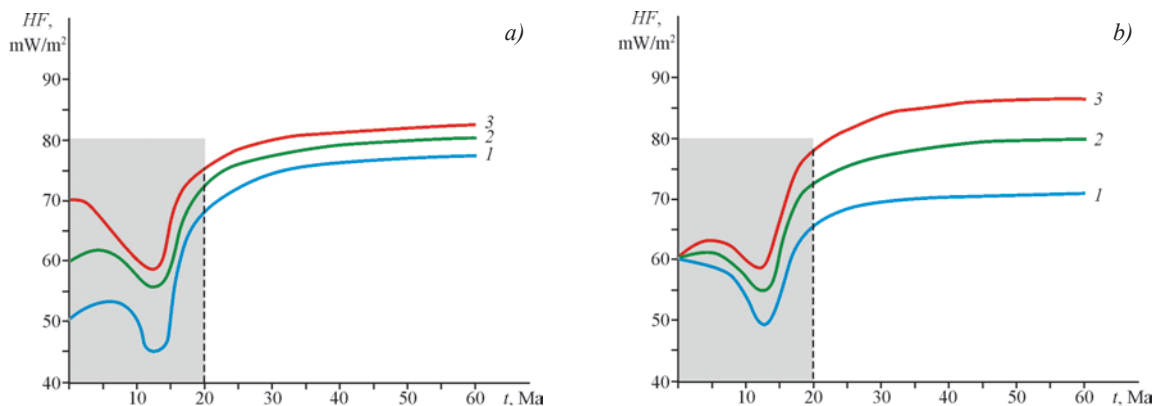


Fig. 8. Evolution of heat flow from the surface above the area of maximum uplift. (a) Options with different values of thermal conductivity  $\lambda$ : 1 – 2.0 (low), 2 – 2.5 (normal), 3 – 3.0 (high) W/m·K with an average value of heat generation  $2.0 \mu\text{W}/\text{m}^3$ . (b) Influence of various rates of heat generation  $H$ : 1 – 1.5 (low), 2 – 2.0 (normal), 3 – 2.5 (high)  $\mu\text{W}/\text{m}^3$  with an average value of thermal conductivity  $2.5 \text{ W}/\text{m}\cdot\text{K}$ . Shaded area – the period of thrusting

in Fig. 4) for different values of thermal conductivity  $\lambda$  (a) and heat generation rate  $H$  (b).

According to the simulation results, the heat flow density drops by about  $10 \text{ mW}/\text{m}^2$  over the limiting fault during the thrusting (shaded area in the figure). The physical basis of this phenomenon is that a layer of a certain thickness (in our model, this is the upper crust) with the same initial temperature distribution gradually moves on a plate with some initial temperature distribution. As a result of the thrust, the “cold” layer is under the “hot” layer and then the temperature equalization stage follows. The early postcollisional stage is characterized by a slight increase in heat flow due to an increase in the thickness of the upper crust with maximum heat generation. Further, the heat flow reaches stable values, since the redistribution of additional load caused by erosion of uplift and sedimentation is very insignificant at this stage due to the local nature of erosion assumed in the model.

### Discussion of the results and conclusions

Table 2 presents a sample of temperatures for all 9 models with three different values of heat generation

$\frac{460}{610}$	$H_1 = 1.5$ $\mu\text{W}/\text{m}^3$		$H_n = 2.0$ $\mu\text{W}/\text{m}^3$		$H_h = 2.5$ $\mu\text{W}/\text{m}^3$	
$\lambda_1 = 2.0 \text{ W}/\text{m}\cdot\text{K}$	$\frac{685}{730}$	$\frac{780}{840}$	$\frac{715}{755}$	$\frac{840}{890}$	$\frac{750}{885}$	$\frac{885}{920}$
$\lambda_n = 2.5 \text{ W}/\text{m}\cdot\text{K}$	$\frac{630}{700}$	$\frac{700}{770}$	$\frac{665}{720}$	$\frac{745}{810}$	$\frac{700}{740}$	$\frac{780}{840}$
$\lambda_h = 3.0 \text{ W}/\text{m}\cdot\text{K}$	$\frac{590}{670}$	$\frac{615}{705}$	$\frac{620}{690}$	$\frac{670}{750}$	$\frac{650}{710}$	$\frac{710}{780}$

Tab. 2. The temperature values ( $^{\circ}\text{C}$ ) under the midpoint of the uplift at the end of the thrusting ( $t = 19.4$  Ma) are left columns and in the post-collisional stage ( $t = 62$  million years) – right columns. The first cell shows the initial temperatures of the selected depths of 20 and 30 km, respectively. Details are given in the text

of the upper crust ( $H_1$ ,  $H_n$ ,  $H_h$ ) – horizontally, and three values of thermal conductivity ( $\lambda_1$ ,  $\lambda_n$ ,  $\lambda_h$ ) – vertically. It shows temperatures at the end of the thrusting  $\sim 20$  million years (left columns in all columns) and 42 million years after the end of the thrusting ( $t = 62$  million years – right columns). The upper values are for a depth of  $\sim 20$  km (the boundary of the upper and lower crust), the lower values for a depth of  $\sim 30$  km (lower crust) below the midpoint (maximum) elevation point,

at a distance of about 80 km to the right of the point  $x_0$  (Fig. 4). Calculations have shown that this is the region of maximum temperatures in the horizontal direction due to the maximum thickening of the crust with high heat generation. The expected result is the maximum temperature increase at the post-collision stage in the case of maximum generation and minimum thermal conductivity ( $H_h$  and  $\lambda_r$ ). The average temperature increase after the end of the thrusting is approximately 200°C for the upper crust (the initial temperature of the model is 460°C for the boundary of the upper and lower crust at a depth of 20 km) and 110°C for a depth of 30 km (in the lower crust). In most variants of thermophysical parameters, the temperature at the final stage of thrusting and at the post-collision stage, with the exception of a high value of thermal conductivity, exceeds the solidus temperature of “wet” granite (shown in bold in Table 2). These results under conditions of local erosion confirm the main conclusions of a one-dimensional simulation of instantaneous thrust about the possibility of the formation of partial melting zones under certain thermal conditions (England, Thompson, 1984).

For the set of selected thermophysical parameters, the calculated maximum temperature range is 590–750°C (from the initial 460°C) and 670–885°C (from the initial 610°C) after a horizontal reduction of 100 km with a thrusting duration of 20 Ma. In the future, the temperature increase rate for 42 million years of post-collisional evolution is much less (compared with the columns on the right), which demonstrates the important role of the initial heating phase during the slow thrusting and the formation of a thickened crust. Thus, with the mid-continental initial temperature, most models provide the possibility of the appearance of a partial melt in the solidus conditions of “wet” granite (the temperatures indicated in bold in Table 2).

The evolution of heat losses at the stage of motion during thrusting and after its termination is studied. The density of the heat flow drops by about 10 mW/m<sup>2</sup> over the fault, along which the process of thrusting occurs. The early postcollisional stage is characterized by a slight increase in heat flow due to an increase of the upper crust thickness, in which heat generation is maximum. Further, the heat flow reaches stable values, since the redistribution of additional load caused by erosion of uplift and sedimentation is very insignificant at this stage due to the local nature of erosion assumed in the model. The maximum values of the heat flow density in the frontal thrust area at the post-collisional stage are 85–95 mW/m<sup>2</sup> with regional background values of 50–70 mW/m<sup>2</sup>. It has been shown that heat losses from the surface after the end of the crust shortening are more dependent on the values of heat generation than on the thermal conductivity of the upper crust.

## Acknowledgements

*This work was supported by the State budget theme No. 0144-2014-0086.*

## References

- Barbey P., Convert J., Moreau B. et al. (1984). Petrogenesis and evolution of an Early Proterozoic collisional orogen: the Granulite Belt of Lapland and the Belomorides (Fennoscandia). *Bull. Geol. Soc. Finl.*, 56, pp. 161–188. <https://doi.org/10.17741/bgsf/56.1-2.010>
- England P., Thompson A.B. (1984). Pressure – temperature – time paths of regional metamorphism. Part I: Heat transfer during the evolution of regions of thickened continental crust. *J. Petrology*, 25, pp. 894–928. <https://doi.org/10.1093/petrology/25.4.894>
- Gaal G., Berthelsen A., Gorbatshev R. et al. (1989). Structure and composition of the Precambrian crust along the POLAR Profile in the northern Baltic Shield. *Tectonophysics*, 162, pp. 1–25. [https://doi.org/10.1016/0040-1951\(89\)90354-5](https://doi.org/10.1016/0040-1951(89)90354-5)
- Gerdas A., Worner G., Henk A. (2000). Post-collisional granite generation and HT – LP metamorphism by radiogenic heating: the Variscan South Bohemian Batholith. *Journal of the Geological Society*, 157, pp. 577–587. <https://doi.org/10.1144/jgs.157.3.577>
- Jaupart C., Mareschal J.-C. (2004). Constraints on crustal heat production from heat flow data. *Treatise on Geochemistry*, V. 3: The Crust. Ed. by R.L. Rudnick. Amsterdam: Elsevier Sci. Pub., pp. 65–84.
- Jaupart C., Mareschal J.-C. (2011). Heat generation and transport in the Earth. New York: Cambridge Univ. Press, 464 p.
- Jaupart C., A. Provost (1985). Heat focusing, granite genesis and inverted metamorphic gradients in continental collision zones. *Earth Planet. Sci. Lett.*, 73, p. 385–397. [https://doi.org/10.1016/0012-821X\(85\)90086-X](https://doi.org/10.1016/0012-821X(85)90086-X)
- Luosto U., Flueh E.H., Lund C.-E. (1989). The crustal structure along the POLAR Profile from seismic refraction investigations. *Tectonophysics*, 162, pp. 51–85. [https://doi.org/10.1016/0040-1951\(89\)90356-9](https://doi.org/10.1016/0040-1951(89)90356-9)
- Mareschal J.-C. (1994). Thermal regime and post-orogenic extension in collision belts. *Tectonophysics*, 238, pp. 471–484. [https://doi.org/10.1016/0040-1951\(94\)90069-8](https://doi.org/10.1016/0040-1951(94)90069-8)
- Parphenuk O.I. (2014). Analiz vliyaniya erozii kollizionnykh podnyatii na protsess ekskumatsii glubinnykh porod (chislennoe modelirovanie) [Analysis of the collisional uplifts erosion influence on the overthrust structures and the process of deep crustal rocks exhumation (numerical modeling)]. *Vestnik KRAUNTs = Bulletin of Kamchatka Regional Association «Educational-Scientific Center»*. *Earth Sciences*, 1(23), pp. 107–20. (In Russ.)
- Parphenuk O.I., Mareschal J.-C. (1998). Numerical modeling of the thermomechanical evolution of the Kapuskasing structural zone, Superior province, Canadian shield. *Izvestiya. Physics of the Solid Earth*, 10, pp. 22–32. (In Russ.)
- Parphenuk O.I. (2015). Uplifts formation features in continental collision structures (evolution modeling). *Russian Journal of Earth Sciences*, 15, ES4002, 8 p. <https://doi.org/10.2205/2015ES000556>
- Parphenuk O.I. (2016). Thermal regime and heat transfer during the evolution of continental collision structures. *Russian Journal of Earth Sciences*, 16, ES6006, 10 p. <https://doi.org/10.2205/2016ES000589>
- Parphenuk O.I., Dechoux V., Mareschal J.-C. (1994). Finite-element models of evolution for the Kapuskasing structural zone. *Can. J. Earth Sci.*, 31(7), pp. 1227–1234. <https://doi.org/10.1139/e94-108>
- Perchuk L.L. (1973). Termodinamicheskii rezhim glubinnoy petrogenеза [Thermodynamic regime of deep petrogenesis]. Moscow: Nauka, 318 p. (In Russ.)
- Perchuk L.L., Krotov A.V., Gerya T.V. (1999). Petrologiya amfibolitov poyasa Tana i granulitov Laplandskogo kompleksa [Petrology of amphibolites of the Tana belt and granulites of the Lapland complex]. *Petrologiya = Petrology*, 7(4), pp. 356–381. (In Russ.)
- Percival J.A. (1990). A field guide through the Kapuskasing uplift, a cross section through the Archean Superior Province. *Exposed Cross-Sections of the Continental Crust*, NATO ASI Ser., 317, pp. 227–283. [https://doi.org/10.1007/978-94-009-0675-4\\_10](https://doi.org/10.1007/978-94-009-0675-4_10)
- Popov Yu.A., Romushkevich R.A., Miklashevskii D.E. et al. (2008). Novye rezul'taty geotermicheskikh i petrotermicheskikh issledovaniy razrezov kontinental'nykh nauchnykh skvazhin [New results of geothermal and petrothermal studies of the sections in continental scientific wells]. *Teplovoe pole Zemli i metody ego izucheniya* [Proc. Int. Conf. «The Earth's Thermal Field and Related Research Methods»]. Ed. Yu.A. Popov. Moscow: RIO RGGRU, pp. 208–212. (In Russ.)
- Reddy J.N. (1984). An introduction to the Finite Element Method. McGraw-Hill: New-York, 459 p.

Rozen O.M., Fedorovskii V.S. (2001). Kollizionnye granitoidy i rassloenie zemnoi kory [Collisional granitoids and stratification of the Earth's crust]. *Trudy GIN RAN* [Proceedings of Geological Institute of RAS], 545, 188 p. (In Russ.)

Sharov N.V. (1993). Litosfera Baltiiskogo shchita po seismicheskim dannym [Lithosphere of the Baltic Shield according to seismic data]. Apatity: KNTs RAN, 145 p. (In Russ.)

Sokolov S.D. (1990). Kontseptsiya tektonicheskoi rassloennosti litosfery: istoriya sozdaniya i osnovnye polozeniya [The concept of tectonic stratification of the lithosphere: the history of foundation and the main aspects]. *Geotektonika = Geotectonics*, 6, pp. 3-19. (In Russ.)

*Tectonophysics*. (1989). Special Issue: The European Geotraverse, Part 5: The Polar Profile. 162(1-2), 171 p.

## About the Author

*Olga I. Parphenuk* – DSc (Physics and Mathematics),  
Leading Researcher, Laboratory of the Theoretical  
Geophysics

Schmidt Institute of Physics of the Earth of the  
Russian Academy of Sciences

Buil. 1, 10, B. Gruzinskaya st., Moscow, 123242,  
Russian Federation

Phone: +7 (499) 254 23 18, e-mail: oparfenuk@ifz.ru

*Manuscript received 19 July 2018;*

*Accepted 20 September 2018;*

*Published 30 November 2018*





## REVIEW ARTICLE

DOI: <https://doi.org/10.18599/grs.2018.4.386-395>

# Mesozoic-Cenozoic climate and the geothermal regime of the oil source Kiterbyutskaya suite of the Arctic region of Western Siberia

V.I. Isaev<sup>1,2\*</sup>, A.A. Iskorkina<sup>1</sup>, G.A. Lobova<sup>1</sup>, T.E. Luneva<sup>1</sup>, E.N. Osipova<sup>1</sup>, R.Sh. Ayupov<sup>2</sup>,  
N.O. Igenbaeva<sup>2</sup>, A.N. Fomin<sup>3</sup>

<sup>1</sup>National Research Tomsk Polytechnic University, Tomsk, Russian Federation

<sup>2</sup>Yugra State University, Khanty-Mansiysk, Russian Federation

<sup>3</sup>Trofimuk Institute of Petroleum Geology and Geophysics of Siberian Branch of Russian Academy of Sciences, Novosibirsk, Russian Federation

**Abstract.** Using the example of paleotemperature modeling of the Kiterbyutskaya suite of the Mesozoic-Cenozoic section, opened by a deep well at the Bovanenkovskoye oil – gas condensate field (Yamal Peninsula), the influence of paleoclimate factors on the thermal history of the Lower Jurassic oil source deposits, the duration of the main phase of petroleum formation and the value of the paleothermometric maximum and oil generation density. The original computer methodology is described, which takes into account the parameters of the tectonic and sedimentation history, as well as the history of the thermophysical properties of the sedimentary formation, including permafrost and glaciers, and not requiring a priori information about the values and nature of the deep heat flow is given.

The features of the model parametrization are shown. The reliability of the results is confidently controlled by the geophysical criterion of the “discrepancy”, comparison with experimental data on the heat flow, and consistency with the drilling data. The presentation is based on the works of the Tomsk School of Geothermics, carried out as part of the development of a methodological base of geothermics as a geophysical oil prospecting method.

**Keywords:** Yamal Peninsula, paleoclimate, Kiterbyutskaya suite, modelling of geothermal regime, hydrocarbon resources, works of the Tomsk School of Geothermics

**Recommended citation:** Isaev V.I., Iskorkina A.A., Lobova G.A., Luneva T.E., Osipova E.N., Ayupov R.Sh., Igenbaeva N.O., Fomin A.N. (2018). Mesozoic-Cenozoic climate and the geothermal regime of the oil source Kiterbyutskaya suite of the Arctic region of Western Siberia. *Georesursy = Georesources*, 20(4), Part 2, pp. 386-395. DOI: <https://doi.org/10.18599/grs.2018.4.386-395>

## Introduction

A quantitative assessment of the prospects for the oil and gas potential of the territories – the assessment of the density of hydrocarbon (HC) resources – is performed by the volumetric-genetic method (basin modeling). The number of generated hydrocarbons is calculated based on the reconstruction of the geothermal regime of oil source sediments (Tissot, 2003; Khutorskoy et al., 2011; Kontorovich et al., 2013; Galushkin, 2016).

The temperature regime of a sedimentary cover, the thermal history of directly source deposits, and, consequently, the degree of realization of their generation potential can be affected by directly (actually) or indirectly (in calculations, reconstructions) by the following paleoclimate factors:

1) the age-old temperature course in the Mesozoic Cenozoic on the surface of the Earth, causing an exogenous source of heat for hydrocarbon generation processes;

2) permafrost strata overlying source deposits and having anomalously high thermal conductivity;

3) ice sheets, peculiar lithologic-stratigraphic complexes, increasing the thickness of the overlying sediments.

Significant research material has been accumulated, giving an estimate of the influence of paleoclimate factors on the temperature regime of sedimentary-volcanic and magmatic complexes (Golovanova et al., 2014; Demezhko, Gornostaeva, 2014; etc.). A series of papers has been published (Lobova et al., 2013; Isaev et al., 2016; etc.), which show the influence of Mesozoic-Cenozoic climatic changes on the thermal history of directly source deposits in the south-east of Western Siberia.

The Arctic region of Western Siberia has unique paleoclimatic features (Kurchikov, Stavitskii, 1987).

\*Corresponding author: Valeriy I. Isaev  
E-mail: [isaevvi@tpu.ru](mailto:isaevvi@tpu.ru)

© 2018 The Authors. Published by Georesurs LLC  
This is an open access article under the CC BY 4.0 license  
(<https://creativecommons.org/licenses/by/4.0/>)

A global event occurred in the Pleistocene – a sharp cooling of the climate. This could lead to cooling of the sedimentary strata, a significant non-stationarity of the temperature field in the entire sedimentary section, including oil source sediments (Kurchikov, 2001). The publication of the Arctic Expedition IODP 302 notes (Nelskamp et al., 2014) that the evolution of temperatures on the Earth's surface has a great influence on the maturity of the source rock: there may be more or less volumes of produced hydrocarbons depending on temporal variations in surface temperatures.

The Upper Jurassic deposits of the Bazhenov Formation ( $J_3 + K_1$ bg) of Western Siberia are the main source of hydrocarbon deposits in the traps of the Upper Jurassic and Cretaceous oil and gas complexes (OGC), as well as a priority shale formation (Kuzmin et al., 2014; Isaev et al., 2018). Due to the strategy

of developing the hydrocarbon resource base of the Russian Federation, exploration and promotion of the oil and gas industry in the north of Western Siberia have been intensified (Igenbaeva, 2015). However, unlike the south-eastern and central regions of the West Siberian petroleum province (WSOGP) (Isaev et al., 2018b), the Bazhenov sediments in the Arctic region vary significantly (Neftegazonosnye basseiny i regiony Sibiri..., 1994) as for concentrations of dispersed organic matter (DOM), often decreasing to 1-2%, and by DOM type, moving to the humus-sapropel type (Database of the Trofimuk Institute of Petroleum Geology and Geophysics of Siberian Branch of Russian Academy of Sciences, 2017).

The article (Isaev et al., 2018a), with a full illustration using the Rostovtsevskaaya 64 well (Yamal Peninsula, Fig. 1), presents a detailed analysis of the impact on the

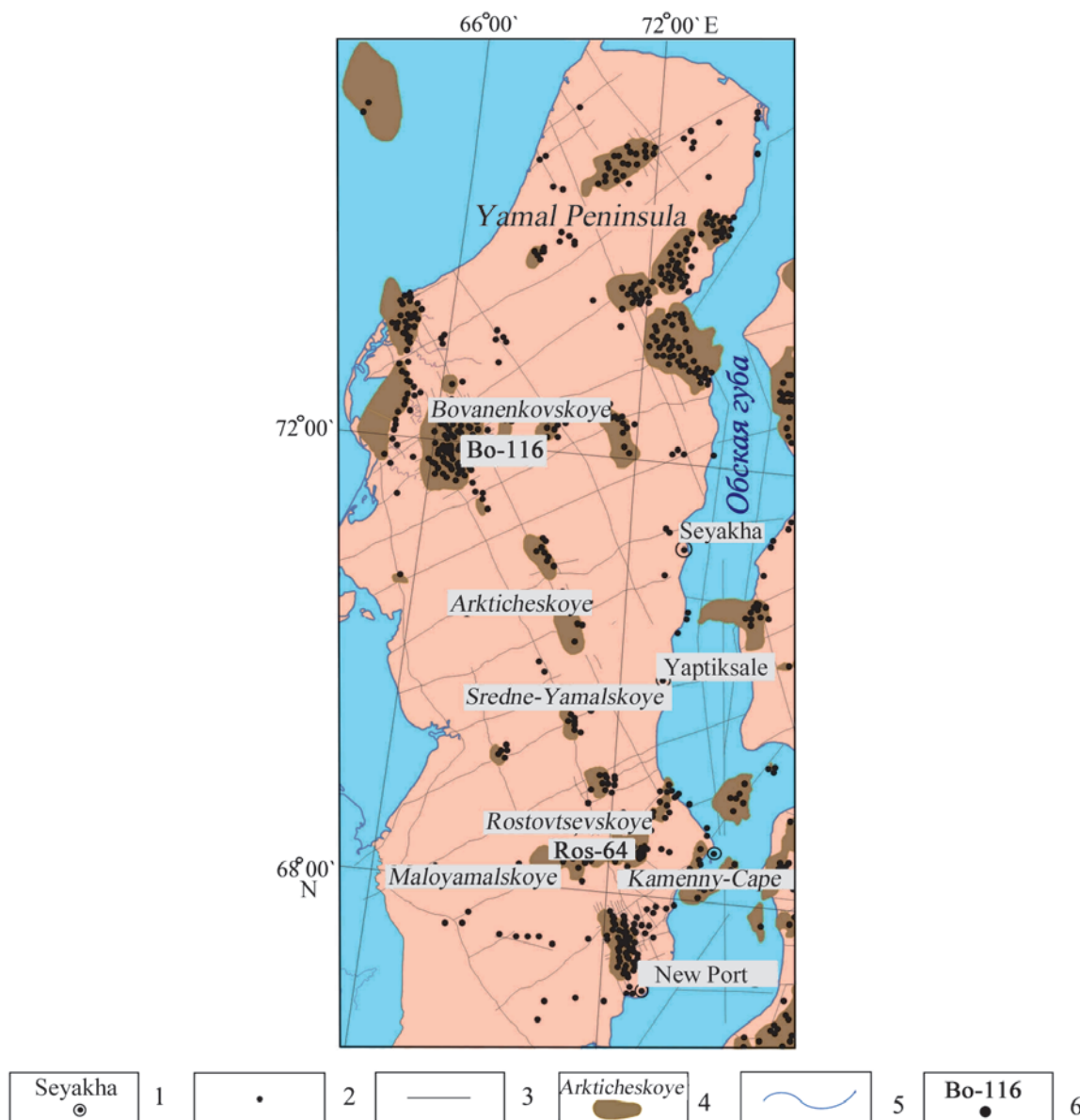


Fig. 1. Review scheme of the research area: 1 – a settlement and its name; 2 – exploration well; 3 – seismic profile of CDPM 2D; 4 – contour of the field and its name; 5 – hydrography and coastline; 6 – simulated well and its index: Ros-64 – Rostovtsevskaaya 64, Bo-116 – Bovanenkovskaya 116

thermal history of the Bazhenov formation of a complex of paleoclimatic factors (the Mesozoic-Cenozoic secular temperature variation on the Earth surface, the secular variation of the Neopleistocene permafrost layer thickness and the secular variation of the thickness of the Late Quaternary ice caps. It has been established that in the paleo-temperature modeling scenario, which takes into account paleoclimate factors, the geological time of the maternal suite in the main oil generation zone is increased by 25 Ma (by 50%), and the absolute paleo-temperature maximum increases by 10°C. Here, the first results were obtained on the evaluation of the role of the Late Quaternary ice caps, which showed their insignificant effect on the thermal regime of the Bazhenov oil-source rock.

At the same time, the geothermal regime of the Kiterbyutskaya suite ( $J_{kt}$ ), which is the source for the formation of hydrocarbon deposits in the traps of the Lower Jurassic and, possibly, pre-Jurassic OGC, is of undoubted interest. The pre-Jurassic (Paleozoic) OGC is one of the priorities for the development of tight oil resources (Polukeev et al., 2013; Lobova et al., 2018). Kiterbyutskaya argillaceous facies, which has an oil source potential, has formed during the time of boreal transgressions in the early Jurassic – Toar. In contrast to the Bazhenov deposits, the dispersed organic matter of the Kiterbyutskaya formation of the Arctic regions (Neftegazonosnye basseiny i regiony Sibiri..., 1994) has more stable concentrations (Database of the Trofimuk Institute of Petroleum Geology and Geophysics of Siberian Branch of Russian Academy of Sciences, 2017).

Therefore, the determination of the influence of paleoclimate factors on the reconstruction of the geothermal regime and on the assessment of the degree of realization of the generation potential of oil source Kiterbyutskaya deposits in the Arctic region of Western Siberia is an important task.

In the work (Iskorkina et al., 2018), the experience of assessing the influence of paleoclimate factors on the calculated geothermal regime of the Kiterbyutskaya formation is given.

The main objective of these studies is the further arguing of the significant influence of paleoclimate factors – the secular variation of temperatures on the Earth's surface and the Neopleistocene permafrost strata – on the calculated geothermal regime of the oil source Kiterbyutskaya suite. And defining the role of ice caps is of particular relevance when assessing the oil and gas potential of the Arctic territories of Western Siberia (Kontorovich et al., 2013). Below are the results of detailed paleotemperature studies of the Kiterbyutskaya deposits, which were penetrated by a deep well in the well-known Bovanenkovskoye field (Yamal Peninsula, Fig. 1). The presentation of the results

is largely based on a review of the published works of the authors, performed as part of the development of the methodological base of geothermics as a geophysical oil prospecting method.

### About the methodology of paleotemperature studies

The restoration of the thermal history of the oil source suite is based on solving the direct and inverse problems of geothermy (Starostenko et al., 2006; Isaev et al., 2018a). The deep heat flow  $q$  is determined by solving the inverse problem of geothermy, which is performed within the parametric description of the sedimentation history and the history of thermophysical properties of the sedimentary layer only, without invoking information about the nature of  $q$  and geodynamics below the base of the sedimentary section. For the conditions of Western Siberia, characterized, starting from the Jurassic time, by the quasistationarity of the deep heat flow (Duchkov et al., 1990; Kurchikov et al., 2001; Isaev et al., 2018), the solution of the inverse geothermy problem – determining  $q$  – in the adopted model has been performed uniquely. The mathematical model in a rigorous mathematical form includes geotemperatures from the definitions of vitrinite reflectance (VR), as “observed”. No separate “calibrations” for VR temperatures are required.

The calculation of paleotemperature consists of two stages. At the first stage, the heat flow  $q$  through the surface of the base of the sedimentary cover, i.e., is calculated from the temperature distribution  $T$  “observed” at the well cut points, i.e., the inverse problem of geothermy is solved – the classical inverse problem of geophysics. At the second stage with a known value of  $q$ , direct geothermal problems are solved – temperatures  $U$  are calculated at given points of the sedimentary sequence  $Z$  (including in the oil source suite) for any given moments of geological time  $t$ .

To solve the inverse problem of geothermics, we use as “observed” both measurements of reservoir temperatures obtained during well tests and geotemperatures recalculated (Isaev, Fomin, 2006) from VR.

The first boundary condition of the model is determined by the temperature of the surface of sedimentation in the Mesozoic-Cenozoic, i.e. paleoclimate factor, and is given as a piecewise linear function of the “arctic” secular temperature pattern on the Earth's surface. The “Arctic” secular temperature pattern built by A.A. Iskorkina is based on a synthesis of published experimental definitions and paleoclimatic reconstructions for the north of the West Siberian Lowland (Iskorkina, 2016).

The formation, existence and degradation of the permafrost in the Neopleistocene and Holocene are



taken into account as a kind of dynamic lithologic-stratigraphic complexes with anomalously high thermal conductivity and thermal diffusivity  $\alpha$ . The formation, existence and degradation of ice mass in the Neopleistocene takes into account their anomalously low density  $\sigma$ . The secular course of the thickness of permafrost and ice sheets was built by A.A. Iskorkina based on a summary of published experimental definitions and paleocryological reconstructions (Iskorkina, 2016; Isaev et al., 2017).

Direct geothermal problems are solved for key points of geological time, corresponding to the start/end times of formation of each suite, overlapping the parent suite, as well as the “breaks” of the secular temperature variations on the Earth’s surface and the “turning points” of formation and degradation of the Neopleistocene permafrost and ice cover.

A quantitative assessment of the influence of paleoclimate on the calculated geothermal regime of oil source sediments is carried out based on an analysis of the variability of the results of four options for paleotemperature reconstructions:

Option 1 – without taking into account paleoclimate factors;

Option 2 – taking into account the secular variation of temperatures on the Earth’s surface, excluding permafrost and glaciers;

Option 3 – taking into account the secular temperature variation, accounting for the dynamics of permafrost;

Option 4 – taking into account the secular variation of temperatures, taking into account the dynamics of permafrost and glaciers.

*The main criterion for the adequacy and preference of the results* of paleotemperature modeling is the optimal consistency (“discrepancy”) of the maximum calculated geotemperatures with the “observed” temperatures of the “maximum paleothermometer” – temperatures determined by VR. The optimality of the “discrepancy” of calculated geotemperatures with “observed” reservoir temperatures is equally important. The optimal “discrepancy” is the mean square difference between the calculated and “observed” values, which is equal to the error of observations. This error is of the order of  $\pm 2^\circ\text{C}$  (Isaev et al., 2018a).

*As the second main criterion* of the adequacy and preference of the results, the degree of consistency of the foci of intense hydrocarbon generation identified by the geotemperature criterion in the maternal suite (Fomin, 2011) with the oil and gas prospecting of the subsoil is established.

*An important criterion* for the reliability of the results of paleotemperature modeling is the consistency of the calculated values of the heat flow density  $q$  with the data of experimental determination of the heat flow density in the study area.

## Parameterization of sedimentation history and thermophysical properties

The dedicated breakdown of the well No. 116 of the Bovanenkovskoye oil – gas condensate field (Fig. 1) from the bottom of the sedimentary cover to the Upper Cretaceous, including the Berezovskaya suite, is taken from the database of the Trofimuk Institute of Petroleum Geology and Geophysics of Siberian Branch of Russian Academy of Sciences (2017). The subdivision of the Lower-Middle Paleogene assemblies, from the Gankinsky to the Irbitsky is borrowed from the materials of A.P. Karpinsky Russian Geological Research Institute (the State Geological Maps of VSEGEI. The map of the Pre-Quaternary formations R (40) -41, R-43, 44 (45) is taken from (<http://vsegei.ru/ru/info/georesource/>)). The overlying strata are dissected on the basis of work (Stratigrafiya neftegazonosnykh basseinov Sibiri, 2002; Volkova, 2011). Within the Bovanenkovsky area, accumulation of sedimentary strata went to the middle of the Miocene (18.5 million years ago, the formation of the Abrosimov Formation). In the Early Bicheul time, for 4 million years, the Abrosimov, Turtass, Novomikhailovsk, Atlym, Tavda, Nyurol, Irbit, Serov and Tibasalinsky formations (238 m) were washed out. From the end of the Bicheul time to the end of Novoportov, the boreal sea coagulation in the Middle Miocene-Early Pliocene was due to accumulation of 143 m thick sediments, which in the subsequent stage of positive tectonic movements over 1.3 million years were denudated. With the onset of the Late Miocene, Pliocene-Quaternary lacustrine-alluvial sediments accumulated.

Thus, when parameterizing the sedimentation-thermophysical model (Table 1), stratigraphic breakdowns were used, taking into account the dynamics of tectonic events during the formation of a sedimentary section (Isaev et al., 2018a).

The density parameter of the rocks  $\sigma$  ( $\text{g}/\text{cm}^3$ ) of each suite was adopted taking into account the actual lithological filling of each stratum. The calculated thermal conductivity of sedimentary rocks  $\lambda$  ( $\text{W}/\text{m}\cdot\text{K}$ ) is used.

For the calculations, petrophysical dependences of the thermal conductivity of  $\lambda$  sediments on their density  $\sigma$  were used. The choice of the coefficients of thermal diffusivity  $\alpha$  ( $\text{m}^2/\text{s}$ ) and specific heat generation  $f$  ( $\text{W}/\text{m}^3$ ) was determined by the lithological composition of the suites, based on published tabular data. The strata of permafrost and ice cover have anomalously high values of thermal conductivity and thermal diffusivity  $\alpha$  (Ivanov, Gavril’ev, 1965; Galushkin, 2007).

Formalized accounting of the permafrost stratum is carried out, starting from 0.52 million years ago, by “instantaneous” (by the standards of geological time, 0.3+3.0 thousand years) the replacement of “normal” sedimentary sediments with 600 m layer with specific

Suite, sequence (stratigraphy)	Thickness, m	Age, mln years ago	Accumulation times, mln years	Density, g/cm	Thermal conductivity, W/m K	Temperature conductivity, m <sup>2</sup> /s	Heat generation, W/m <sup>3</sup>
Neopleistocene <i>Q-N<sub>2</sub></i>	-	0.015-0.00	0.015	-	-	-	-
	-500	0.02-0.015	0.005	0.92	2.25	1.2 -006	1.22 -007
	-	0.04-0.02	0.02	-	-	-	-
	-1000	0.05-0.04	0.01	0.92	2.25	1.2 -006	1.22 -007
	-	0.120-0.050	0.070	-	-	-	-
	+1000	0.130-0.120	0.010	0.92	2.25	1.2 -006	1.22 -007
	-	0.177-0.130	0.047	-	-	-	-
	+500	0.182-0.177	0.005	0.92	2.25	1.2 -006	1.22 -007
	300	0.18215-0.1820	0.00015	2.10	2.09	1.05 -006	1.22 -006
	300	0.1823-0.18215	0.00015	2.10	1.3	7 -007	1.22 -006
	-600	0.1826-0.1823	0.0003	-	-	-	-
	-	0.5167-0.1826	0.3341	-	-	-	-
Quarter + Pliocene <i>Q-N<sub>2</sub></i>	212	4.1-0.520	3.58	2.04	1.29	6.5 -007	1.1 -006
<i>N<sub>1-2</sub></i>	-143	4.1-5.4	1.3				
Novoportov <i>N<sub>1-2</sub></i>	80	5.4-8.4	3	2.08	1.33	7 -007	1.2 -006
Tavolzhan <i>N<sub>1</sub></i>	25	8.4-12.5	4.1	2.08	1.33	7 -007	1.2 -006
Bischeul <i>N<sub>1</sub></i> <i>bsch</i>	38	12.5-14.5	2	2.08	1.33	7 -007	1.2 -006
<i>N<sub>1</sub></i>	-238	14.5-18.5	4				
Abrosimov <i>N<sub>1</sub></i>	10	18.5-23.0	4.5	2.08	1.33	7 -007	1.2 -006
Turtass <i>P<sub>3</sub> tur</i>	20	23.0-28.0	5	2.08	1.33	7 -007	1.2 -006
Novomikhaylov <i>P<sub>3</sub> nvm</i>	15	28.0-30.0	2	2.08	1.33	7 -007	1.2 -006
Atlym <i>P<sub>3</sub> atl</i>	37	30.0-34.0	4	2.08	1.33	7 -007	1.2 -006
Tavda <i>P<sub>2</sub> tv</i>	50	34.0-42.6	8.6	2.08	1.33	7 -007	1.2 -006
Nyuroi <i>P<sub>2</sub> nl</i>	37	42.6-50.4	7.8	2.08	1.33	7 -007	1.2 -006
Irbit <i>P<sub>2</sub> ir</i>	5	50.4-55.0	4.6	2.09	1.35	7 -007	1.2 -006
Serov <i>P<sub>1</sub> sr</i>	20	55.0-58.0	3	2.09	1.35	7 -007	1.2 -006
Tibasalinsky <i>P<sub>1</sub> tb</i>	44	58.0-63.7	5.7	2.09	1.35	7 -007	1.2 -006
Gankinsky <i>K<sub>2</sub>+</i> <i>P<sub>1</sub> gn</i>	35	63.7-73.0	9.3	2.11	1.37	7 -007	1.25 -006
Berezovskaya <i>K<sub>2</sub> b</i>	279	73.0-89.0	16	2.15	1.41	7.5 -007	1.25 -006
Kuznetsov <i>K<sub>2</sub> kz</i>	37	89.0-92.0	3	2.18	1.43	8 -007	1.25 -006
Marresalinsky <i>K<sub>2</sub>-K<sub>1</sub> mr</i>	523	92.0-102.0	10	2.26	1.49	8 -007	1.25 -006
Yaronsky <i>K<sub>1</sub> jar</i>	168	102-108.5	6.5	2.39	1.6	8 -007	1.25 -006
Tanopchinsky <i>K<sub>1</sub> tn</i>	746	108.5-133.2	24.7	2.44	1.62	8 -007	1.25 -006
Akhsy <i>K<sub>1</sub> ah</i>	522	133.2-142.7	9.5	2.44	1.64	8 -007	1.25 -006
Bazhenov <i>J<sub>3</sub>+K<sub>1</sub> bg</i>	15	142.7-149.3	6.6	2.42	1.62	8 -007	1.3 -006
Nurminsky <i>J<sub>2</sub> nr</i>	83	149.3-161.7	12.4	2.42	1.62	8 -007	1.3 -006
Malyshevsky <i>J<sub>2</sub> ml</i>	84	161.7-171.0	9.3	2.45	1.63	8 -007	1.3 -006
Leontievsky <i>J<sub>2</sub> ln</i>	90	171.0-173.0	2	2.47	1.65	8 -007	1.3 -006
Vymsky <i>J<sub>2</sub> vm</i>	143	173.0-175.0	2	2.45	1.63	8 -007	1.3 -006
Laydinsky <i>J<sub>2</sub> ld</i>	83	175.0-177.0	2	2.47	1.65	8 -007	1.3 -006
Nadoyakhsky <i>J<sub>2</sub>+J<sub>1</sub></i> <i>nd</i>	73	177.0-182.5	5.5	2.45	1.63	8 -007	1.3 -006
Kiterbyutskaya <i>J<sub>1</sub> kt</i>	68	182.5-184.0	1.5	2.47	1.65	8 -007	1.3 -006
Sharapovsky <i>J<sub>1</sub> shr</i>	85	184.0-186.0	2	2.45	1.63	8 -007	1.3 -006
Levinsky <i>J<sub>1</sub> lv</i>	111	186.0-186.70	0.7	2.47	1.65	8 -007	1.3 -006
Zimny <i>J<sub>1</sub> zm</i>	13	186.7-200.2	13.5	2.45	1.63	8 -007	1.3 -006
Section thickness, m	3370						

Table 1. A parametric description of the sedimentation history and thermophysical properties of the sedimentary sequence exposed by the Bovanenkovskaya well No. 116 (Iskorkina et al., 2018). The brown fill shows the accumulation times of the source-material Bazhenov and Kiterbyutskaya suites and their parametric description. Gray fillings show erosion of Paleogene-Neogene deposits. The blue fill shows the times of formation, existence and degradation of the permafrost strata, the light blue shows the times of formation, existence and degradation of the glaciers

thermal characteristics. Then, this layer of frozen rocks was present in the sedimentary cover for 334 000 years. Further, “instantly” ( $0.3 + 0.15 + 0.15$  thousand years), the frozen ground degrades in a volume of 300 m. And, further, frozen rocks exist in a volume of 300 m to the present during the last 182 000 years.

The recording of the ice cover is carried out starting from 0.182 million years ago. For 5 thousand years, a 500-meter glacier with its thermal characteristics was formed and existed in such a volume for 47 thousand years. Then, over 10 thousand years, the glacier's capacity has grown to 1500 m, and in such a volume it existed 70 thousand years. Further, over 10 thousand years, the glacier is reduced to 500 m and existed for 20 thousand years. By the time of 15 thousand years ago (the end of Sartan time) the glacier was completely degraded.

### Reconstruction of the geothermal regime of the Kiterbyutskaya suite

**Solution of the inverse problem of geothermy.** Comparison of the calculated and “observed” geotemperatures are given in Table. 2. Since the “observed” (measured) temperatures (including those determined by VR) have an error of the order of  $\pm 2^\circ\text{C}$ , then *options 1 and 2* of the solutions (not accounting, not full accounting of paleoclimate factors) cannot be considered as acceptable. In these cases, the “residuals” exceed the optimum by 2 times and much more, and in option 1, the difference with the temperature according to VR reaches  $18^\circ\text{C}$ . In the case of paleoclimate (*options 3 and 4*), both the “discrepancies” for reservoir temperatures and the convergence with the “maximum paleothermometer” are optimal and about equivalent. It seems the most optimal (acceptable) is *option 3*.

*Analysis of the calculated values of the heat flux density from the base of the sedimentary section* shows that when the factors of paleoclimate are taken into account, the heat flow increases. *The reliability of the results of paleotemperature modeling* of the Bovanenkovskaya borehole 116 is supported by the

good consistency of the obtained *calculated* values of the heat flow density  $60\text{--}62\text{ mW/m}^2$  with the calculated values (Isaev et al., 2018a) of the heat flow density in the Rostovtsevskaya well 64 is  $49\text{--}50\text{ mW/m}^2$  (Fig. 1). This is confirmed by experimental determinations of the heat flow density for the Yamal Peninsula. The range of experimental definitions for the Yamal Peninsula is  $47\text{--}58\text{ mW/m}^2$ , with the established pattern of the heat flow density increasing in the north-west direction (Khutorsky et al., 2013).

**Solutions to direct problems of geothermy.** An analysis of the thermal history of the Kiterbyutskaya suite (Table 3) in the well section Bovanenkovskaya 116 indicates that, in *option 1* (without taking into account all paleoclimate factors), the oil source series “survived” the shortest and “coolest” main oil generation phase (MOGP).

In *variants 2, 3 and 4* (taking into account the factors of paleoclimate), the Kiterbyutskaya suite has “rich” thermal histories of MOGP. The main phases of oil formation in these variants have different values of the absolute maxima of paleotemperatures.

In *option 3*, the presence of a permafrost stratum with high thermal conductivity and thermal diffusivity leads to the maximum calculated values of the heat flow density, which, in turn, leads to a longer duration of the MOGP and increases the calculated geotemperature of the mother sediments to the maximum values.

Note that the addition of the ice sheet (*option 4*) had little effect on the calculated value of the heat flux density from the base, and, as a consequence, on the intensity and duration of the MOGP.

As noted above, the Kiterbyutskaya suite is the source of the formation of hydrocarbon deposits in the traps of the Lower Jurassic and, possibly, the pre-Jurassic hydrocarbons bearing sequence. In this regard, it is important to assess the consistency of the foci of intensive generation of Kiterbyutskaya oil, identified by the geothermal criterion in the well section, with the test results of the Lower Jurassic formations. In the Bovanenkovskaya area, the Kiterbyutskaya formation,

Depth, m	Measured temperatures, °	Measuring method	Option 1		Option 2		Option 3		Option 4	
			Value	Difference	Value	Difference	Value	Difference	Value	Difference
2610	94	formation	100	+6	97	+3	96	+2	97	+3
2657	97	formation	102	+5	99	+2	97	0	99	+2
2795	103	formation	107	+4	104	+1	103	0	104	+1
3050	113	formation	116	+3	113	0	112	-1	113	0
2615	120	by VR	102	-18	113	-7	119	-1	115	-5
Standard deviation ("residuals"), °			±9		±4		±1		±3	
Calculated heat flow from the base, $\text{mW/m}^2$			57		59		62		60	

Table 2. Comparison of measured and calculated subsoil temperatures in well No. 116 of Bovanenkovskoye oilfield – gas condensate field, using (Iskorkina et al., 2018). Brown fill shows the options that are optimal by the criterion of «discrepancy»



Time, mln years ago	«Arctic» secular temperature pattern, °C	Thickness of frozen rocks, m	Thickness of ice flow, m	Depth of Kiterbyutskaya suite, m	Geotemperatures of Kiterbyutskaya suite, °				
					Option 1	Option 2	Option 3	Option 4	
								Geotemperatures	Depth of Kiterbyutskaya suite, m (accounting for the ice cover)
0	-4	300	-	3127	118	116	115	115	3111
0,015	-10	300	-	3126	118	115	115	114	3110
0,02	-8	300	500	3126	118	115	115	113	3610
0,030	-5	300	500	3125	118	116	114	113	3609
0,04	-6	300	500	3125	118	115	114	112	4109
0,050	-7	300	1500	3125	118	116	114	111	4608
0,070	-4	300	1500	3123	118	115	113	109	4609
0,110	-5	300	1500	3121	118	115	112	107	4609
0,120	-6	300	1500	3121	118	114	111	107	4609
0,130	-7	300	500	3120	118	114	111	106	3609
0,150	-6	300	500	3119	118	114	111	106	3608
0,177	-7	300	500	3118	118	114	122	106	3607
0,1820	-7	300	-	3118	118	114	119	106	3108
0,1826	-7	600	-	3118	118	114	112	106	3087
0,200	-8	600	-	3117	118	114	111	106	3107
0,240	-9	600	-	3115	118	113	111	106	3107
0,5167	-10	600	-	3100	114	112	119	114	3089
0,5197	-11	-	-	3100	117	112	126	114	2907
0,520	-11	-	-	3100	117	112	118	114	3127
1,8	-13	-	-	3034	114	109	115	110	3051
3,2	+5	-	-	2962	111	120	126	121	2968
4,1	+4	-	-	2915	110	119	125	120	2915
4,9	+4	-	-	3003	113	121	127	123	3003
5,4	+4	-	-	3058	115	124	130	125	3058
8,4	+5	-	-	2978	112	118	127	122	2978
10	+6	-	-	2968	111	122	127	123	2968
12,5	+6	-	-	2953	110	121	127	122	2953
14,5	+6	-	-	2915	110	121	126	122	2915
18,5	+7	-	-	3153	120	132	138	133	3153
23	+8	-	-	3143	119	132	138	133	3143
28	+8	-	-	3123	118	131	137	132	3123
30	+9	-	-	3108	117	131	137	132	3108
34	+9	-	-	3071	116	130	136	131	3071
35	+9	-	-	3065	116	130	135	130	3065
42,6	+12	-	-	3021	114	131	136	131	3021
50	+15	-	-	2986	112	132	137	132	2986
50,4	+15	-	-	2984	112	132	137	132	2984
55	+15	-	-	2979	112	132	137	133	2979
58	+16	-	-	2959	111	132	136	132	2959
63,7	+16	-	-	2915	109	130	135	130	2915
70	+16	-	-	2891	108	128	134	129	2891
73	+15	-	-	2880	107	127	133	128	2880
85	+13	-	-	2671	98	116	121	116	2671
89	+13	-	-	2601	95	113	118	114	2601
92	+13	-	-	2564	94	111	116	112	2564
100	+15	-	-	2146	77	95	99	96	2146
102	+15	-	-	2041	73	91	95	92	2041
108,5	+15	-	-	1873	67	85	88	85	1873
120	+16	-	-	1526	54	72	75	73	1526
134	+15	-	-	1083	34	55	57	55	1083
135	+15	-	-	1028	32	52	55	53	1028
142,5	+15	-	-	616	22	38	39	38	616
Calculated heat flow from the base, mW/m²					57	59	62	60	

Tab. 3. Estimated geotemperatures of the Kiterbyutskaya suite in the section of the well Bovanenkovskaya 116, using (Iskorkina et al., 2018). Option 1 – without taking into account paleoclimate factors. Option 2 – taking into account the “arctic” secular temperature pattern. Option 3 – taking into account the “arctic” secular temperature pattern and the Neopleistocene permafrost. Option 4 – taking into account the “arctic” secular temperature pattern, the Neopleistocene permafrost and ice cover. Brown fill shows the temperature of the main oil generation phase (MOGP), dark brown fill shows the temperature maximum of MOGP. The gray fill indicates the times of erosion of the Paleogene-Neogene deposits

according to the simulation results, has been located in the main zone of oil formation since the Marresala time (100 million years ago). And for about 15 million years, before the main erosion in the Neogene, the sequence closely approached the lower gas formation zone, warming up to 138°C (Table 3). And, indeed, the well Bovanenkovskaya 116 revealed the oil-and-gas-saturated Lower Jurassic formations Yu6, Yu10 and Yu12.

## Conclusions and discussion

1. On the representative section of the Bovanenkovskoye field of the Yamal Peninsula, it has been established that taking into account the “arctic” secular variation of temperatures on the Earth’s surface and the Neopleistocene permafrost allows us to correctly reconstruct the thermal history of the oil source rocks of the Kiterbyutskaya suite.

2. Accounting for paleoclimate leads to an increase in the estimated duration of the hydrocarbon formation by 10 million years and an increase in the calculated paleotemperature maximum by 18°C, and, therefore, provides a more correct estimated density of Kiterbyutskaya oil.

3. The reliability of the results of paleotemperature modeling is confidently controlled by the geophysical criterion of the “discrepancy”, comparison with experimental data on heat flow in the study area, consistency with drilling and well testing data.

4. The results of assessing the role of Late Quaternary ice sheets (on the lands of the Yamal Peninsula) make it possible to argue the insignificant influence of the ice sheet on the thermal regime of oil source rocks of the Kiterbyutskaya suite.

5. The results obtained for the Kiterbutskaya suite of the Arctic region of Western Siberia are in complete agreement with the nature of the previously obtained estimates of the significant influence of the Mesozoic-Cenozoic climate on the geothermal regime of the Bazhenov Formation of the Yamal Peninsula.

It is important to note the following. A quick calculation of the density of the generation of the Kiterbyutskaya oil shows (Iskorkina et al., 2018) that not taking into account the paleoclimatic factors, leading to a decrease in the intensity and duration of the main oil generation phase, leads to an underestimation of the prognostic hydrocarbon resources by 30%. A similar calculation of the generation density of Bazhenov oil (Isaev et al., 2018a) showed an underestimation of the prognostic hydrocarbon resources by 40-50%. The express calculation cumulatively takes into account the times of the oil source formation in the main oil generation window.

It should be suggested why, in paleotemperature modeling of both Bazhenov and Kiterbyutskaya

maternal sediments, accounting for the ice cover had little effect on the magnitude of the calculated heat flow density from the base  $q$ , and on the intensity and duration of the main oil generation phase. This result may be explained by the fact that the temperature wave of “disturbance” of the thermal model in the upper part of the section – reaches fully to depths of about 3000 m not earlier than in 0.2-0.3 million years (Khristoforov, Abrosimova, 2012). Such a “delay” was established by us earlier (Isaev, Fomin, 2006; Osipova et al., 2015). Obviously, this “lag” is more concerned with the influence of ice caps, whose age was assumed to be no more than 0.18 Ma.

This article provides an overview of the publications of the Tomsk Research School of Geothermals, which consistently, based on borehole observations and computer modeling, develops the idea of the evolution of the geothermal conditions of oil source deposits in Western Siberia. This methodology formulates new exploration tasks that can be solved by measuring, mapping and modeling the spatial-temporal parameters of geothermal fields.

## Acknowledgments

*The authors thank Professor V.I. Starostenko and Professor M.D. Khutorskoy for the constant attention to our research.*

## References

- Demezhko D., Gornostaeva A.A. (2014). Reconstructions of long-term ground surface heat flux changes from deep-borehole temperature data. *Russian Geology and Geophysics*, 55(12), pp. 1471-1475. <https://doi.org/10.1016/j.rgg.2014.11.011>
- Duchkov A.D., Galushkin Yu.I., Smirnov L.V., Sokolova L.S. (1990). Evolyutsiya temperaturnogo polya osadochnogo chekhla Zapadno-Sibirskoi plity [The evolution of the sedimentary cover temperature field of the West Siberian Plate]. *Geologiya i geofizika = Russian Geology and Geophysics*, 10, pp. 51-60. (In Russ.)
- Fomin A.N. (2011). Katagenez organicheskogo veshchestva i neftegazonosnost' mezozoiskikh i paleozoiskikh otlozhenii Zapadno-Sibirskogo megabasseina [Catagenesis of organic matter and petroleum potential of the Mesozoic and Paleozoic sediments of the West Siberian megabasin]. Novosibirsk: INGG SO RAN, 331 p. (In Russ.)
- Galushkin Yu.I. (2007). Modelirovanie osadochnykh basseinov i otsenka ikh neftegazonosnosti [Modeling of sedimentary basins and evaluation of their oil and gas content]. Moscow: Nauchnyi Mir, 456 p. (In Russ.)
- Galushkin Yu.I. (2016). Non-standard Problems in Basin Modelling – Switzerland: Springer, 274 p.
- Golovanova I.V., Sal'manova R.Y., Tagirova C.D. (2014). Method for deep temperature estimation with regard to the paleoclimate influence on heat flow. *Russian Geology and Geophysics*, 55(9), pp. 1130-1137. <https://doi.org/10.1016/j.rgg.2014.08.008>
- Igenbaeva N.O. (2015). Resource potential and environmental risks of oil and gas development of the Northern districts of KHAMO-Yugra. *Vestnik Yugorskogo gosudarstvennogo universiteta* [Yugra State University Bulletin], S2(37), pp. 176-178. (In Russ.)
- Isaev V.I., Fomin A.N. (2006). Centers of generation of bazhenov- and togur-type oils in the southern Nyuro'l'ka megadepression. *Geologiya i geofizika = Russian Geology and Geophysics*, 47(6), pp. 734-745. (In Russ.)
- Isaev V.I., Iskorkina A.A., Kosygin V.Yu., Lobova G.A., Osipova E.N., Fomin A.N. (2017). Integrated assessment of paleoclimate factors of reconstructing thermal history of petromaternal Bazhenov suite in arctic regions of Western Siberia. *Izvestiya Tomskogo politekhnicheskogo universiteta. Inzhiniring georesursov* [Bulletin of the Tomsk Polytechnic University. Geo Assets Engineering], 328(1), pp. 13-28. (In Russ.)

- Isaev V.I., Iskorkina A.A., Lobova G.A., Fomin A.N. (2016). Paleoclimate's factors of reconstruction of thermal history of petroleum bazhenov and togur suites southeastern West Siberia. *Geofizicheskii zhurnal*, 38(4), pp. 3-25. (In Russ.)
- Isaev V.I., Lobova G.A., Stotskiy V.V., Fomin A.N. (2018). Geothermy and zoning of shale oil prospects of the Koltogor-Urengoy paleorift (southeastern part of West Siberia). *Geofizicheskii zhurnal*, 40(3), pp. 54-80. <https://doi.org/10.24028/gzh.0203-3100.v40i3.2018.137173> (In Russ.)
- Isaev V.I., Iskorkina A.A., Lobova G.A., Starostenko V.I., Tikhotskii S.A., Fomin A.N. (2018a). Mesozoic–Cenozoic Climate and Neotectonic Events as Factors in Reconstructing the Thermal History of the Source-Rock Bazhenov Formation, Arctic Region, West Siberia, by the Example of the Yamal Peninsula. *Izvestiya. Physics of the Solid Earth*, 2, pp. 310-329. <https://doi.org/10.1134/S1069351318020064> (In Russ.)
- Isaev V.I., Lobova G.A., Mazurov A.K., Starostenko V.I., Fomin A.N. (2018b). Zoning of mega-depressions by shale oil generation density of Togur and Bazhenov source suites in the southeast of Western Siberia. *Geologiya nefii i gaza = Oil and Gas Geology*, 1, pp. 15-39. (In Russ.)
- Iskorkina A.A. (2016). Paleoclimate factors of reconstructing thermal history of the petromaternal bazhenov suite of the Arctic region in Western Siberia. *Izvestiya Tomskogo politekhnicheskogo universiteta. Inzhiniring georesursov* [Bulletin of the Tomsk Polytechnic University. Geo Assets Engineering], 32(8), pp. 59-73. (In Russ.)
- Iskorkina A.A., Prokhorova P.N., Stoskiy V.V., Fomin A.N. (2018). Reconstructions of geothermal mode of the petromaternal Kiterbutsk suite of the Arctic region in Western Siberia taking into account the influence of paleoclimate. *Izvestiya Tomskogo politekhnicheskogo universiteta. Inzhiniring georesursov* [Bulletin of the Tomsk Polytechnic University. Geo Assets Engineering], 329(2), pp. 49-64. (In Russ.)
- Ivanov N.S., Gavril'ev R.I. (1965). Teplofizicheskie svoystva merzlykh gornykh porod [Thermophysical properties of frozen rocks]. M.: Nauka, 74 p.
- Khristoforov A.V., Abrosimova I.S., Burganov B.T. (2012). Interference of the temperature waves. Laboratory experiment. *Georesursy = Georesources*, 1(43), pp. 28-30. (In Russ.)
- Khutorskoi M.D., Podgorniy L.V., Suprunenko O.I., Kim B.I., Chernykh A.A. (2011). Termotomograficheskaya model' i prognoz neftegazonosnosti osadochnogo chekhla shel'fa morya Laptevykh [Thermotomographic model and oil and gas potential prediction of the sedimentary cover of the Laptev Sea shelf]. *Doklady akademii nauk = Proc. of the Academy of Sciences*, 440(5), pp. 663-668. (In Russ.)
- Khutorskoy M.D., Akhmedzyanov V.R., Ermakov A.V. et al. (2013). Geotermiya arkticheskikh morey [Geothermy of Arctic seas]. Moscow: GEOS, 232 p. (In Russ.)
- Kontorovich A.E., Burshtein L.M., Safronov P.I., Gus'kov S.A., Ershov S.V., Kazanenkov V.A., Kim N.S., Kontorovich V.A., Kostyreva E.A., Melenevskiy V.N., Livshits V.R., Malyshev N.A., Polyakov A.A., Skvortsov M.B. (2013). Historical-geological modeling of hydrocarbon generation in the Mesozoic–Cenozoic sedimentary basin of the Kara Sea (basin modeling). *Russian Geology and Geophysics*, 54(8), pp. 917-957. <https://doi.org/10.1016/j.rgg.2013.07.011> (In Russ.)
- Kurchikov A.R. (2001). Geotermicheskii rezhim uglevododorodnykh skoplenii Zapadnoi Sibiri [Geothermal regime of hydrocarbon accumulations in Western Siberia]. *Geologiya i geofizika = Russian Geology and Geophysics*, 42(11-12), pp. 1846-1853. (In Russ.)
- Kurchikov A.R., Stavitskiy B.P. (1987). Geotermiya neftegazonosnykh oblastei Zapadnoi Sibiri [Geothermy of oil and gas regions of Western Siberia]. Moscow: Nedra, 134 p. (In Russ.)
- Kuzmin Iu.A., Kuzmenkov S.G., Polukeev S.M., Novikov M.V., Korkunov V.V. (2014). Hard-to-recover oil reserves of Bazhenov deposits in KhMAO-Yugra. *Nedropol'zovanie XXI vek*, 3, pp. 56-63. (In Russ.)
- Lobova G.A., Luneva T.E., Kirillina M.S. (2018). Zoning of oil-gas potential of preJurassic reservoirs in Nyuro'l'ka megadepression (using paleotemperature modeling and drilling). *Izvestiya Tomskogo politekhnicheskogo universiteta. Inzhiniring georesursov* [Bulletin of the Tomsk Polytechnic University. Geo Assets Engineering], 329(3), pp. 123-133. (In Russ.)
- Lobova G.A., Osipova E.N., Krinitsyna K.A., Ostankova Yu.G. (2013). The effect of paleoclimate on geometry mode and oil generation potential of Bazhenov formation (at Tomsk region latitudes). *Izvestiya Tomskogo politekhnicheskogo universiteta* [Bulletin of the Tomsk Polytechnic University], 322(1), pp. 45-50. (In Russ.)
- Neftegazonosnye basseiny i regiony Sibiri [Oil and gas bearing basins and regions of Siberia] (1994). Is. 2: Zapadno-Sibirskii bassein [West Siberian basin]. Ed. A.E. Kontorovich, V.S. Surkov, A.A. Trofimuk et al. Novosibirsk: SO RAN, 201p. (In Russ.)
- Nelskamp S., Donders T., van Wess J.-D., Abbink O. (2014). Influence of Surface Temperatures on Source Rock Maturity: An Example from the Russian Artic. *ROGTEC*, 18, pp. 26-35.
- Osipova E.N., Lobova G.A., Isaev V.I., Starostenko V.I. (2015). Petroleum potential of the lower cretaceous reservoirs of Nyuro'l'ka megadepression. *Izvestiya Tomskogo politekhnicheskogo universiteta* [Bulletin of the Tomsk Polytechnic University], 326(1), pp. 14-33. (In Russ.)
- Polukeev S.M., Shpilman A.V., Kuzmin Iu.A., Korkunov V.V., Novikov M.V., Kuzmenkov S.G. (2013). Stabilization of oil production in Ugra by means of hard to recover reserves – myth or reality? *Nedropol'zovanie XXI vek*, 5, pp. 12-19. (In Russ.)
- Starostenko V.I., Kutas R.I., Shuman V.N., Legostaeva O.V. (2006). Obobshchenie statsionarnoi zadachi geotermii Releya-Tikhonova dlya gorizonta'nogo sloya [Generalization of the stationary problem of the Rayleigh-Tikhonov geothermy for a horizontal layer]. *Izvestiya. Physics of the Solid Earth*, 12, pp. 84-91. (In Russ.)
- Stratigrafiya neftegazonosnykh basseinov Sibiri [Stratigraphy of Siberian oil and gas basins] (2002). Book 9: Kainozoi Zapadnoi Sibiri [Cenozoic of Western Siberia]. Ed. V.S. Volkova. Novosibirsk: SO RAN, 246 p. (In Russ.)
- Tissot B.P. (2003). Preliminary Data on the Mechanisms and Kinetics of the Formation of Petroleum in Sediments. Computer Simulation of a Reaction Flowsheet. *Oil & Gas Science and Technology – Rev. IFP*, 58(2), pp. 183-202.
- Volkova V.S. (2011). Paleogene and Neogene stratigraphy and paleotemperature trend of West Siberia (from palynologic data). *Russian Geology and Geophysics*, 52(7), pp. 709-716. <https://doi.org/10.1016/j.rgg.2011.06.003>

## About the Authors

**Valery I. Isaev** – DSc (Geology and Mineralogy), Professor, Department of Geology, School of Earth Sciences & Engineering, National Research Tomsk Polytechnic University; Leading Researcher, Department of Oil and Gas, Ugra State University  
30, Lenin Ave., Tomsk, 634050, Russian Federation  
Phone: +7 (3822) 701-777 ad. 2942  
E-mail: isaevvi@tpu.ru

**Albina A. Iskorkina** – PhD (Geology and Mineralogy), Expert of the Information-Analytical Department  
National Research Tomsk Polytechnic University  
30, Lenin Ave., Tomsk, 634050, Russian Federation

**Galina A. Lobova** – DSc (Geology and Mineralogy), Associate Professor, Department of Geology, School of Earth Sciences & Engineering  
National Research Tomsk Polytechnic University  
30, Lenin Ave., Tomsk, 634050, Russian Federation

**Tatyana E. Luneva** – PhD Student, Department of Geology, School of Earth Sciences & Engineering  
National Research Tomsk Polytechnic University  
30, Lenin Ave., Tomsk, 634050, Russian Federation

**Elizaveta N. Osipova** – PhD (Geology and Mineralogy), Associate Professor, Department of Geology, School of Earth Sciences & Engineering  
National Research Tomsk Polytechnic University  
30, Lenin Ave., Tomsk, 634050, Russian Federation

**Roman Sh. Ayupov** – PhD (Engineering), Head of the Oil and Gas Department, Institute of Environmental Management  
Ugra State University  
16, Chekhov st., Khanty-Mansiysk, 628012, Russian Federation



*Natalya O. Igenbaeva* – PhD (Geography), Associate Professor, Oil and Gas Department, Institute of Environmental Management  
Ugra State University  
16, Chekhov st., Khanty-Mansiysk, 628012, Russian Federation

*Alexander N. Fomin* – DSc (Geology and Mineralogy), Head of the Laboratory of Oil and Gas Geochemistry  
Trofimuk Institute of Petroleum Geology and Geophysics of Siberian Branch of Russian Academy of Sciences  
3, Ak. Koptug ave., Novosibirsk, 630090, Russian Federation

*Manuscript received 20 June 2018;*

*Accepted 16 August 2018;*

*Published 30 November 2018*



# The study of the relationship between thermal conductivity and porosity, permeability, humidity of sedimentary rocks of the West Siberian Plate

A.D. Duchkov\*, D.E. Ayunov, S.V. Rodyakin, P.A. Yan

*Trofimuk Institute of Petroleum Geology and Geophysics of Siberian Branch of Russian Academy of Sciences, Novosibirsk, Russian Federation*

**Abstract.** The determination of correlation between thermal conductivity and structural parameters (porosity, permeability, humidity) of sedimentary rocks is a very urgent task. This article analyzes and compares the results of measurements of these parameters for ~300 samples of Mesozoic sandstones and siltstones from the core of 18 wells drilled in the north-eastern and southern regions of the West Siberian plate. The thermal conductivity of all samples was measured in the dry state and some (90 samples) – after saturation with water. Porosity and permeability are determined for 280 and 230 samples, respectively. The obtained data are used to establish linear correlation connections between thermal conductivity, porosity and permeability. The most interesting are rather stable dependences of thermal conductivity of dry and water-saturated samples between themselves and with porosity. The established correlation dependences are interesting in practical terms. Some of them can be used to approximate the thermal conductivity of water-saturated rocks by measurements of dry rocks or even only by the porosity value. The relationship between the thermal conductivity of sedimentary rocks and porosity can be used for rapid assessment of porosity of rocks on advanced measurements of thermal conductivity of a full-size core. It is obvious that the revealed correlation connections require further clarification.

**Keyword:** West Siberian plate, Mesozoic sandstones and siltstones, thermal conductivity, porosity, permeability, humidity, correlation dependence

**Recommended citation:** Duchkov A.D., Ayunov D.E., Rodyakin, S.V., Yan P.A. (2018). The study of the relationship between thermal conductivity and porosity, permeability, humidity of sedimentary rocks of the West Siberian Plate. *Georesursy = Georesources*, 20(4), Part 2, pp. 396-403. DOI: <https://doi.org/10.18599/grs.2018.4.396-403>

## Introduction

The thermal conductivity coefficient (hereinafter thermal conductivity,  $\lambda$ ) quantitatively characterizes the process of heat transfer in the material (rock). This parameter (as well as other thermal properties – thermal diffusivity, heat capacity) is necessary when estimating heat flow and depth temperatures, when performing thermo-hydrodynamic and basin modeling, and calculating heat exchange processes in rocks. It should be noted that, until now, all information on the thermal conductivity of rocks is based on the study of core samples in laboratory conditions, as it is not yet possible to develop reliable equipment for measuring thermal properties of rocks directly in wells (Novikov et al., 2008).

The results of measurements of thermal conductivity of rocks of the sedimentary cover of the West Siberian Plate, obtained from studying the heat flow, are

summarized and analyzed in a number of monographs (Kurchikov, Stavitskii, 1987; Teplovoe pole nedr Sibiri..., 1987; Balobaev, 1991, Lipaev et al., 2001). Analysis of the results showed that the thermal conductivity of sedimentary rocks is determined by the composition of the mineral skeleton, porosity ( $\phi$ ) and permeability ( $k$ ) of the rock, as well as the type of fluid that fills the pores (air, water, oil). Thus, the thermal conductivity of water-saturated samples ( $\lambda_w$ ) usually significantly exceeds the thermal conductivity of the same, but dry samples ( $\lambda_s$ ), which is explained by the multiple difference in thermal conductivity of water and air (0.6 and 0.025 W/m/K, respectively). To estimate  $\lambda_w$ , it is necessary to saturate the dry samples with water and repeat the measurements, i.e. significantly complicate the experiments. In this regard, a very urgent task is to determine the correlation dependences between  $\lambda_s$  and  $\lambda_w$ , as well as between  $\lambda_s$ ,  $\lambda_w$  and structural parameters (porosity and permeability) of rocks, which would allow to evaluate, even if roughly, the missing data. Accumulated during the study of heat flow information on the thermal conductivity of sedimentary rocks of the West Siberian Plate is largely

\*Corresponding author: Albert D. Duchkov  
E-mail: [duchkovad@ipgg.sbras.ru](mailto:duchkovad@ipgg.sbras.ru)

© 2018 The Authors. Published by Georesursy LLC  
This is an open access article under the CC BY 4.0 license  
(<https://creativecommons.org/licenses/by/4.0/>)

unsuitable for establishing correlations due to problems with the selection of samples collections and differences in equipment and measurement techniques.

The situation noticeably changed after high-performance instruments were created and widely used in the Russian Federation that allow rapid measurements of thermal properties of rocks: Thermal Comparator, TK (Kalinin et al., 1983) and especially Scanning Thermal Measuring Meter, ITS (Popov et al., 1983; Nikitin et al., 2016). These devices are equally metrologically provided (use one set of standards). Approximately the same for these devices and the depth of penetration of the heat signal into the rock (about 10 mm). All this allows us to reasonably compare the results obtained by these devices. The use of this equipment led, in a relatively short time, to a significant increase in the amount of experimental data (including in Western Siberia). The most detailed studies of the thermal properties of sedimentary rocks of the West Siberian Plate were carried out in 1995-2008 by the team of Yu.A. Popov. First of all, it is necessary to note the study of hundreds of samples of sandstones, aleurolites, basalts from the full-sized core of ultra-deep Tyumen well (SG-6) and En-Yakhinskaya well (SG-7) (Popov, et al., 1996; Popov et al., 2008). These works made it possible to form a general idea of the change in the thermal conductivity of rocks in almost the entire section (from Cretaceous to Triassic deposits) of the sedimentary cover of the West Siberian Plate. In the same period, studies were carried out to study the relationship between the thermal conductivity of sedimentary rocks and other physical properties on a specially selected collection of samples from the core of the Middle-Ob region wells (Popov et al., 2003). The collection consisted of 143 samples of sandstones and aleurolites of the Cretaceous and Jurassic age from a depth of 1360-3000 m. The porosity of the samples varied from 9.6 to 30.4%, and the permeability was 0.01-200 mD. All measurements of thermal conductivity were performed on the device ITS. The authors (Popov et al., 2003) studied dry and water-saturated standard samples with a diameter of 2.5 cm and a length of 3 cm, cut from a full-sized core along and across the layering. Accordingly, the authors obtained the values of thermal conductivity along ( $\lambda_l$ ) and across ( $\lambda_\perp$ ) lamination and showed that the average values of  $\lambda_l$  were greater than  $\lambda_\perp$  by about 20%. The authors trust the  $\lambda_l$  values more, since this component is less affected by the deconsolidation caused by decompression. The thermal conductivity of dry samples varied from 1 to 2.76 W/m/K, and water-saturated from 1.3 to 3.4 W/m/K. Analysis of the results allowed us to reveal fairly close linear and exponential dependencies connecting the thermal conductivity of samples with their porosity and permeability. For example, one can give two regression equations:

$$\lambda_w/\lambda_s = 0,87 + 0,04 \cdot \phi \quad (R^2=0,75, N=143), \quad (1)$$

$$\lambda_w/\lambda_s = 0,95 + 0,03 \cdot \phi \quad (R^2 = 0,72), \quad (2)$$

which are obtained in (Popov et al., 2003; Popov et al., 2008), respectively. In these formulas (and subsequent ones),  $R^2$  is a parameter characterizing the degree of reliability of the linear approximation;  $N$  is the number of measured samples;  $\phi$  is in %.

We have obtained new data on the thermal conductivity of two collections of samples of sedimentary rocks of the same composition and age from cores of wells drilled in the northeast and southern regions of the West Siberian Plate. These collections are divided not only by geography, but also by the type of instrument used to measure thermal conductivity. In both cases, the thermal conductivity was measured on standard cores cut from a full-sized core perpendicular to its axis (parallel to lamination) and having a diameter and height of about 3.7-3.8 mm. This report discusses the results of these studies.

### **Collection 1 – samples from the core of the wells of the north-eastern part of the West Siberian plate**

#### ***Collection 1 overview***

Collection 1 includes 129 samples of Cretaceous and Jurassic sandstones and siltstones from cores of seven wells (Medvezhya-31, Suzunskaya-4, Gorchinskaya-1, Yuzhno-Noskovskaya-318, Deryabinskaya-9, Vostok-1, 3), drilled mainly in the North-East West-Siberian plate. The location of the wells and the primary results of the measurements are indicated in the work (Duchkov et al., 2013). The collection covers part of the section from 1,800 to 4,200 m. For measurements of  $\lambda$ , a “Thermal Comparator” (Kalinin et al., 1983) was used, the sensor of which was located at the ends of standard cores, regardless of the location of the layers in the core. First, the thermal conductivity of all samples was measured in the air-dry state ( $\lambda_s$ ). Then, a part of the collection (90 samples) was saturated with water according to the standard method and the  $\lambda_w$  values were measured. For 93 and 53 samples measured by the  $\phi$  and the  $k$ , respectively. The porosity of the rocks in the samples varies from 1 to 29% (mostly from 4 to 15%), and the permeability – from <0.001 to 440 mD (one sample – 1117 mD). In general, the thermal conductivity of dry samples varies from 0.6 to 2.6 W/m/K. According to the histogram (Fig. 1), the average value of  $\lambda_s$  is 1.8-2 W/m/K.

After saturation with water, the thermal conductivity of samples increases on average by 20-40% and varies from 1.6 to 3.2 W/m/K. The average value of  $\lambda_w$  is 2.6-2.8 W/m/K (the ratio of  $\lambda_w/\lambda_s$  varies from 1.1 to 2.1). Saturation of rocks with water leads not only to an increase in their thermal conductivity, but also to a relative leveling of its values along the section. The



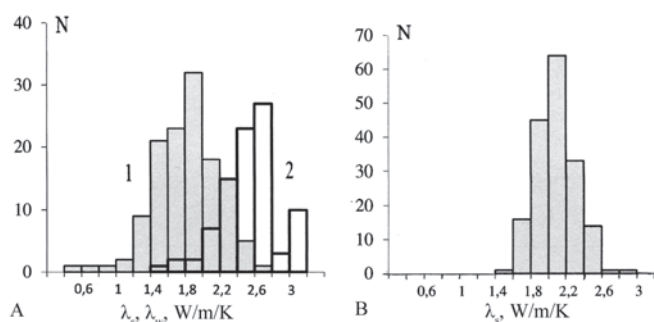


Fig. 1. Histograms of thermal conductivity values of Mesozoic sandstones and aleurolites from the core of the northeastern (Collection 1, A) and southern (Collection 2, B) parts of the West Siberian Plate: A1 – dry samples ( $N = 129$ ), A2 – saturated samples ( $N = 93$ ), B – dry samples ( $N = 175$ ).  $N$  is the number of samples

Cretaceous and Jurassic formations are virtually identical in thermal conductivity.

The obtained results were used to search for correlations between the measured parameters  $\lambda_s$ ,  $\lambda_w$ ,  $\lambda_w/\lambda_s$ ,  $\phi$  and  $k$ .

A direct comparison of  $\lambda_s$  and  $\lambda_w$  shows the presence of a fairly close positive correlation dependence between them (Fig. 2):

$$\lambda_w = 1,52 + 0,56 \lambda_s (R^2 = 0,51, N = 90). \quad (3)$$

Some statistical data characterizing dependence (1) are given in the caption inscription to Figure 2. The scatter of the points of the correlation field is associated with the effect on thermal conductivity, in addition to porosity and fluid type, unaccounted changes in the mineral composition and structural and textural features of the rock.

As already noted, the thermal conductivity of sedimentary rocks is largely determined by their porosity ( $\phi$ ). There is an inverse linear relationship between these parameters. The regression equation obtained by measuring the  $\lambda_s$  and  $\phi$  samples from

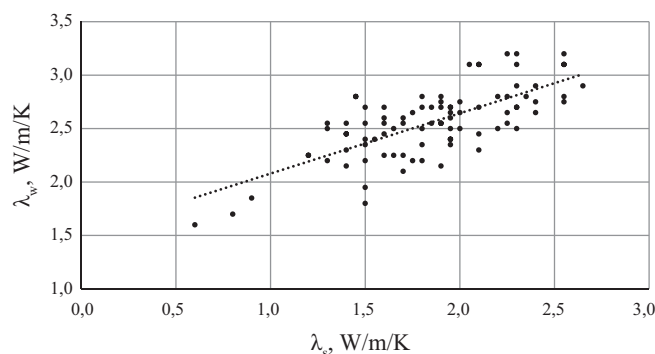


Fig. 2. Collection 1. Linear correlation between the measured values of  $\lambda_s$  and  $\lambda_w$ . The linear regression equation (line):  $\lambda_w = 1.52 + 0.56 \lambda_s$  ( $R^2 = 0.51$ ,  $N = 90$ ). The standard deviation of individual values of  $\lambda_w$  from the regression line is 0.26 W/m/K. Hereinafter,  $R^2$  is a parameter characterizing the degree of reliability of linear approximation;  $N$  is the number of samples

Collection 1 has the form:

$$\lambda_s = 2,43 - 0,05 \phi (R^2 = 0,54, N = 93). \quad (4)$$

Most  $\phi$  measurements were performed on samples with a porosity in the range of 5-15%. This interval  $\phi$  is characterized by the largest scatter of measured values of  $\lambda_s$  (the standard deviation of individual values of  $\lambda_s$  from the regression line is 0.35 W/m/K). When interpreting the relationship of thermal conductivity with  $\phi$ , it should be borne in mind that  $\lambda$  responds to changes in total porosity (the total volume of all pores). When measuring porosity, open porosity is usually recorded on samples, depending on the volume of communicating pores.

The correlation between the values of  $\lambda_w$  and  $\phi$  is much weaker, since in this case the contrast of thermal conductivity of the rock matrix and the filling fluid is much less than in dry rocks:

$$\lambda_w = 2,95 - 0,03 \phi (R^2 = 0,34, N = 54). \quad (5)$$

Formulas (3-5) can be used for a rough estimate of  $\lambda_s$  by the values of  $\phi$ , and as well for the thermal conductivity of water-saturated samples by the values of  $\lambda_s$  or even just  $\phi$ . This is necessary in cases where thermal conductivity measurements cannot be performed due to the lack of equipment or suitable core samples. Using the formula (4), we can estimate the average thermal conductivity of the mineral skeleton (matrix) of the samples ( $\lambda_m$ ), setting  $\phi = 0$ . In the rocks of our collection  $\lambda_m$  is 2.5 W/m/K.

In the works (Popov et al., 2003; Popov et al., 2008), it was suggested to use the ratio  $\lambda_w/\lambda_s$  for studying correlation relationships. Figure 3 shows the correlation between this parameter and  $\phi$  according to our data. The regression equation is:

$$\lambda_w/\lambda_s = 1,04 + 0,03 \cdot \phi (R^2 = 0,69, N = 54). \quad (6)$$

Obviously, this correlation dependence is the most reliable of those given earlier (parameter  $R^2$  has a maximum value), and it also corresponds well to equations (1) and (2) obtained from studying collections of rocks from other regions of the West Siberian Plate.

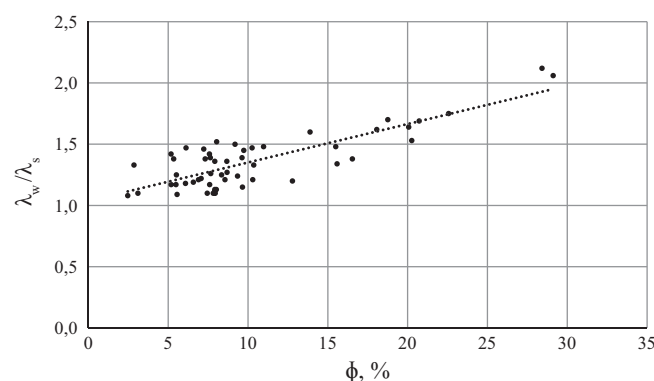


Fig. 3. Collection 1. Linear correlation between the values of the ratio of thermal conductivity of water-saturated and dry samples ( $\lambda_w/\lambda_s$ ) and their porosity. The linear regression equation:  $\lambda_w/\lambda_s = 1.04 + 0.03 \phi$  ( $R^2 = 0.69$ ;  $N = 54$ )

The dependence can be used to estimate the thermal conductivity of water-saturated sedimentary rocks by the values of  $\lambda_s$  and  $\phi$ .

It is known that between porosity and permeability of sedimentary rocks there is a correlation. Accordingly, there should be a correlation relationship between thermal conductivity and permeability. This was confirmed in (Popov et al., 2003), in which the values of  $\lambda_w/\lambda_s$  and  $k$  were compared for 60 rock samples from the core of the Middle-Ob region wells and an exponential increase of  $\lambda_w/\lambda_s$  from 1.3 to 2.3 was found as permeability from 0.03 to 100 mD (the correlation equation is not given in this work). We verified the existence of correlations between  $\lambda_s$ ,  $\lambda_w$ ,  $\lambda_w/\lambda_s$ , and  $k$  using the data we have. Previously it was stated that the permeability of 93 samples from Collection 1 basically varied from <0.001 to 440 mD. More than half of the samples are poorly permeable rocks ( $k < 0.001$ ), which must be excluded during the correlation. Due to the significant range of changes in permeability, the logarithm ( $\lg k$ ) is normally used to represent it. As a result, the equation for the inverse linear correlation between  $\lambda_s$  and  $k$  for 53 samples has the form similar to (4):

$$\lambda_s = 1,8 - 0,21 \cdot \lg k \quad (R^2 = 0,37, N = 53), \quad (7)$$

where the dimension  $k$  is in mD. With an increase in permeability (and porosity) in the rock, the amount of air that conducts heat poorly increases, and, accordingly, the effective thermal conductivity of the sample decreases.

For a smaller amount of data (26 samples in total), the correlation between the thermal conductivity of water-saturated rocks ( $\lambda_w$ ,  $\lambda_w/\lambda_s$ ) and their permeability was considered. The corresponding regression equations are:

$$\lambda_w = 2,58 - 0,15 \cdot \lg k \quad (R^2 = 0,29, N = 26) \text{ K}, \quad (8)$$

$$\lambda_w/\lambda_s = 1,44 + 0,13 \cdot \lg k \quad (R^2 = 0,41, N = 25) \text{ K}. \quad (9)$$

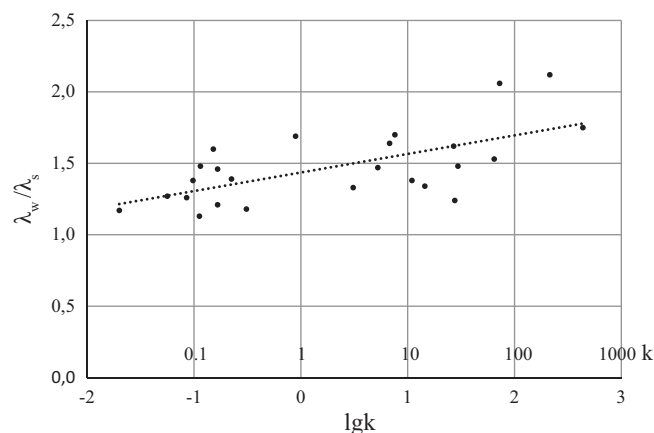


Fig. 4. Collection 1. Linear inverse correlation between the measured values of thermal conductivity of samples ( $\lambda_w/\lambda_s$ ) and their permeability ( $k$  in mD;  $\lg k$ ). Regression equation:  $\lambda_w/\lambda_s = 1,44 + 0,13 \cdot \lg k$  ( $R^2 = 0,41$ ;  $N = 25$ )

The most stable last correlation is shown in Fig. 4. It follows from equation (9) that, according to our data,  $\lambda_w/\lambda_s$  increases from 1.2 to 1.9 as  $k$  increases from 0.03 to 100 mD, i.e. noticeably slower than according to the work (Popov et al., 2003).

It was noted above that the correlation equations (3, 5, 6) can be used to approximate the thermal conductivity of water-saturated samples of sedimentary rocks by the values of  $\lambda_s$  and  $\phi$ . As an example, such calculations were performed by us for samples from the Vostok wells, the results of measurements and calculations are shown in Table 1 (Duchkov et al. 2014). First, the calculated values of  $\lambda_w^*$  by  $\lambda_s$  (Eq. (3)). Then, parameter  $\phi$  determines the values of  $\lambda_w^{**}$  (Eq. (5)). And, finally, the  $\lambda_w^{***}$  values are calculated from  $\lambda_s$  and  $\phi$  (Eq. (6)).

A comparison of the experimental and calculated values of  $\lambda_w$  shows that the difference between them for individual samples can be significant. And this is not surprising, since the regression equation allows us to estimate only the average of several  $\lambda_w$ , corresponding to one particular value of  $\lambda_s$  or  $\phi$ , or their combination. However, the average calculated values of  $\lambda_w$  for all samples differ from the experimental average by no more than 3-5%. It is clear that the estimated results for samples of rocks not included in our collection may be somewhat worse. But in any case, when conducting geothermal studies (for example, studying heat flow, calculating deep temperatures), it is more expedient to use the calculated values of  $\lambda_w$  (they will be much closer to the truth) than the thermal conductivity of dry samples. This is especially true for sedimentary rocks with high porosity.

	Sampling depth, m	, %	Thermal conductivity, W/m/K				
			s	w	* w	** w	*** w
1	2058	28,33	0,6	1,6	1,8	2	1,3
2	2067	29,12	0,9	1,85	2,0	2	1,9
3	2072	28,42	0,8	1,7	2,0	2	1,6
4	2127	12,79	1,5	1,8	2,4	2,5	2,2
5	2299	13,89	1,5	2,4	2,4	2,5	2,3
6	2317	18,76	1,5	2,55	2,4	2,3	2,5
7	2472	7,6	2,1	2,45	2,7	2,7	2,7
8	2520	20,73	1,3	2,2	2,2	2,3	2,3
9	2528	20,07	1,4	2,3	2,3	2,3	2,4
10	2617	20,26	1,6	2,45	2,4	2,3	2,8
11	2679	18,07	1,6	2,6	2,4	2,4	2,7
12	2744	22,57	1,4	2,45	2,3	2,2	2,6
13	2806	16,54	1,85	2,55	2,6	2,4	3,0
14	3067	15,58	1,9	2,55	2,6	2,4	3,0
15	3184	15,5	2,1	3,1	2,7	2,5	3,3
Average				2,33	2,35	2,32	2,44

Table 1. Measured and calculated by the formulas (3, 5, 6) values of thermal conductivity of samples of water-saturated rocks from Mesozoic sediments exposed by the Vostok-1 (samples No. 1-6, 10-12) and Vostok-3 (samples No. 7-9, 3-15) wells;  $\lambda_s$ ,  $\lambda_w$ ,  $\phi$  – measured values of thermal conductivity and porosity;  $\lambda_w^*$ ,  $\lambda_w^{**}$  and  $\lambda_w^{***}$  are the values of thermal conductivity calculated by the formulas (3, 5, 6), respectively

## Collection 2 – samples from the cores from the wells located in the southern part of the West Siberian plate

### Collection 2 Overview

Collection 2 includes 175 samples of sandstones and aleurolites of Jurassic age selected from cores of 10 wells (Biazinskaya-1, Kasmanskaya-1,2; Nadezhdinskaya-1, Optimistic-1, Pogranichnaya-2, Rakitinskaya-4,5,7; Uzasskaya-1), drilled in the southern part of the plate (Novosibirsk region). The collection contains samples from the Tyumen ( $J_{1-2}$ ) and Vasyugan ( $J_3$ ) suites, approximately in equal proportions (96 and 79 samples) from depths of 2430-2780 m. Thus, the studied collections significantly differ not only in the number of samples taken, but also according to the size of the sampling interval (Collection 1 – 2400 m interval, 129 samples were selected; Collection 2 – 350 m interval, 175 samples were selected). As before, standard cores were studied – cylinders cut from a full-sized core perpendicular to its axis (parallel to lamination) and having a height and diameter of about 37-38 mm. In the course of the research, the thermal conductivity of only dry cores was measured, and their porosity and permeability were determined. It was found that  $\phi$  varies from 0.54 to 19.3%,  $k$  – from <0.001 to 120 mD. An ITS device was used to measure thermal conductivity (Popov et al., 1983). Scanning took place along the axis of the standard core. At the same time, the position of the scanning line relative to the stratification of the core was not specifically tracked (as in the study of Collection 1).

The thermal conductivity of dry cores varies from 1.4 to 2.9 W/m/K, the average value of  $\lambda_s$  is 2.1 W/m/K. The samples taken from the Tyumen ( $J_{1-2}$ ) and Vasyugan ( $J_3$ ) suites are almost identical in thermal conductivity: 1.70-2.63 and 1.45-2.57 W/m/K, respectively. According to the histogram (Fig. 1), the bulk of the samples from Collection 2 has a thermal conductivity of 2.0-2.2 W/m/K, i.e. about 0.2 W/m/K higher than the main group of samples Collection 1. Thus, it should be stated that, in terms of average thermal conductivity, dry samples of the same type and same age rocks gathered in two collections representing different, fairly distant parts of West Siberian plates differ by about 10%. It can be assumed that this difference is associated with the use of different thermal conductivity meters (TK and ITS) in the study of Collections 1 and 2. However, the data presented in the work (Popov et al., 2003) do not seem to confirm this assumption. According to these data, dry sandstones and aleurolites from the upper Jurassic and lower Cretaceous of the Middle-Ob region are characterized (measured on ITS) with an average thermal conductivity of about 1.7-1.8 W/m/K different from our estimates. In this regard, it is possible that the described variations in the mean values of  $\lambda$  are

associated with changes in the mineral composition and structural features of the rocks in the sections of different regions. This problem requires a special, more detailed, consideration. From the identified differences, we can conclude that the data obtained from several collections of samples should be interpreted separately and only then be solved the question of combining them. Below we will show it on the example of data for the Collection 2.

### Correlations between $\lambda_s$ and $\phi$ , $k$

When studying the samples of Collection 2, only the values of  $\lambda_s$ ,  $\phi$ , and  $k$  were measured. When comparing 170 pairs of  $\lambda_s$ ,  $\phi$  values, a correlation dependence is obtained, the regression equation of which has the form:

$$\lambda_s = 2,47 - 0,04 \cdot \phi \quad (R^2 = 0,43; N = 170). \quad (10)$$

Comparison of equations (4) and (10) shows that they are completely identical. This allows one to add the measurement results of  $\lambda_s$ ,  $\phi$  for both collections and to obtain the correlation dependence of the sum of the data (Fig. 5). The regression equation for the total dependence is:

$$\lambda_s = 2,49 - 0,05 \cdot \phi \quad (R^2 = 0,5; N = 263). \quad (11)$$

Thus, despite the differences in the sampling sites of Mesozoic sandstones and aleurolites of the West Siberian Plate and their quantity, identical correlation dependences between the measured values of  $\lambda_s$  and  $\phi$  were obtained (equations (4, 10, 11)). It would be interesting to check the stability of this dependence on the collections of other samples.

From equation (11) it follows that the thermal conductivity of the mineral skeleton  $\lambda_m$  ( $\lambda_s$  value at  $\phi = 0$ ) of samples from Collections 1 and 2 is the same and is 2.5 W/m/K (Fig. 5). At the same time, judging by the work (Popov et al., 2003), rocks similar to the type and age from Middle-Ob region should differ significantly in the composition of the mineral skeleton, since their average  $\lambda_m$  is 3.2-3.6 W/m/K, i.e. much higher than our values.

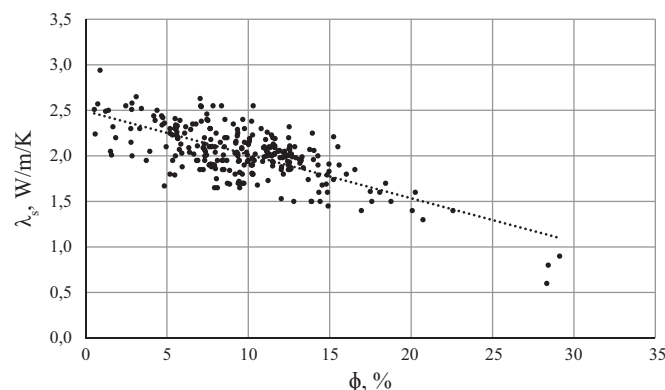


Fig. 5. Linear inverse correlation dependence between the measured values of thermal conductivity ( $\lambda_s$ ) and ( $\phi$ ) of all samples from Collections 1 and 2. Regression equation:  $\lambda_s = 2.49 - 0.05\phi$  ( $R^2 = 0.5$ ;  $N = 263$ )



As already noted, the permeability of rocks in the Collection 2 (173 samples) varies from  $<0.001$  to 120 mD. After elimination of poorly permeable rocks ( $<0.001$  mD), 109 samples remain in Collection 2, and the correlation relationship between  $\lambda_s$  and  $\lg k$  and the corresponding regression equation are determined:

$$\lambda_s = 2 - 0,13 \lg K_{np} \quad (R^2 = 0,17; N = 109). \quad (12)$$

Despite the greater number of samples measured, this correlation dependence is generally less reliable ( $R^2 = 0.17$ ) than that obtained earlier in the study of Collection 1 (equation (7),  $R^2 = 0.37$ ). A comparison of the correlation equations (formulas (7) and (12)) shows that the regression lines in both cases have approximately the same slope, but are shifted relative to each other by approximately 0.2 W/m/K. In this situation, combining these two collections is not reasonable.

### Factors affecting the type of correlation relationship between $\lambda_s$ and $\phi$

All the obtained correlation dependences are characterized by a significant scatter of data. To clarify the causes of variation, the authors checked according to Collection 2 data the influence of a number of factors (permeability, the content of cement and quartz with  $\lambda = 7.7$  W/m/K). This became possible, since all samples of the Collection 2 were subjected, among other things, to petrographic analysis.

To test the effect of the permeability factor, the samples were divided into three groups: “poorly permeable” ( $<0.001$  mD), “medium permeable” (0.2-3 mD), and “high permeable” ( $>3$  mD). For each group of samples, the presence of correlations between  $\lambda_s$  and  $\phi$  was checked (Fig. 6).

It was established that a relatively small sets of “high-permeable” samples shows the maximum variation of porosity values for samples with close thermal conductivity and does not reveal a correlation link between  $\lambda_s$  and  $\phi$ . The rest of the sets are characterized by fairly stable, having the same slope correlation

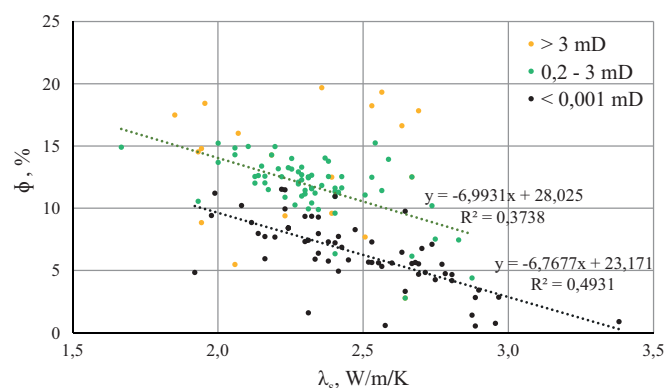


Fig. 6. Collection 2. Connections between porosity and thermal conductivity and linear trends for groups of “poorly permeable”, “medium-permeable” and “high-permeable” samples

dependencies between the studied parameters. However, they are shifted relative to each other so that the porosity of “poorly permeable” samples is lower by 5% than  $\phi$  “medium-permeable” samples with the same thermal conductivity.

The study of the effect of the cement content in samples (clay and carbonate) was carried out separately for the groups of “poorly permeable” and “medium-permeable” samples. In each group, three sets of samples were considered on the cement content in the mineral skeleton: less than 10%, 10-30% and more than 30%. Again, the correlation dependences between  $\lambda_s$  and  $\phi$  were constructed from these groups. In all sets of both samples groups, close correlation dependences between the studied parameters were found.

The study of the effect of quartz content in the samples was also conducted separately for the groups of “medium-permeable” and “poorly permeable” samples. According to the total content of quartz in the mineral skeleton, three sets were taken: less than 25%, 25-50% and more than 50%. On the correlation diagram,  $\lambda_s$  and  $\phi$ , the samples showed no obvious differences. Thus, it can be stated that of the three different factors considered (permeability, cement and quartz content), it is permeability that has the main influence on the nature of the correlation dependence between  $\lambda_s$  and  $\phi$ . When constructing such a relationship, it is desirable to remove from the samples the values of  $\lambda_s$  obtained for samples whose permeability exceeds 3 mD. It is likely that these conclusions are valid for the other correlation dependences considered in the article.

### Conclusion

In the course of the research, two collections of samples (a total of ~ 300 samples) of sedimentary rocks from core 17 wells drilled in the north-east and southern regions of the West Siberian Plate were studied. Two devices – Thermal comparator (Kalinin et al., 1983) and Scanning thermal conductivity meter (Popov et al. 1983) – have been used to measure the thermal conductivity of all samples in a dry state and some (90 samples) after saturation with water. Porosity and permeability are determined for 280 and 230 samples, respectively. Studies have shown, as should be expected, that the thermal conductivity of sedimentary rocks is determined primarily by the porosity and type of fluid (air, water) that saturates the pores. In our experiments, after saturation with water, the thermal conductivity of sedimentary rocks (average porosity 12-15%) increased on average by 20-40%. This shows how important it is to use the corresponding values of the thermal conductivity for different geothermal calculations, at least assessed by empirical correlation. The relevance of experimental research in the scouting for such connections between thermal conductivity and

its determining factors is unquestionable. We used our data to establish relationships between  $\lambda_s$  and  $\lambda_w$ ,  $\phi$ ,  $\lg k$ ;  $\lambda_w$  and  $\phi$ ,  $\lg k$ ;  $\lambda_w/\lambda_s$  and  $\phi$ ,  $\lg k$ . All the resulting regression equations for convenience are summarized in Table 2 with the numbers of the regression equations preserved.

First of all, it is necessary to note the presence of stable ( $R^2 = 0.43-0.54$ ) bonds  $\lambda_s$  with  $\lambda_w$  and  $\phi$ . The same correlation dependences  $\lambda_s$  and  $\phi$  (equations 4, 10, 11) for both collections and their sum were obtained, despite the different numbers of samples in the sets (93-263 samples) and the places of their selection. At the same time, it should be pointed out that in all studied samples, Mesozoic sedimentary rocks of the same type and age are presented. Therefore, an urgent task is to check the indicated relationships  $\lambda_s$  and  $\phi$  on collections involving other sediments.

Significantly less in the considered collections of samples for which there are measured values of  $\lambda_w$  and  $\phi$ . However, it is for them that the most stable connection ( $R^2 = 0.68$ ) between  $\lambda_w/\lambda_s$  and  $\phi$  was obtained. The corresponding regression equation (6) satisfactorily corresponds to the correlations (1 and 2) obtained earlier for other regions of the West Siberian Plate (Popov et al., 2003; Popov et al., 2008). In these works, the opinion is expressed that the correlations between  $\lambda_w/\lambda_s$  and  $\phi$  are inherent in different types of rocks, which probably indicates their universal character for sedimentary rocks.

It was not possible to obtain stable correlations between thermal conductivity and permeability of samples. So, for 109 dry samples of Collection 2, a regression equation was obtained (equation 12), for which the degree of reliability of the linear

approximation  $R^2$  is only 0.17. The relationship between permeability and thermal conductivity of water-saturated rocks (equations 8, 9) is somewhat more stable, but they were obtained in just 26 samples.

The considered correlation dependences are undoubtedly of practical interest. First, some of them (equations 3-6) can be used for an approximate estimate of  $\lambda_w$  from the measured values of thermal conductivity of dry rocks or only their porosity. The example given in the article (Table 1) showed that in this case one can get results that correspond to the measured ones.

A very important fact is the presence of correlations of thermal conductivity of dry sedimentary rocks with their porosity and permeability. Thus, the established relationship (equation 11) can be used to quickly estimate the porosity of rocks using previously measured  $\lambda_s$  values. Hence, using anticipatory measurements of  $\lambda_s$  of the core, it is possible to identify highly porous rock intervals, which can be further studied in more detail by traditional methods. To apply this technique, it will be necessary to measure the thermal conductivity of a full-sized core (better than air-dry) and, using the correlation links  $\lambda_s$  with  $\phi$ , to estimate changes in the porosity of rocks with depth. Thermal conductivity of dry rocks is measured much easier and faster than porosity (and permeability), especially when using modern express equipment such as ITS.

It is obvious that the identified correlations, which are of great importance for the rapid assessment of the thermal and structural properties of sedimentary rocks, require further clarification. It is necessary to continue the work on increasing the volume of samples of measured parameters for different types of rocks and geological provinces, as well as analyzing and refining the correlation dependencies considered in the article.

## Acknowledgments

*The study was carried out according to the plan of basic research works of the Department of Geophysics, Trofimuk Institute of Petroleum Geology and Geophysics of Siberian Branch of Russian Academy of Sciences, with financial support from the Russian Foundation for Basic Research grant No. 16-35-00211.*

## References

- Balobaev V.T. (1991). Geotermiya merzloi zony litosfery severa Azii [Geothermy of the frozen zone of the lithosphere of the north of Asia]. Novosibirsk: Nauka, 194 p. (In Russ.)
- Duchkov A.D., Sokolova L.S., Ayunov D.E., Zlobina O.N. (2013). Thermal conductivity of sediments in high-latitude West Siberia. *Russian Geology and Geophysics*, 54(12), pp. 1522-1528. <https://doi.org/10.1016/j.rgg.2013.10.015> (In Russ.)
- Duchkov A.D., Sokolova L.S., Rodyakin S.V., Chernysh P.S. (2014). Thermal conductivity of the sedimentary-cover rocks of the West Siberian Plate in relation to their humidity and porosity. *Russian Geology and Geophysics*, 55(5-6), pp. 784-792. <https://doi.org/10.1016/j.rgg.2014.05.021> (In Russ.)
- Kalinin A.N., Sokolova L.S., Duchkov A.D., Cherepanov V.Ya. (1983). Issledovaniya teplovogo komparatora primenitel'no k izmereniyam

Samp. coll.	Eq. no.	Parameters	Regression equations	$R^2$	N
	1	$w/\lambda_s$	$w/\lambda_s = 0.87 + 0.04 \cdot \phi$	0,75	143
	2	$w/\lambda_s$	$w/\lambda_s = 0.95 + 0.03 \cdot \lg k$	0,85	-
1	3	$\lambda_s, w$	$w = 1,52 + 0,56 \cdot \lambda_s$	0,51	90
1	4	$\lambda_s, \phi$	$\phi = 2,43 - 0,05 \cdot \lambda_s$	0,54	93
1	5	$w, \phi$	$w = 2,95 - 0,03 \cdot \phi$	0,34	54
1	6	$w/\lambda_s$	$w/\lambda_s = 1,04 + 0,03 \cdot \phi$	0,68	53
1	7	$\lambda_s, \lg k$	$\lg k = 1,8 - 0,21 \cdot \lambda_s$	0,37	53
1	8	$w, \lg k$	$w = 2,58 - 0,15 \cdot \lg k$	0,29	26
1	9	$w/\lambda_s, \lg k$	$w/\lambda_s = 1,44 + 0,13 \cdot \lg k$	0,41	25
2	10	$\lambda_s, \phi$	$\phi = 2,47 - 0,04 \cdot \lambda_s$	0,43	170
1+2	11	$\lambda_s, \phi$	$\phi = 2,49 - 0,05 \cdot \lambda_s$	0,5	263
2	12	$\lambda_s, \lg k$	$\lg k = 2 - 0,13 \cdot \lambda_s$	0,17	109

*Table 2. Correlation dependences between thermal conductivity, porosity and permeability of samples of sedimentary rocks of the West Siberian Plate. Note: Regression equations (1 and 2) are given in (Popov et al., 2003; Popov et al., 2008), respectively. Equations (3-12) are obtained by the authors.  $R^2$  is a parameter characterizing the degree of reliability of linear approximation; N is the number of samples;  $\phi$  – in %*

teploprovodnosti gornykh porod [Research of the thermal comparator in relation to measurements of thermal conductivity of rocks]. *Geologiya i geofizika = Geology and Geophysics*, 3, pp. 116-122. (In Russ.)

Kurchikov A.R., Stavitskii B.P. (1987). Geotermiya neftegazonosnykh oblastei Zapadnoi Sibiri [Geothermy of oil and gas regions of Western Siberia]. Moscow: Nedra, 134 p. (In Russ.)

Lipaev A.A., Gurevich V.M., Lipaev S.A. (2001). Teplovyie svoistva gornykh porod neftyanykh mestorozhdenii Tatarstana [Thermal properties of rocks of oil fields of Tatarstan]. Kazan: KMO Publ., 205 p. (In Russ.)

Nikitin D.S., Khutorskoi M.D., Nikitin A.S. (2016). Beskontaktnye izmereniya teplofizicheskikh svoistv gornykh porod na ustanovke TS14 [Non-contact measurements of thermal-physical properties of rocks on TC14 device]. *Protsessy v geosredakh = Processes in GeoMedia*, 3(7), pp. 246-254. (In Russ.)

Novikov S.V., Popov Yu.A., Tertychnyi V.V. et al. (2008). Vozmozhnosti i problemy sovremennoogo teplovogo karotazha [Opportunities and problems of modern thermal logging]. *Geologiya i razvedka = Geology and exploration*, 3, pp. 54-57. (In Russ.)

Popov Yu., Tertychnyi V., Romushkevich R. et al. (2003). Interrelations between thermal conductivity and other physical properties of rocks: experimental data. *Pure and applied geophysics*, 160, pp. 1137-1161. <https://doi.org/10.1007/PL00012565>

Popov Yu.A., Romushkevich R.A., Gorobtsov D.N. et al. (2008). Teplovyie svoistva porod i teplovoi potok v raione bureniya sverkhglubokoi En-Yakhinskoi skvazhiny [Thermal properties of rocks and heat flow in the area of ultra-deep drilling in the En-Yakhinskaya well]. *Geologiya i razvedka = Geology and exploration*, 2, pp. 59-65. (In Russ.)

Popov Yu.A., Romushkevich R.A., Popov E.Yu. (1996). Thermophysical studies of rocks of the Tyumen ultradeep well section. V kn.: *Tyumenskaya sverkhglubokaya skvazhina (interval 0-7502 m). Rezul'taty bureniya i issledovaniya* [Book: Tyumen ultradeep well (interval 0-7502 m). Results of drilling and research]. *Sbornik dokl. Nauchnoe burenie v Rossii* [Coll. papers: Scientific drilling in Russia]. Is. 4. Perm: KamNIIGIS, pp. 163-175. (In Russ.)

Popov Yu.A., Semenov V.G., Korostelev V.M. et al. (1983). Opredelenie teploprovodnosti gornykh porod s pomoshch'yu podvizhnogo istochnika tepla [Determination of thermal conductivity of rocks using a movable heat source]. *Izvestiya. Physics of the Earth*, 7, pp. 86-93. (In Russ.)

Teplovoe pole nedr Sibiri [Thermal field of Siberia depths] (1987). Ed. E.E. Fotiadi. Novosibirsk: Nauka, 195 p. (In Russ.)

## About the Authors

*Albert D. Duchkov* – DSc (Geology and Mineralogy), Professor, Chief Researcher

Trofimuk Institute of Petroleum Geology and Geophysics of Siberian Branch of Russian Academy of Sciences

3 Ak. Koptug ave., Novosibirsk, 630090, Russian Federation

*Dmitry E. Ayunov* – PhD (Physics and Mathematics), Senior Researcher

Trofimuk Institute of Petroleum Geology and Geophysics of Siberian Branch of Russian Academy of Sciences

3 Ak. Koptug ave., Novosibirsk, 630090, Russian Federation

*Sergey V. Rodyakin* – Junior Researcher

Trofimuk Institute of Petroleum Geology and Geophysics of Siberian Branch of Russian Academy of Sciences

3 Ak. Koptug ave., Novosibirsk, 630090, Russian Federation

*Petr A. Yan* – PhD (Geology and Mineralogy), Head of laboratory

Trofimuk Institute of Petroleum Geology and Geophysics of Siberian Branch of Russian Academy of Sciences

3 Ak. Koptug ave., Novosibirsk, 630090, Russian Federation

*Manuscript received 04 July 2018;*

*Accepted 26 September 2018;*

*Published 30 November 2018*



# Complex structural-tectonic zoning of the north-eastern part of the Barents Sea shelf

D.S. Nikitin<sup>1</sup>\*, D.A. Ivanov<sup>2</sup>

<sup>1</sup>Geological Institute of the Russian Academy of Sciences, Moscow, Russian Federation

<sup>2</sup>Voronezh State University, Voronezh, Russian Federation

**Abstract.** The large amount of geological and geophysical data obtained in recent decades for the north-eastern part of the Barents Sea shelf makes their visual comparative analysis difficult, and the use of automated classification methods, in particular, multidimensional statistics, become relevant.

The perspectives of the statistical approach to the processing and interpretation of multi-sign geological and geophysical information are considered. The objective performance of the method of identifying classes (tectonic structures) within the studied area is determined by statistically justified methods that are independent of the subjective factor. The structural-tectonic schemes for reflecting horizons are clarified, at the level of which the main stages of large-scale tectonic reorganizations occur.

**Keywords:** Barents Sea shelf, statistic analysis, structural-tectonic zoning

**Recommended citation:** Nikitin D.S., Ivanov D.A. (2018). Complex structural-tectonic zoning of the north-eastern part of the Barents Sea shelf. *Georesursy = Georesources*, 20(4), Part 2, pp. 404-412. DOI: <https://doi.org/10.18599/grs.2018.4.404-412>

## Introduction

In the north-eastern part of the Barents Sea shelf in recent decades, a large amount of geological and geophysical studies have been performed to predict oil and gas content (Pavlov et al., 2008; Velichko et al., 2010; Pavlov, 2012; Tektonicheskaya karta., 1998; Khutorskoy et al., 2008; Shipilov, Tarasov, 1998; Rostov et al., 2002; Fedukhin et al., 2002, etc.).

The article presents the results of statistical analysis of geological and geophysical information, which helped to clarify the structural-tectonic schemes for reflecting horizons, at the level of which the main stages of large-scale tectonic reorganizations occur. The spatial model (structural and block models, three-dimensional model of faults) of the northeastern part of the Barents Sea shelf, built by the authors earlier (Nikitin et al., 2017; Nikitin, Ivanov, 2016; Nikitin, etc., 2015) served as the basis for the statistical analysis.

New materials obtained by the authors provided the basis for updating and detailing the existing interpretations of previous data on the deep structure of the north-eastern part of the Barents Sea. The article presents new results of a complex structural-tectonic zoning of the north-eastern part of the Barents Sea shelf,

obtained as a result of a statistical analysis of geological and geophysical information.

## Object of study

The study area is geographically located in the northeast of the Arctic shelf of the Barents Sea between the two archipelagos of insular land – Frantz Josef Archipelago (FJA) and Novaya Zemlya (Fig. 1).

By the nature of seismic records and the distribution of potential geophysical fields, the studied area can be divided into two parts: the north-west and the south-east. The structure of the East Barents depression belongs to the northwestern part. The southeastern part is represented by the Novaya Zemlya forearc structural region, formed by the uplifts of the Admiralty, Pankratiev and Cape Zhelaniya, as well as the deflections of Sedov, Mak, Gulf Stream and Karpov (Fig. 2). The East-Barents depression, made by rocks of Middle Paleozoic-Mesozoic age, has a sedimentary cover thickness of 18 to 20 km. The thickness of the consolidated part of the Earth's crust ranges from 10 to 15 km, the Moho border is located at a depth of 27 to 33 km. The crust is thinned due to reduction of the granite-gneiss layer (Sakulina et al., 2007).

During the transition from the East Barents depression to the Novaya Zemlya forearc structural region, the structure of the Earth's crust, the shape of potential field anomalies, and the nature of magmatism change dramatically. The basement surface is stepped up in a southeastern direction and formed by multi-level

\*Corresponding author: Dmitry S. Nikitin  
E-mail: [ndsnomination@mail.ru](mailto:ndsnomination@mail.ru)

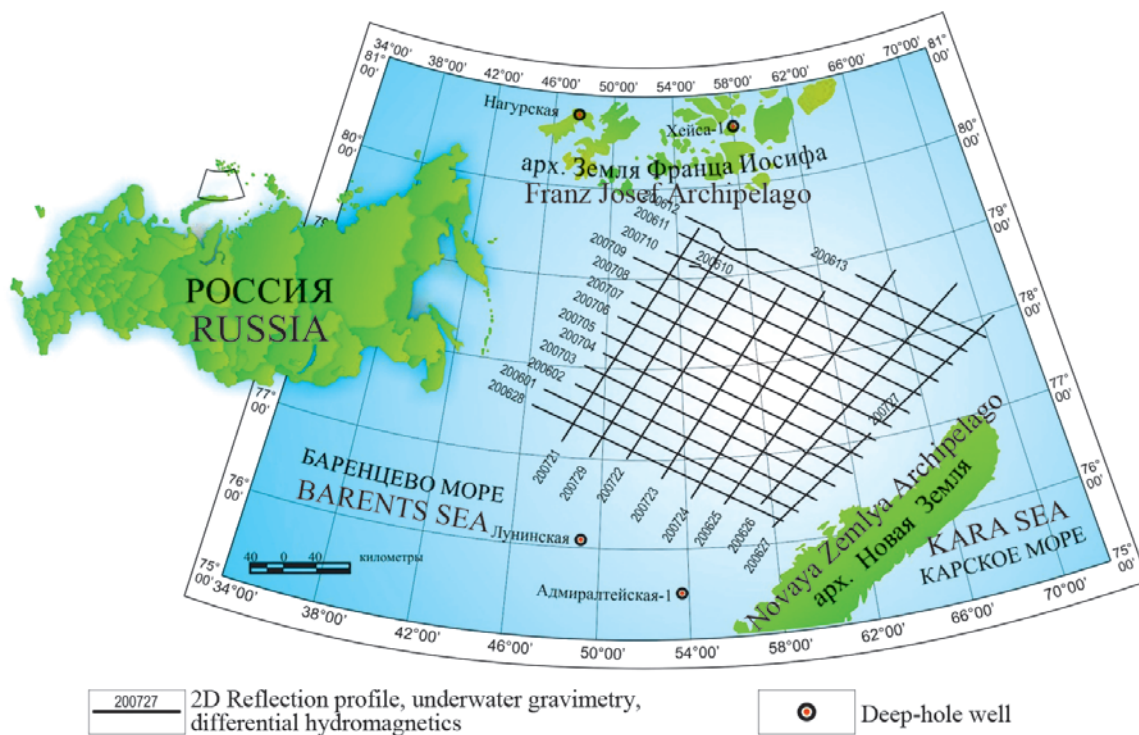


Fig. 1. Location of the study area

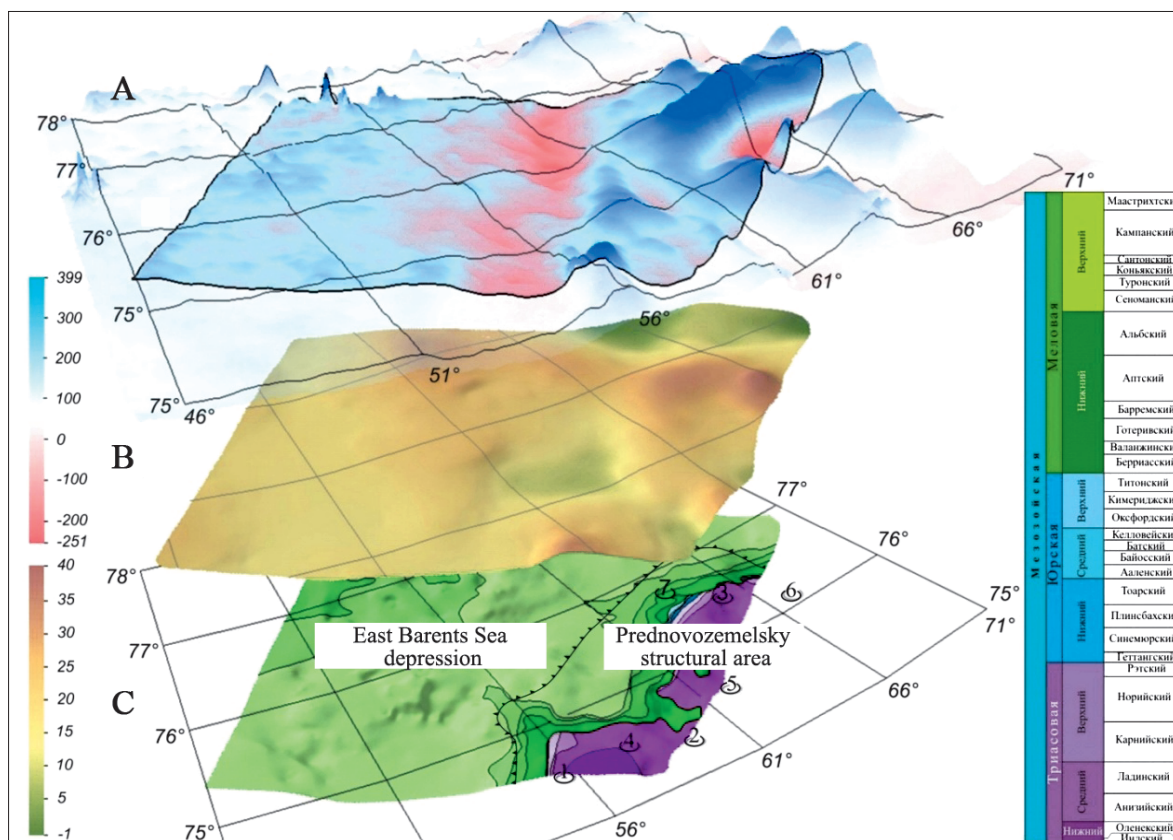


Fig. 2. Map of anomalous magnetic field (A), map of anomalous gravitational field (B), geological map of pre-Quaternary formations (C): 1-3 – elevated blocks of the Earth's crust: 1 – Admiralty, 2 – Pankratiev, 3 – Cape Zhelaniya; 4-7 – subsided blocks of the Earth's crust: 4 – Sedov, 5 – Maka, 6 – Gulf Stream, 7 – Karpov

blocks disintegrated and pulled over the crystalline base of the East Barents Sea depression. The thickness of the crust increases to 36-38 km, but at the same time there are significant fluctuations in the thickness of the sedimentary cover and the granite-metamorphic layer.

The boundary between the East Barents Sea depression and the Novaya Zemlya forearc structural region is traced by zones of deep faults. In the central part of the study area, it is expressed in a magnetic field of a wide, linear negative anomaly of northeast strike. The



anomalous zone has a width of 40 to 80 km. Within its limits, the northeastern and sub-meridional thrusts traced from the Novaya Zemlya orogen are replaced by normal faults of the northeastern direction. On the eastern side of the depression, there is an immersion of blocks of the Novaya Zemlya forearc structural region. On reflection-time section of this structural area, the introduction of large intrusions is noted, the upper edges of which are located at depths from 8 to 10 km (Pavlov et al., 2008; Pavlov, 2012).

In compiling the tectonic scheme, the results of thematic works (Verba, Ivanov, 2000), published materials, tectonic maps and charts (Shipilov, Tarasov, 1998) were used. In tectonic terms, the territory under consideration belongs to the Svalbard Plate, which is characterized by a heterogeneous structure.

Within the study area, it is assumed the Grenville age of the basement forming, as well as for the most part of the northern Barents Sea shelf (Shipilov, Tarasov, 1998). According to other authors (Suprunenko et al., 1998), the study area belongs to the epi-Baikal shelf plate, with pre-Baikal rigid blocks soldered into it (Frantz Josef Archipelago).

In the geological structure of the north-eastern part of the Barents Sea shelf, three structural-tectonic levels (STL) are distinguished: the lower – pre-Paleozoic folded basement, the intermediate – lower middle-Paleozoic and upper, which includes sediments from

Upper-Devonian to Quaternary. These structural levels are separated by surfaces of regional stratigraphic and angular inconsistencies (reflecting horizon (RH) VI (C) and III<sub>2</sub> (D<sub>3</sub>)), reflecting significant changes in the structural plans of the sedimentary cover of the study area.

Tectonic zoning patterns are available for the Lower-Middle Paleozoic sediment complex (OG III<sub>2</sub> (D<sub>3</sub>)) and on the top of the Triassic sediments (OG B (T-J)) (Fig. 3).

In addition, in the history of the development of the Upper Paleozoic-Mesozoic STL, the stages of large-scale tectonic reorganizations in the Early Permian period, at the Triassic and Jurassic, and in the Neocomian period are also distinguished.

### Geometric Analysis

The analysis included the study of the parameters of spatial (strike azimuth) and quantitative (density) distribution of faults, selected according to the results of seismic exploration of 2D CDP seismic reflection method. The study method is the construction of rose diagrams of the strike of faults.

Rose diagrams (azimuth rose plots) are one of the oldest and most widely used methods of graphic representation of measurements of the occurrence of the entire set of different rank disturbances of rock continuity (from microcracks to faults) recorded by various research methods. They can display any one

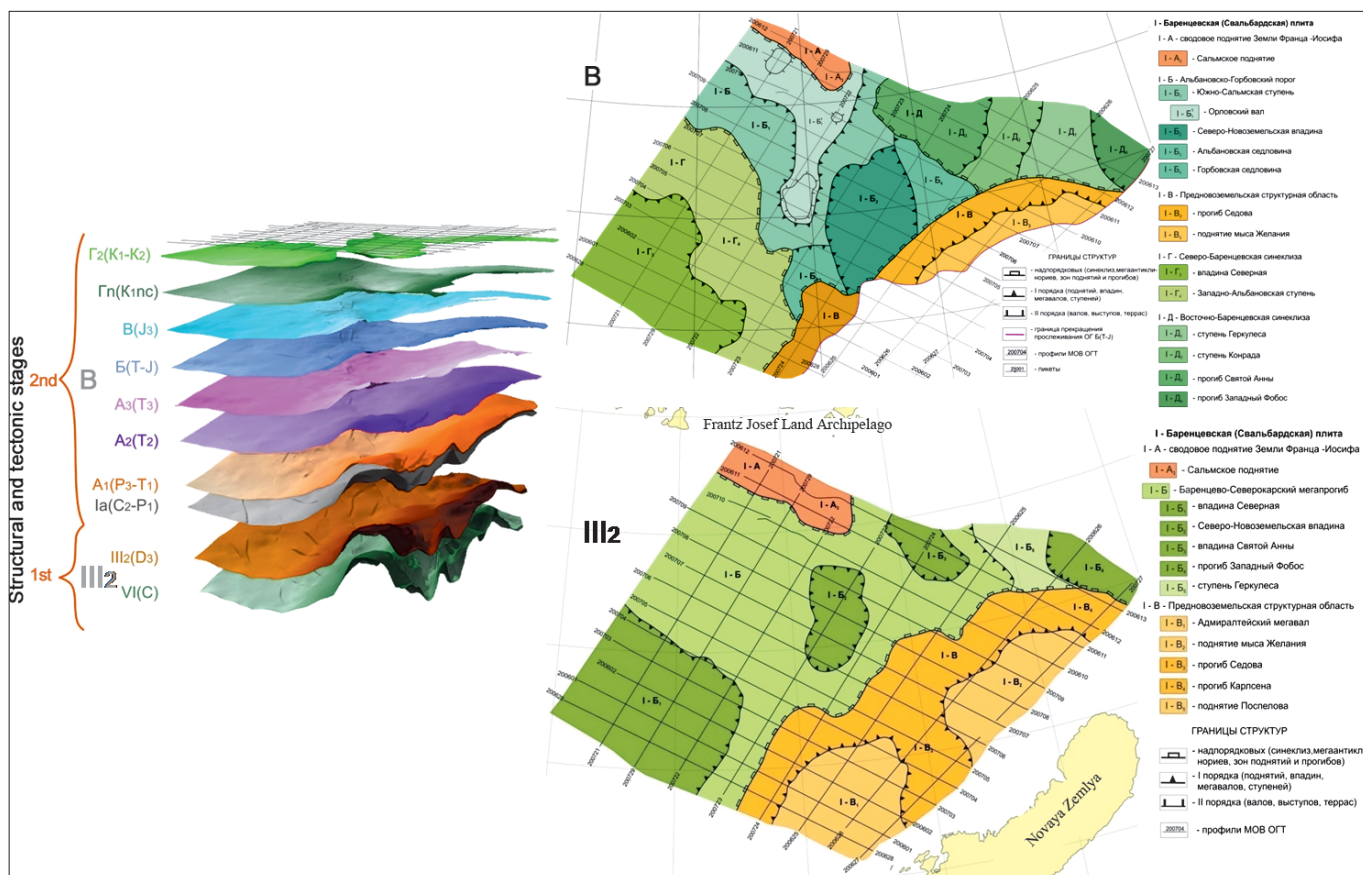


Fig. 3. Schemes of tectonic zoning along the roof of the Triassic deposits (B) and the Lower-Middle Paleozoic complex (III<sub>2</sub>) (according to the Arctic Sea Geological Expedition with the addition of authors)



measurement element, and with a combination of two or three such diagrams, two or three measurement elements can be shown (strike, direction of fall, angles of fall).

In our case, the number of structural-tectonic disturbances was plotted as a percentage, the total number of measurements was taken as 100%, and the percentage of measurements for each group was calculated.

For the analysis, three levels of structural-tectonic disturbances were used, identified according to the results of spatial modeling (Nikitin, Ivanov, 2016).

The first level in terms of the relative density of the distribution of structural-tectonic disturbances is represented by two fault systems (Fig. 4).

The first system of faults is located in the azimuth range of the NNW 360° – NNE 20° and SSW 190° – SSE 170°. The second system of faults is in the azimuth section of the SE 135° – ESE 120° and WNW 280° – NW 315°.

Fault systems are obliquely crossing each other at an angle of  $\approx 40^\circ$ . The identified two fault systems are a consequence of the manifestation and identify two differently oriented regional (?) Stress fields in the history of the sedimentary cover.

The second level in terms of the relative density of the distribution of structural-tectonic disturbances is represented mainly by the north-north-western strike in the azimuth section of the NW 315° – NNW 370° and SSE 10° – SE 135° (Fig. 5).

The constancy of the strike of structural-tectonic disturbances is noted, which indicates that the faults are of one genesis and age range. Such a deformation structure is an element of self-organization of sedimentary rocks under conditions of constant exposure to excessive

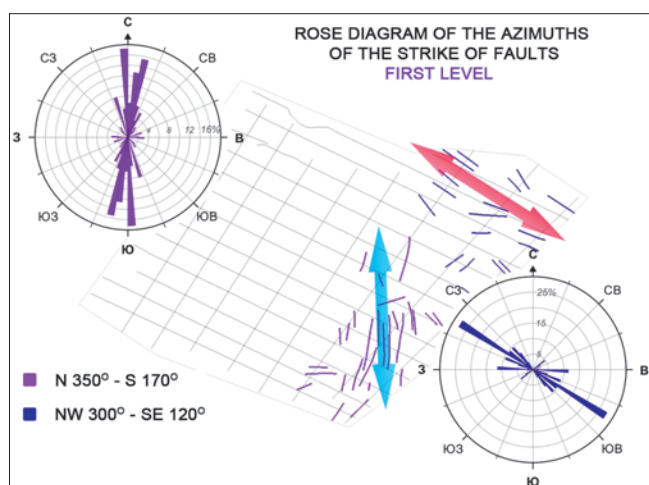


Fig. 4. Scheme of the first level of structural-tectonic disturbances. Rose diagram of spatial orientation of structural and tectonic disturbances. The rose diagram shows the azimuths of the strike of faults in the horizontal plane, the length of the petals corresponds to the total length of the faults with the corresponding strike azimuth in the selected scale

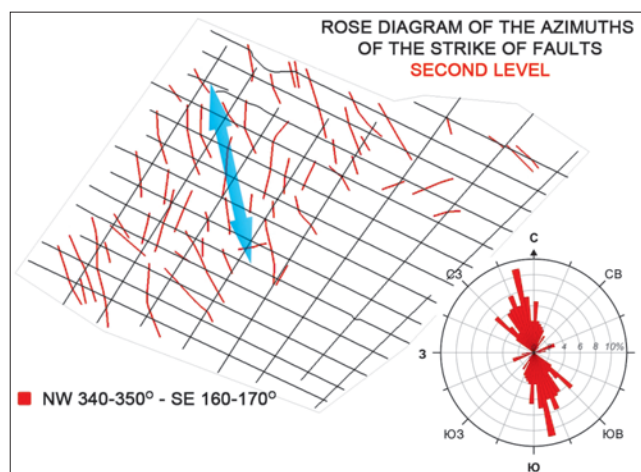


Fig. 5. Scheme of the second level of structural-tectonic disturbances. The detailed description see in Fig. 4

stresses and a natural condition of existence at constant equilibrium.

The third level in terms of the relative density of the distribution of structural-tectonic disturbances is represented by two fault systems (Fig. 6).

The first system of faults is located in the azimuth range of the NW 320° – NNW 360° and SSE 160° – SE 160°. The second system of faults is located in the azimuth range of the SW 225° – SE 135° and NW 315° – 45° NE.

Fault systems are orthogonal to each other and form an angle of  $\approx 90^\circ$ . The identified fault systems identify two differently oriented regional (?) stress fields in the history of the sedimentary cover.

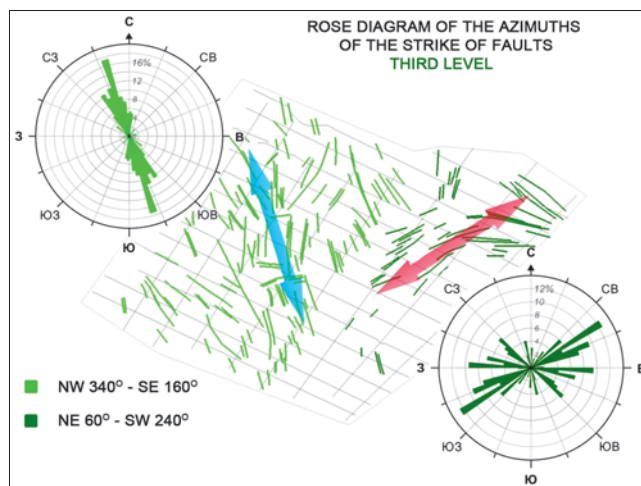


Fig. 6. Scheme of the third level of structural-tectonic disturbances. The detailed description see in Fig. 4

### Statistical analysis

Statistical analysis was carried out on 23 signs of different types of geological and geophysical data (information on eleven reflecting horizons, dividing structural-material complexes and geophysical fields). To exclude features that have strong correlations from the processing, a matrix of paired correlations between

the values of the absolute marks of reflecting horizons (RH) and the thickness of the structural-compositional sedimentary complexes (SCC) belonging to the Lower-Middle Paleozoic structural tectonic level was calculated.

According to the results of processing, there are strong correlations between the absolute marks of all RH and the thickness of the rocks separating them from the SCC. This indicates the inheritance of the development of the territory and individual structures within the framework of this structural sedimentation cycle. Therefore, for further joint processing with geophysical fields, only the altitude values for RH VI and the power of the SCC between RH VI and RH III2 were used. Moreover, it is precisely for the surface III2 (D3) that there is a structural-tectonic scheme. It is used for a comparative analysis of the results of classification.

As a method of multidimensional classification, a type of cluster analysis method was used – the K-means method. The advantage of the method, as in the whole cluster analysis, is the ability to split objects by several indicators. At the same time, cluster analysis does not impose any restrictions on the type of objects under consideration, which makes it possible to consider sets of initial data of arbitrary nature in various units of measurement.

This classification method is based on dividing the set of the studied objects into statistically homogeneous aggregates or clusters. The resulting clusters consist of statistically similar objects. Objects belonging to different clusters should differ significantly. In our case, the elementary units of a territory of 500×500 meters in size, corresponding to the cells of the constructed mesh surfaces are objects of clustering. The selected clusters will correspond to parts of the territory that are supposed to be interpreted from the standpoint of tectonic zoning. As a result of the classification, for each cell of the territory we get an additional attribute – a class number from 3 to 10, depending on the partitioning parameters. Based on this attribute, a point map of the coordinates X, Y is visualized on the screen and compared with the existing pattern of structural-tectonic regionalization along the surface III2 (D3).

According to the number of clusters formed, zoning schemes of the territory for 4, 5, 6, 7, 8, 9 and 10 classes are sequentially constructed (Fig. 7).

When reviewing the results, it is noted that the boundaries of superorder structures stand out by 70%, starting with the 7th grade and more (Fig. 7c-e).

A complete coincidence of structures, parts and boundaries is noted for superorder structures, for example, for the Salmsk uplift, for the Novaya Zemlya forearc structural region. The structures of the first order clearly delineate the North depression in the southwest, and the Admiralty megaswell in the southeast of the region.

The most optimal, from our point of view, is the result of classification into 8 classes. In Fig. 8 classes are adapted to the color palette of the original map.

After constructing a three-dimensional model of the map obtained as a result of the classification into 8 classes taking into account faults, we can judge that the structures of the first order have a more complicated morphology. So the 3rd class, framing the Novaya Zemlya forearc structural area, is a transitional area with the Barents – North-Kara depression. The region allocated to the 3rd class, allocated in the northern part of the territory, can also be considered as a transitional to the arched uplift of Franz Josef Archipelago (Fig. 9).

For a comparative assessment of the values of the distributions of individual signs, on the basis of which clustering was carried out, “box” diagrams were used. In general, this type of diagram consists of two elements – a “box” and “whiskers” or “tails”. When preparing data for such a presentation, the entire range of available values is divided into quartiles with the boundary values of 25, 50, and 75%. Central quartiles – 25-50% and 50-75% – are graphically placed in a rectangle – box. Extreme quartiles – 0-25% and 75-100% – are depicted as linear forms called tails or whiskers. In the center of the box is a median value in the form of a point or line. The graph allows us to estimate the symmetry of the distributions and the spread of values. In addition, outliers and hurricane values that are significantly different from the normal distribution predicted for a given data set (by mean value and median) and deviations in values of more than three standard deviations are shown in a circle or asterisks. An important advantage of box diagrams is the possibility of simultaneously comparing several distributions.

Figure 10 shows the box diagram for the absolute values of the reflecting horizon VI for all selected classes of objects. Based on the analysis of the diagram (Fig. 10), it is noted that according to the median values and the 50% center line, the classes are individualized 5, 6, 7 and 8, belonging to the depressions of the Barents-North-Kara deflection and the Novaya Zemlya forearc structural region. Statistically indistinguishable classes for this indicator are bordering classes 2 and 3. They correspond to the transition zone between negative and positive superorder structures. Classes 1 and 4 are also statistically similar, however, in terms of their location on the map, the first corresponds to the main bed of the Barents-North Kara deflection, and the 4th corresponds to the structure that separates the uplifts within Novaya Zemlya forearc region.

Figure 11 shows the box diagram of the thickness of the deposits between RH VI and III2 for all selected classes of objects.

By the nature of the distribution of power and the median value (2900 m), 3rd class is sharply



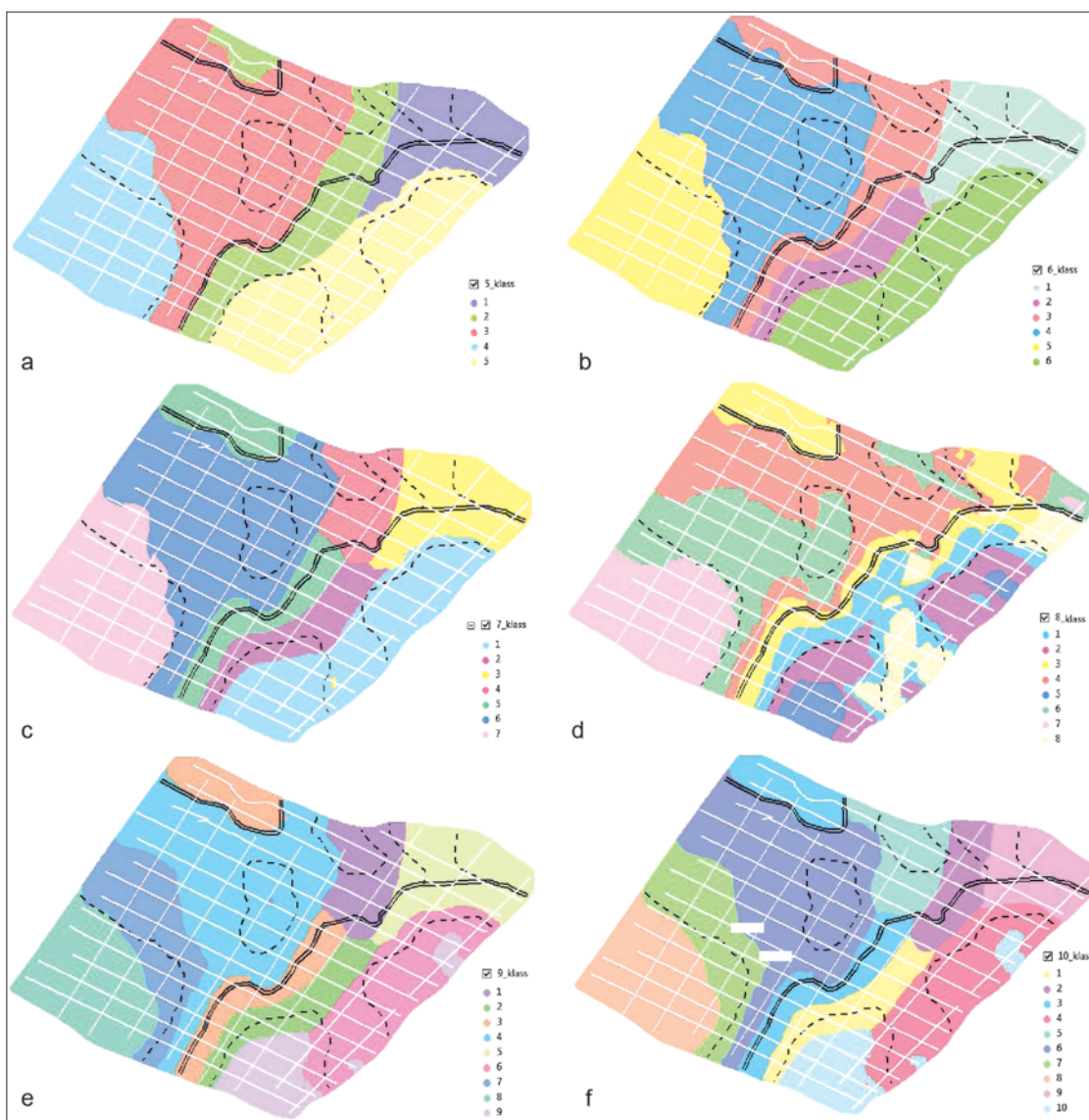


Fig. 7. The result of clustering by the K-medium method of the Lower-, Middle Paleozoic structural-tectonic: a – 5 classes; b – 6 classes; c – 7 classes; d – 8 classes; e – 9 classes; f – 10 classes; - - - the boundaries of the structures of the first order; === – boundaries of superorder structures

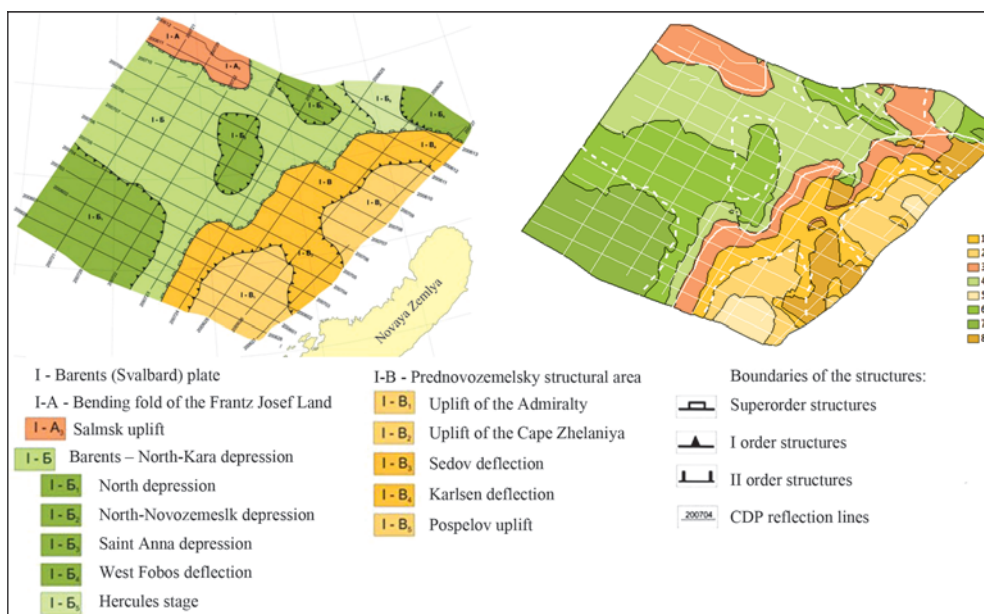


Fig. 8. Example of comparison of the initial structural map and a map constructed using multidimensional analysis. Shows the division into 8 classes



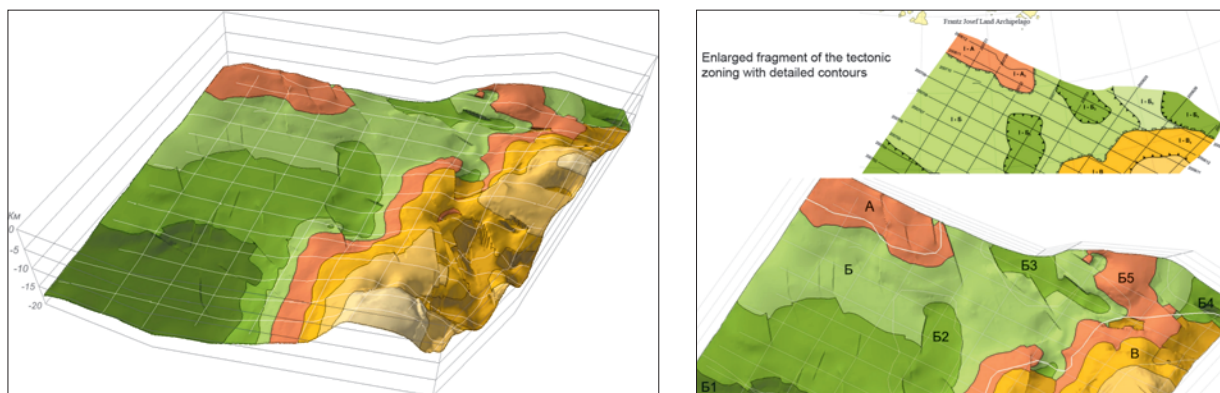


Fig. 9. Volumetric model of the RH VI with superimposed boundaries of tectonic structures obtained according to the statistical processing

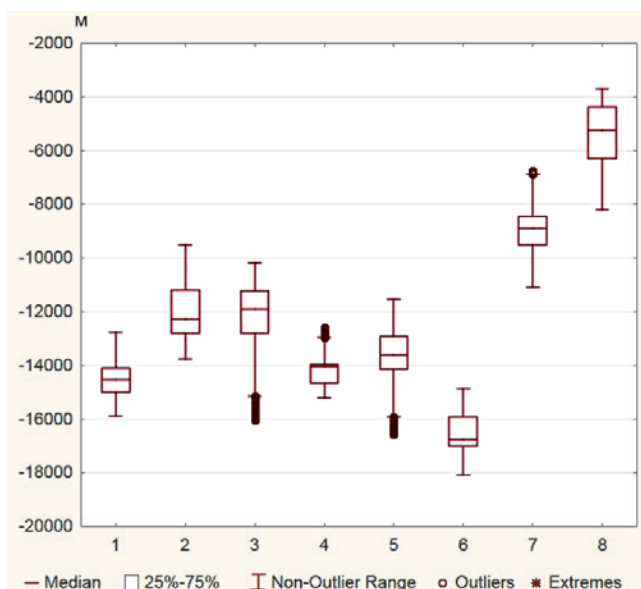


Fig. 10. Box diagram of the distribution of absolute marks for selected classes of objects

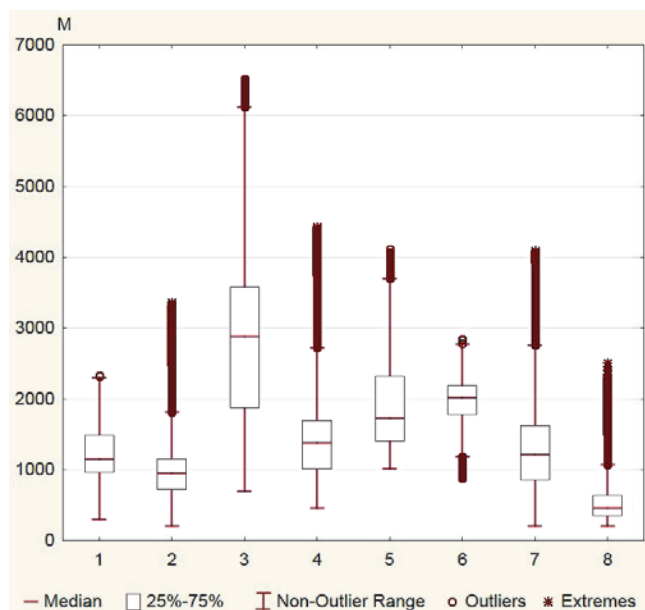


Fig. 11. Box diagram of the distribution of power between RH VI and III2 for selected classes of objects

distinguished. According to these parameters, it is unambiguously separated from the 2nd class (the median value is 1000 m), despite the fact that they are statistically similar in the values of their absolute marks (Fig. 10). The characteristics of the power distribution also clearly allow us to distinguish the 8th and partially 2nd classes, the first corresponds to the areas with the maximum absolute marks of the territory, the last – with the minimum. The remaining classes – 1, 4, 5, 6 and 7th – provide significantly overlapping distributions and can be interpreted only with the help of information about their spatial distribution.

### Characteristics of geophysical fields

In the distribution of the absolute values of the magnetic field for the selected classes of objects, distinctly individualized groups are absent (Fig. 12).

In Figure 12, several groups of classes with a close distribution of the magnetic field are distinguished by span and median values. These are classes 1, 2 and 4, spatially corresponding to the slope parts of the uplift of the Novaya Zemlya forearc structural region and the flattened part of the Barents – North Kara deflection. The second group of classes (3 and 5) has a similar range of distributions with a higher median value for the 5th class. These classes are distinctly separated spatially: the 3rd corresponds to the near-slope parts of positive supra-order structures, the 5th corresponds to their apical parts. The nature of the distributions and the absolute values of the magnetic field for the 7th and 8th classes are very close, with different spatial localization within the site. The smallest scatter of values or a uniform character has a magnetic field within the 6th class – 30-50 nT. This class corresponds to the intermediate depths of the Barents – North Kara deflection.

The box diagrams of the distribution of the gravitational field values for the selected classes of objects in Fig. 13 are ranked by median values.

According to the absolute values of the gravitational

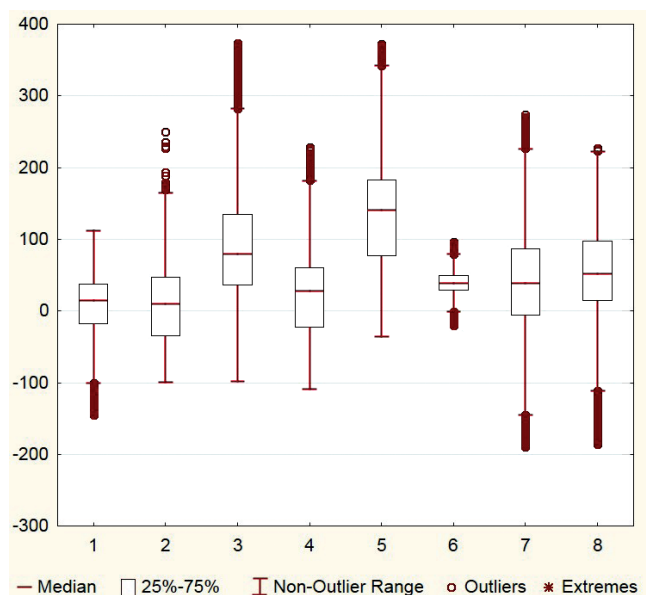


Fig. 12. Box diagram of the distribution of magnetic field values for selected classes of objects

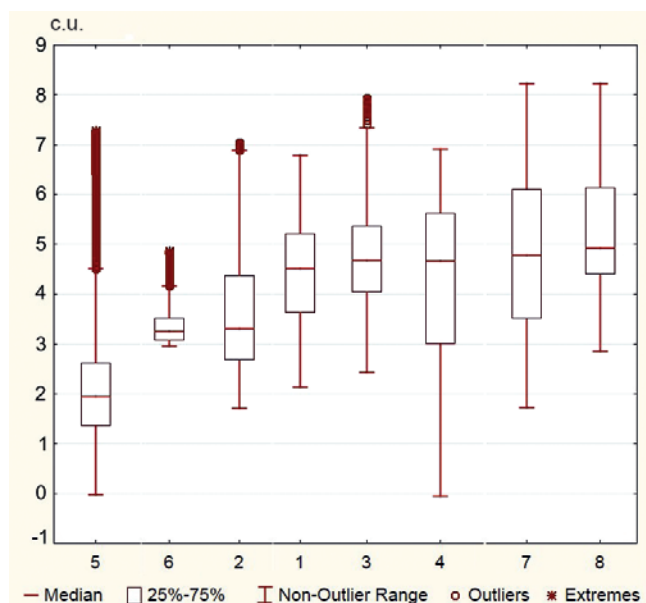


Fig. 13. Box diagram of the distribution of gravitational field values for selected classes of objects

field, only the 5th class can be distinguished, which corresponds to the apical part of the Novaya Zemlya forearc structural region. It has minimal absolute field values, a symmetric distribution, and an average 50% of the distribution, overlapping with other distributions only in the tail portions. The minimum dispersion, as in the case of a magnetic field, has a gravitational field for the 6th class. The distributions of the gravitational field for the other selected classes largely overlap and have close median values.

Thus, none of the individual signs of a structural nature or a geophysical field makes it possible to unambiguously regionalize the territory with the necessary degree of detail. For this, it is necessary to share the complex of features and methods of

multivariate statistical analysis. The classification values of individual signs can be estimated based on factor loadings.

## Conclusions

The objective performance of the method of identifying classes (tectonic structures) within the study area by statistically sound methods independent of the subjective factor has been determined.

The result of the zoning of the Lower Middle Paleozoic complex of rocks is quite comparable with the existing tectonic schemes, moreover, he specifies them. The boundaries of the superstructure are programmed at 70%, starting with 7 or more division classes. The boundaries of the structures of the 1st order are represented by a more complex morphology with a detailed internal structure and are partially outlined by discontinuous disturbances.

The most important basis for tectonic zoning of a sedimentary cover are structural maps of reflecting horizons taking into account tectonic disturbances.

## Acknowledgments

This work was supported by the Russian Foundation for Basic Research (grant No. 18-35-00236 mol\_a) and the program of the Presidium of the Russian Academy of Sciences P47.

## References

- Fedukhin N.V. et al. (2002). Model' stroeniya litosfery Barentsevskogo shel'fa po dannym glubinnoy seysmorazvedki [The model of the Barents shelf lithosphere structure according to the deep seismic studies]. Murmansk: Fund of the Marine Arctic Geological Expedition (MAGE). (In Russ.)
- Khutorskoy M.D., Viskunova K.G., Podgornyykh L.V. et al. (2008). Geotemperaturnaya model' zemnoy kory Barentseva morya: issledovaniya vvol' geotransversov [Geotemperature model of the Barents Sea crust: research along geotransverses]. *Geotektonika = Geotectonics*, 2, pp. 55-67. (In Russ.)
- Nikitin D.S., Gorsky P.P., Khutorskoy M.D., Ivanov D.A. (2017). Analysis and numerical simulation of the potential fields in Barents sea Northeastern part. *Monitoring, nauka i tekhnologii*, 1(30), pp. 6-15. (In Russ.)
- Nikitin D.S., Ivanov D.A. (2016). Structural and tectonic conditions of oil and gas content of Northeast part of the Barents sea shelf. *Monitoring, nauka i tekhnologii*, 2(27), pp. 48-54. (In Russ.)
- Nikitin D.S., Ivanov D.A., Zhuravlev V.A., Khutorskoy M.D. (2015). Three-dimensional geological and geothermal model of sedimentary cover in the north-eastern part of the Barents Sea shelf in connection with the development of hydrocarbon resources. *Georesursy = Georesources*, 1(60), pp. 13-19. <https://doi.org/10.18599/grs.60.1.3> (In Russ.)
- Pavlov S.P., Shlykova V.V., Grigor'eva B.M. et al. (2015). Otchet po ob'ektu «Utochnit' geologicheskoe stroenie i perspektivy neftegazonosnosti vostochnogo borta Severo-Barentsevskoy vpadiny» [To clarify the geological structure and petroleum potential of the eastern side of North Barents depression. Report]. Murmansk: MAGE JSC. (In Russ.)
- Pavlov S.P. (2012). Geological structure and petroleum potential of the north-eastern part of the Barents Sea according to geophysical data. *Diss. cand. geol.-min. nauk* [Cand. geol. and min. sci. diss.]. Murmansk. (In Russ.)
- Roslov Yu.V. et al. (2002). Otchet o sozdani modeli glubinnoy geologicheskogo stroeniya Barentsevomorskoy neftegazonosnoy provintsii na osnove novoy tekhnologii kompleksnoy obrabotki dannykh MOV, MPV i GSZ na oporyakh profilyakh v perekhodnoy zone «susha-more» [Report on the modelling of deep geological structure of the Barents Sea oil and gas province on the basis of new technologies for data integration]. St. Petersburg: GNPP «Sevmorgeo». (In Russ.)
- Sakulina T.S., Verba M.L., Ivanova N.M., Roslov Yu.V., Belyaev I.V.

(2007). Glubinnoe stroenie severnoi chasti Barentsevo-Karskogo regiona vdol' profilya 4-AR [The deep structure of the northern part of the Barents-Kara region along the 4-AR profile]. Sbornik materialov 7-go foruma: Toplivno-energeticheskii kompleks Rossii [Coll. papers: 7th forum «Fuel and Energy Complex of Russia»]. St.Petersburg, pp. 371-374. (In Russ.)

Shipilov E.V., Tarasov G.A. (1998). Regional'naya geologiya neftegazonosnykh osadochnykh basseynov Zapadno-Arkticheskogo shel'fa Rossii [Regional geology of oil and gas bearing sedimentary basins of the Western Arctic shelf of Russia]. Apatity: «KNTs RAN» Publ. 306 p. (In Russ.)

Suprunenko O.I., Evdokimov N.K., Shkola I.V., Bro E.G., Dibner V.D., Makar'ev A.A., Stolbov N.M., Ustinov N.V. (1998). Perspektivy neftegazonosnosti arhipelaga Zemlya Frantsa-Iosifa [Oil and gas potential of the archipelago Franz Josef Land]. *Geologo-geofizicheskie kharakteristiki litosfery arkticheskogo regiona* [Geological and geophysical characteristics of the lithosphere of the Arctic region], 2, pp. 153-168. (In Russ.)

Tektonicheskaya karta morey Karskogo i Laptevykh i Severa Sibiri [Tectonic Map of the Kara and Laptev Seas and the North of Siberia]. (1998). Scale 1:2 500 000. Ed. N.A. Bogdanova, V.E. Khaina. Moscow: Federal Service for Geodesy and Cartography of Russia. (In Russ.)

Velichko B.M., Shlykova V.V., D'yachenko A.B. et al. (2010). Otchet po ob'ektu «Kompleksnoe geologo-geofizicheskoe issledovanie severovostochnoy chasti Barentsevomorskogo shel'fa» [Integrated geological and geophysical studies of the northeastern part of the Barents Sea shelf. Report]. Murmansk: MAGE JSC. (In Russ.)

Verba M.L., Ivanov G.I. (2009). Tektonicheskaya karta Barentsevo-Karskogo regiona masshtaba 1:2500 000: neftegeologicheskii i geoeologicheskii prognoz [Tectonic map of the Barents-Kara region

of 1: 2500 000 scale: oil-geological and geo-ecological forecast]. *Trudy 9-i konferentsii RAO/CIS Offshore* [Proc. 9th RAO/CIS Offshore Conf.]. St.Petersburg: KhIMIZDAT, V.1, pp. 19-23. (In Russ.)

### About the Authors

*Dmitry S. Nikitin* – Researcher, Laboratory of Heat and Mass Transfer

Geological Institute of the Russian Academy of Sciences

7, Pyzhevsky lane, Moscow, 119017, Russian Federation

*Dmitry A. Ivanov* – PhD (Geology and Mineralogy), Associate Professor, Department of Historical Geology and Paleontology

Voronezh State University

1, Universitetskaya sq., Voronezh, 394018, Russian Federation

*Manuscript received 25 July 2018;*

*Accepted 12 October 2018; Published 30 November 2018*





# Geothermal monitoring as a way to predict volcanic eruptions and estimate geothermal energy resources

A. V. Muravyev

*Geological Institute of the Russian Academy of Sciences, Moscow, Russian Federation*

*E-mail: amur1909@mail.ru*

**Abstract.** Geothermal monitoring is an effective tool for predicting volcanic eruptions, as well as for assessing the geothermal energy potential of geothermal areas. Increased magmatic activity, an indicator of which is the penetration of hot volcanic gases through faults, has been observed in recent years on the Elbrus volcano. Since Elbrus is a year-round resort of world importance, in order to control volcanic and seismic activity, forecast and reduce the risks of eruption and earthquakes, it is recommended to drill an observation well on the slope of Elbrus with the installation of an underground fiber-optic system for temperature and pressure monitoring. In combination with microseismic, gravimetric and inclinometric observations, satellite IR imaging and geochemical gas testing, the continuously obtained information on the thermodynamic conditions of the subsoil will provide a reliable complex for the operational forecast of natural geophysical disasters. Utilization of the geothermal energy of the magma chamber in the artificial circulation systems of small GeoPPs, water injection from the surface and obtaining superheated water and steam from producing wells will reduce the risks of eruption and at the same time provide the resort with environmentally friendly thermal and electric power. Technological justification for the construction of a GeoPP will also require exploratory drilling to the area of hot rocks, therefore information on the distribution of temperature and pressure along the wellbore is doubly valuable.

In geothermal fields that are under development, to assess the spatial heterogeneity of the filtration characteristics can be a useful method of “thermal interference testing” – as a complement or alternative to hydrodynamic interference testing. It is recommended to conduct such an experiment at the North Mutnovsky geothermal field.

**Key words:** Geothermal, monitoring, fiber optic measuring systems, Elbrus, Mutnovsky, volcano, prediction, volcanic eruptions, geothermal energy resources, thermal interference testing

**Recommended citation:** Muravyev A.V. (2018). Geothermal monitoring as a way to predict volcanic eruptions and estimate geothermal energy resources. *Georesursy = Georesources*, 20(4), Part 2, pp. 413-422. DOI: <https://doi.org/10.18599/grs.2018.4.413-422>

## 1. Introduction

Geothermal monitoring in the areas of modern volcanism is aimed at solving two main problems – the forecast of eruptions and the assessment of prospects for the development of geothermal energy. These two sets of tasks are closely interrelated. The study of the geothermal activity of volcanoes in the interparoxysmal stage provides a basis for the conclusion about the geological conditions, risks and economic efficiency of the development of geothermal energy near the volcano. On the other hand, active taking away of the heat of the magmatic chamber during the operation of the geothermal power plant (GeoPP) leads to continuous cooling of the interior beneath volcano, which can reduce the risks of eruptions. The artificial circulation system, which gives energy to GeoPP, may include dozens of

injection wells with water injection from surface sources and dozens of production wells with the removal of superheated steam to the surface at a temperature of about 240-300°C. It is well known, the cost of electricity produced by GeoPP is few times lower than that obtained at diesel thermal power plants. The practical inexhaustibility of volcanic energy resources and the environmentally friendly nature of their utilization by means of closed-cycle system makes geothermal energy extremely unique and attractive.

## 2. Geothermal monitoring of the Mutnovsky volcano

Mutnovsky volcano, located about 70 km from the city of Petropavlovsk-Kamchatsky, is an ideal site for geothermal monitoring due to the presence of extensive fumarole fields (Bottom and Top fields), located in its Lower (North-East) crater, as well as modern Active funnel, which are within relatively easy reach for researchers and tourists. Regular studies of the thermal

regime were started by B.G. Polyak and his colleagues in 1961, 1963 (Polyak, 1965, 1966; Vakin et al., 1966) and continued in 1980 and 1981 (Muravyev et al., 1983; Polyak et al., 1985; Vakin et al., 1986). Thermal imaging of fumarole fields using platinum resistance thermometers at various depth sections (15 cm, 50 cm and 100 cm), panoramic IR imaging of the sides of the Active funnel, as well as measurements of the temperature and flow rate of fumarole gas and hot springs, allowed us to estimate the thermal power of the fumarole fields of the North-Eastern crater (about 380 MW) and to draw a conclusion about the relative stability of the thermal regime of the volcano in the interparoxysmal stage. Thus, geothermal survey with an interval of 17-18 years on the Bottom field of the North-Eastern crater did not reveal any fundamental changes in the pattern of temperature distribution in the soil (Fig. 1). Only the relative heating of the soil was found in the 80-ies in the Northern part of the fumarole field, located near the exit of extrusions and necks, according to the binding to the detailed geological map of the volcano (Selyagin, 2016).

Throughout the history of the formation during the Holocene, Mutnovsky volcano was characterized by relatively frequent (with a periodicity of 4-60 years) phreatic-magmatic eruptions of medium and low power, with the predominant NW direction of explosions (Melekestsev et al., 1987). In 1980, just in time for field work on Mutnovsky, the nearby Gorely volcano, having with Mutnovsky common magmatic chamber, started to

erupt. The increased heating of the soil at the Bottom field in 1980-81 fits into the tendency of increasing activity of volcanic processes, which eventually led to another episode of the explosive activity of Mutnovsky with a phreatic explosion on March 17, 2000 (Zelenskii et al., 2002).

A large amount of atmospheric precipitation in the area of the volcano provides a high level of natural soil moisture and groundwater supply. Water penetrating through cracks and channels to the depth of tens and hundreds of meters into the hot rocks area continuously flushes through volcanic rocks and is discharged in the form of steam hydrotherms and hot springs, creating prerequisites for the development of geothermal energy. These hydrogeothermal resources, in the form of superheated steam and hot groundwater, were discovered by drilling. In 1999 on the basis of the North-Mutnovsky geothermal field, the Upper Mutnovsky GeoPP with a capacity of 12 MW was put into operation, and in 2002 two power units of Russia's largest Mutnovsky GeoPP with a capacity of 50 MW were put into operation, which together cover about 17% of the electricity consumption of the Kamchatka territory; in the future, it is expected to include new power units with an increase in the capacity of Mutnovsky GeoPP to 200 MW (<https://minzkh.kamgov.ru/shema-i-programma-razvitia-energetiki-kamcatskogo-kraa>).

To control the risks of eruptions in the future, as well as to increase the efficiency of the GeoPPs, it is advisable to continue geothermal monitoring of the Mutnovsky

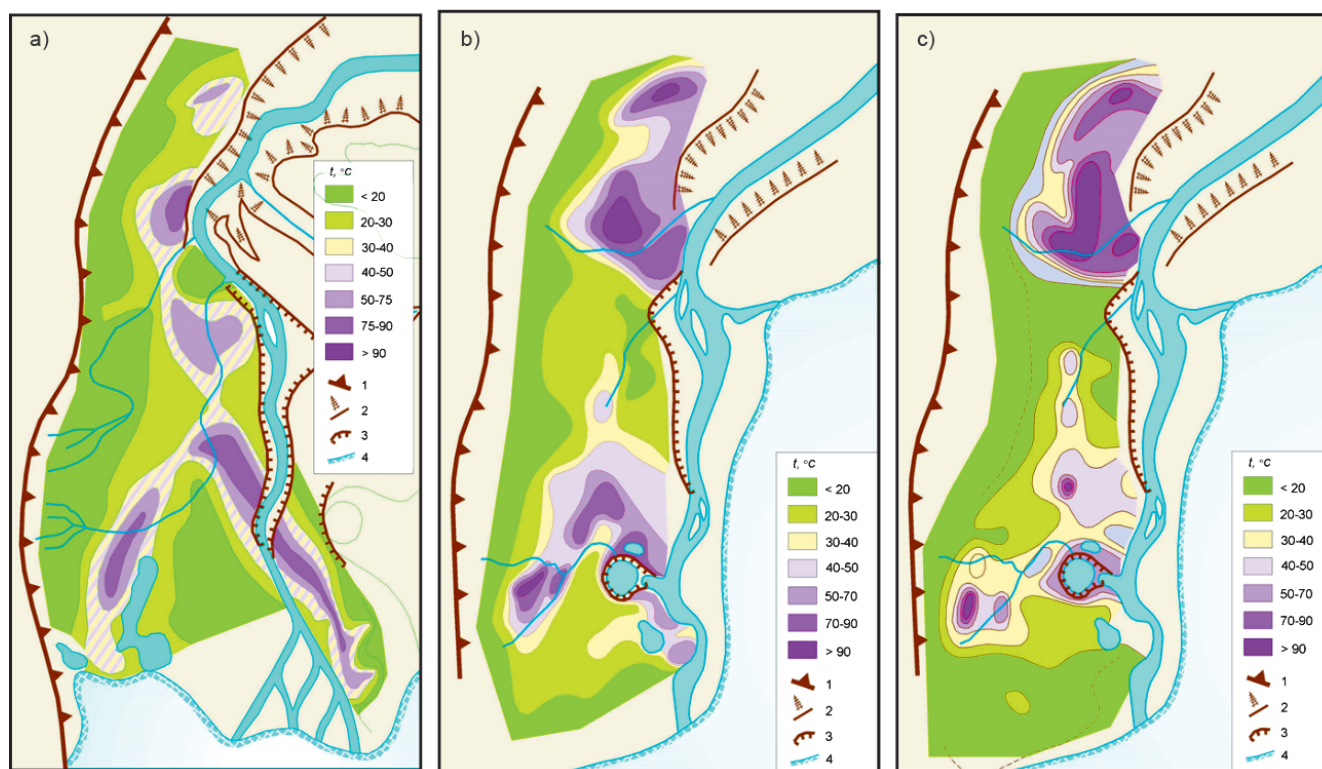


Fig. 1. Subsurface soil temperature at a depth of 15 cm on the Bottom fumarole field, NE crater, Mutnovsky volcano, in 1963, 1980 and 1981 (Polyak, 1965; Muravyev, et al., 1983)

field at a qualitatively new level. Dozens of wells in the North Mutnovsky geothermal field are currently out of operation due to insufficient flow of coolant. This means that the circulation system is inefficient and needs to be optimized. The stopped deep wells (depth over 2000 m) are excellent candidates for transfer them to the category of observational with installation in them of systems of underground monitoring with sensors of temperature and pressure. The network of such support wells will create the basis for the method of hydraulic monitoring. This method is based on the analysis of the time of passage and changes in the amplitude of the pressure pulse transmitted from the perturbing well to the reacting (observation) wells. It is widely used in the development of oil and gas fields to assess the anisotropy of filtration properties and to identify hydrodynamic relationships between wells (Stewart, 2011). The pressure pulse created by suspending production or, conversely, by pumping water into a previously inactive well is recorded by digital downhole gauges with a sufficiently high resolution of pressure (0.03 kPa) and temperature (0.005°C). Such metrological parameters are standard for modern downhole quartz gauges ([www.slb.com](http://www.slb.com)). If the pressure change is not recorded for a long period of time, significantly exceeding the estimated time, the hydrodynamic connection between the wells is absent. If a change in pressure is noted, the studies continue to produce a response curve. Quantitative interpretation of the interference testing data is performed using a hydrodynamic interpretation programs such as Saphir™ or PanSystem™.

Although modern downhole gauges automatically measure both pressure and temperature, in practice, only the pressure parameter is used for hydrodynamic interpretation by oil companies. The temperature is mainly used to adjust the rheological properties of reservoir fluids. This is due to the fact that the heat pulse is subject to relatively rapid relaxation due to heat exchange with all host rocks, while the pressure pulse propagates only within the reservoir and in the absence of hydrodynamic barriers can be registered at a distance of 1-1.5 km from the disturbing well. However, in the author's opinion, in case of application of the method of interference testing on the geothermal field, both measured parameters can be effectively used: pressure and temperature. Preconditions of success of the use of such «thermodynamic» interference test are following:

- The identity of the equations of thermal conductivity and diffusivity makes it possible to apply similar algorithms for the interpretation of hydrodynamic and thermal interference testing data.

- The high permeability of the reservoir at the geothermal field and, consequently, the rapid filtration of the coolant from the perturbing well allows us to expect that the amplitude of the thermal pulse at the observation

well will be large enough ( $>1^{\circ}\text{C}$ ) for reliable quantitative interpretation.

- Relatively close distances between wells (about 100-200 m) also contribute to the rapid passage of the pulse.

- It is possible to create a high amplitude pulse by pumping water with a contrasting temperature (cold water – in hot rocks).

- The efficiency of the experiment can be improved by the use of chemical markers (tracers) when injected into active well.

Comparison of the results of classical hydrodynamic and thermal methods of interference testing in the framework of the same experiment will allow to evaluate the effectiveness of the latter, and if successful, to recommend it for use at sites where hydrodynamic interference testing is ineffective, for example, in gas fields.

In our case, interference testing at the Mutnovsky geothermal field can be recommended in order to create a hydrodynamic model of the field, determine the filtration and capacitive properties of the natural reservoir, identify high conductivity zones and impermeable barriers, plan geological and technological measures to improve the efficiency of development.

### 3. Geological risks in the area of mount Elbrus

The main sources of potential emergencies in the area of Elbrus are, along with climatic, geological factors: volcanism and seismicity. Accelerated melting and collapse of glaciers, snow avalanches and mudflows are also largely determined by the heating of soils, the release of warm gases and sources on the slopes of Elbrus, as well as seismic activity. The frequency of catastrophic eruptions of mount Elbrus is several hundred years. The last strong eruption with a radius of dispersion of volcanic bombs to 700-800 km occurred about 1800 years ago (Bogatikov et al., 1998; Rogozhin et al., 2001; Izmeneniya okruzhayushchei sredy i klimata..., 2007). In recent years, once again there has been an increase in the level of seismicity and heating of the surface of the volcanic cone, which may indicate the activation of processes in the magmatic chamber (Izmeneniya okruzhayushchei sredy i klimata..., 2008; <https://geocenter.info/article/sejsmicheskaja-aktivnost-vulkana-elbrus>). The volcanic structure of Elbrus is characterized by the absence of extensive fumarole fields and obvious signs of modern volcanic activity in the crater, but there are indirect signs of activation of the volcano in recent years. Few small fumaroles on the saddle and the side of the crater have been revealed, marked by a warming of the soil to  $+21^{\circ}\text{C}$  on the Western side that led to the emergence of a colony of green moss at the height of 5621 meters, while the surrounding air is cooled to  $-20^{\circ}\text{C}$  and below (Likhodeev, 2013). Analysis



of the Earth's surface temperature in the area of the summit craters of Elbrus according to NOAA satellites, the temperature of mineral springs in the vicinity of the volcano, indicate a pronounced thermal anomaly associated with the volcano, and magnetotelluric and gravimetric data indicate the presence of a subsurface magmatic chamber and a deeper parent vent under the volcanic structure (Bogatikov, 2006).

Scientists from the Institute of Physics of the Earth have been carried out for a number of years comprehensive geophysical studies, including regime measurements of the temperature in the tunnel built on the slope of the Elbrus within the framework of the Neutrino project, as well as measurements of the temperature of fumarole, the surface of the volcano slope and the temperature of the bottom layer of the water of the newly formed lake at the foot of the Small Azau glacier (Global'nye izmeneniya prirodnoi sredy..., 1997; Rogozhin et al., 2001; Likhodeev, 2013; Gorbatiykov et al., 2018; etc.). The geothermal gradient of 160 mK/m was established by measurements on the walls of the gallery. The researchers conclude that the development of thermal processes on the surface of the volcanic construction of Elbrus led to the intensive melting of some glaciers in recent years. The depth of the lower (parental) magmatic chamber is estimated at a depth of 20 to 40 kilometers. According to the updated data, the upper magmatic chamber beneath the volcanic construction is located in the range of depths of 1-10 km below sea level, its dimensions are within 8-9 km, and the temperature of the upper edge of the chamber is about 850 °C (Likhodeev, 2013).

Microseismic sounding (MSS) studies along the submeridional profile through the Eastern summit of the Elbrus have confirmed the presence of two magmatic foci in the distinct region of low shear wave velocities (Gorbatiykov et al., 2018). The depth of the upper hearth is estimated at 7-13 km below sea level, and the lower – at depths from 18 to 40 km, and to depths above 50 km there is no distinct lower boundary of the hearth. Despite the certain value of all existing methods of observing the temperature regime of the Elbrus volcano, they do not solve the problem of the operational forecast of the eruption. Perhaps, only satellite IR-surveying under condition of regular repeated researches can give the reliable short-term forecast. However, such studies are expensive and performed with long interruptions, so that with the sudden development of the process, observers can easily miss the moment of a sharp increase in the activity of the volcano and the transition to the critical phase.

A more cost – effective solution, in addition to providing a continuous flow of information, can be the installation of temperature monitoring sensors as close as possible to the magmatic chamber. Due to the

activation of volcanic processes, the task of complex monitoring of changes in geophysical fields around the Elbrus is very relevant. First of all, it is important to control the dynamics of changes in the various precursors of the eruption, which are: reducing the depth of the hypocenters of microseismic events, deformation (in particular, swelling) of the Earth's surface in the area above the magmatic focus, the increase in the temperature of the subsoil near the volcano and the change in the gas-hydrogeochemical composition of fluids from fumaroles and thermal sources. A consistent decrease in the depth of the hypocenters indicates the rise of magma to the surface. In some cases, the rate of magma rise was able to accurately predict the time of eruption three months before the event, for example, Kilauea volcano, Hawaii, in 1959 (Rasp, 1982). However, the probability of accurate prediction of the beginning of the eruption from microseismic data is much higher for effusive eruptions of shield volcanoes of Hawaiian type.

Elbrus belongs to stratovolcanoes, which show more insidious behavior, because their magma is more acidic in composition, and therefore is more viscous and slow-moving. The main source of energy of eruptions of stratovolcanoes is a durable accumulated pressure of volcanic gases, which are the most important factor causing volcanic eruptions (Rasp, 1981). Swelling of the surface due to the pressure of the accumulated gases may indicate the approach of an explosive eruption with the greatest risks to the population due to its suddenness and catastrophic consequences. Historical examples of such catastrophes as the destruction of Pompeii during the eruption of Vesuvius (79), the ruin of St. Pierre during the eruption of Mont Pele, Martinique (1902), the eruption of St. Helens, USA (1980), etc., pose the problem of the need to improve the accuracy of forecasts of time, nature and scale of natural disasters.

#### 4. Objectives of subsurface monitoring

Especially valuable information can be given by the systems of underground monitoring of temperature, pressure and microseismicity, installed in sufficiently deep inclined wells, directed towards the magmatic focus. The sensors must meet the requirements of high accuracy and long-term stability of measurements in an aggressive environment (hydrogen sulfide, acid solutions, etc.). The measuring system should be placed along the entire wellbore in order to obtain a spatial dynamic picture of the thermal field, variations in reservoir pressure and groundwater level, localization of seismic events. Modern technologies make it possible to place a multiparameter measuring system in a well on a single geophysical cable. It is believed that the magma is heated in the upper volcanic chamber under the Elbrus to 1000-1100°C, so the geothermal gradient in an inclined

well drilled in the direction of the magmatic focus can be 140-160 mK/m, and the temperature at the bottom of the well depth of 1800 m can reach 260-290°C even with the assumption of a purely conductive nature of heat transfer from the edge of the magmatic chamber to the surface. However, an additional convective heating of the volcanic construction is possible by penetration of hot volcanic gases from the magma hearth through the faults in volcanic rocks. In addition, with the increase of magmatic activity, the deep temperatures will also grow, so it is necessary to apply technological solutions designed for high temperatures.

The specified requirements are met by fiber-optic monitoring systems (FOS), widely used in the oil industry to monitor steam injection, high-temperature production, as well as geothermal wells. The capabilities of most modern downhole electronic sensors are limited to a temperature of 177°C ([www.slb.ru](http://www.slb.ru)), and they are more susceptible to aggressive environments and to damage due to mechanical shocks and vibration.

Drilling an exploration well in the hot rock area will allow to study both the thermal regime in the bowels of the volcano, and also the presence of groundwater, their chemical composition, the degree of fragmentation and permeability of rocks. All this is important not only to control the risks of the eruption, but as well to assess the prospects of environmentally friendly geothermal energy for the further development of the resort infrastructure.

The question arises, where and to what depth it is advisable to conduct drilling to solve the whole complex of tasks?

As noted, the well should be inclined towards the magmatic focus, up to 1800 m deep, drilled in compliance with all safety measures and considering the risks of abnormally high temperatures, pressures and hydrogen sulfide during the penetration of volcanic gas pockets and fault zones. It is necessary to take into account the inevitable natural difficulties – sharply dissected terrain, harsh climate and tenuous air at high altitude, high hardness of rocks and extremely high «environmental sensitivity» of the resort area. In the event that the well shows the prospects for the development of geothermal energy resources, a fairly extensive site for the construction of a GeoPP complex and a network of geothermal wells, protected from avalanches and mudflows, may be required.

As one of the possible options for the drilling site, the author recommends considering a relatively flat area near the Mir station (Fig. 2) cable car «Azau» (about 3400 m above sea level). There are likely to be other suitable sites for geothermal exploration drilling on the slope of Elbrus. The main conditions required here is the availability of the access way for drilling equipment and the safety of operations.



*Fig. 2. View of the valley Azau from the station «Mir» cable car (photo: Mochalov, 2017). A flat area at an altitude of about 3400 m with an access road is a potentially convenient place for drilling exploration and/or observation geothermal well*

## 5. Underground monitoring systems

Modern fiber-optic (FO) systems for underground monitoring have a number of undoubted advantages in comparison with near-surface thermal sensors and satellite IR imaging:

- Real temperature measurements can be carried out in maximum proximity to the object of study (magmatic chamber).
- Continuity of observations provides operational control in case of sudden changes in the thermal regime.
- The amount of incoming information in the monitoring process is easily optimized by recording data in standby mode.
- Automatic transmission of data in real time – through the satellite system SCADA in the center of data collection and analysis provides convenience and safety.
- There is a real opportunity to control changes in gas-hydrothermal activity on the faults connecting the magmatic chamber with the surface.
- Carrying out a complex of various geophysical measurements in the well with the help of sensors installed on a single geophysical (optical) cable provides high information content of the system and reliability of the forecast of eruptions.

The disadvantage is a fairly high cost of the project drilling and completion of the well with the FO monitoring system.

## 6. Technological solutions

Successful and repeatedly tested technological solutions for underground monitoring in extremely harsh conditions are developed, in particular, in the leading oil service companies-Schlumberger and Weatherford. Fiber-optic measuring system, in contrast to electronic sensors resistant to mechanical shock, vibration, corrosive chemicals and can withstand much higher temperature and pressure.

Schlumberger, which has been operating in Russia since 1991, has a Sensa™ fiber optic monitoring system that enables reliable and accurate wellbore temperature profile data to be received and transmitted in real time. The FO temperature profile monitoring system for steam injection wells is designed for operating temperatures up to 250°C; the system also has a built-in discrete pressure and temperature sensor. In oil production, temperature monitoring is most often used in such a method of extraction as steam assisted gravity drainage (SAGD). The dynamics of changes in the temperature profile along the horizontal section of the trunk is used to increase the efficiency of steam injection into the formation and helps to identify the places of breakthrough and inflow of fluids (water, steam, gas, oil) into the well.

Weatherford monitoring systems offer a wide variety of technical solutions for underground monitoring and include, in addition to temperature and pressure sensors, options such as downhole seismic receivers and flow meters. The optimal configuration is selected depending on the tasks to be solved in oil and gas production, steam injection and geothermal wells. An important advantage of these systems is that the sensors are mounted on a single cable. In the arsenal of the company there are systems designed for operating temperatures up to 300°C and aggressive environment, which is especially important for solving problems of volcanology. Sensors on the FO cable are divided into two groups – discrete, the principle of which is based on the use of Bragg gratings, and distributed temperature sensors (DTS), using the refraction of the beam in the MM light guide. Usually, combinations of sensors of different types are used due to the capabilities of a special three-core optical cable (Fig. 3).

**Fiber Optic cable.** FO cable has three cores: two single-mode (SM), designed only to work with sensors on Bragg gratings, and one multimode (MM), serving to measure the profile of the distributed temperature (DTS). The cable is protected from external chemical and mechanical influences. Up to 8 seismic receivers, or a system of 12 micro-temperature sensors, as well

as various combinations of pressure-temperature (PT) gauges with other sensors can be installed on each SM core.

**PT sensors on Bragg gratings.** The principle of operation of the sensors on the Bragg gratings (FBG) is as follows. The light beam is directed through the light guide core. Part of the beam of light – only at the wavelength of the lattice-is reflected back. Applied strain changes the length of the FBG reflected wave. Surface equipment detects the wavelength shift due to the deformation of the sensor. The factory calibration allows to convert the wavelength measurement in terms of pressure and temperature values.

**DTS (Distributed Temperature Sensing) technology.** Multi-mode optical fiber is used for continuous monitoring of the temperature profile along the wellbore. In the DTS system, the fiber optic cable itself is a distributed temperature sensor. DTS measurements are based on the principle of Raman backscattering. The intensity of the measured signal depends on the energy state of the optical fiber. The temperature is calculated by the ratio of the peak intensities of the Stokes /anti-Stokes. The DTS system can be used to detect gas and water breakthrough, dynamics of thermal field change along the wellbore. The accuracy of the DTS temperature measurement is improved in combination with the use of point sensors as reference measuring devices.

**Seismic monitoring – Clarion™ system.** An example of a successful project is the monitoring of microseismic events, pressure and temperature in the T-24 well at the Tengiz field (Kazakhstan) ([www.weatherford.com](http://www.weatherford.com)). Microseismic sensors were installed in an abandoned production well, which was transferred to the category of observation. At the customer's request, the monitoring system has to work for many years, so the Clarion™ long-life optical seismic system has been selected (Fig. 4). The operation of passive accelerometer sensors in the well is supported by the FO system; while there is absolutely no downhole electronics, which ensures high reliability of this sensor system. The design of the spit consists of eight seismic receivers installed at different

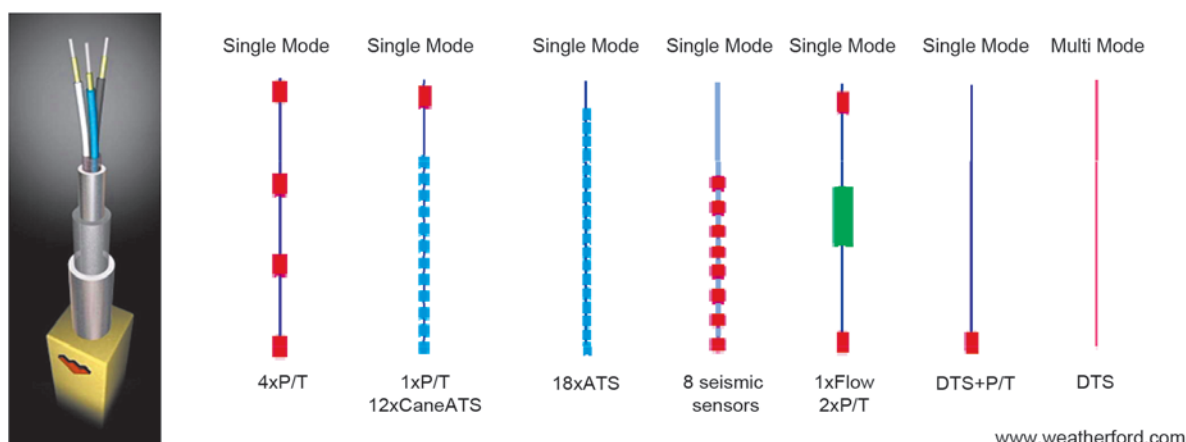


Fig. 3. Flexible sensor configuration in Weatherford fiber optic monitoring systems ([www.weatherford.com](http://www.weatherford.com))



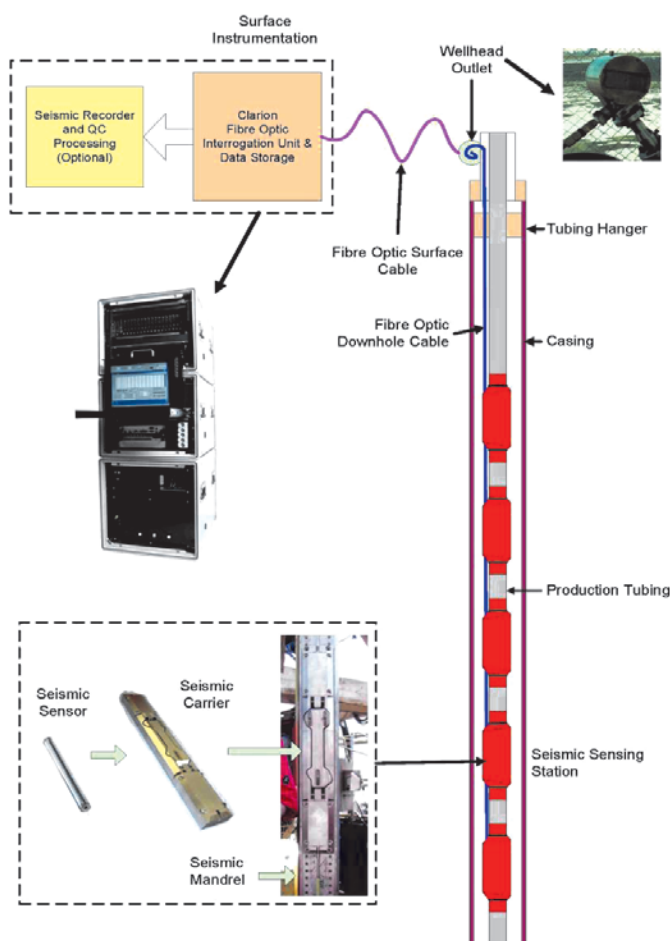


Fig. 4. Clarion™ Borehole Seismic Fiber Optic System. The installation process at the Tengiz field ([www.weatherford.com](http://www.weatherford.com))

depths, each of which includes three accelerometers in coordinates (XYZ). The total length of the sensors cable assembly was more than 500 m. Seismic receivers are mounted on specially designed mandrels as part of the completion layout. Fiber optic cable is fixed with clamps on each section of tubing – to the wellhead. After installation at a given depth, the sensors were deployed perpendicular to the casing string, closely connected to the geological formation through the cement ring. Deployed sensor holders are also designed to isolate seismic sensors from noise in the production tubing, increasing the signal-to-noise ratio. Since the output signal is a laser beam, there is no electrical interference in the downhole system. Physical orientation of sensors in the wellbore was carried out to minimize the error in the evaluation of localization of microseismic events. This was done using a special tool and a gyroscope inside the tubing. Orientation sets the absolute direction of the X and Y sensors relative to the magnetic North. Surface equipment, located at a distance of several hundred meters from the wellhead, were connected via optical cable and put into operation to record data in October 2006, to the present time, there is recorded data in continuous mode. By promoting the front of microseismic events it is possible to control the process

of field development within a radius of 15 km. Similarly, on Elbrus it is possible to track the dynamics of magma movement to the surface and the moments of formation of faults in the Earth's crust.

**LxData™ Technology.** LxData™ technology with an operating temperature of up to 300°C, designed specifically for steam injection wells, is the most cost-effective solution with the use of underground monitoring systems ([www.weatherford.com](http://www.weatherford.com)). It is designed for the installation of up to 40 temperature micro-sensors on one FO cable along wellbore, with a pressure sensor at the end of the cable (Fig. 5; Table. 1).

The arrangement of downhole sensors allows the use of configurations with 10, 20 or 40 temperature sensors and individual placement of sensors and the step between them (Fig. 6). The system provides accurate real-time temperature measurements, which makes it possible to monitor the intensity of hot volcanic gases release from faults and to forecast eruptions promptly. This does not require calibration of downhole and ground fiber optic lines, and the sensors can be reused if necessary. The LxData system is a cost-effective, alternative solution

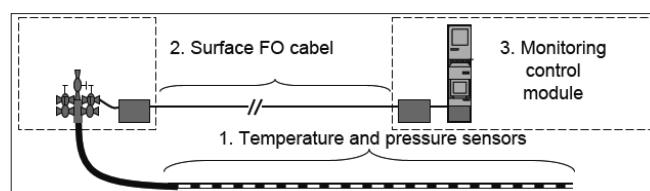


Fig. 5. Layout of downhole sensors and the surface part of the monitoring system

Parameter	Value
<b>Operating Performance</b>	
Temperature Measurement Range	-40° to 300°C
Temperature Accuracy	+/- 0.5°C
Temperature Resolution	+/- 0.01°C
Update Rate	1s/channel
Typical Operating Lifetime	>10 Years
<b>System Configuration</b>	
Number of Channels/ Cabinet	Up to 32
Number of Sensing Points/Sensor Cable	40 +
Maximum Sensor Cable Length	1800 m
Nominal Sensor Spacing	20 m
Maximum Surface Cable Run	5000 m
<b>Surface Instrument Module</b>	
Cabinet Housing Type	NEMA Enclosure
Surface Power Requirements	500W (Integrated UPS w/Battery Backup)
Data Transfer Protocol	MODBUS over TCP
Surface Cable Operating Temperature	-50°C to 85°C
<b>Environmental Conditions</b>	
Maximum Non-Operating Temperature (sensing cable)	300°C
Maximum Pressure (sensing cable)	500 to 8500 kPa
Cabinet Storage Temperature	-20°C to 50°C

Table 1. Specifications of the LxDATA™ monitoring system ([www.weatherford.com](http://www.weatherford.com))

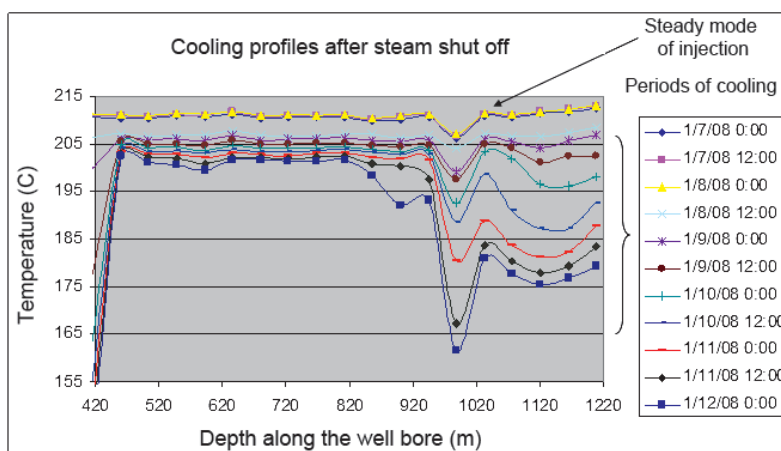


Fig. 6. An example of thermal monitoring with the LxDATA™ system. The dynamics of temperature variation along the well bore for five days after stopping the injection of steam shows the zone of inflow of formation fluid in the range of 960-1000 m

for high temperature monitoring. Instead of an expensive three-core cable, it uses an optical fiber placed together with temperature micro-sensors in a capillary tube 1/4" of corrosion-resistant alloy Inconel 718/625. At the end of the capillary is placed a pressure micro-sensor with an operating pressure of 8.5 MPa (Fig. 7). To implement the descent of the sensor system in the directional well used flexible tubing (coiled tubing) (Fig. 8). The monitoring system is controlled from the surface of the room where the ground equipment for reading and storing data is installed (Fig. 9). From the wellhead (through the cable input) to the control centre, transmission of signals is via the ground-based optical cable. Operational control is carried out in real time, through the graphical user interface and playback system. The data is stored in the memory of the device, where it is stored for three months with a sequential update of the record. Remote configuration and software updates as well as access to data via web applications are possible.

At the wellhead, it is advisable to install an automatic monitoring system with geochemical sensors of the concentration of acidic volcanic gases ( $\text{H}_2\text{S}$ ,  $\text{CO}_2$ ,  $\text{SO}_2$ ,  $\text{HCl}$ ,  $\text{HF}$ ). These components, along with water vapor, represent at least 95% of the gas volume of volcanic and geothermal systems and serve as indicators of volcanic activity. For example, monitoring of the amount of  $\text{SO}_2$  emanations in the Caldera of Kilauea volcano, conducted by researchers since 1979, showed that in the periods immediately preceding the eruptions, there



Fig. 9. Hardware rack of the control center (a) and control panel (b) of 19" size ([www.weatherford.com](http://www.weatherford.com))

was a significant increase in the intensity of removal of sulfur dioxide (Sutton, Ellias, 2014). Thus, a month before the eruption in March 2008, the amount of  $\text{SO}_2$  carried out doubled.

## 7. Cost-effective monitoring options

There are options that do not require drilling, but provide valuable operational information about volcanic activity. First of all, we are talking about the monitoring of the thermal state and gas-hydrogeochemical composition of fluids in the fumarole fields in the saddle and the Eastern part of the slope, in the zone of Hot Narzans, and, if possible, in the crater of the volcano. In other words, where there are already or are likely to be signs of increased heat

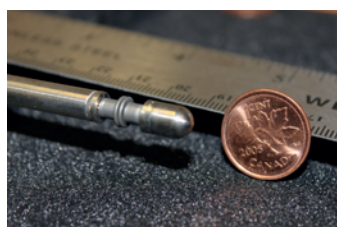


Fig. 7. Pressure sensor at the end of the capillary line ([www.weatherford.com](http://www.weatherford.com))

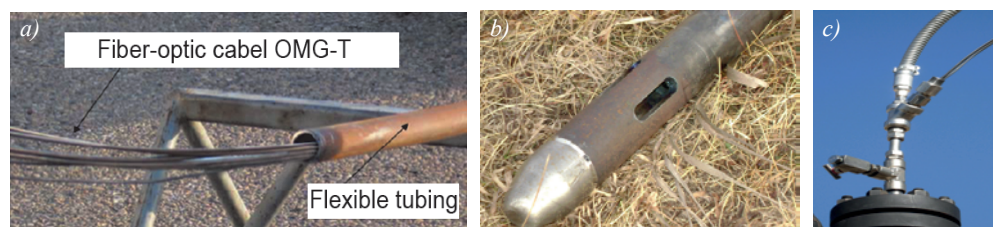


Fig. 8. Flexible tubing (a, b) with a diameter of 1.25" for the installation of T-P sensors in the well; (c) Cable entry at the wellhead ([www.weatherford.com](http://www.weatherford.com))



and mass transfer from the magma chamber due to the migration of hot gases through faults. It is advisable to install infrared thermal imagers on fumarole fields in order to continuously monitor the temperature of the soil surface in the areas of the greatest fumarole activity. Satellite data transmission can provide a rapid response in the event of an eruption. The installation of sensors to monitor the temperature and concentration of volcanic gases in the craters of the volcano makes sense only in the case of signs of geothermal activity and the possibility of open access to the crater. Currently, the craters are under the thickness of ice and snow, although on the Eastern wall of the Lateral crater (Fig. 10) participants in the tourist routes marked weak fumaroles. In addition to temperature sensors near fumaroles, it is advisable to install geochemical sensors of volcanic gas concentration.



Fig. 10. Side crater, on the east wall of which weak fumaroles are marked (photo from the Internet)

## Summary

Geothermal monitoring is an effective tool for forecasting volcanic eruptions, as well as assessing the geothermal energy potential of volcanic areas.

The method of “thermal interference testing” as a supplement or alternative to hydrodynamic interference testing can be quite successful in assessing the spatial heterogeneity of the filtration characteristics in the underground circulation system in geothermal and gas fields, carried out in order to improve the efficiency of development. It is recommended to conduct such a trial at the North Mutnovsky geothermal field.

In order to monitor volcanic activity and assess the prospects for the development of geothermal energy in the region, it would be advisable to drill on the slope of the Elbrus volcano an observation well up to 1800 m deep, directed towards the magmatic chamber. As possible locations for the drill sites should consider the area in the vicinity of the Mir station of the ropeway Azau.

To improve the reliability of the forecast of sudden volcanic eruptions, it is recommended to use

modern fiber-optic telemetry systems of underground monitoring, including array of temperature, pressure and microseismic events sensors.

## Acknowledgements

*The author is grateful to colleagues B.G. Polyak, M.D. Khutorskoy and V.Y. Lavrushin for valuable advice and comments. Work is performed under the State budget theme No. 0135-2015-0021.*

## References

- Bogatikov O.A. (2006). Issledovanie «spyashchikh» vulkanov [The study of «sleeping» volcanoes]. Sb.: Lektsii laureatov Demidovskoi premii (1993-2004) [Coll. papers: Lectures of the Demidov Prize winners (1993-2004)]. Ekaterinburg: Ekb. Univer. publ., pp. 483-495. (In Russ.)
- Bogatikov O.A. et al. (1998). Radiouglerodnoe datirovaniye golotsenovykh izverzhenii vulkana El'brus (Severnoy Kavkaz, Rossiya) [Radiocarbon dating of the Holocene eruptions of Elbrus volcano (North Caucasus, Russia)]. *Dokl. RAN = Proc. of the Russian Academy of Sciences*, 363(2), pp. 219-221. (In Russ.)
- Global'nye izmeneniya prirodnoi sredy i klimata [Global environmental and climate change]. (1997). *Izbrannyye nauchnyye trudy GNTPR*. Ed. Ak. Laverova N.P. M.: 433 p. (In Russ.)
- Gorbatikov A.V., Rogozhin E.A., Stepanova M.Yu., Kharazova Yu.V., Rybin A.A., Sysolin A.I., Andreeva N.V. (2018). Osobennosti glubinnogo stroeniya i vulkanicheskoi aktivnosti gory El'brus po kompleksu geologo-geofizicheskikh dannykh [Features of the deep structure and volcanic activity of Mount Elbrus using the complex of geological and geophysical data]. V Sb.: *Problemy tektoniki i geodinamiki zemnoi kory i mantii* [Coll. papers: Problems of tectonics and geodynamics of the crust and mantle]. Moscow: GEOS, V.2, pp. 149-154. (In Russ.)
- Izmeneniya okruzhayushchei sredy i klimata. Prirodnye i svyazannyye s nimi tekhnogennyye katastrofy [Environmental and climate change. Natural and related technological disasters]. (2007). Program No. 16 of the Presidium of the Russian Academy of Sciences. Vol.1: Seismic processes and catastrophes, recent volcanism. Ed.: Laverov N.P. Moscow: IGEM RAN, 198 p. (In Russ.)
- Izmeneniya okruzhayushchei sredy i klimata. Prirodnye i svyazannyye s nimi tekhnogennyye katastrofy [Environmental and climate change. Natural and related technological disasters]. (2008). Program No. 16 of the Presidium of the Russian Academy of Sciences. Vol.2: The newest volcanism of Northern Eurasia: patterns of development, volcanic danger, connection with deep-seated processes and changes in the natural environment and climate. Ed.: Kovalenko V.I., Yarmolyuk V.V., Bogatikov O.A. Moscow: IGEM RAN, IFZ RAN. (In Russ.)
- Likhodeev D.V. (2013). Issledovanie teplovogo i navedennogo volnovykh protsessov v raione El'brusskogo vulkanicheskogo tsentra [Study of thermal and induced wave processes in the area of the Elbrus volcanic center]. *Avtoref. diss. k.f.-m.n.* [Abstract Cand. phys. and math. sci. diss.]. Moscow.
- Melekestsev I.V., Braitseva O.K., Ponomareva V.V. (1987). Dinamika aktivnosti vulkanov Mutnovskii i Gorelyi v golotsene [Dynamics of activity of Mutnovsky and Gorely volcanoes in the Holocene]. *Vulkanol. i seismologiya = Volcanology and seismology*, 3, pp. 3-18. (In Russ.)
- Mochalov A. Climbing to Elbrus – photo essay. <http://www.mochaloff.ru/elbrus-azau>
- Muravyev A.V., Polyak B.G., Turkov V.P., Kozlovtsseva S.V. (1983). Povtornaya otsenka teplovoi moshchnosti fumarol'noi deyatel'nosti vulkana Mutnovskogo (Kamchatka) [Re-evaluation of the thermal power of the fumarole activity of the Mutnovsky volcano (Kamchatka)]. *Vulkanol. i seismologiya = Volcanology and seismology*, 5, pp. 51-63. (In Russ.)
- Polyak B.G. (1965). Teplovaya moshchnost' mezhparoksizmal'noi stadii aktivnosti Mutnovskogo vulkana [Thermal power of the interparoxysmal stage of activity of the Mutnovsky volcano]. *Doklady AN SSSR* [Proc. of the USSR Academy of Sciences], 162(3), pp. 643-646. (In Russ.)
- Polyak B.G. (1966). Geotermicheskie osobennosti oblasti sovremennogo vulkanizma [Geothermal features of the area of modern volcanism]. Moscow: Nauka, 180 p. (In Russ.)
- Polyak B.G., Bezukh B.A., Kaftan V.I. et al. (1985). Opyt nazemnnoi IK-s'emki dlya otsenki temperatury i teploizlucheniya termal'nykh polei vulkana Mutnovskogo (Kamchatka) [Experience of ground-based IR imaging to assess the temperature and radiation of thermal fields of the Mutnovsky volcano (Kamchatka)]. *Vulkanol. i seismologiya = Volcanology and seismology*, 3, pp. 54-63. (In Russ.)



Rasp Kh. (2013). Vulkany i vulkanizm [Volcanoes and volcanism]. Moscow: Mir, 344 p. (In Russ.)

Rogozhin E.A., Sobisevich L.E. et al. (2001). Geodinamika, seysmotektonika i vulkanizm Severnogo Kavkaza [Geodynamics, seismotectonics and volcanism of the North Caucasus]. Ed.: Ak. Laverov N.P. Report. 338 p. (In Russ.)

Selyangin O.B. (2016). Stroenie, veshchestvo i blizpoverkhnostnye ochagi vulkanov Mutnovskii i Gorelyi (Mutnovskii geotermal'nyi raion, Kamchatka) [Structure, substance and near-surface foci of the Mutnovsky and Gorely volcanoes (Mutnovsky geothermal area, Kamchatka)]. Part I-IV. V kn.: *Gornyi informatsionno-analiticheskii byulleten'* [Book: Mining information and analytical bulletin], special issue no. 31. Gornaya kniga publ., pp. 348-438. (In Russ.)

Stewart G. (2011). Welltest design and analysis. PenWell Corp., Tulsa, USA. 1483 pp.

Sutton A.J. and Elias T. (2014). One Hundred Volatile Years of Volcanic Gas Studies at the Hawaiian Volcano Observatory. In: Characteristics of Hawaiian Volcanoes. Editors: M.P. Poland, T. J. Takahashi, and C.M. Landowski., Ch.7. P.295-320. USGS Professional Paper 1801.

Vakin E.A., Kirsanov I.T., Kirsanova T.P. (1976). Termal'nye polya i goryachie istochniki Mutnovskogo vulkanicheskogo massiva [Thermal fields and hot springs of the Mutnovsky volcanic massif]. *Gidrotermal'nye sistemy i termal'nye polya Kamchatki* [Hydrothermal systems and thermal fields of Kamchatka]. Vladivostok, pp. 85-114. (In Russ.)

Vakin E.A., Kirsanov I.T., Pronin A.L. (1966). Aktivnaya voronka Mutnovskogo vulkana [The active funnel of the Mutnovsky volcano]. *Byull. vulk. st.* [Bull. volc. Art.], 40, pp. 25-35. (In Russ.)

Vakin E.A., Pilipenko G.F., Sugrobov V.M. (1986) Obshchaya kharakteristika Mutnovskogo mestorozhdeniya i prognoznaya otsenka resursov. Geoterm. i geokhim. issl-ya vysokotemperaturnykh gidroterm [General characteristics of the Mutnovsky field and the prediction resource estimate. Geothermal and geochemical studies of high-temperature hydrotherm]. Moscow: Nauka, pp. 6-40. (In Russ.)

Zelenskii M.E., Ovsyannikov A.A., Gavrilenko G.M., Senyukov S.L. (2002). Izverzhenie vulkana Mutnovskii (Kamchatka) 17 marta 2000 g. [Mutnovsky volcano eruption (Kamchatka) on March 17, 2000]. *Vulkanologiya i seismologiya = Volcanology and seismology*, 6, pp. 25-28. (In Russ.)

## About the Author

*Alexander V. Muravyev* – PhD (Geology and Mineralogy), Chief Researcher, Heat and Mass Transfer Laboratory

Geological Institute of the Russian Academy of Sciences

7, Pyzhevsky lane, Moscow, 119017, Russian Federation

*Manuscript received 11 July 2018;*

*Accepted 16 September 2018;*

*Published 30 November 2018*



ISSN 1608-5043 (Print)  
ISSN 1608-5078 (Online)

Key title: «Georesursy»  
Parallel title: «Georesources»

# GEORESOURCES

A peer-reviewed scientific and technical journal published since 1999

The journal is included/indexed in:

WEB OF SCIENCE™ CORE COLLECTION

**EMERGING SOURCES  
CITATION INDEX**

Web of Science Core Collection (ESCI)



CAS (Chemical Abstracts Service) databases



GeoRef database



EBSCOhost™ databases



Directory of Open Access Journals (DOAJ)

---

The full-text electronic versions of the articles published in the Journal  
are freely available to the public on our website: **[www.geors.ru](http://www.geors.ru)**

---

Contacts:  
Deputy Chief Editor - Daria Khristoforova  
E-mail: [mail@geors.ru](mailto:mail@geors.ru)  
Tel: +7 (843) 239-05-30